



**ERA ORA**

**EUROPEAN  
RADAR OPTICAL  
RESEARCH ASSEMBLAGE**

An EC research project  
co-funded by the Environment and Climate Programme within the topic  
*Space Techniques Applied to Environmental Monitoring and Research  
Methodological Research*

**FINAL REPORT**

prepared by

**P. Ferrazzoli, L. Guerriero, G. Schiavon, D. Solimini**

March 2002

Contract N° ENV4-CT97-0465





# Contents

<b>1</b>	<b>Introduction</b>	<b>7</b>
1.1	Overview of the project . . . . .	7
1.2	Radar and Optical/IR Data Library . . . . .	9
1.3	Model Library . . . . .	9
1.4	Selected applications . . . . .	12
1.5	Opening and maintenance of the Library . . . . .	12
1.6	ERA-ORA-based papers . . . . .	12
<b>2</b>	<b>Radar and Optical/IR Data</b>	
	<b>(WP 101)</b>	<b>15</b>
2.1	Available data . . . . .	15
2.1.1	DLR . . . . .	15
2.1.2	ESA/ESTEC . . . . .	16
2.1.3	GAMMA . . . . .	16
2.1.4	UAW . . . . .	17
2.1.5	UCL . . . . .	18
2.1.6	UPS . . . . .	18
2.1.7	UTOV . . . . .	19
2.1.8	USFD . . . . .	19
2.1.9	UVAL . . . . .	20
2.2	Data calibration and validation . . . . .	20
2.2.1	On the quality of remote sensing data . . . . .	20
2.3	Overview of relevant crop data features . . . . .	22
2.3.1	Summary of radar and optical data . . . . .	22
2.3.2	Summary of ground data . . . . .	26
2.3.3	Comparing crop $\sigma^0$ 's at different sites . . . . .	27
<b>3</b>	<b>Data Analysis and Synergy</b>	
	<b>(WP 201)</b>	<b>49</b>
3.1	Objectives . . . . .	49
3.2	Introduction . . . . .	49
3.2.1	The role of the ERA-ORA D.D.L. . . . .	50
3.3	On the information content of data . . . . .	50
3.4	Synergy studies in agriculture based on AirSAR data . . . . .	51

3.4.1	Crop discrimination: qualitative data analysis. . . . .	54
3.4.2	Classification of agricultural surfaces . . . . .	54
3.5	RASAM observation of seasonal development of crops . . . . .	62
3.5.1	Winter Wheat . . . . .	62
3.5.2	Corn (Maize) . . . . .	64
3.5.3	Rape (Canola) . . . . .	66
3.5.4	Sugar Beet . . . . .	66
3.6	Radar-Optical synergy in agriculture . . . . .	69
3.7	Elements of synergy in snow cover measurements . . . . .	72
<b>4</b>	<b>The Model Library</b>	
	<b>(WP 102, WP 202)</b>	<b>77</b>
4.1	Introduction . . . . .	77
4.2	Overview of the models . . . . .	78
4.2.1	UTOV model features . . . . .	78
4.2.2	POLSCAT model features . . . . .	78
4.2.3	UPS model features . . . . .	79
4.3	The models . . . . .	79
4.3.1	UTOV model description . . . . .	79
4.3.2	The POLSCAT model . . . . .	81
4.3.3	UPS model . . . . .	84
4.4	Model tests and validation . . . . .	84
4.4.1	UTOV model validation . . . . .	84
4.4.2	POLSCAT model test and validation . . . . .	97
<b>5</b>	<b>Towards Retrieval</b>	
	<b>(WP 203)</b>	<b>109</b>
5.1	Objectives . . . . .	109
5.2	Retrieval of crop parameters . . . . .	109
5.2.1	General aspects . . . . .	109
5.2.2	Data assimilation and use of the UTOV model . . . . .	110
5.3	Retrieval of soil moisture . . . . .	113
<b>6</b>	<b>Conclusions and Recommendations</b>	<b>117</b>
6.1	The Data Library (WP101) . . . . .	117
6.1.1	Data calibration . . . . .	117
6.2	Remote sensing data in agriculture (WP 201) . . . . .	118
6.2.1	Classifying and monitoring crops . . . . .	118
6.2.2	Monitoring bare soil and plant moisture . . . . .	119
6.3	The Model Library (WP 102, WP 202) . . . . .	119
6.3.1	The problem of the model inputs . . . . .	120
6.4	Towards data assimilation and retrieval (WP 203) . . . . .	121
6.5	Suggesting future satellite radar features . . . . .	122
6.6	General conclusions and recommendations . . . . .	123

<b>A The Wageningen Agricultural University Data Set</b>	<b>125</b>
A.1 The Flevoland agricultural test site .....	125
A.2 The MAESTRO-I campaign in The Netherlands .....	125
A.3 Ground data collection .....	127
A.4 The JPL AirSAR-91 campaign in The Netherlands .....	129
A.5 Vegetation map .....	129
<b>B Data Structure and Format</b>	<b>135</b>
<b>C Papers on pilot applications of the ERA-ORA Library</b>	<b>143</b>



# Chapter 1

## Introduction

### 1.1 Overview of the project

European RAdar-Optical Research Assemblage (ERA-ORA) is a Concerted Action co-funded by the European Commission within the RTD Programme on Environment and Climate (Fourth Framework Programme) in the field of space techniques applied to environmental monitoring and research.

The project has taken place in the years from 1998 till 2001, has been coordinated by Prof. D. Solimini, Università Tor Vergata, Rome, and has been monitored by Dr. Michel Schoupe, CEC, DG XII, who succeeded to the former officer Alan Cross.

Institutions from eight European Countries and an international organisation took part in the project:

- DLR (Deutsche Forschunganstalt für Luft- und Raumfahrt), Institut für Hochfrequenztechnik, Oberpfaffenhofen, Germany
- ESA/ESTEC, Wave Interaction and Propagation Section, Noordwijk, The Netherlands
- GAMMA Remote Sensing A.G., Muri, Switzerland
- Landbouwniversiteit Wageningen, Waterhuishouding, The Netherlands (UAW)
- Università Tor Vergata, Dipartimento di Informatica, Sistemi e Produzione, Roma, Italy (UTOV)
- Universitat de Valencia, Departamento de Termodinámica, Spain (UVAL)
- Université Catholique de Louvain, Laboratoire de Télécommunications et de Télédétection, Louvain-la-Neuve, Belgium (UCL)
- Université Paul Sabatier, Centre d'Études Spatiales de la Biosphère, Toulouse, France (UPS)
- University of Sheffield, Centre for Earth Observation Science, Great Britain (USFD)

The researchers who contributed to the project include the following (Table 1.1)

Institution	Scientist				
DLR	Christiane Schmillius (now with Uni. Jena)	David Hounam	Irena Hajsek		
ESA	Maurice Borgeaud				
GAMMA	Tazio Strozzi	Urs Wegmüller	Andreas Wiesman		
UAW	Dirk Hoekman	Martin Visser			
UCL	Albert Guissard	Stanislaw Matusiak	Pierre Defourny	Xavier Blaes	
UPS	Thuy Le Toan	Malcom Davidson			
USFD	Shaun Quegan	Mark Lomas			
UTOV	Domenico Solimini (coordinator)	Paolo Ferrazzoli	Giovanni Schiavon	Leila Guerriero	Fabio Del Frate
UVAL	José Moreno	Maria-Carmen González Sampedro			

Table 1.1: Institutions and scientists participating in ERA-ORA.

The essential objective of this Concerted Action is to improve the tools and methods to analyze and interpret microwave remote sensing data acquired over different areas of Europe.

Radar is sensitive to environmental parameters, like soil moisture and roughness, vegetation type and biomass, snow water equivalent, etc. However, the full exploitation of radar potential in environmental applications has been hindered by the fragmentation and particularization of model and application tools and by the restricted amount of (expensive) experimental data at the disposal of a single researcher.

Joining different sets of already available experimental data and theoretical models yields a value-added enlarged set forming an enhanced research tool. Indeed, benefits are expected by the availability of measurements obtained in different conditions and for various surface types, and of theoretical models based on different approaches.

A pool of European researchers has put in common radar data (with corresponding ground truth) and the eventual simultaneous optical/IR measurements, as well as computer programs for theoretical microwave backscattering modeling. The ensemble of data and software forms the ERA-ORA Library. The Library is organized as a tree of directories, starting from the “eraora” root directory. One subdirectory tree, containing introductory descriptions and information on formats, data, and possibly simulation computer programs, pertains to each project partner. Data and software reside on the site “<http://eraora.disp.uniroma2.it>”, where a handbook can be found which gives the needed details about

content and use of deposited files (see also Appendix B). Data are freely available for non-commercial applications, provided their sources are duly acknowledged.

Interested researchers can contact Paolo Ferrazzoli (ferrazzoli@disp.uniroma2.it), Giovanni Schiavon (schiavon@disp.uniroma2.it) or Domenico Solimini (solimini@disp.uniroma2.it) for further information.

The Library can be schematically subdivided into data and model sections. The Data Library (D.L.) includes radar data taken over land, covering agricultural, forest and snow-covered sites in Europe. For some sites, interferometric coherence and simultaneous optical/IR reflectances are also available. Samples of radiometric measurements are also included, since passive data can turn out to be quite useful in view of their possible synergy with scatterometer data.

Radar signatures and optical reflectances are usually accompanied by significant ground data (soil moisture and roughness, vegetation biomass, leaf area index, snow water equivalent, etc.).

A second section of the Library, the Model Library (M.L.) assembles three theoretical models for microwave backscattering simulation.

The features of data and models deposited in the ERA-ORA Library make this latter potentially useful for a variety of studies on microwave remote sensing, e.g.,

- understanding the information content of measurements and determining their statistical features;
- to assess, improve and use theoretical modeling;
- assessing the enhancement of accuracy in classification deriving by a synergistic use of different techniques and/or instruments;
- to devise and develop procedures to retrieve bio- geophysical parameters of interest to users, such as agricultural crop biomass, soil moisture, and snow water equivalent;
- to define efficient radar configurations for future missions.

In addition, cross-checks among data collected over different sites is expected to enhance the overall reliability of the measurements.

## 1.2 Radar and Optical/IR Data Library

The data Library includes field-average values of backscattering coefficients, degree of coherence (tandem) covariance matrices (polarimetric), relevant statistics (e.g., histograms) and selected statistical parameters of backscattering coefficients, or optical/IR reflectances. An overview of the remote sensing data present in the Library is given in Table 1.2. Significant ground data usually accompany the remote measurements.

## 1.3 Model Library

The Model Library includes three theoretical models, based on the Radiative Transfer (RT) Theory, which simulate microwave backscattering from soil and vegetation.

- A multiple-scattering model by Tor Vergata (UTOV) computes co- and cross-polar backscattering from crops.
- *POLSCAT* is a RT model contributed by UCL, which simulates the polarimetric radar response from vegetation, using leaf, branch, trunk, and soil parameters as input.

Institution	Site	Sensor	N° of fields	N° of data
DLR	Altmühltal	ERS	> 40	> 6,500
	Bayern	E-SAR		
	Lechfeld	Daedalus		
ESA	Flevoland	ERS	> 360	> 19,000
GAMMA	Bern	ERS	> 120	> 244,000
	Central Plain	RASAM		
	Davos	NA-SCATT		
	Kaunertal	NA-SCATT		
	Flevoland	ERS		
	Uecht	NA-SCATT		
M. Zeeland	ERS			
UAW	Flevoland	AirSAR	> 482	> 1,256,000
UCL	Hesbaye	ERS	4	32
UPS	M. Zeeland	ERS	48	150
	Lozère	ERS		
		J-ERS		
		SIR-C		
UTOV	Montespertoli	AirSAR	24	> 136,000
		TMS		
USFD	Driffield	ERS	72	> 28,000
	Feltwell	AirSAR		
UVAL	Barrax	AirSAR	12	> 28,000
		AVIRIS		
<b>TOTAL</b>			<b>&gt; 1,100</b>	<b>&gt; 1,700,000</b>

Table 1.2: Radar and optical/IR data present in the ERA-ORA Library at the end of March 2002.

- A four-layer (crown, trunk, understory, and grass) vector RT model contributed by UPS/CESBIO, computes backscattering coefficients and the Müller matrix for arboreous vegetation. The bistatic scattering coefficients can be obtained by some minor modifications of the program.

The models describe the soil as a lossy homogeneous half-space with rough boundary and the vegetation as an ensemble of discrete elements like discs (deciduous leaves) and cylinders (coniferous leaves, stems, branches, trunks). Although the models use the same electromagnetic approach, they differ from each other in their structure and computational details.

Among other input data, the computer codes can use the experimental ground truth contained in the D.L.. When the ground data are not sufficient, auxiliary inputs, such as vegetation morphological parameters derived from growth models, can be assigned.

An overview of relevant features of the models available in the ERA-ORA Library is provided by Table 1.3

Features	UTOV	UCL	UPS
Radiative Transfer Theory	x	x	x
Coherent / Incoherent	Inc	Inc	Inc*
Layered medium + soil	x	x	x
Multiple scattering	x		
Discrete scatterers	x	x	x
Forests		x	x
Crops	x	x	
P.D.F. of scatterer dimensions	*	x	x
P.D.F. of scatterer orientation	*	x	x
Input: scatterer dimensions	*	x	x
Input: scatterer permittivity	*	x	x
Infinite cylinder approximation	x	x	x
Generalized Rayleigh Gans approx.	x	x	x
Physical Optics approximation	x	x	
Resistive sheet approximation		x	
Output: $\sigma_{hh}$ , $\sigma_{vv}$ , $\sigma_{hv}$ , $\sigma_{vh}$	x	x	x
Output: Müller matrix		x	x

Table 1.3: Schematic features of models present in the ERA-ORA Library.

\* Branch scattering is formulated through a coherent approach to take clusters into account.

\* The software provided in the Tor Vergata model includes a routine which computes vegetation input parameters (scatterer dimensions, orientation, permittivity, and their probability distribution functions) as functions of the plant height.

## 1.4 Selected applications

The availability of a large collection of radar/optical/IR data related to a wide variety of surfaces and climatic conditions, with different features due to their multi-temporality, multi-frequency, and multi-polarization, can result in a novel powerful tool for applications. To suggest the usefulness of the ERA-ORA D.L. and show the first results, use of the Library has been made in three main fields.

- Assessment of the information content of multi-site radar and optical data.  
Cross-polar measurements at C-band, like the ones ENVISAT will acquire, appear to contain substantial information on crop canopies. Lower frequencies, e.g., L-band, are also promising for crop discrimination and monitoring.
- Classification of agricultural crops by multi-configuration radar data.  
The classification exercise has been based on a neural network algorithm using some of the multi-polarization and/or multi-date sets of C-band measurements provided by different institutions. The results allow conclusions on the benefits attainable from increasing the number of polarizations and/or of measurements dates. Testing a scheme of inter-year dynamic classification has also been made possible by the availability of such a large ensemble of data.
- Retrieval of crop canopy parameters.  
Monitoring crop development by radar exploits the sensitivity of microwave data both to the dimensions of the plant elements and to their water content. The important and difficult problem of estimating vegetation parameters, such as leaf area index and biomass density, by means of SAR acquisitions has been considered with specific reference to wheat fields. The retrieval scheme uses multi-temporal sets of C-band measurements in conjunction with a crop growth model and a scattering theoretical model. The procedure has been tested for two ERA-ORA sites, in the U.K. and in Switzerland, with different climatic conditions.

It is stressed that the unusual extent of the ERA-ORA Library offer a new and large variety of application opportunities and its exploitation by interested users would probably require several years. The results discussed in this report (see also the papers in appendix) are samples of the expected outcome, which, hopefully, will induce additional researchers to investigate the practical use of microwave remote sensing.

## 1.5 Opening and maintenance of the Library

The ERA-ORA Library is accessible to the open scientific community, subject to suitable acknowledgments of the sources of data.

It is pointed out that it is possible to contribute new data to the ERA-ORA Library, which, hopefully, will keep growing.

The Library is maintained by the Tor Vergata University team.

## 1.6 Scientific papers regarding ERA-ORA

Although the exploitation of the ERA-ORA Library is in its initial stage, the results that are being obtained have given the opportunity of presenting papers to several conferences.

- M.C. González-Sampedro, L. Alonso-Chorda, J.C. Fortea, and J.F. Moreno, “SAR/optical synergy for the retrieval of water content parameters in the Barrax area of Spain”, *European Geophysical Society XXV General Assembly*, Nice, France, 25-29 April 2000.
- P. Ferrazzoli, L. Guerriero, J.-P. Wigneron, A. Chanzy, S. Quegan, G. Cookmartin, A. Quesney, and O. Taconet, “Testing of microwave model for wheat with different sets of multitemporal data”, *Progress in Electromagnetic Research Symposium*, Cambridge, MA, U.S.A., July 2000.
- M.C. González-Sampedro, L. Alonso-Chorda, J.C. Fortea, and J.F. Moreno, “Improvement of retrievals of soil/canopy water content through polarimetric-SAR/hyperspectral-optical data synergy”, *EOS/SPIE International Symposium on Remote Sensing*, Barcelona, Spain, 25-29 September 2000.
- D. Solimini, P. Ferrazzoli, M. Borgeaud, D. Hoekman, J. Moreno, S. Quegan, and T. Strozzi, “Potential of radar in agricultural applications: comparison among results over different European sites”, *13<sup>th</sup> National Electromagnetics Meeting*, Como, Italy, 25-29 September 2000.
- A Guissard, S. Matusiak, and M. Leysen, “A polarimetric radiative transfer model for radar remote sensing of land targets”, *ERS-ENVISAT Symposium*, Gothemburg, Sweden, 16-20 October 2000.
- A Guissard, S. Matusiak, and E. Robin, “Polarimetric radiative transfer model applied to radar remote sensing of vegetation and forest covers”, *8<sup>th</sup> International Symposium on Physical Measurements and Signatures in Remote Sensing*, Aussois, France, 8-12 January 2001.
- P. Ferrazzoli, “SAR for agriculture: Advances, problems and prospects” (Keynote address), *Proc. 3<sup>rd</sup> International Symposium Retrieval of Bio- and Geophysical Parameters from SAR Data for Land Applications*, Sheffield, U.K., 11-14 September 2001, pp. 47-56.
- M.C. González-Sampedro, T. Le Toan, M.W.J. Davidson, and J. Moreno, “Assessment of crop discrimination using multi-site databases”, *Proc. 3<sup>rd</sup> International Symposium Retrieval of Bio- and Geophysical Parameters from SAR Data for Land Applications*, Sheffield, U.K., 11-14 September 2001, pp. 63-68.
- F. Del Frate, G. Schiavon, D. Solimini, M. Borgeaud, D. Hoekman, and M. Vissers, “The potential of SAR in crop classification using multi-configuration data”, *Proc. 3<sup>rd</sup> International Symposium Retrieval of Bio- and Geophysical Parameters from SAR Data for Land Applications*, Sheffield, U.K., 11-14 September 2001, pp. 93-98.
- F. Del Frate, P. Ferrazzoli, L. Guerriero, T. Strozzi, U. Wegmüller, G. Cookmartin, and S. Quegan, “Monitoring crop cycles by SAR using a neural network trained by a model”, *Proc. 3<sup>rd</sup> International Symposium Retrieval of Bio- and Geophysical Parameters from SAR Data for Land Applications*, Sheffield, U.K., 11-14 September 2001, pp. 239-244.

Other papers have been or are going to be submitted to conferences and peer-reviewed journals.



## Chapter 2

# Radar and Optical/IR Data (WP 101)

### 2.1 Available data

All participating institutions contributed data to the ERA-ORA Library, which has been filled generally following the guidelines reported in Appendix B. The contributions by each institution relative to the different sites is overviewed in the following.

#### 2.1.1 DLR

Data collected by different sensors and procedures over three sites are present.

##### **Altmühltal, DE**

The radar data set consists in backscattering coefficients measured by ERS (both ascending and descending orbits) in the years 1995, 1996, and 1997 over 4 forest stands of beech, spruce, pine and poplar.

Ground data include details on the imaged surface and on the arboreous vegetation, such as basal area, biomass, and geometry.

##### **Bayern, DE**

This site has been overflown by the DLR ESAR in the course of the TerraDew campaign carried out in June 2000 over 30 fields, with crops (maize, oat, triticale, sugarpea, futter clover, winter and summer barley, wheat, potato) and pasture.

The radar data set consists of co- and cross-polarized ( $vv$ ,  $hh$ ,  $hv$ ,  $vh$ ) backscattering coefficients measured at C- and X-bands at three different times on the same days over different parcels (up to 4) of each field.

The ground data include crop height and row separation and, in particular, the plant volumetric soil moisture for each field parcel measured around the time of each radar overpass.

**Lechfeld, DE**

This site has been imaged by a Daedalus multispectral scanner (11 bands, including one in the thermal infrared).

The optical/IR data set consists of radiances measured in the different bands over 16 crop fields (beets, rape, turnip, summer and winter barley, wheat) in mid May and mid July 1992.

Ground data consist of total biomass, volumetric moisture, crop height and plant row distance.

**2.1.2 ESA/ESTEC****Flevoland, NL**

The data base contains multi-temporal average backscattering coefficients taken by ERS over a variety of agricultural surface types, including, among others, bare soil, grass, barley, maize, oilseedrape, potatoes, peas, beans, sugar beet, and wheat, for a total of about 175 fields. Measurements refer to the years 1993, 1994, 1995, and 1996, with up to 27 measurements per year per field.

The radar data are accompanied by a crop map for each year.

**2.1.3 GAMMA**

A variety of data (radar, scatterometric, radiometric) has been contributed, relative to agricultural surfaces, forest, and snow, on different sites.

**Bern, CH**

This data set refers to interferometric ERS SAR data acquired on 26 forest areas and includes a single tandem pair over snow-covered terrain. It consists of the field-averaged backscattering coefficients of the two interferometric images and of the average degree of interferometric coherence, as well as of the corresponding standard deviations. Eight tandem pairs for one year (April 1995 to April 1996) are included

Ground data relate to forest type and, when applicable, to snow thickness and type.

**Central Plain, CH**

The set of data contains measurements taken by the RASAM (University of Bern) instrument over various types of fields, including bare soil, maize, sugar beet, potato, rape, and wheat.

It includes backscattering coefficients averaged from measurements taken on a specific day on a specific field at  $hh$ ,  $vv$ ,  $hv$ , and  $vh$  polarizations, at the frequencies of 2.5, 3.1, 4.6, 7.2, 10.2, and 11.0 GHz, and at 8 incidence angles (0 to 70°, step 10°). Data refer to a period of 8 years (1984-1991) with several days (up to 43) of measurement each year

The emissivities contemporarily measured at the same polarizations, frequencies, angles of observation and days are also generally available for the same fields.

The corresponding ground data files include information on average volumetric soil moisture (0-4 cm layer), density (0-4 cm layer), and texture, surface roughness, average height of canopy layer, above surface vegetation water content and dry matter fraction, and fraction of soil covered by vegetation at normal observation direction. The roughness of some bare fields is described by the whole profile, which is important in view of a deeper comprehension of the scattering from rough surfaces and of new approaches to modelling.

### **Davos, CH and Kaunertal (Ötztaler Alps), AT**

The available data have been acquired by a network-analyzer based scatterometer (University of Bern) operating at 5 and 35 GHz over bare and snow-covered terrain on 37 and 23 days, respectively, in 1994 and 1995. Average backscattering coefficients at  $hh$ ,  $vv$ , and  $hv$  polarizations are provided for each frequency at 5 incidence angles ( $20^\circ$  to  $60^\circ$ , step  $10^\circ$ ). Corresponding standard deviations are included.

Ground data include details on soil type and, when snow is present, thickness, density, permittivity, temperature, fraction and column height of liquid water, as well as information on layers and range of air temperature.

### **Flevoland, NL**

The data set consists of interferometric data acquired by 4 ERS-1 repeat-passes on bare soil and on crops in 1991 and by 4 ERS-1/ERS-2 tandem passes in 1995. For each pair, average backscattering coefficients, 1-day repeat degree of coherence, and corresponding standard deviations are included for 14 bare soil parcels and for several (up to 18) fields, with various cover types, such as grass, potato, maize, sugar beet, wheat.

Ground data include details on soil status, crop coverage, crop description, sowing, harvest, and tillage periods.

### **Moosseedorf and Uecht, CH**

The set of data collected on this site has essentially the same features as that of Davos and Kaunertal. They consist in multi-angle, multi-polarization backscattering coefficients at 5 and 35 GHz over snow covers, measured on 14 days in 1993, 1994, and 1996.

Ground data include soil type, thickness, density, permittivity and temperature of snow, fraction and column height of liquid water, information on snow layers, and range of air temperature.

### **Zeeland, NL**

This radar data set is similar to that of Flevoland. It contains interferometric data (backscattering coefficient, degree of coherence and standard deviations) relative to 12 ERS-1 repeat-pass pairs of images acquired between January and March 1994 over 8 bare-soil fields.

Ground data consist of information on soil type, average r.m.s. height obtained by a laser profiler, and moisture measurements by a Time Domain Reflectometer (0-5 cm depth).

#### **2.1.4 UAW**

The Agricultural University of Wageningen has contributed a large radar and ground data set relative to the Flevoland (Netherlands) site, as detailed in Appendix A.

### **Flevoland, NL**

The test site was imaged in two different years, 1989 (MAESTRO Campaign) and 1991 (MAC-Europe Campaign). While in 1989 only one flight took place in mid August, four flights occurred in 1991, from mid June till the end of July. In all cases the sensor was the three-frequency polarimetric AirSAR, which

overflow an agricultural area with a large variety of crops. The angles of incidence are in the range  $25^\circ$  to  $65^\circ$ .

Field-averaged complex elements of P-, L-, and C- band backscattering covariance matrices are available, together with the corresponding standard deviations and histograms (50 samples between minimum and maximum values for modulus, 36 samples between  $-180^\circ$  and  $+180^\circ$ , step  $10^\circ$  for phase).

Detailed ground measurements are provided for 16 fields (6 bare soil, 4 wheat, 2 each for potato, sugar beet and corn) in 1989 and for 33 fields (10 each for wheat and potato, 9 sugar beet and 4 corn) in 1991, on each date. Various surface parameters are available. In case of bare terrain, r.m.s. soil surface roughness transverse and parallel to cultivation (both mean values and standard deviations), exponential and Gaussian autocorrelation lengths transverse and parallel to cultivation (both mean values and standard deviations), volumetric and gravimetric soil moisture content in the layers at depths 0-5 cm, 10-15 cm, and 20-25 cm (both mean values and standard deviations). In the case of crops, the mean values of crop cover and height, plant fresh and dry weights, plant moisture content, and leaf area index are added.

### 2.1.5 UCL

#### Belgium

The modulus of single-look complex images and the degree of coherence (mean values and standard deviation) are available for 8 fields (two each) of wheat, sugar beet, potato, and maize, together with ground information. The image processing, yielding a pixel size of 40 m by 40 m, was carried out by the InSAR processor developed by the Spatial Center of Liège - CSL. The backscattering values were extracted from a tandem pair of ERS 1/2 images acquired on the 13<sup>th</sup> and 14<sup>th</sup> of June 1996, with an interferometric baseline of 94 meters. In order to keep the full information content of these images, they were neither resampled nor geometrically corrected.

The ground data provide canopy cover fraction, crop height, phenological stage, distance between rows of plants and between 2 plants in the same row, gravimetric soil moisture (average on 6 samples per field), average soil density (6 samples per field), rainfall during the hour of the satellite overpass, 24 hours and 5 days cumulative rainfall before image acquisition.

These data were provided by Prof. P. Defourny of the Department of Environmental Science and Land use Planning-Geomatic of the Université Catholique de Louvain.

### 2.1.6 UPS

UPS/CESBIO has made available radar data on bare soil parcels and forest stands.

#### Middle Zeeland, NL

This data set contains backscattering coefficients (average and standard deviation) measured on 13 different days in January, February and March 1994 by the ERS-1 SAR over 7 bare soil fields (not temporarily imaged). The corresponding ground truth consists of information on tillage technique (seedbed, harrowed, old plough, new plough), volumetric soil moisture, and roughness data in terms of surface height standard deviation and correlation length parallel and perpendicular to tracks obtained by a laser profilometer.

**Lozère, FR**

Average and standard deviation of backscattering coefficients, measured by ERS, JERS and SIR-C, are provided for 14 forest stands of Austrian pine of various ages.

**2.1.7 UTOV**

Both multi-frequency polarimetric AirSAR and optical/IR data are provided for a variety of land categories, including bare soil, crops, forest, and olive groves. The measurements were supported by the Italian Space Agency within the MAC-Europe campaign and were coordinated by Paolo Pampaloni, CNR/IROE, Firenze.

**Montespertoli, IT**

The polarimetric radar measurements present in the data base refer to three different dates (22 and 29 June, 14 July 1991), P-, L- and C- bands, and two incidence angles, i.e., 35° and 50°. In addition to bare soil with different roughness, fields with various crops, like alfalfa, wheat, sunflower, colza, and corn were imaged. Arboreous vegetation includes 5 stands of mixed deciduous forest and three olive groves. Optical/IR data for the same area are present, as collected by the TMS in 10 bands.

Radar data consist of the elements of the backscattering covariance matrix and include field-averaged values, standard deviations, module histograms (50 samples between minimum and maximum values) and *hhvv* phase histogram (36 samples between -180° and +180°, step 10°). TMS measurements include the average, standard deviation and histograms (20 samples between minimum and maximum values) of the radiance in each of the 10 bands.

The detailed ground data, relative to selected fields of the above crop types, include gravimetric and volumetric moisture at depths 0-5 cm and 5-10 cm, surface height standard deviation and correlation length, row direction, phenological state, crop height, fresh and dry biomass of stems and leaves, stem density, main stem diameter and height, LAI, number of leaves per stem, and area and thickness of leaves. In the case of bare soil, a number of parameters are provided, including tillage technique and track directions, gravimetric moisture and bulk density in layers at three depths (0-2.5 cm, 2.5-5 cm, 5-10 cm), surface height standard deviation and correlation length both parallel and perpendicular to tracks. Ground truth for forests and olive groves consists of trunk density and diameter, total height, and basal area.

**2.1.8 USFD**

USFD/SCEO makes available both multitemporal ERS data (Driffield site) and multi-frequency polarimetric AirSAR measurements (Feltwell site).

**Driffield, UK**

Field-average backscattering coefficients measured by ERS-2 on 13 dates from February till August 1997 are provided for 12 fields containing oil-seed rape, winter wheat, spring barley and potato.

Ground truth includes temperature, texture (percentage of sand, clay and loam), volumetric moisture and roughness parameters (r.m.s. surface height, Gaussian autocorrelation length) of soil, and a quite detailed crop characterization. This considers plant coverage and area density, thickness of the layers into which the crop canopy is subdivided (bottom, middle, top), number of scatterers in each layer, leaf

dimensions and gravimetric moisture in each layer, stems per plant and leaves per stem (in the lower and upper layer), stem dimensions and their gravimetric moisture, branches per stem, branch dimensions and their gravimetric moisture, pods/ears per branch, and pod/ear dimensions and gravimetric moisture.

### Feltwell, UK

The ERA-ORA data files contain data relative to 60 fields and forest stands, imaged at the end of July 1991 at P-, L-, and C-band. Barley, potato, sugar beet, and wheat are represented by 10 fields each, as well as grass and conifer stands. Both scatter and Müller covariance matrices and statistics are provided.

### 2.1.9 UVAL

#### Barrax, SP

Polarimetric multi-frequency AirSAR data and AVIRIS measurements in 224 bands taken in June and July 1991 are available for fields with irrigated and dry barley, maize, alfalfa, wheat and bare soil.

Radar data files include backscattering covariance matrices, field-averaged values, standard deviations, module histograms (50 samples between minimum and maximum values) and *hhvv* phase histogram (36 samples between  $-180^\circ$  and  $+180^\circ$ , step  $10^\circ$ )

The AVIRIS data files contain minimum, maximum, and average values of the radiance in each of the 224 bands, together with the corresponding standard deviations.

Ground measurements consist of soil data and crop information. Soil is characterized by mean values and standard deviations of volumetric and gravimetric soil moisture at various depths (0-2 cm, 0-5 cm, 5-10 cm). Crops are described by phenology, height, cover fraction, area density, fresh and dry biomass, canopy water content, and leaf area index.

## 2.2 Data calibration and validation

A major task undertaken has been in checking the quality of the data. A tool for validation is the comparison among data relative to similar types of surfaces. From this point of view, the availability of a wide ensemble of data makes the ERA-ORA Library rather interesting and more effective than the usually limited data bases available to individual groups. In the following, details on some problems encountered in data calibration and validation are reported, in the hope that a share of the ERA-ORA experience in this domain, could result in a more effective exploitation of SAR measurements.

It should be remarked that the assessment of the ERA-ORA data quality has required careful and lengthy analyses on a huge amount of data.

### 2.2.1 On the quality of remote sensing data

The quality of most data available in the library appears to be good, at least for scientific studies. In many cases, data had been validated and published by the same experimenter providing them. As a further validation, cross checks between homogeneous data sets have been carried out, as well as comparisons with results published in the literature, and eventual discrepancies have been noted and discussed.

### AirSAR data

As an example of the procedures followed to further improve the quality of polarimetric data, we report the one implemented at USFD for the measurements on the Feltwell site. The routine for calibrating the scattering matrix elements was tested and modified and the field boundaries were rechecked for a selected sub-set of data. Then the calibration and polygon analyses were rerun for all the available data. After cross-checking all these results, the required parameters, extracted from the Müller matrix and from four of the separate scattering matrix images used to form the 16-look Müller matrix were consolidated. This was done for the C-, L- and P-band data relative to a substantial set of fields. Polygons showing anomalous behaviour (for example, single extremely bright pixels or thin lines occurred in single looks, particularly at P-band, which greatly distorted field statistics) were removed. By this recheck, the number of polygons with acceptable data could be increased from the original set, with a substantial improvement of the contribution to the ERA-ORA database. It is worth mentioning that having all four scattering matrix image data available at all frequencies enables stability of parameters to be investigated; this varies markedly with frequency, with much greater variation at lower frequencies. Note that a commentary on the data has also been provided within a *readme* file, which helps potential users to make best use of them.

An additional subsequent quality checking pointed out that there is some form of error (around 1%) in the Müller matrices for several of the pixels. The error is not obvious, but shows up as follows. Most of the parameters needed for the ERA-ORA database come from the covariance matrix, which by its nature must be positive definite. However, some of the eigenvalues associated with these matrices appeared to be negative, which cannot happen for positive definite matrices. Using a different check for positive definiteness (based on positivity of a certain set of determinants) this condition was often found violated. This is probably due to the data compression used by JPL. A note to this effect has been added to the *readme* file.

Another problem experienced on AirSAR data (Barrax site) has been that differences in measured values due to variations in the incidence angle can be as significant as potential calibration issues and even temporal changes. When this is the case, suitable models have to be assumed when making multi-angular comparisons, and, anyway, particular care must be exerted when drawing conclusions. Note that this type of problem can affect optical data too, when solar elevation changes from measurement to measurement.

Over all, the polarimetric AirSAR data present in the library generally show consistent values of  $hh$ ,  $hv$  and  $vv$  signatures, whereas correlation coefficients and phases are occasionally questionable.

It is also worth noting that P-band signatures show a certain dispersion for values lower than about -25 dB. This cannot be simply explained on the basis of scene properties, but needs deeper statistical investigations, e.g., by histogram analysis.

### Scatterometer data

GAMMA has carried out an investigation of RASAM and NA-based scatterometer data in terms of mean signatures and time series, with the purpose of critically analysing the accuracy and stability of the contributed data.

The amplitude data from the ground-based scatterometer RASAM were considered accurate enough to be used as reference data, since they were carefully calibrated with stable reference targets and, after all, their quality was already demonstrated in other works.

### ERS data

GAMMA compared ERS SAR data with those of RASAM at C-band,  $vv$  polarization and at a nearby incidence angle in an experiment for monitoring the seasonal development of maize and sugar beet. Comparison between data collected on potato and bare-soil fields with different roughness and soil moisture was also carried out. For the crop data acquired over Flevoland in 1991 and the bare soil data acquired over Middle Zeeland, the agreement between RASAM and ERS SAR data was found acceptable, consistently with the known good calibration of the ERS data.

In one instance (Flevoland site, GAMMA 1995 data), some inconsistency was noted, probably due to a gain underestimation in the procedure followed for calibrating that particular set of data. It was decided to keep these data in the DL and to complete the *readme* file with the relevant information and comments on the absolute radiometric calibration, both because of the high value of these data for a multi-temporal analysis of the test-site where they were acquired, and because these data are rather unique, since they also include coherence values. On the other hand, re-calibration of these measurements after H. Laur et al. [1] may be feasible, if needed.

### Optical/IR data

Radiances have been provided. Calibration features will be eventually discussed simultaneously with data analysis.

## 2.3 Overview of relevant crop data features

### 2.3.1 Summary of radar and optical data

The majority of available radar and optical data refer to agricultural surfaces with a variety of crops, or, especially in winter, to bare soil.

Among the data that have been analyzed in detail, three main data set categories can be identified.

1. Multitemporal, but single frequency single polarization: ERS with RASAM (C-band,  $vv$ ).
2. Polarimetric, with short-term multitemporality: AirSAR with possible addition of RASAM C-band.
3. Polarimetric radar and optical.

The following Tables 2.1 to 2.3 summarise the features of the three groups of data referring to crops and bare soil.

MULTITEMPORAL ERS + RASAM						
Site	Flevoland	Flevoland	Driffield	Central Plain	Zeeland	Zeeland
Sensor	ERS	ERS	ERS	RASAM	ERS	ERS
Years	'93-'96	'95	'97	'84-'91	'94	'94
BUSHES	-	5	-	-	-	-
CORN/MAIZE	12	5	-	4	-	-
SUGARBEET	155	5	-	2	-	-
POTATO	176	5	3	2	-	-
RAPE	4	2	3	2	-	-
BARLEY	30	-	3	-	-	-
WHEAT	183	5	3	4	-	-
LUCERNE	-	3	-	-	-	-
GRASS	121	5	-	-	-	-
OAT	-	-	-	-	-	-
ONION	-	5	-	-	-	-
PEAS	7	5	-	-	-	-
FLAX		5	-	-	-	-
BARE SOIL	11	2	-	-	2	8
Notes	(1)	(2)	(3)	(4)	(3)	(2)

Table 2.1: Number of multitemporal data takes deposited before December 2000.

Notes:

(1) – N. fields  $\times$  n. years; crop maps.

(2) – Accompanied by coherence values; coarse ground data.

(3) – Detailed ground data.

(4) – (N. fields with at least 6 samples/year)  $\times$  n. years; detailed ground data.

MULTIPOLARIZATION AirSAR + RASAM					
Site	Barrax	Montespertoli	Feltwell	Flevoland	Central Plain
Years	'91	'91	'91	'89	'84-'91
Sensor	AirSAR	AirSAR	AirSAR	AirSAR	RASAM
FOREST	-	2	10	-	-
SUNFLOWER	-	3	-	-	-
CORN/MAIZE	4	1	-	4	6
SUGARBEET	-	-	10	10	7
POTATO	-	-	10	11	11
RAPE/CANOLA	-	1	-	4	6
BARLEY	6	-	10	7	-
WHEAT	1	5	10	26	17
LUCERNE	1	3	-	2	-
GRASS	-	-	10	-	11
OAT	-	-	-	-	2
ONIONS	-	-	-	5	-
PEAS	-	-	-	-	1
BARE SOIL	2	3	-	11	$\approx 300$
Notes	(1)	(2)	(3)	(4)	(5)

Table 2.2: Number of polarimetric data takes deposited before December 2000.

Notes:

(1) – 2 overpasses; detailed ground data.

(2) – 3 overpasses; detailed ground data.

(3) – No ground data.

(4) – Detailed ground data.

(5) – For crops:  $n$ . fields  $\times$   $n$ . years ( $1 < n$ . overpasses/year  $< 25$ ); for bare soils: total number of fields  $\times$  years  $\times$  overpasses  $\approx 300$ ; detailed ground data.

AirSAR + OPTICAL		
Site	Barrax	Montespertoli
Year	'91	'91
Sensor	AVIRIS + AirSAR	TMS + AirSAR
FOREST	-	2
SUNFLOWER	-	3
CORN/MAIZE	4	1
RAPE/CANOLA	-	1
BARLEY	4	-
WHEAT	1	5
LUCERNE	1	-
BARE SOIL	2	-
Notes	(1)	(2)

Table 2.3: Number of “simultaneous” radar and optical data takes (deposited before December 2000).

Notes:

(1) – 2 overpasses; detailed ground data.

(2) – 2 overpasses; detailed ground data.

### 2.3.2 Summary of ground data

Available ground truth data are summarized in Table 2.4 for crops.

GROUND DATA							
Site		Barrax	Montespertoli	Driffield	Flevoland	Central Plain	Zeeland
Years		'91	'91	'97	'89	'84-'91	'94
Soil moisture:							
	gravimetric	X	X	X	X	X	X
	volumetric	X	X	X	X	X	X
Soil roughness:							
	$\sigma_z$	-	X	X	X	X	X
	Correlation length	-	X	X	X	X	X
	Whole profile	-	-	-	-	X	-
Canopy:							
Height		X	X	-	X	X	-
Cover (%)		X	-	X	X	X	-
Density ( $m^{-2}$ )		X	X	X	-	-	-
Volume		-	-	X	-	-	-
Fresh weight							
	total	X	X	X	X	X	-
	components	-	X	X	-	-	-
Dry weight							
	total	X	X	X	X	X	-
	components	-	X	X	-	-	-
LAI		X	X	X	X	-	-
Stem/ear dimensions		-	X	-	-	-	-
Leaf dimensions		-	X	-	-	-	-
Notes		(1)	(2)		(3)	(4)	(5)

Table 2.4: Available ground measurements (deposited before December 2000).

Notes:

- (1) – Some data not available.
- (2) – Height standard deviation  $\sigma_z$  and correlation length for bare soil only; data available for 10 fields.
- (3) – Data available for 16 fields.
- (4) – Profiles for bare soil only.
- (5) – Prevaillingly bare soil.

### 2.3.3 Comparing crop $\sigma^0$ 's at different sites

Figures 2.1 to 2.24 show comparisons among selected  $\sigma^0$ 's mainly measured over crops in different sites, while some forest and bare soil signatures have been included, for suitable cross-checking. The diagrams derive from three kinds of data assemblies:

1. Multitemporal radar signatures collected by ERS SAR and RASAM (C-band,  $vv$  polarization,  $30^\circ$ );
2.  $hh$ ,  $hv$  and  $vv$  multifrequency AirSAR signatures collected at Barrax, Montespertoli and Flevoland sites, with incidence angles from  $\sim 40^\circ$  to  $\sim 50^\circ$ ;
3. AirSAR signatures with nearly simultaneous optical reflectances (Barrax and Montespertoli sites).

These diagrams are intended as examples of the outcome of the analysis on part of the ERA-ORA data set, which, as already noted, consists of a considerably large amount of diverse measurements.

It should be noted that only polygon average values are shown in the figures. More in-depth statistical analysis, based on standard deviations and histograms, when available, can be carried out for a more complete characterization of the radar response of the various crops.

In spite of the somewhat partial character of the analysis, the results reported in the figures already show the potential of the ERA-ORA library and pave the road to more advanced specific studies, based on quantitative analysis, models, and statistical analysis.

#### Multitemporal patterns

Multitemporal  $\sigma^0$  patterns collected by ERS SAR and RASAM over different sites and years are shown in Figures 2.1 (potato fields), 2.2 (sugar beet) and 2.3 (wheat). Among the many data available for Flevoland, only 10 patterns per crop type per year have been plotted. Available coherence data are also included. Figure 2.1 shows a wide site-to-site and year-to-year variability in the first periods of the years. This is related to the various rain, snow and frost events, since the backscatter is dominated by soil. In a later period, after day  $\sim 150$ ,  $\sigma^0$ 's are closer to each other, since vegetation backscatter becomes dominant. For 4 fields out of 5, coherence trends show an enhanced minimum occurring at  $\sim$ day 200, i.e., in full growth.

Most of the previous comments apply also to the sugar beet trends of Figure 2.2, in which the coherence minimum is observed for 3 fields over 5.

Wheat patterns are shown in Figure 2.3. As far as  $\sigma^0$  is concerned, a general decreasing trend is observed in the first period of the year in almost all patterns. A minimum occurs between day  $\sim 150$  and day  $\sim 200$ . This  $\sigma^0$  decrease is due to two simultaneous factors, i.e. soil drying and development of vertical absorbing structures, such as ears and stems. The degree of coherence is relatively high and does not show significant temporal trends. This result is not easy to explain. Possible hypotheses are:

- the lower plant moisture of wheat with respect to other crops in the same days
- the high plant density producing a reduction in pixel-to-pixel variability.

Figure 2.4 compares the  $\sigma^0$  trends of wheat and barley with those of other crops. The previously discussed minimum is observed in all wheat patterns and, to a lesser extent, in the barley patterns, while it is absent in the other crops. This result is interesting for both applications and signature interpretation.

At Driffield and in the Swiss Central Plain detailed ground measurements were carried out. Figure 2.5 shows wheat  $\sigma^0$  trends jointly with patterns of fresh biomass and soil moisture. Ground data indicate that Driffield fields were less moist and showed longer biomass cycles.  $\sigma^0$  trends are in general agreement with these properties. More quantitative analyses, based on modelling, can be carried out for further understanding.

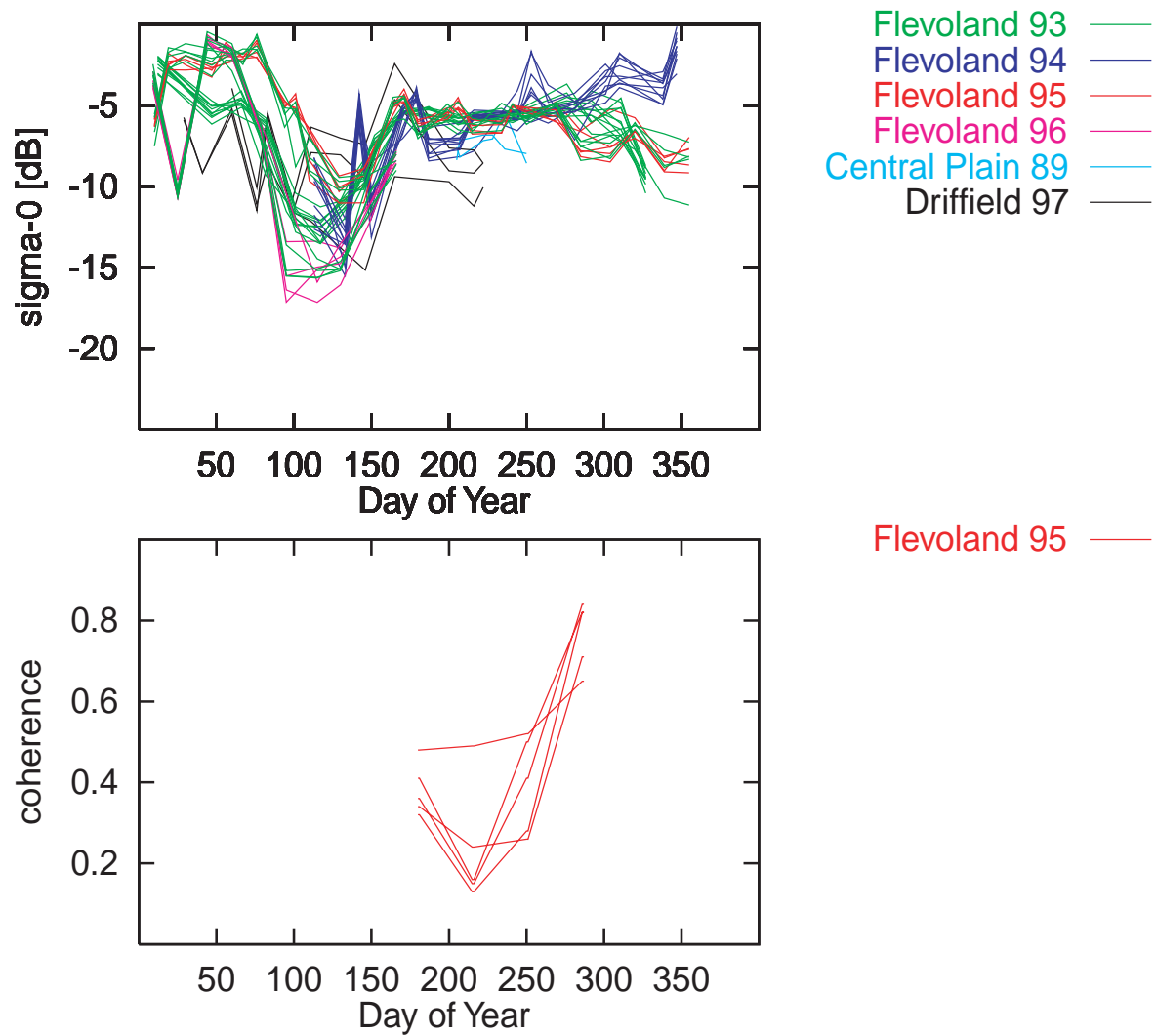


Figure 2.1: Multitemporal patterns of backscattering coefficient (top) and degree of coherence (bottom) for potato fields.

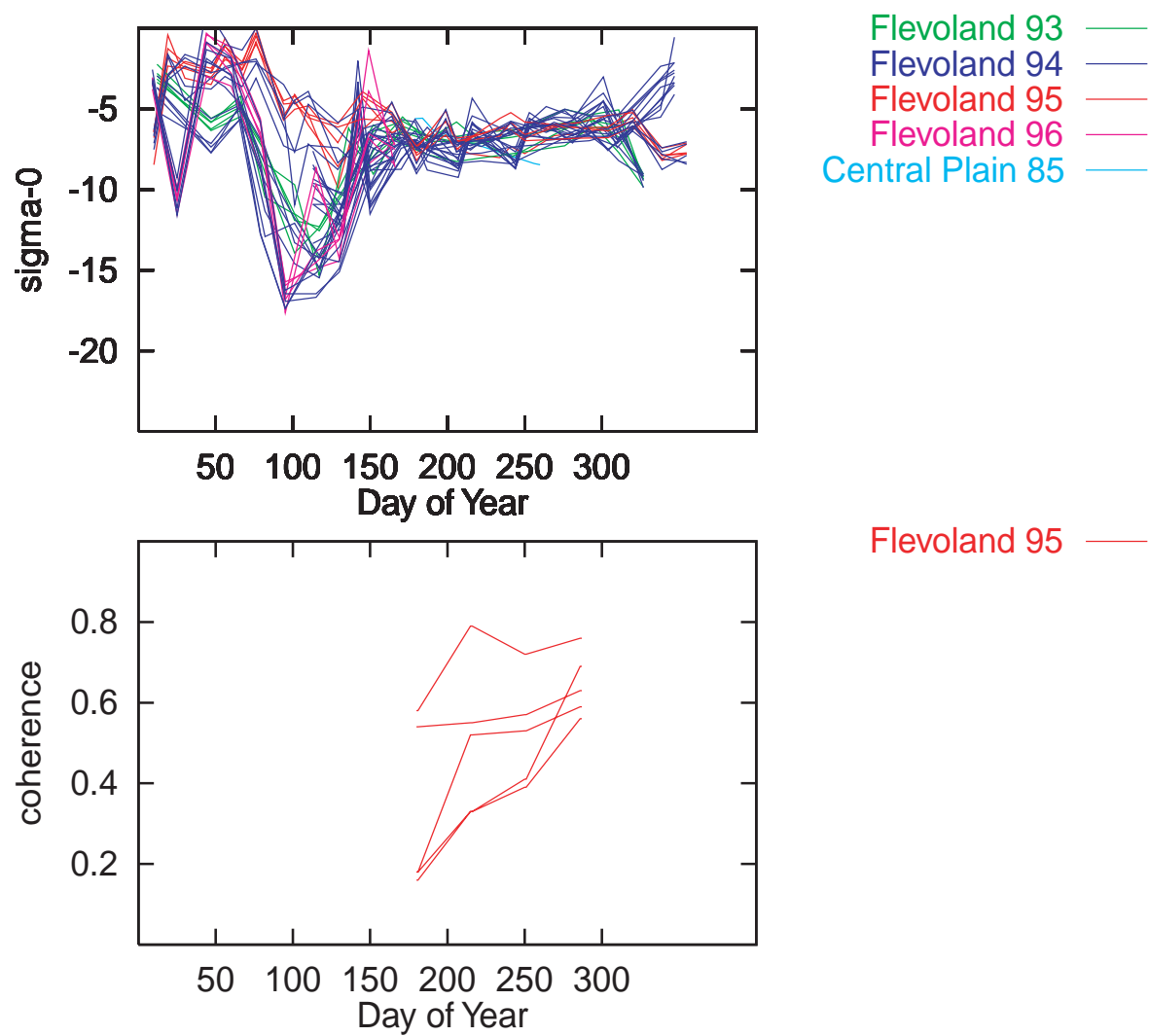


Figure 2.2: Multitemporal patterns of backscattering coefficient (top) and degree of coherence (bottom) for sugar beet fields.

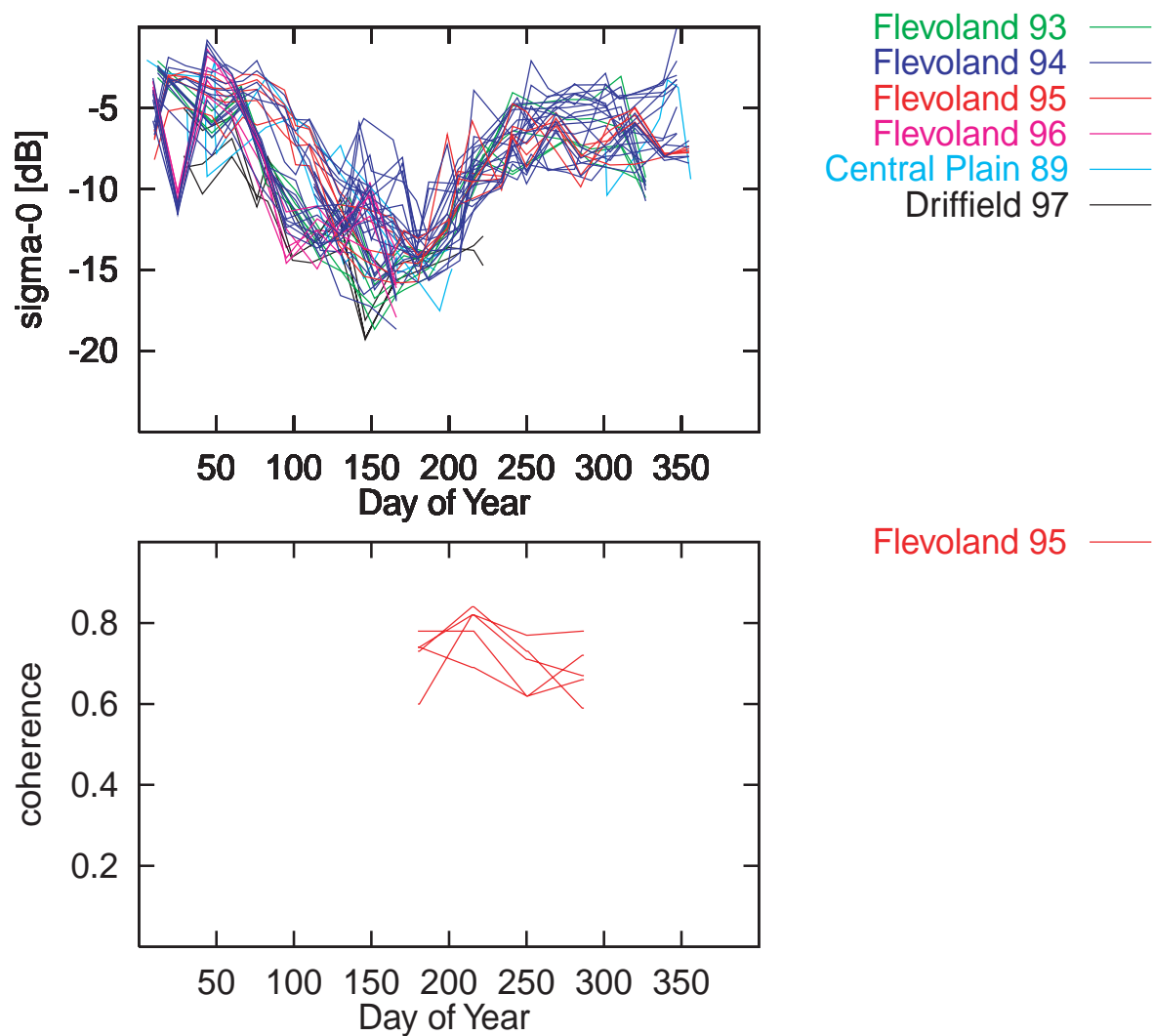


Figure 2.3: Multitemporal patterns of backscattering coefficient (top) and degree of coherence (bottom) for wheat fields.

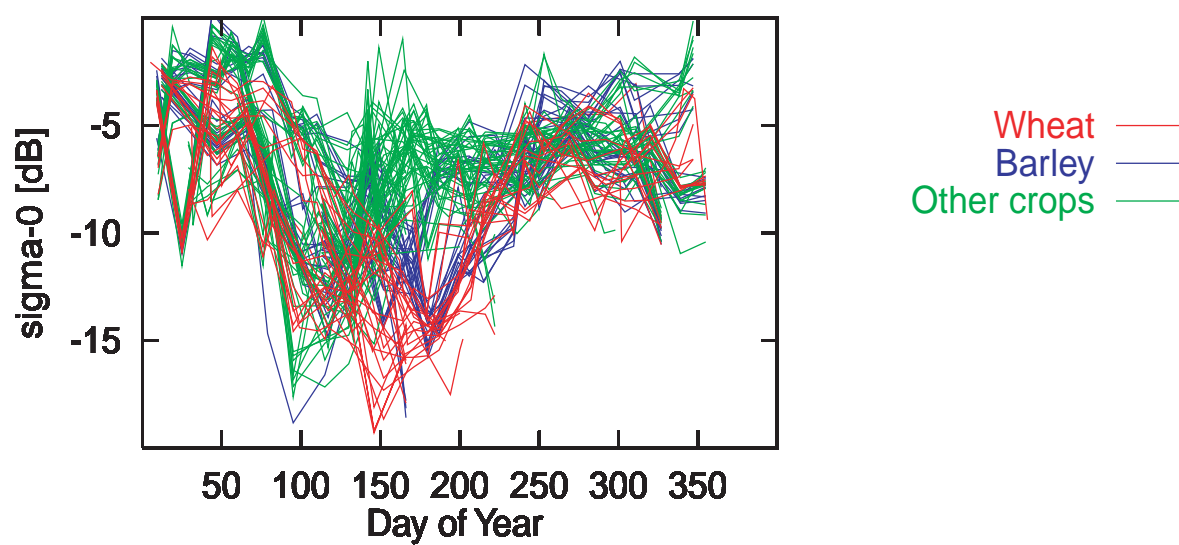


Figure 2.4: Multitemporal patterns of backscattering coefficient for wheat and barley fields as compared with other crop types.

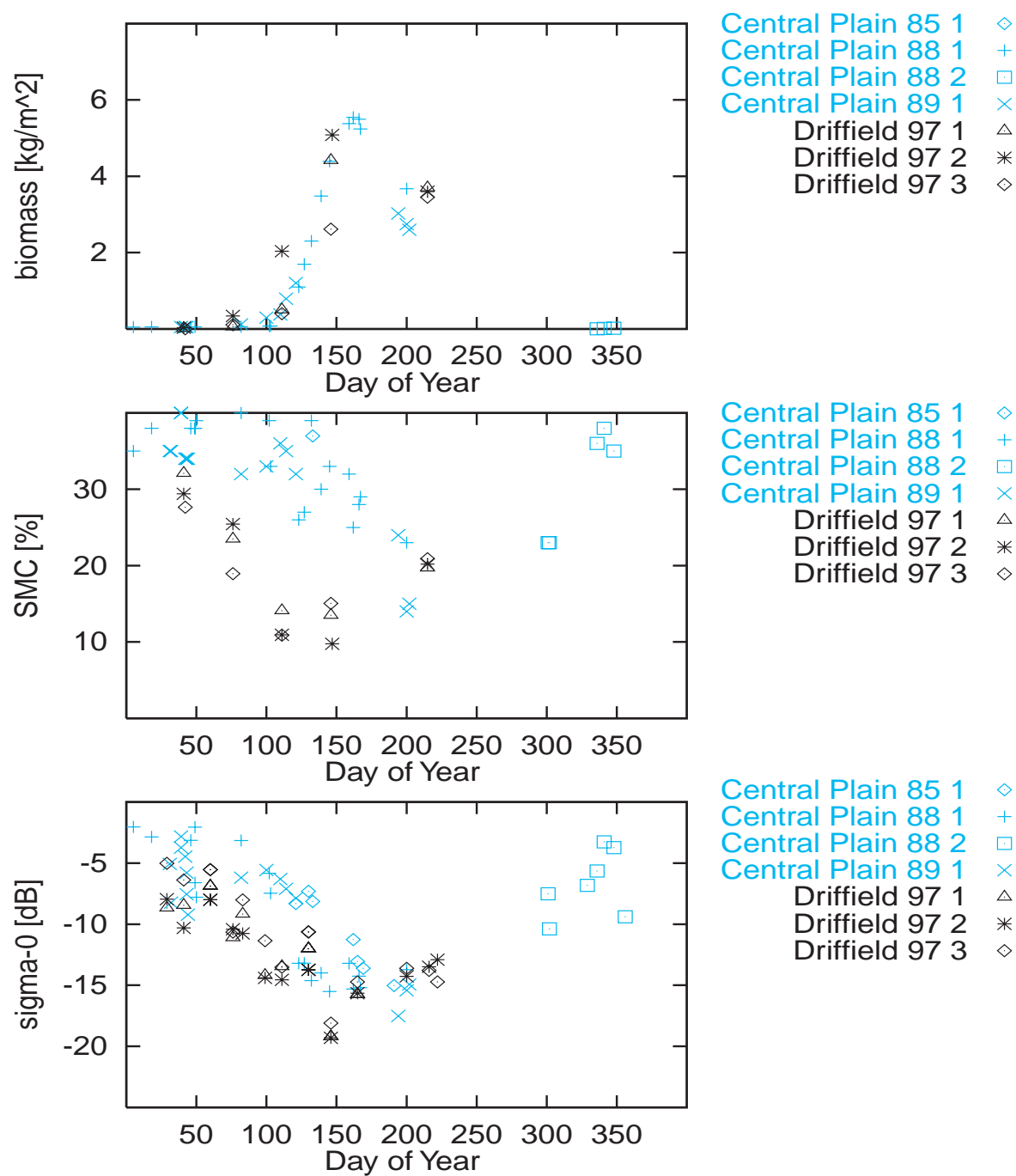


Figure 2.5: Backscattering coefficient of wheat fields (bottom), together with corresponding fresh biomass (top) and soil moisture content (middle) as functions of time.

### Multifrequency polarimetric patterns

A comparison between multifrequency AirSAR patterns measured over different surface types (with or without vegetation) is shown in Figures 2.6 for  $\sigma_{hh}^0$ , 2.7 for  $\sigma_{hv}^0$ , and 2.8 for  $\sigma_{vv}^0$ .

Forest, potato, wide leaf (i.e., potato, maize, sugar beet and sunflower), wheat, and bare soil signatures collected at Barrax, Flevoland and Montespertoli have been included. Wide leaf fields have been subdivided into “early stage” (plant water content  $\lesssim 1 \text{ kg}\cdot\text{m}^{-2}$ ) and “developed” (plant water content  $\gtrsim 1 \text{ kg}\cdot\text{m}^{-2}$ ). Bare soil fields have been subdivided between “smooth” ( $\sigma_z \lesssim 1.5 \text{ cm}$ ) and “rough” ( $\sigma_z \gtrsim 1.5 \text{ cm}$ ). The figures confirm several conclusions about vegetation signatures available in the literature, but may also expand our understanding of the subject. The largest contrast among different categories is observed at  $hv$  polarization (Figure 2.7) due to the lower soil contribution. The trends shown in Figure 2.7 may be related to some typical dimensions of the vegetation elements. For forests, where a wide range of dimensions are present (trunks, large branches, small branches, twigs, leaves) the trends are rather flat. Developed wide leaf canopies show low values at P-band, while backscatter due to stems, leaves and petioles is appreciable at L-band. This effect is more enhanced in potato fields. For early stage and wheat crops (small elements) a more evident increase is observed between L- and C-band. Signatures of bare soils at  $hv$  polarisation are lower than the ones of the crops. However, roughness effects are evident. At  $hh$  and  $vv$  polarization (Figures 2.6 and 2.8) we observe a lower contrast, a reduced difference between crops and bare soils, and some peaks probably due to double bounces. The effect of this mechanism is widely influenced by variations in stem density and stem dimensions, especially at  $vv$  polarization.

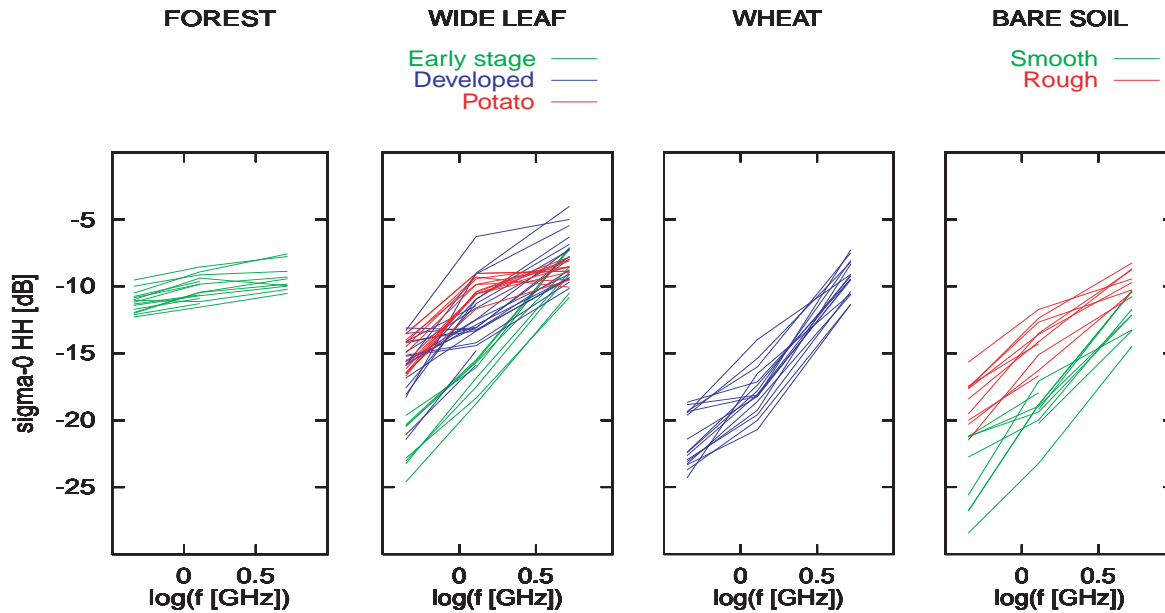


Figure 2.6: Backscattering coefficient at  $hh$  polarisation as a function of frequency for different types of surface.

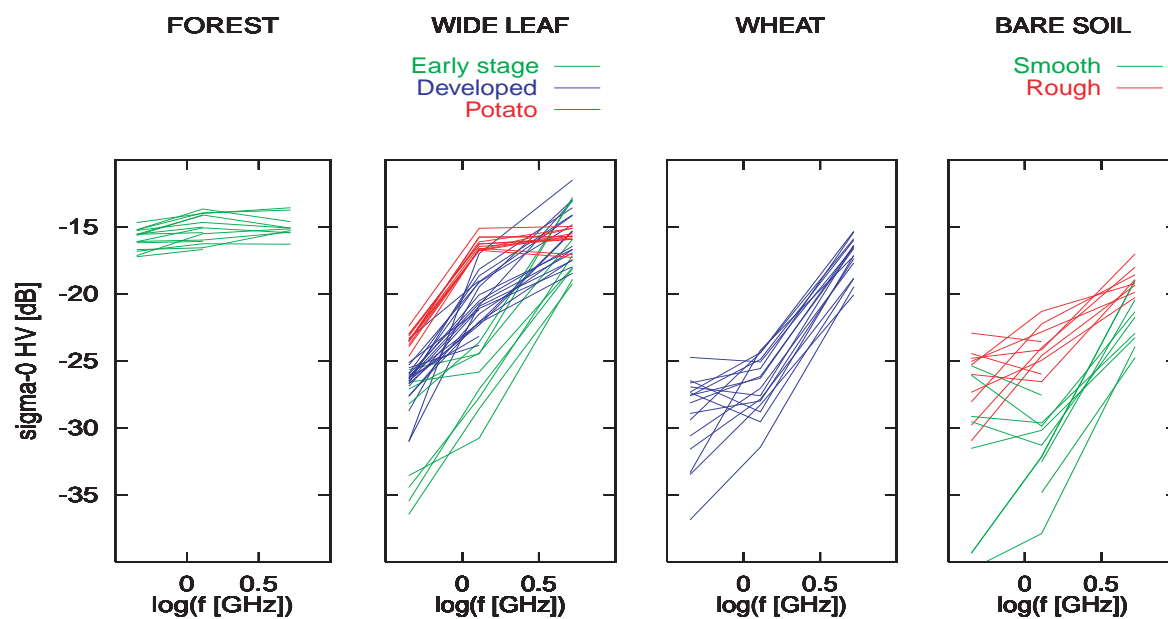


Figure 2.7: Cross-polarised backscattering coefficient  $\sigma_{hv}^0$  as a function of frequency for different types of surface.

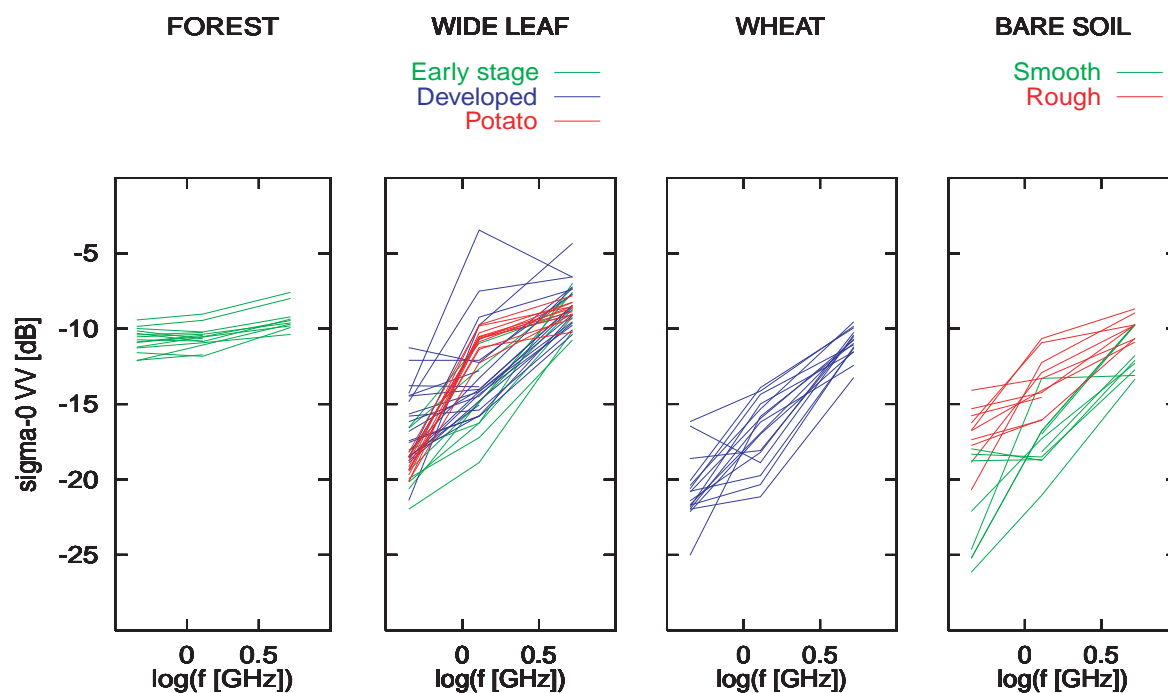


Figure 2.8: Backscattering coefficient at  $vv$  polarisation as a function of frequency for different types of surface.

### Multifrequency, multipolarization and multiangle patterns

The data library includes microwave parameters measured with the ground-based radiometer-scatterometer RASAM for fully grown wheat, corn, sugar beet, potato and rape, grass, and bare soil. The microwave parameters are available for many fields of each of these surface categories. Besides the mean values, the standard deviation of each parameter is included, since the fluctuations can be useful indicators of the state of the surface, e.g., of strong changes in soil moisture.

The following figures, Figs. 2.9–2.14, report selected examples of backscattering coefficients (here  $\gamma = \sigma^0 / \cos \theta$ ), at various polarizations as functions of frequency for different angles of incidence.

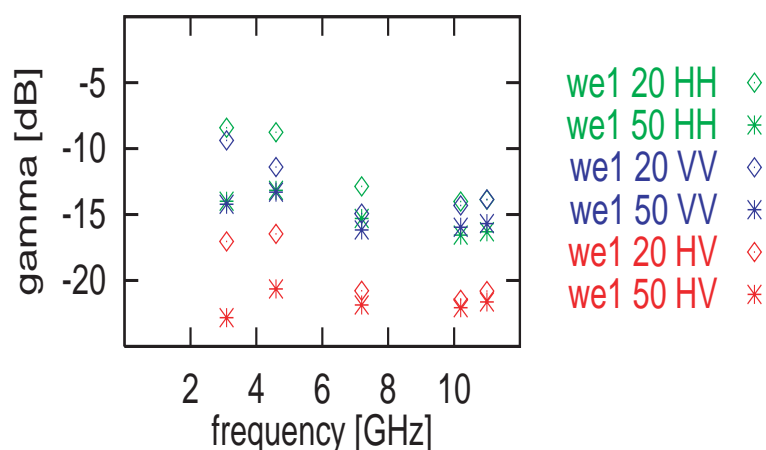


Figure 2.9: Frequency trend of wheat mean (26 measurements) signature  $\gamma = \sigma^0 / \cos \theta$ . Typical vegetation parameters are: vegetation height, 100 cm; plant density, 730 plants·m<sup>-2</sup>; wet biomass, 6–7 kg·m<sup>-2</sup>; dry matter fraction, 0.2–0.35.

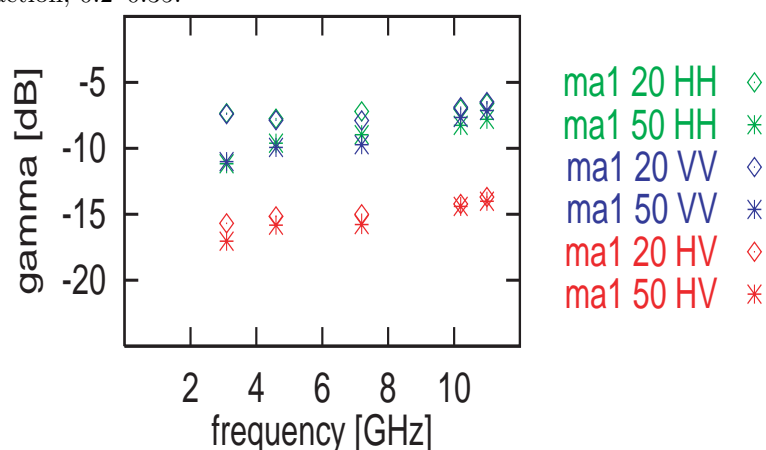


Figure 2.10: Frequency trend of corn mean (30 measurements) signature  $\gamma = \sigma^0 / \cos \theta$ . Typical vegetation parameters are: vegetation height, 220 cm; plant density, 7.2 plants·m<sup>-2</sup>; wet biomass, 6–8 kg·m<sup>-2</sup>; dry matter fraction, 0.17–0.40; leaf thickness, 0.22 mm.

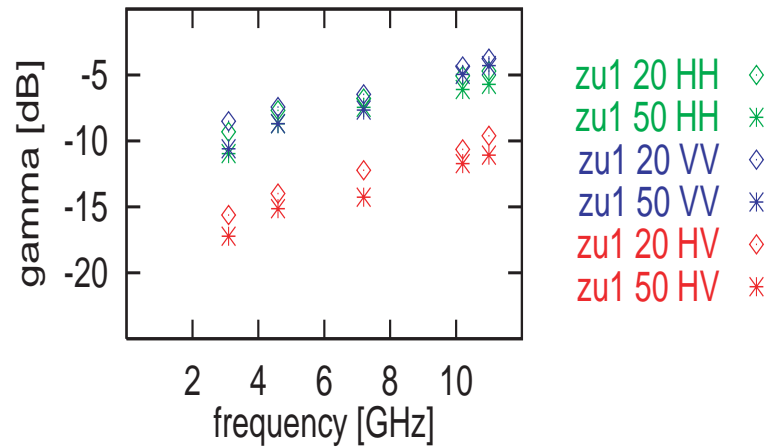


Figure 2.11: Frequency trend of sugar beet mean (15 measurements) signature  $gamma = \sigma^0 / \cos \theta$ . Typical vegetation parameters are: vegetation height, 45 cm; plant density,  $6.4 \text{ plants}\cdot\text{m}^{-2}$ ; wet biomass (without beet),  $4.6 \text{ kg}\cdot\text{m}^{-2}$ ; dry matter fraction, 0.14–0.20; leaf thickness, 0.25–0.35 mm.

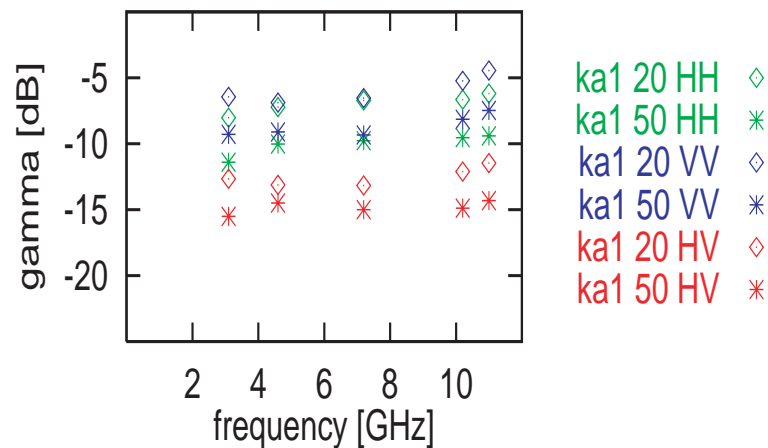


Figure 2.12: Frequency trend of potato mean (29 measurements) signature  $gamma = \sigma^0 / \cos \theta$ . Typical vegetation parameters are: vegetation height, 28–45 cm; plant density,  $3\text{--}4.5 \text{ plants}\cdot\text{m}^{-2}$ ; wet biomass (without root),  $1.1 \text{ kg}\cdot\text{m}^{-2}$ ; dry matter fraction, 0.10–0.18; leaf thickness: 0.25 mm.

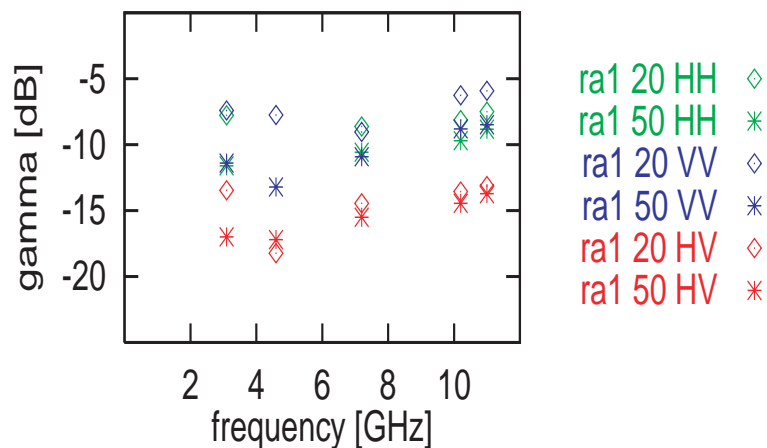


Figure 2.13: Frequency trend of rape mean (9 measurements) signature  $gamma = \sigma^0 / \cos \theta$ . Typical vegetation parameters are: vegetation height, 120–140 cm; plant density, 68 plants·m<sup>-2</sup>; wet biomass, 4.2 kg·m<sup>-2</sup>; dry matter fraction, 0.13–0.30.

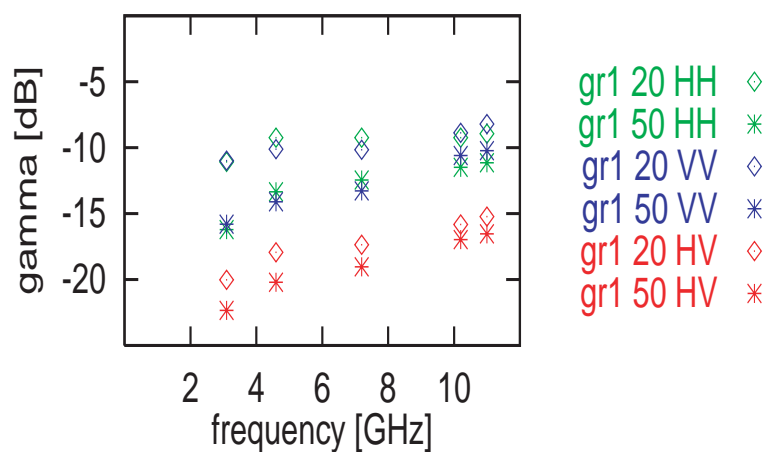


Figure 2.14: Frequency trend of grass mean (13 measurements) signature  $gamma = \sigma^0 / \cos \theta$ . Typical vegetation parameters are: vegetation height, 20–70 cm; wet biomass, 1–3 kg·m<sup>-2</sup>; dry matter fraction, 0.15–0.25.

The microwave parameters of a bare soil with surface aggregates look similar to those of vegetation, especially if the soil is dry (Fig. 2.15), since the aggregates act as volume scatterers. From our data we find that bare soil with aggregates and vegetation can best be distinguished by the ratio  $\sigma_{hv}^0/\sigma_{vv}^0$ , for frequencies below 5 GHz and incidence angles between  $30^\circ$  and  $50^\circ$ . For suitable comparison the frequency trend of signatures of smooth bare soil after heavy rain is shown in Fig. 2.16.

Data from further fields in particular conditions are also present in the data base. In particular, there are interesting measurements on crops in their mature stage, i.e., close to harvest. The following figures, Figs. 2.17–2.21, report selected examples of backscattering coefficients at various polarizations as functions of frequency for different angles of incidence.

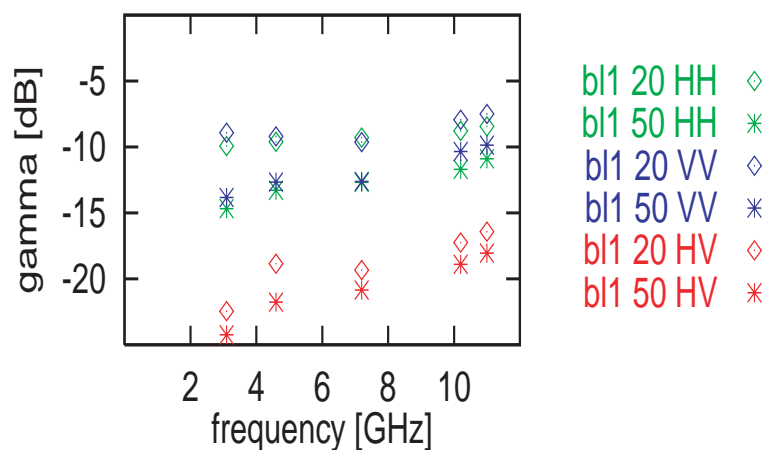


Figure 2.15: Mean (15 measurements) frequency trend of signatures of bare (rough) soil with surface aggregates, as is usual after mechanical cultivation. Typical soils parameters are: volumetric soil moisture, 0.1–0.3; r.m.s. surface height, 1.0–1.6 cm; correlation length, 3.0–4.5 cm (for an exponential model). Here  $gamma = \sigma^0 / \cos \theta$ .

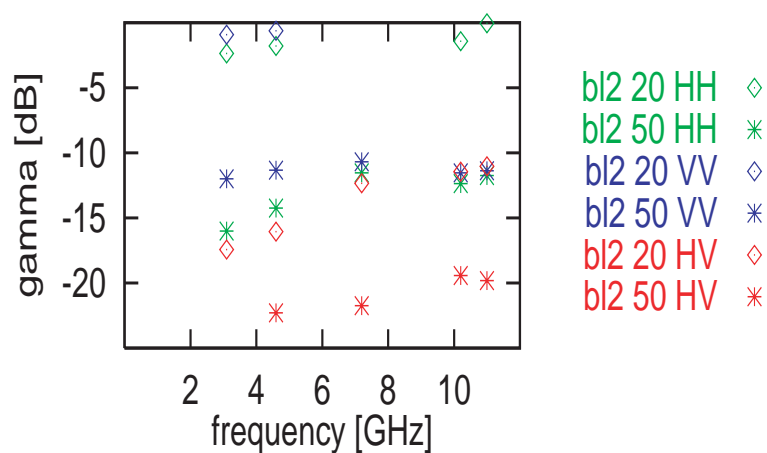


Figure 2.16: Frequency trend of bare (smooth) soil mean signature  $gamma = \sigma^0 / \cos \theta$ . Typical soils parameters are: volumetric soil moisture, 0.33; r.m.s. surface height, 0.87 cm; correlation length, 3.81 cm (for an exponential model).

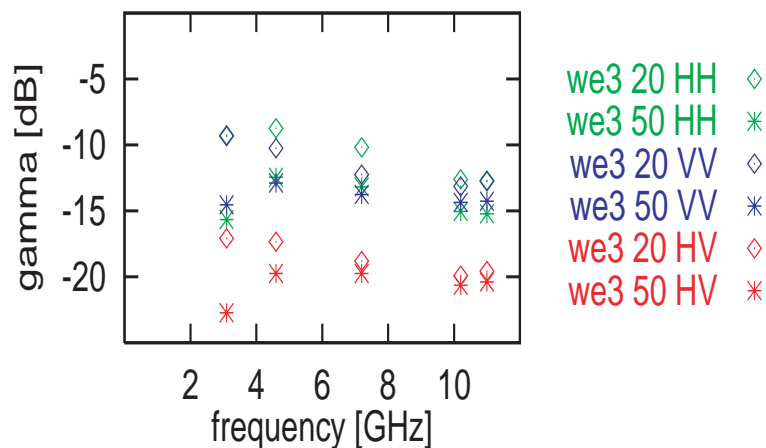


Figure 2.17: Frequency trend of (preharvest) wheat mean (8 measurements) signature  $gamma = \sigma^0 / \cos \theta$ . Typical vegetation parameters are: vegetation height, 100 cm; plant density, 730 plants $\cdot$ m $^{-2}$ ; wet biomass, 6 kg $\cdot$ m $^{-2}$ ; dry matter fraction, 0.40 (total plant), 0.55 (ears).

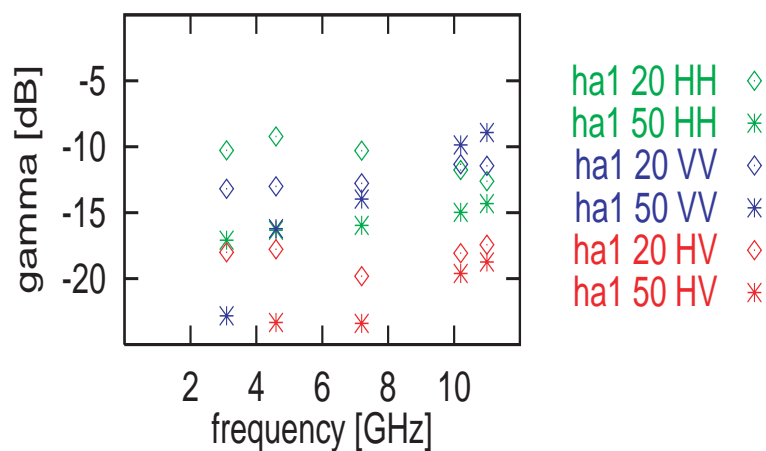


Figure 2.18: Frequency trend of (preharvest) oat signature  $gamma = \sigma^0 / \cos \theta$ . Typical vegetation parameters are: vegetation height, 100 cm; plant density, 400 plants $\cdot$ m $^{-2}$ ; wet biomass, 3.4 kg $\cdot$ m $^{-2}$ ; dry matter fraction, 0.45; volumetric soil moisture (0-5cm), 0.11.

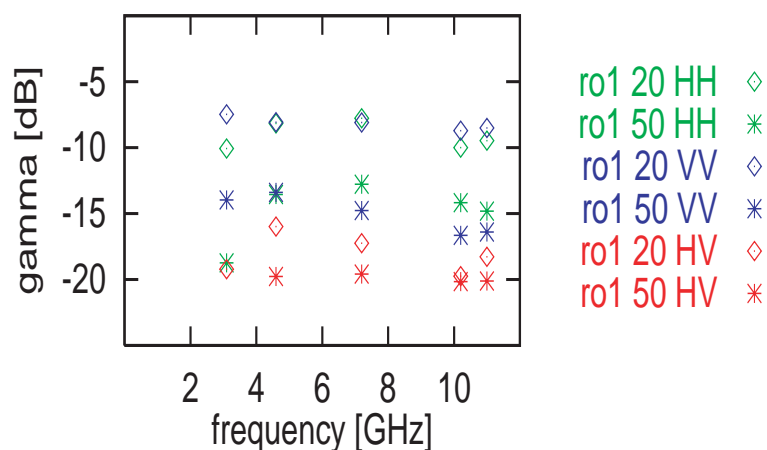


Figure 2.19: Frequency trend of (preharvest) rye mean (2 measurements) signature  $\gamma = \sigma^0 / \cos \theta$ . Typical vegetation parameters are: vegetation height, 140 cm; wet biomass, about  $2.5 \text{ kg}\cdot\text{m}^{-2}$ ; dry matter fraction, 0.71 (total plant).

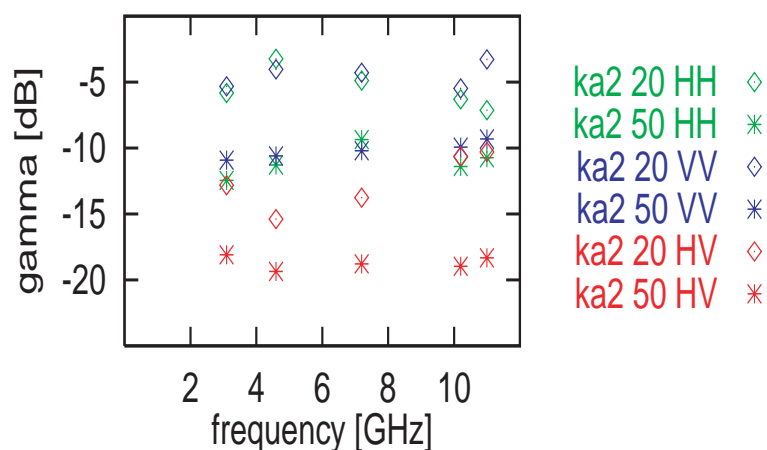


Figure 2.20: Frequency trend of (preharvest) potato mean (8 measurements) signature  $\gamma = \sigma^0 / \cos \theta$ . Typical vegetation parameters are: vegetation height, 0 cm; plant density,  $4 \text{ plants}\cdot\text{m}^{-2}$ ; wet biomass (dead leaves)  $0.26 \text{ kg}\cdot\text{m}^{-2}$ ; dry matter fraction, 0.86; volumetric soil moisture (0-5cm), 0.22.

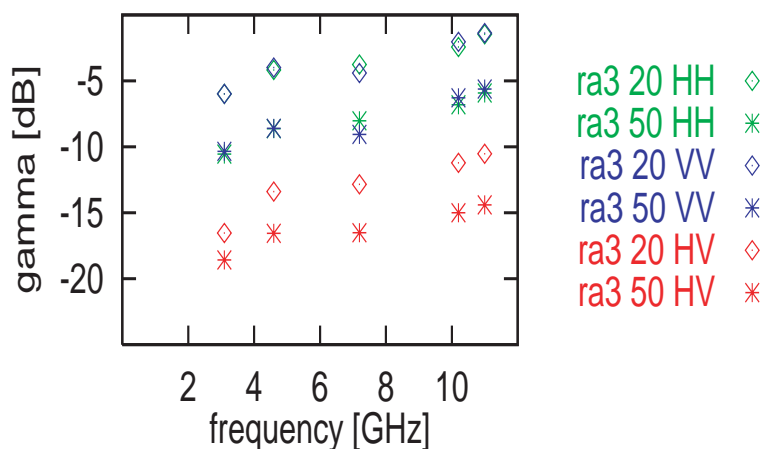


Figure 2.21: Frequency trend of (winter unfrozen) rape mean (6 measurements) signature  $\gamma = \sigma^0 / \cos \theta$ . Typical vegetation parameters are: vegetation height, 15 cm; plant density, 68 plants  $\cdot m^{-2}$ ; wet biomass, 1.0  $kg \cdot m^{-2}$ ; dry matter fraction, 0.12; volumetric soil moisture (0-5cm), 0.30–0.38. Air temperature,  $> 3^\circ C$ .

Another interesting feature is the behaviour of  $\sigma^0$  at high incidence angles, which have demonstrated their usefulness in crop discrimination. A comparison among the different frequency trends is shown in Figs. 2.22 ( $vv$  polarization) and 2.23 ( $hv$  polarization) for an incidence angle of  $50^\circ$ .

The diagrams presented in this section are just a few suggestive samples from the data stored in the ERA-ORA Data Distributed Library. Many other interesting features can be appreciated by combining measurements contributed by different groups.

### Radar and optical/IR signatures

Assembling radar and optical data is another attractive attribute of the ERA-ORA D.D.L.

As an example, Fig. 2.24 compares radar and optical signatures collected at Barrax (14 and 15 July 1991) and Montespertoli (29 June and 1 July 1991) over wide leaf (maize and sunflower), wheat and dry barley fields. In particular,  $\sigma_{hv}^0$  multifrequency patterns and optical reflectance spectra are plotted. It is seen that the three vegetation categories are well discriminated by the microwave patterns. Dry barley fields are markedly discriminated also by the optical spectra, which show a typical dry-vegetation behaviour. Wide leaf trends are in general agreement with each other and show an evident “step” between visible and near-infrared wavelengths. However, the behaviour of TMS wheat reflectances is not easy to be interpreted and needs further investigations.

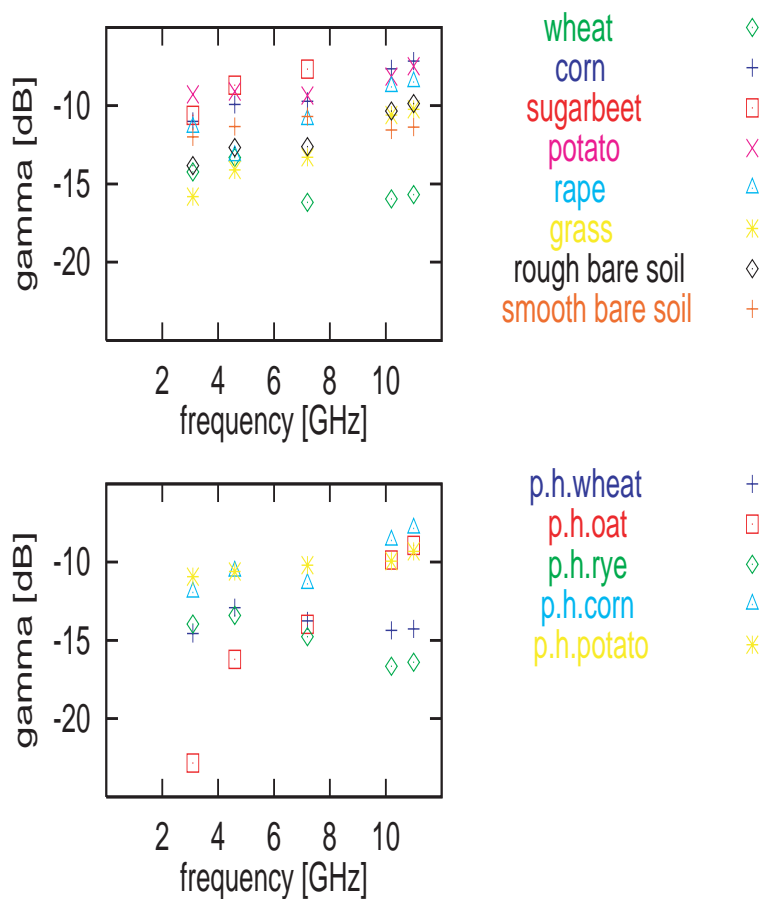


Figure 2.22: Comparison among frequency trends at 50°, *vv* polarization.

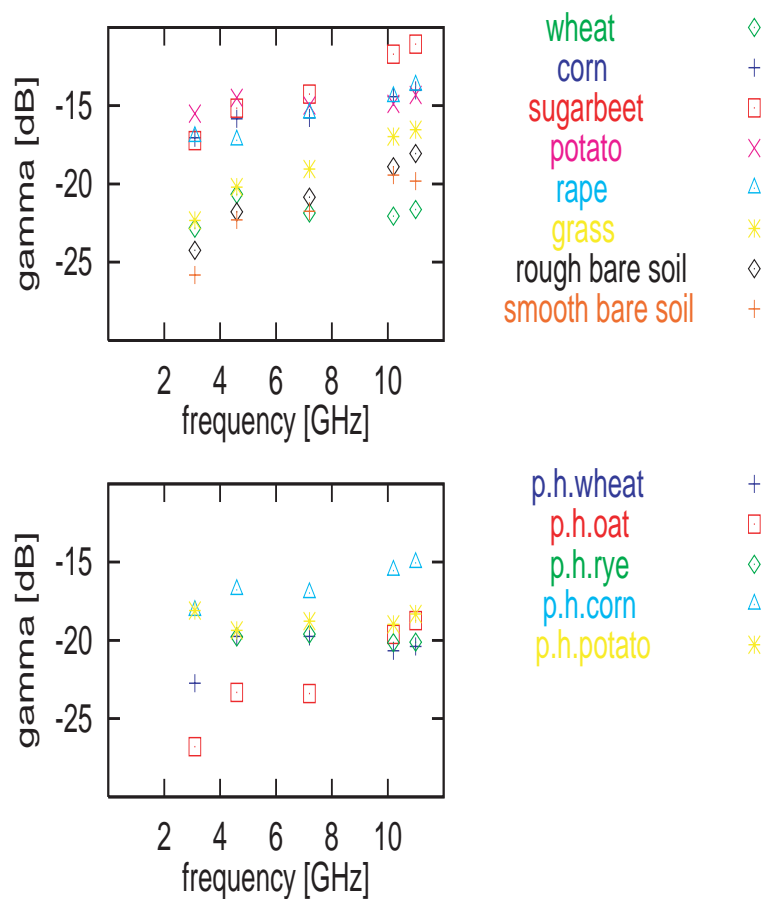


Figure 2.23: Comparison among frequency trends at  $50^\circ$ ,  $hv$  polarization.

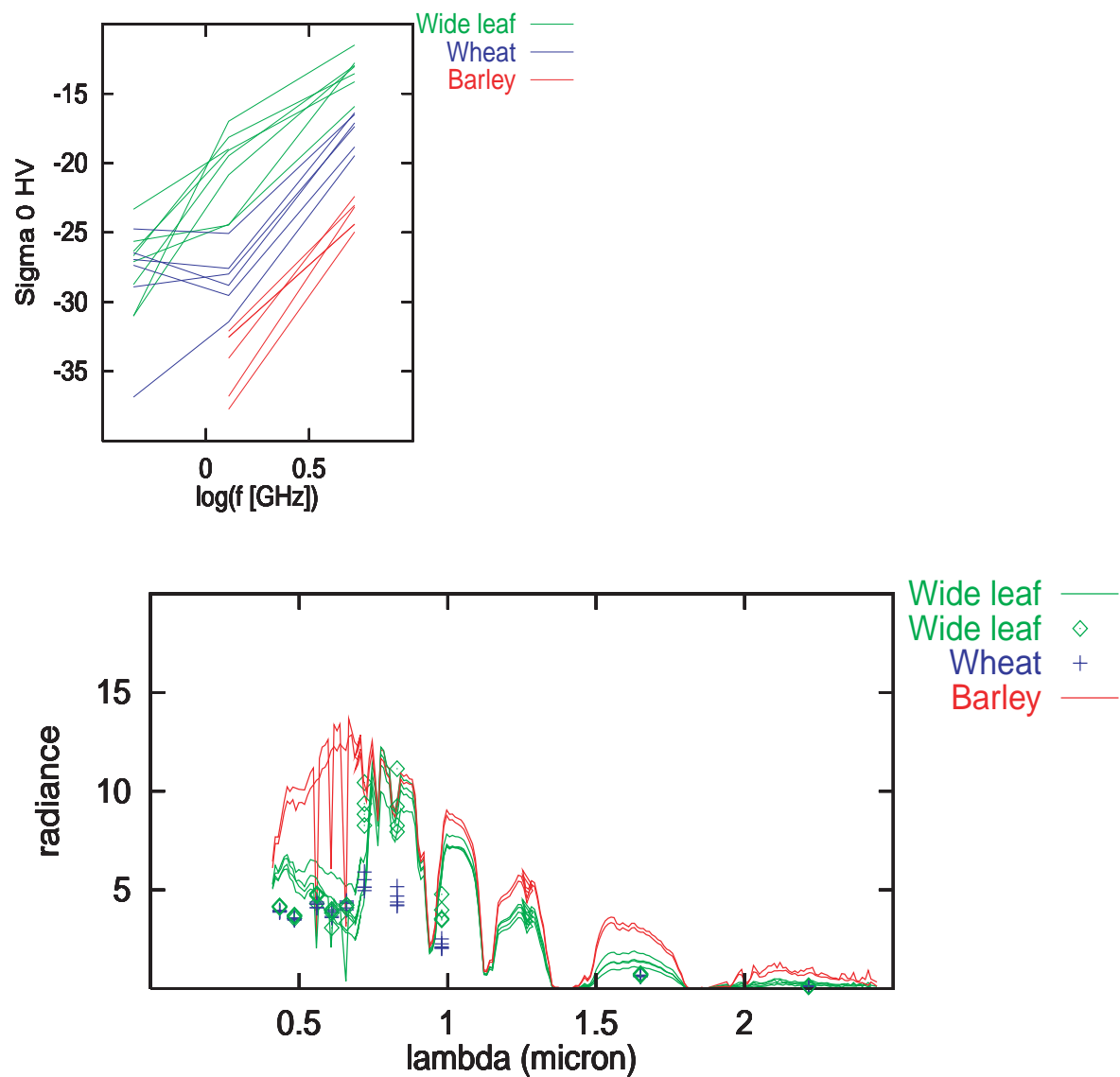


Figure 2.24: Cross-polarised backscattering coefficient vs. frequency and optical/IR radiance vs. wavelength for different crop types.



# Bibliography

- [1] H. Laur, P. Meadows, J.I. Sanchez, and E. Dwyer, ERS-1 SAR Radiometric Calibration, *Proceedings of the CEOS SAR Calibration Workshop*, ESA WPP-048, Sept. 1993.



## Chapter 3

# Data Analysis and Synergy (WP 201)

### 3.1 Objectives

This chapter reports selected results of the data analysis carried out by the Working Party on Synergy (WP 201), based on the ERA-ORA D.D.L., mainly aimed at investigating possible synergy among various kinds of data, i.e., complementarity of multitemporal, multifrequency and multipolarization radar and optical/IR data.

In particular, ERS and AirSAR signatures collected in different sites are compared in order to understand the information they contain about crops. A specific study of the wide AirSAR data set provided by UAW on the Flevoland site in 1991 is summarized. Then the multitemporal signatures collected in Switzerland by the RASAM scatterometer are discussed, because of their synergistic potential. The role of optical reflectances in conjunction with backscattering coefficients is also overviewed.

Although the chapter is focused on agricultural applications, the potential of snow cover radar signatures is also discussed.

### 3.2 Introduction

The potential of SAR in agricultural applications has been demonstrated in several studies [1]-[8]. The main objectives of the investigations fall into the following application fields:

- to classify different crop species,
- to monitor the seasonal cycle of growth of any single crop,
- to identify anomalous behaviours.

Reliable remote sensing applications may be proposed once  $\sigma^\circ$  (or other measured electromagnetic parameters such as the degree of coherence) are demonstrated to be sensitive to variables such as:

- typical geometrical characteristics of single crops (for classification);

- dimensions and orientation of crop elements (for monitoring);
- plant permittivity.

In spite of several efforts, classification and monitoring techniques are still limited, since, in several cases, variations of plant parameters are observed to produce minor effects on  $\sigma^\circ$ . In order to overcome this problem, sensor parameters (i.e., frequency, incidence angle, polarization) have to be carefully optimized to achieve adequate sensitivity. However, other severe problems stem from the effects of simultaneous variations of several soil and plant parameters, which makes it difficult to identify the causes of  $\sigma^\circ$  variations. As an example, the crop growth process occurring in springtime is generally simultaneous with drying out of the soil. Both processes produce  $\sigma^\circ$  variations, making it difficult to single out the causes of the observed effects. In order to overcome the above mentioned limits, which could prevent operational use of microwave remote sensing, synergy among various data sources should be exploited. First of all, SAR could operate in multifrequency and/or multipolarization and/or multiangle configuration. Classification and monitoring potentials are, in this way, improved with respect to single configuration observations. Other benefits may be attained by repeated overpasses over single fields (multitemporal techniques). Finally, further advantages may be offered by joining  $\sigma^\circ$  measurements with coherence data and/or simultaneous observations with optical instruments.

### 3.2.1 The role of the ERA-ORA D.D.L.

The ERA-ORA Data Distributed Library appears suitable to investigate the potential of synergy in remote sensing applications, since it contains data collected by different instruments in different situations.

- Several multitemporal ERS SAR signatures are available, covering growth cycles of various crop types. Observations took place in several sites and, in some cases, were repeated in different years. Sometimes, amplitude data are accompanied by coherence data.
- In some sites, fields were observed by the AirSAR, i.e., a 3-frequency, fully polarimetric instrument. Some observations are partially multitemporal. In the Spanish and Italian sites, SAR data are accompanied by a set of optical measurements.
- The Swiss Central Plain site was observed by the RASAM scatterometer, operating at 5 frequencies, 4 polarizations ( $hh$ ,  $vv$ ,  $hv$ ,  $vh$ ) and several angles of incidence. For some fields, RASAM signatures are available on different dates, covering the seasonal development of agricultural crops.

The availability of such a wide data library allows one to investigate various kinds of synergy, i.e. multifrequency, multipolarization, multitemporal and multisensor (e.g., joining SAR observations with optical observations), and, in particular, how additional channels in terms of frequency, incidence angle and polarization may improve the discrimination of agricultural crops and the study of their developments.

The obtained results are just examples, which are also intended for suggesting further applications of the D.D.L..

## 3.3 On the information content of data

Both multitemporal and multifrequency/multipolarization techniques may provide useful information. As an example, the signatures of 3 crops, potato, sugarbeet, and wheat, are here considered. Several

sample fields of these crops have been observed in some ERA-ORA sites. Fig. 3.1 compares multitemporal ERS trends collected over many different fields and in different sites and years. In the upper part of the figure, 3 different codes are associated with different crop types, while in the lower part, codes are sites and/or years. The forthcoming observations apply.

- During vegetation development, i.e. from Day of Year  $\sim 150$  to Day of Year  $\sim 200$ ,  $\sigma^\circ$ 's of wheat fields are clearly lower than  $\sigma^\circ$ 's of potato and sugarbeet fields. This behaviour may be explained by the differences in crop geometry: wheat vertical elements, such as ears and thin stems, produce enhanced absorption at C-band.
- In the other periods of the year, when soil scattering dominates,  $\sigma^\circ$  variations are mainly due to soil conditions (moisture effects, essentially). As a consequence, small differences are observed among samples belonging to the same site/year, while site-to-site or year-to-year variations may be large.

Fig. 3.1 indicates that a single-frequency, single-polarization radar, such as ERS SAR, may be useful for classification, provided multitemporal data are used. Also crop monitoring could be accomplished, provided a-priori information about soil conditions is available.

These same 3 crops have been considered in Fig.3.2, where multifrequency polarimetric AirSAR observations are compared. In particular, reference has been made to the  $hv$  polarization, which has been demonstrated to be powerful for vegetation. The figure shows C-band  $\sigma^\circ$ 's vs. L band  $\sigma^\circ$ 's. The same coding as in Figure 1 is adopted for upper and lower plots. The upper plots indicate that there is a reasonable potential for classification. It is interesting to note that plots agree well with some previous studies carried out over limited data sets. The lower plots indicate that data are reliable, since no apparent site effects are noted.

In general, the upper plots of Figs. 3.1 and 3.2 show that both multitemporal and multifrequency polarimetric data have a good information content, with the potential of yielding useful results after suitable classification or retrieval algorithms are applied. Moreover, the lower plots indicate that site and/or year effects are evident over bare soils, mainly due to moisture variations, while they are low for developed crops. Among other things, this observation indicates a general reliability of the ERA-ORA data library.

### 3.4 Synergy studies in agriculture based on AirSAR data

The results of the previous Section indicate that both multitemporal and multifrequency/multipolarization data sets are useful for agricultural applications. Moreover, ERA-ORA data collected in different sites/years appear to be consistent.

In order to carry out a specific and quantitative investigation, we have taken the wide data set of the AirSAR signatures collected at the Flevoland site in 1991. This data set is suitable to investigate radar classification capability and synergy among multi-parameter techniques, since signatures span 3 frequencies, are fully polarimetric and cover more than 350 fields with 9 vegetation species. Moreover, data are partially multitemporal, since the site was overflowed four times in summer.

In order to simplify the application of the algorithms, a limited data subset, including fields observed all 4 times and within a limited incidence angle range ( $50^\circ$ - $55^\circ$ ), has been selected. Seven crop types have been considered, i.e., wheat, sugarbeet, rape, potato, grass, corn and barley.

The study is subdivided into two parts. First of all, multitemporal patterns are plotted for several polarizations at L- and C-band. The main crop features are identified and interpreted by means of previous

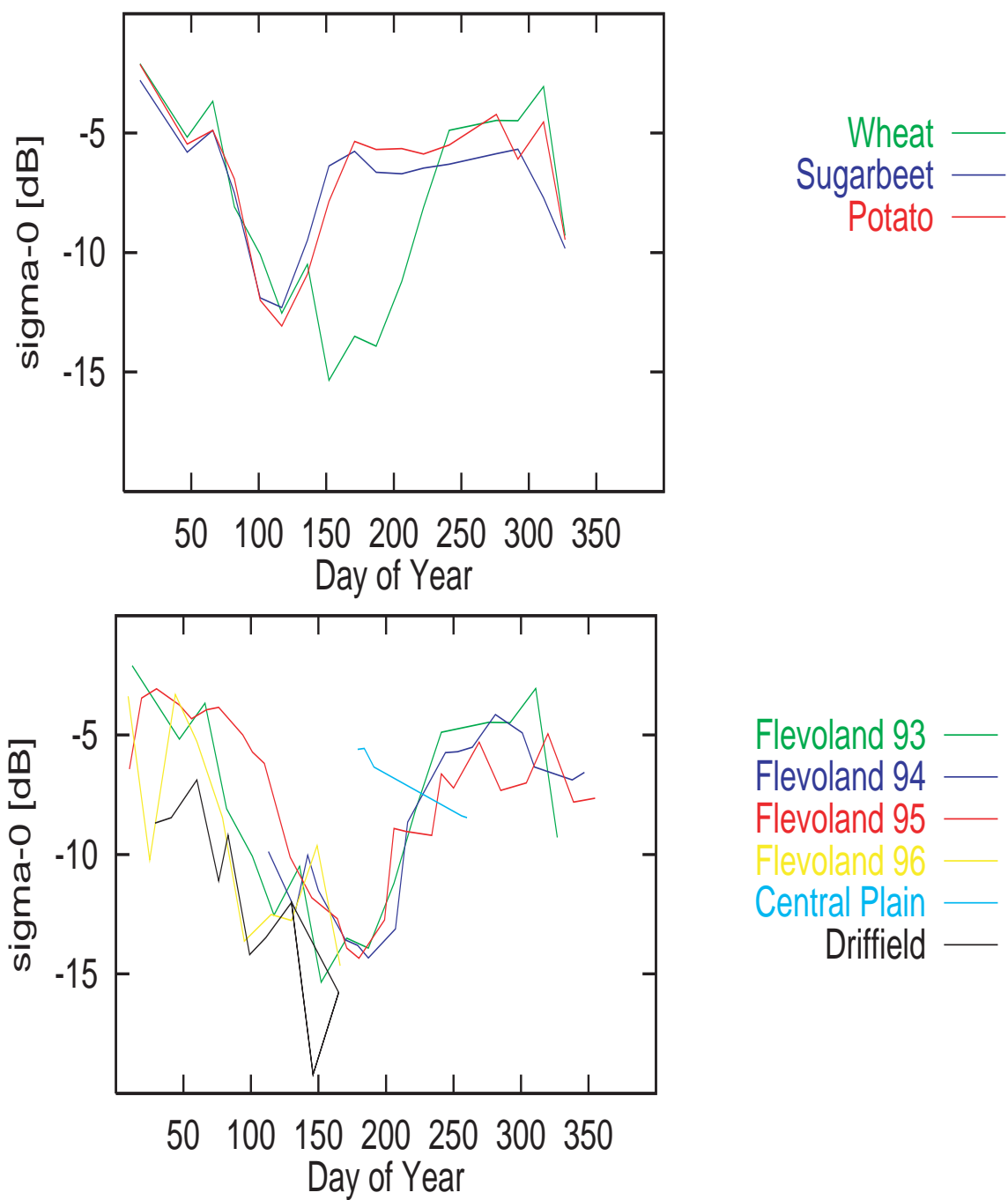
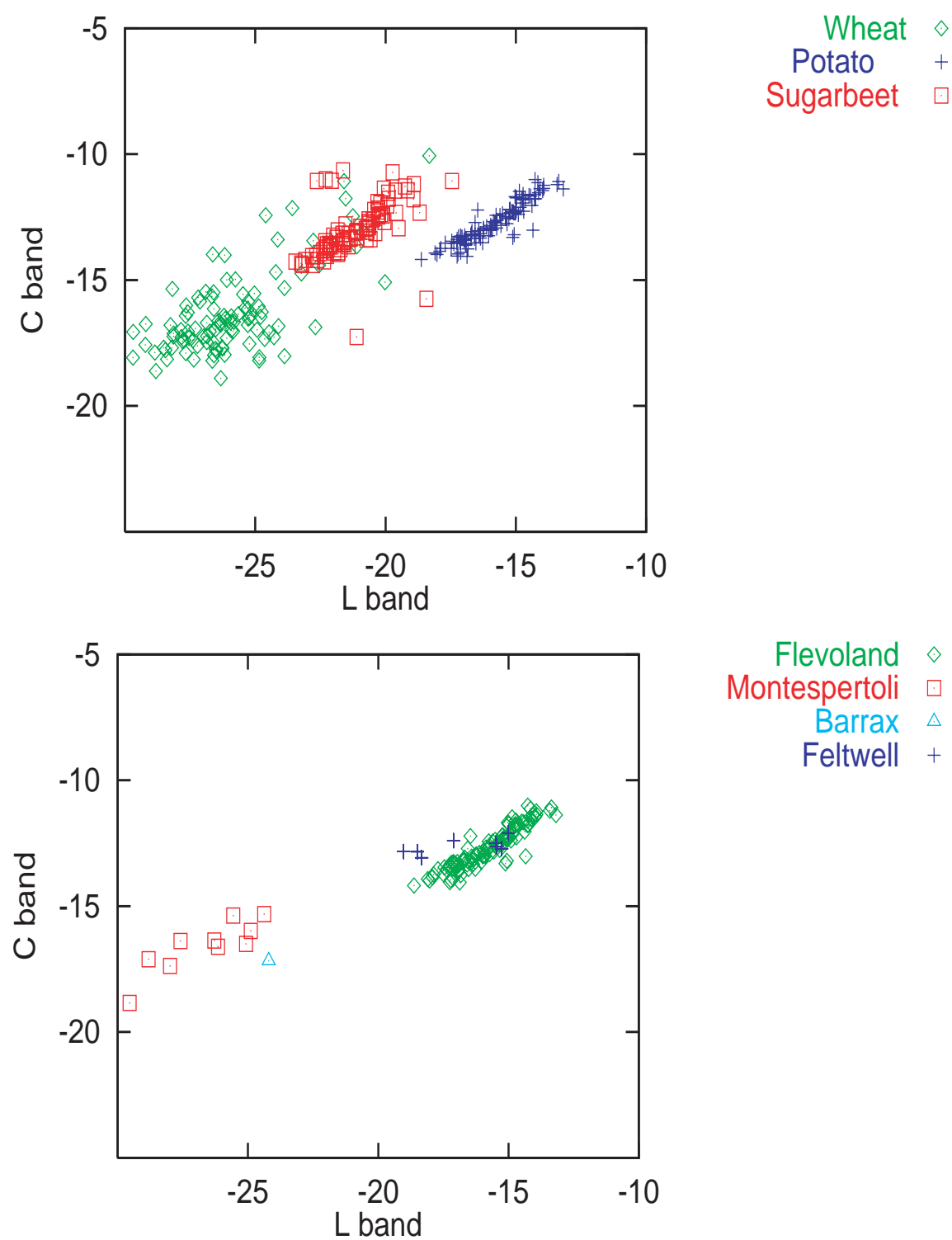


Figure 3.1: Examples of ERS SAR multitemporal signatures.

Figure 3.2: Examples of AirSAR C-band  $\sigma_{hv}^0$ 's vs. L band  $\sigma_{hv}^0$ 's.

experience, based also on the understanding of electromagnetic interaction mechanisms. The second step is strictly quantitative: a neural network classification algorithm is applied to the 7 crop species. Results are shown and the improvement attained by a synergistic use of multipolarization and/or multitemporal techniques is discussed.

### 3.4.1 Crop discrimination: qualitative data analysis.

Some important polarimetric features have been selected, also based on previous experience, and multitemporal patterns at L- and C-band have been plotted.

Fig. 3.3 shows the trends of absolute  $\sigma_{hv}^{\circ}$ 's. It appears that L-band data are more suitable for discriminating potato from other crops, while C-band allows one to easily identify rape before harvest. Ground data are not sufficiently detailed to explain these features. However, measurements carried out in Switzerland indicate the evidence of larger twigs in potato and smaller twigs (or pods) in rape. These properties, which are typical of the geometries of these crops in every site, may explain the observed features. The lowest  $\sigma_{hv}^{\circ}$ 's are observed for wheat and grass, i.e. vegetation characterized by small vertical elements producing absorption and low crosspolar backscatter. Multitemporal information is particularly important for corn and barley: an evident  $\sigma_{hv}^{\circ}$  increase is observed between the second and the third overpass, for both crops. This is due to plant growth for the case of corn, while it is due to ear bending for barley.

Fig. 3.4 shows the  $\sigma_{hv}^{\circ}/\sigma_{vv}^{\circ}$  ratios. While for most crops no important information is added with respect to Fig. 3.3, this figure is interesting for wheat and sugarbeet, particularly at C-band for the last two overpasses. For wheat, the  $\sigma_{hv}^{\circ}$  values are generally low, but the  $\sigma_{hv}^{\circ}/\sigma_{vv}^{\circ}$  ratio looks useful for discrimination. For sugarbeet, wide leaf scattering produces relatively high  $\sigma_{hv}^{\circ}$ 's, but low  $\sigma_{hv}^{\circ}/\sigma_{vv}^{\circ}$ 's.

Figs. 3.5 and 3.6 show cross-to-copolar ratios at circular and  $45^{\circ}$  linear polarization, respectively. At C-band and for the last overpasses, the lowest values are observed for wide leaf (potato, sugarbeet, corn). Vertical wheat elements produce high cross polarization ratios here, while they were low in  $hv$  (see Fig. 3.4). According to Fig. 3.7, the information content of the  $hh - vv$  correlation coefficient is essentially similar to that of Figs. 3.5 and 3.6.

Selected considerations useful in interpreting the signature trends are summarized in Table 3.1. It may be observed that these results are in agreement with previous ones based on more limited data sets [9].

### 3.4.2 Classification of agricultural surfaces

The Flevoland '91 AirSAR signatures have been used to carry out a classification exercise intended to assess the improvement of accuracy brought by progressively richer (in terms of polarizations and measurement dates) sets of data.

The classification algorithm consists of a neural network with feedforward configuration. The neural network simulator (SNNS) developed at the University of Stuttgart (Germany) [10] provided the basic software for the algorithm implementation. The net consists of a multilayer perceptron with two hidden layers. Training has been pursued by a scaled conjugate gradient (SCG) algorithm. This is a member of the class of conjugate gradient methods, general purpose second order techniques that help to minimize goal functions of several variables. Second order indicates that such methods use the second derivatives of the error function, while a first-order technique, like standard backpropagation, only uses the first derivatives. For the purpose of classification, the values of the output nodes were coded in binary form and the class selection has been made according to a winner-and-take approach.

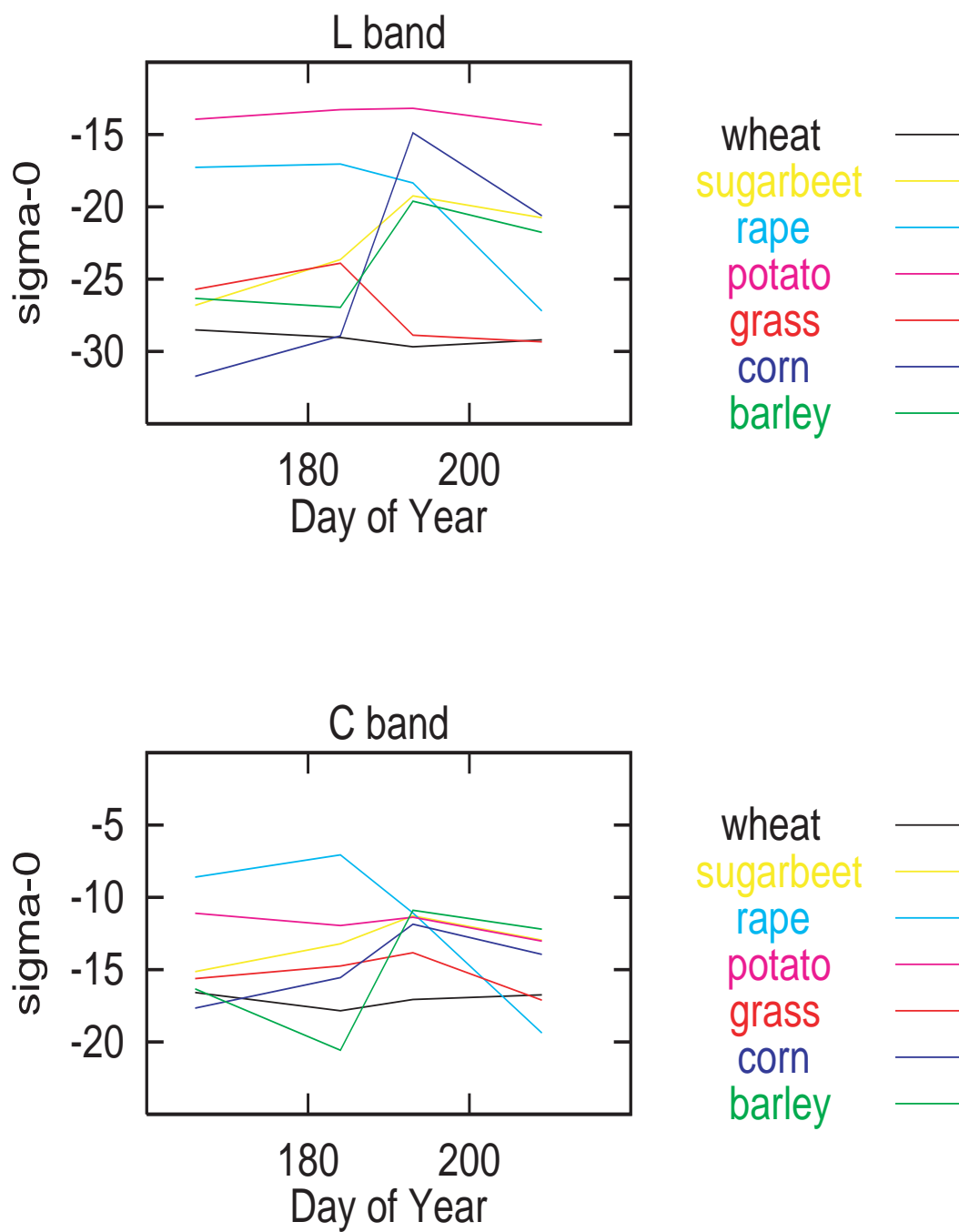


Figure 3.3: Examples of  $\sigma_{hv}^0$  multitemporal trends.

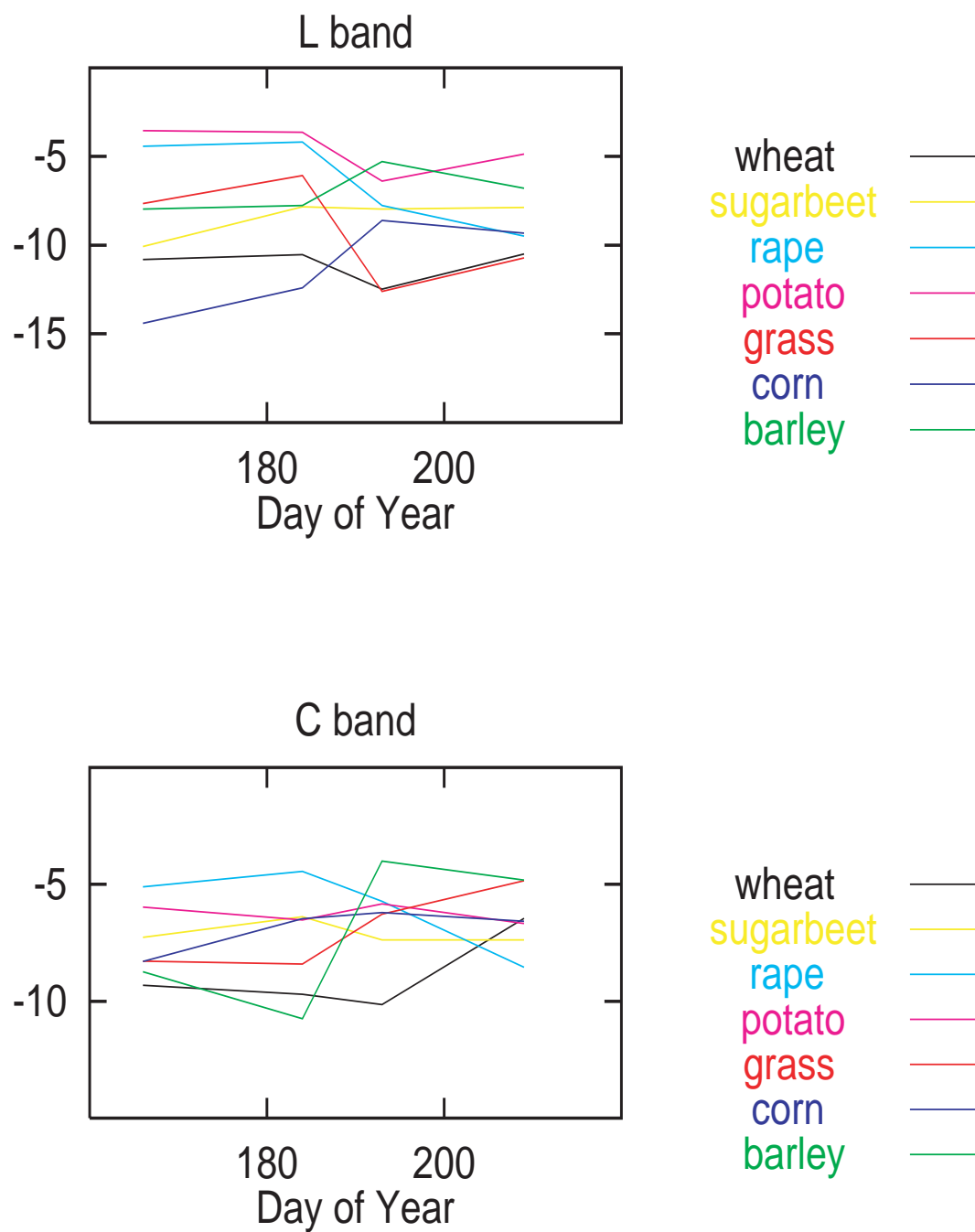


Figure 3.4: Examples of  $\sigma_{hv}^0/\sigma_{vv}^0$  multitemporal trends.

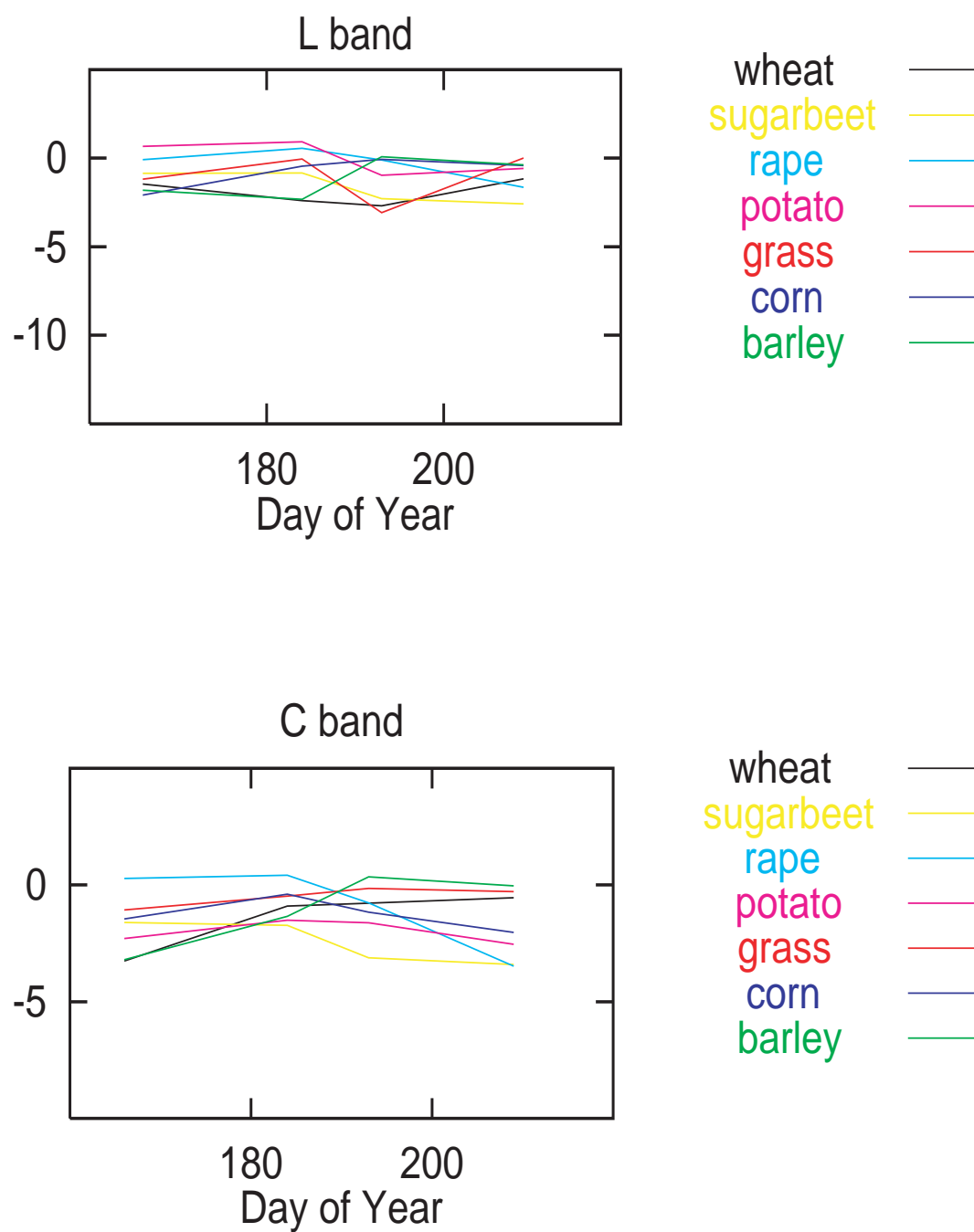


Figure 3.5: Examples of  $\sigma_{RR}^0/\sigma_{RL}^0$  multitemporal trends.

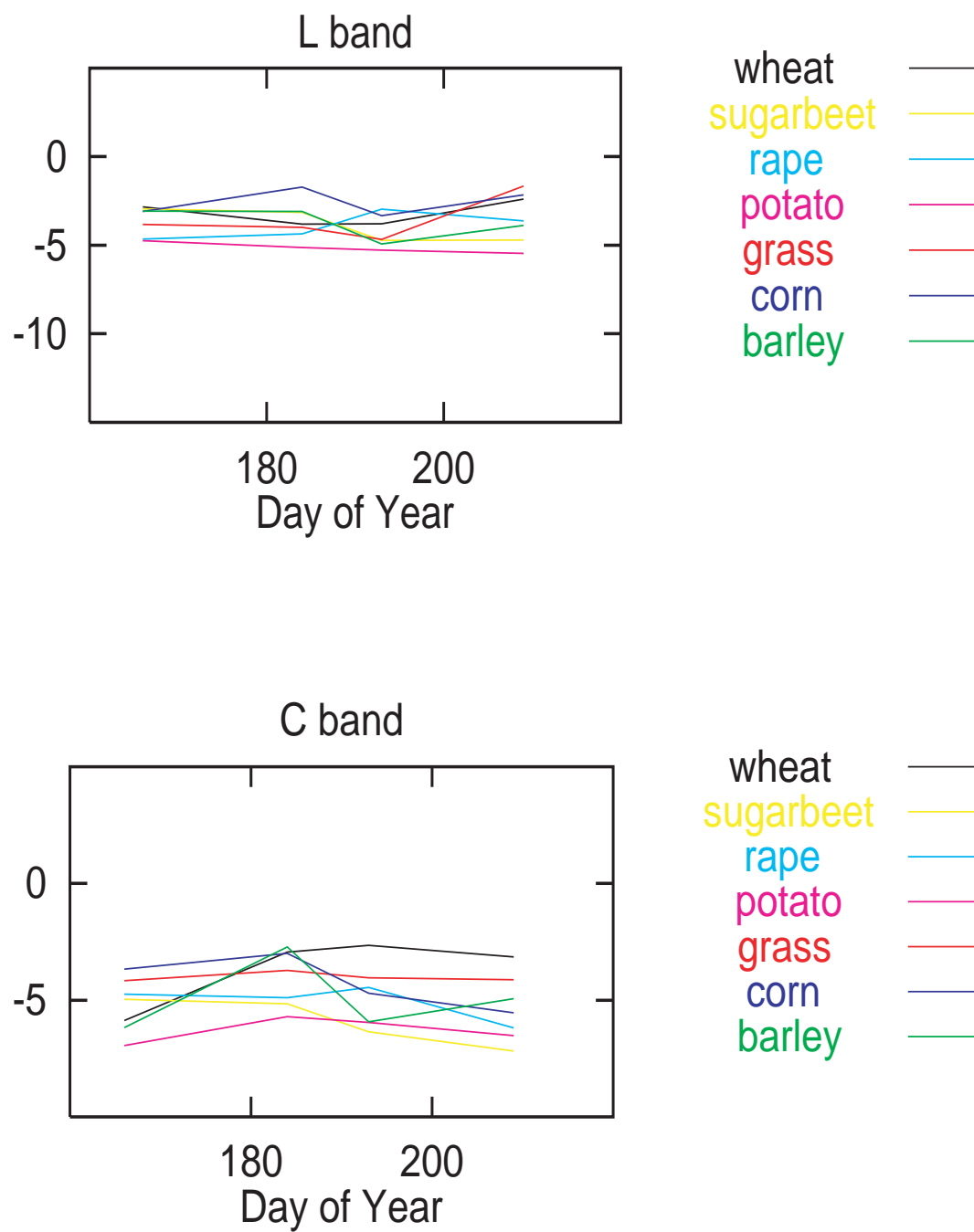


Figure 3.6: Examples of  $\sigma_{45^\circ}^0 \text{cross} / \sigma_{45^\circ}^0 \text{co-pol}$  multitemporal trends.

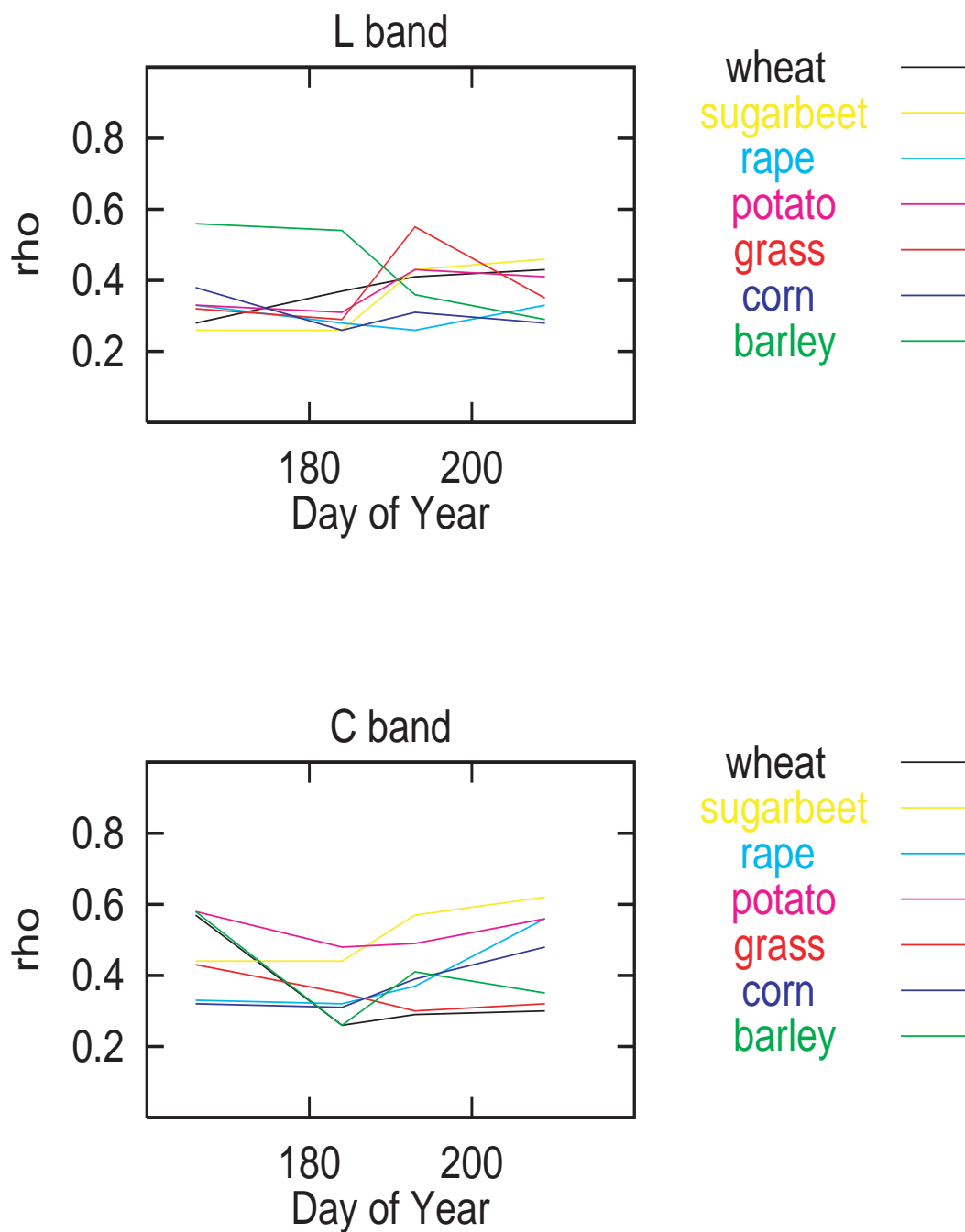


Figure 3.7: Examples of multitemporal trends of correlation coefficient  $\rho_{hhvv}$ .

First of all, a training set of backscattering coefficients has been generated, by selecting the C-band 50° data relative to a number of fields of the following crops:

- 10 fields of barley
- 2 fields of corn
- 11 fields of grass
- 28 fields of potato
- 4 fields of rape
- 23 fields of sugarbeet
- 33 fields of wheat

within the total number of fields imaged on the Flevoland'91 site. Multipolarization and/or multitemporal C-band  $\sigma^0$ 's of the above fields have trained the NN algorithm. The required number of epochs varied from 60 for the maximum number (6) of input channels to 1100 for the single-input net. Then, the trained network has been used to classify the fields of the test set, which included the remaining Flevoland'91 fields, i.e.:

- 4 fields of barley
- 2 fields of corn
- 8 fields of grass
- 25 fields of potato
- 3 fields of rape
- 19 fields of sugarbeet
- 18 fields of wheat

The work has been repeated several times using different subsets of the available data. First of all, a very simple data set has been taken, i.e.,  $\sigma^0$  for C-band,  $vv$  polarization, one single flight. The data set complexity has gradually been increased, up to the most complete case, relative to C-band,  $hh$ ,  $vv$  and  $hv$  polarizations, 4 flights. The obtained results are shown in Table 3.2.

Quite low percentages of misclassified samples have been achieved in the last cases, although only C-band and linear polarizations (without phase information) have been considered.

This is a promising result in view of the future exploitation of the Envisat ASAR data, although before extrapolating the results obtained in this exercise, the effects of the different incidence angles should be assessed. Moreover, the fine ground resolution of the AirSAR has allowed us to identify even relatively small fields, whereas this will not be the case for the coarser resolution Envisat ASAR.

CROP TYPE	DISCRIMINANT PROPERTY	EXPLANATION
POTATO	high HV(L-band)	larger twigs ( $\sim 4$ mm)
RAPE	high HV(C-band)	smaller twigs ( $\sim 2$ mm)
SUGARBEET	high $\rho_{hhvv}$ (C-band) low HV/VV (C-band) low RR/RL (C-band)	“facet” scattering
CORN	$hv$ (L-band) increase at beginning of July	crop growth (leaf and petiole scattering)
WHEAT	low HV/VV (C-band) high RR/RL (C-band) high 45x/45 (C-band)	vertical cylinders
BARLEY	low HV(C-band) in June increase in July	ear bending

Table 3.1: Interpretation of polarimetric features.

SELECTED SIGNATURES (C-band)	% OF MISCLASSIFIED FIELDS
$\sigma_{vv}^0$ , 1 flight	44.3
$\sigma_{vv}^0$ , 4 flights	16.5
$\sigma_{vv}^0 + \sigma_{hh}^0 + \sigma_{hv}^0$ , 1 flight	8.9
$\sigma_{vv}^0$ , 4 flights + $\sigma_{vv}^0 + \sigma_{hh}^0 + \sigma_{hv}^0$ , 1 flight	6.3
$\sigma_{vv}^0 + \sigma_{hh}^0 + \sigma_{hv}^0$ , 4 flights	3.8

Table 3.2: Classification results.

### 3.5 RASAM observation of seasonal development of crops

Another rich set of multi-parameter observations has been collected by the radiometer-scatterometer RASAM in dedicated measurement campaigns. In order to monitor the temporal variations of multifrequency, multiangle and multipolarization active microwave parameters during the seasonal development of agricultural crops, the instrument was installed between two fields, so that it was possible to get data from both. During the season 1987/88 winter wheat and corn were measured. The winter wheat was then followed by rape, the corn by winter wheat, both measured during the 1988/89 season. The temporal variations of the microwave parameters of sugar beet were obtained in another field. This kind of data is also very attractive to test or create models, since, besides scatterometer data, soil and vegetation parameters are also available. In the following, some relevant features of multi-temporal backscattering coefficients at different polarizations are shown and discussed, trying to bring out the potential of these measurements in crop discrimination and monitoring. The observed significant canopy conditions are also reported to enhance the understanding of the radar signatures.

#### 3.5.1 Winter Wheat

The phenological stages of the winter wheat field observed during the season 1987/88 are presented in Table 3.3, while the temporal trends of co- and cross-polarized  $\gamma = \sigma^0 / \cos \theta$  at  $20^\circ$  and  $50^\circ$  and for 3.1 GHz (S), 4.6 GHz (C) and 10.2 GHz (X) are shown in Fig. 3.8, together with the temporal trends of soil moisture and plant water content for suitable comparison.

For the small incidence angle ( $< 20^\circ$ )  $\sigma^0$ 's decrease during the growth of wheat, then increase at the end of the season, when the vegetation is drying. They are strongly correlated with the water content of the vegetation. For the larger incidence angle, the wheat canopy does not only act as an absorbing medium over the soil, but it contributes to the backscattering. Its contribution increases with increasing incidence angle. For vertical polarization the contribution of the vertically orientated vegetation is larger than at horizontal polarisation. If we look at the polarization dependence of  $\sigma^0$ 's at 3.1 GHz and incidence angles  $\theta > 30^\circ$ , we find that on day 127  $\sigma_{hh}^0 > \sigma_{vv}^0$  because the 50 cm-high wheat is more transparent at horizontal polarization. Later, on days 162 and 200, this is still true, but now  $\sigma_{vv}^0$  has significantly increased because of the contribution of the vegetation, especially at larger incidence angles, so that  $\sigma_{vv}^0$  becomes larger than  $\sigma_{hh}^0$ . This polarization behaviour at 3.1 GHz seems to be a useful signature to

Day	Date	Stage
64	Oct. 28, 1987	sowing
54	Nov. 7, 1987	germination
31	Nov. 30, 1987	6-8cm high, winter stage
61	Mar. 1, 1988	restart of growth
113	Apr. 22, 1988	elongation
149	May 28, 1988	79 cm high, ears appear
166	Jun. 14, 1988	end of growth
175	Jun. 23, 1988	bloom
207	Jul. 25, 1988	harvest

Table 3.3: Phenological stages of winter wheat during multitemporal observation.

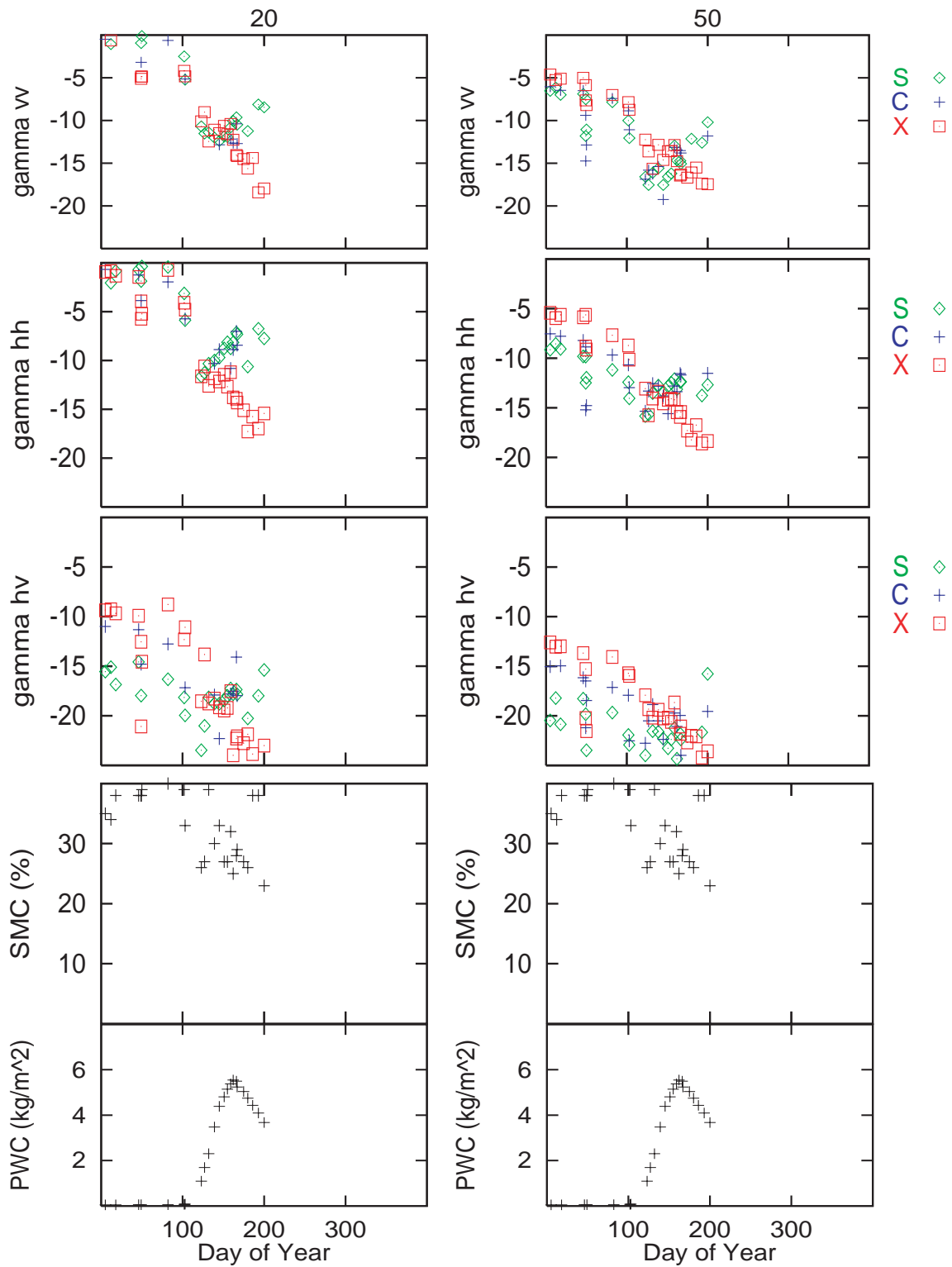


Figure 3.8: Multitemporal trends of co- and cross-polarized  $\gamma = \sigma^0 / \cos\theta$ , SMC, and PWC for a wheat field.

classify wheat. On the other hand, if we look at the temporal development of  $\sigma^0$ 's, the signatures are highly dependent on the incidence angle.

Some differences are found by comparison of the above data with those collected during the season 1988/89 on a very similar winter wheat field. In 1989 the backscattering coefficients were lower than in 1988 between day 120 and 130. This can be explained by the different soil moisture, since in 1988 the soil was dry while in 1989 the soil remained wet in that period. However, for both seasons we find the same variations of the angular dependence of  $\sigma^0$ . This may indicate that the temporal variation of the angular dependence of  $\sigma^0$  can be a tool for wheat identification.

### 3.5.2 Corn (Maize)

The phenological stages of corn observed during the season 1987/88 are presented in Table 3.4. The temporal trends of co- and cross-polarized  $\gamma = \sigma^0 / \cos \theta$  at  $20^\circ$  and  $50^\circ$  and for 3.1 GHz (S), 4.6 GHz (C) and 10.2 GHz (X) are shown in Fig. 3.9, together with the temporal trends of soil moisture and plant water content for suitable comparison.

The variation with time of the backscattering coefficients depends on the incidence angle. At  $0^\circ$  and  $10^\circ$  the growing vegetation leads to a decrease of  $\sigma^0$ , while at  $70^\circ$  the contribution from the soil is smaller than that from the corn canopy. Therefore, very small or very large incidence angles would be appropriate to monitor the vegetation growth. At  $50^\circ$   $\sigma^0$  increases with the corn growth, and the contribution from bare soil is smaller than that from the vegetation covered field if the soil is either dry or smooth (day 139). If the latter is wet and rough, the values are close to those for the fully grown corn. For bare soil and low vegetation, the soil moisture variations cause significant changes of  $\sigma^0$ , but this is not observed for grown corn. The ripening causes a decrease of  $\sigma^0$ . Harvest considerably increases  $\sigma^0$  at small incidence angles, whereas  $\sigma^0$  remains almost unchanged at  $50^\circ$ . For grown corn  $\sigma_{vv}^0$  and  $\sigma_{hh}^0$  are similar, while for bare soil and again after harvest,  $\sigma_{vv}^0$  is larger than  $\sigma_{hh}^0$ , especially at 3.1 GHz. At cross-polarization  $\sigma_{hv}^0$  is about 6 dB smaller than at like polarization. The behaviour of the cross-polarized backscattering is very similar to that of the like polarization. The differences between bare soil and corn are a little more obvious at cross polarization, and  $\sigma_{hv}^0$  increases with increasing frequency. To distinguish between bare soil and corn with a radar at  $50^\circ$  incidence angle, dry conditions are preferred, because  $\sigma^0$  for dry soil is smaller than for corn, smooth soil making the distinction easier.

Day	Date	Stage
126	May 5, 1988	sowing
135	May 14, 1988	germination
198	Jul. 16, 1988	bloom, growth of cobs
205	Jul. 23, 1988	end of growth
275	Oct. 1, 1988	yellowing of leaves
298	Oct. 24, 1988	harvest
301	Oct. 27, 1988	sowing of winter wheat

Table 3.4: Phenological stages of corn during multitemporal observation.

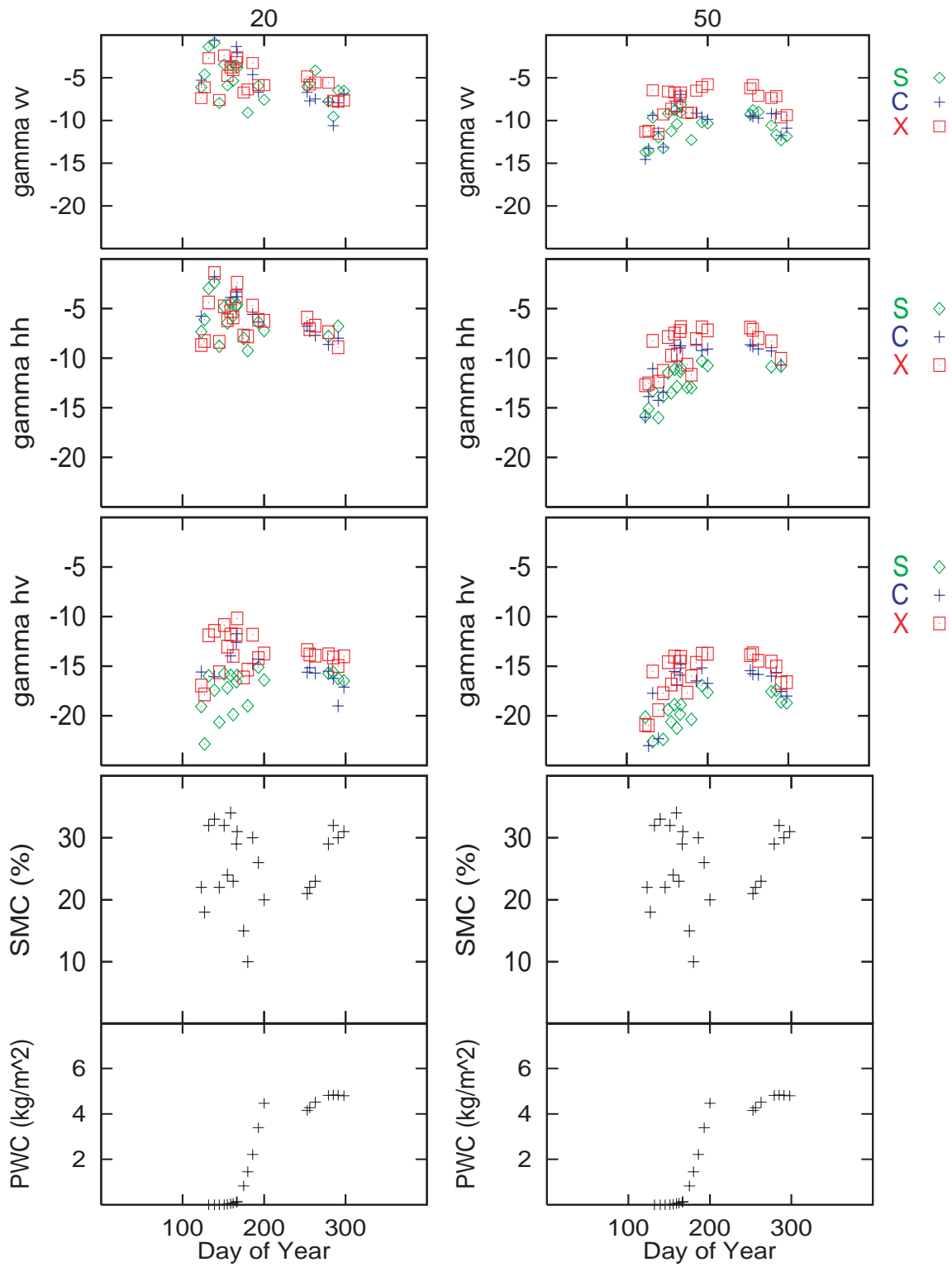


Figure 3.9: Multitemporal trends of co- and cross-polarized  $\gamma = \sigma^0 / \cos \theta$ , SMC, and PWC for a corn field.

Day	Date	Stage
114	Sep. 8, 1988	sowing, aggregates
108	Sep. 14, 1988	germination
64	Oct. 28, 1988	15 cm high, winter stage
80	Mar. 21, 1989	restart of growth
105	Apr. 15, 1989	start of bloom
114	Apr 24, 1989	growth of pods with seeds
143	May. 23, 1989	end of bloom and growth
		ripening, drying
194	Jul. 13, 1989	harvest
		stubble field

Table 3.5: Phenological stages of rape during multitemporal observation.

### 3.5.3 Rape (Canola)

As before, the phenological stages of rape observed during the season 1987/88 are presented in Table 3.5 and the temporal trends of co- and cross-polarized  $\gamma = \sigma^0 / \cos \theta$  at  $20^\circ$  and  $50^\circ$  and for 3.1 GHz (S), 4.6 GHz (C) and 10.2 GHz (X) are shown in Fig. 3.10, with soil moisture and plant water content.

Until day 80 the large leaves and the soil lead to a strong backscattering at the incidence angle of  $50^\circ$ . Then, during the growth in spring the leaves become more randomly oriented, and the backscattering decreases. The appearance of the pods increases the backscattering at 4.6 and 7.2 GHz, while the values at lower and at higher frequencies do not change much.

### 3.5.4 Sugar Beet

Typical phenological stages of sugar beet fields are reported in Table 3.6. The essential features of  $\sigma^0$  for sugar beet are summarized as follows. Backscattering increases strongly with increasing frequency, since there are leaves perpendicular to the wave vector at every incidence angle, which cause specular reflection. This also may explain the small differences between  $\sigma^0$  at different polarizations.  $\sigma^0$  also increases with the growing vegetation. The cross-polarized backscattering coefficient is about five times smaller than the like-polarization. Its spectral and angular dependence is similar to that of the like-polarization. As far as the temporal variation is concerned, in the first period of the year a wide site-to-site and year-to-year

Day	Date	Stage
110	Apr. 20.	sowing
184	Jul. 3.	25 cm high
		soil cover fraction: 40%
210	Jul. 29,	leaves grown-up
290	Oct. 17	harvest

Table 3.6: Phenological stages of sugar beet during multitemporal observation.

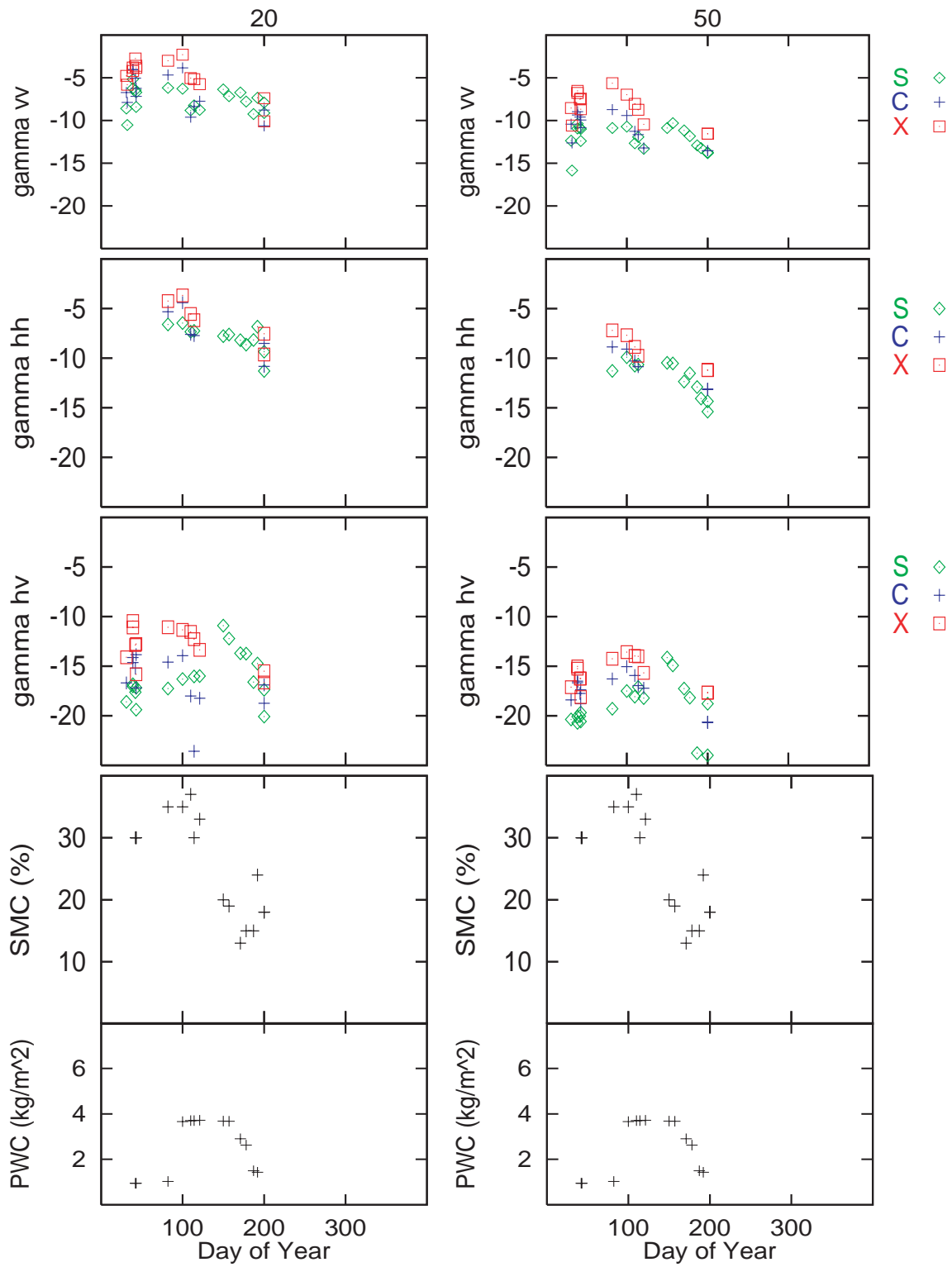


Figure 3.10: Multitemporal trends of co- and cross-polarized  $gamma = \sigma^0 / \cos \theta$ , SMC, and PWC for a rape field.

variability is observed due to various rain events, since the backscattering is dominated by soil. In a later period, after  $\sim$ day 150, the  $\sigma^0$  values are stable and close to each other, since backscatter from vegetation becomes dominant. After harvest ( $\sim$ day 300) the backscattering is again dominated by the soil. The angular dependence of  $\gamma = \sigma^0 / \cos \theta$  measured by RASAM at 4.6 GHz is shown in Fig. 3.11 for day 184 and in Fig. 3.12 for day 260. A small decrease of  $\gamma$  at incidence angles lower than  $30^\circ$  can

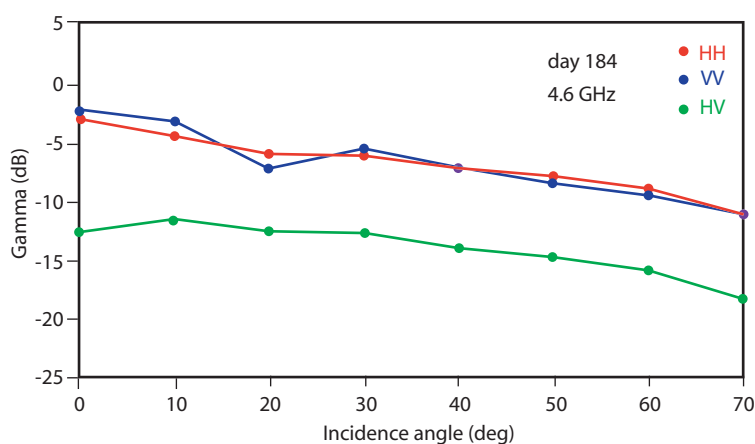


Figure 3.11: Sugarbeet angular signatures at day 184.

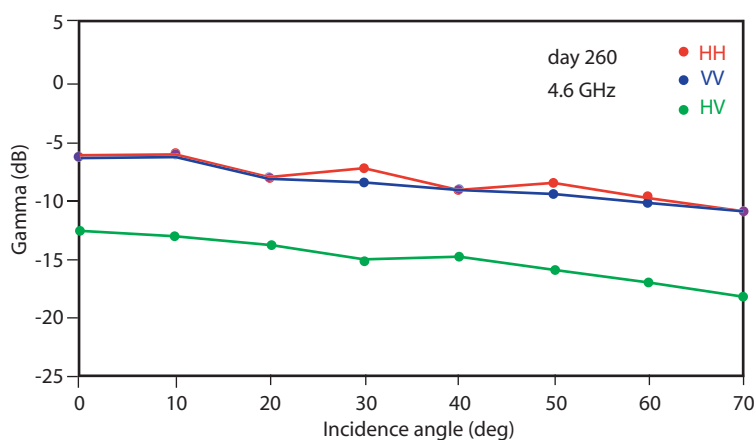


Figure 3.12: Sugar beet angular signatures at day 260.

be observed from day 184 to day 260 due to the increasing effect of the vegetation as an absorbing medium over the soil. However, peculiar signatures are the small difference between  $\gamma_{vv}$  and  $\gamma_{hh}$ , the generally flat trend with incidence angle and the high cross-polarization response. Again, we assume the presence of leaves perpendicular to the wave vector, causing specular reflection, at every observation angle.

### 3.6 Radar-Optical synergy in agriculture

The synergy between radar and optical instruments has been investigated by the University of Valencia group. In particular, the possibility of combining both kinds of data for the retrieval of surface bio-geophysical parameters, mainly water content, has been considered.

There are several similarities and differences in the problem as seen from the point of view of the optical domain or the radar domain. In general, for vegetation, there are three aspects to take into account:

- Canopy architecture
- Geometry of illumination/observation
- Water content and leaf chemical pigments

Canopy architecture and geometry of observation affect radar scattering. However, information on leaf chemical constituents is contained in optical data only. A typical green vegetation spectrum is mainly described by the absorptions due to chlorophyll in the wavelength range 0.4-0.7  $\mu\text{m}$  (Fig. 3.13) and the absorptions due to water in the range 0.9-2.5  $\mu\text{m}$  (Fig. 3.14). There are other absorption bands in vegetation spectra due to other constituents such as lignin. The decoupling of specific absorptions for leaf pigments and water, each affecting a different spectral range, is the main advantage of optical data for the retrieval of both water and leaf chemical constituents (chlorophyll).

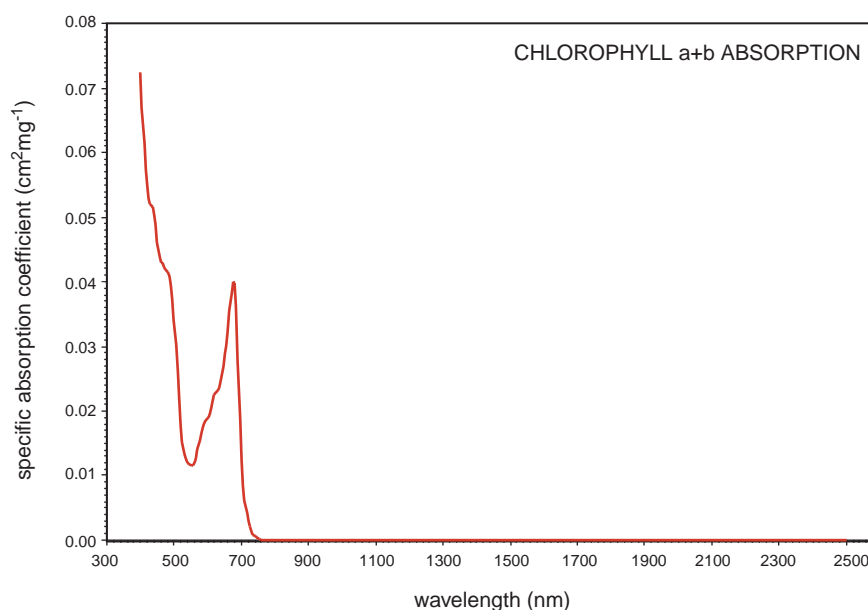


Figure 3.13: Green vegetation absorption spectrum: effect of chlorophyll.

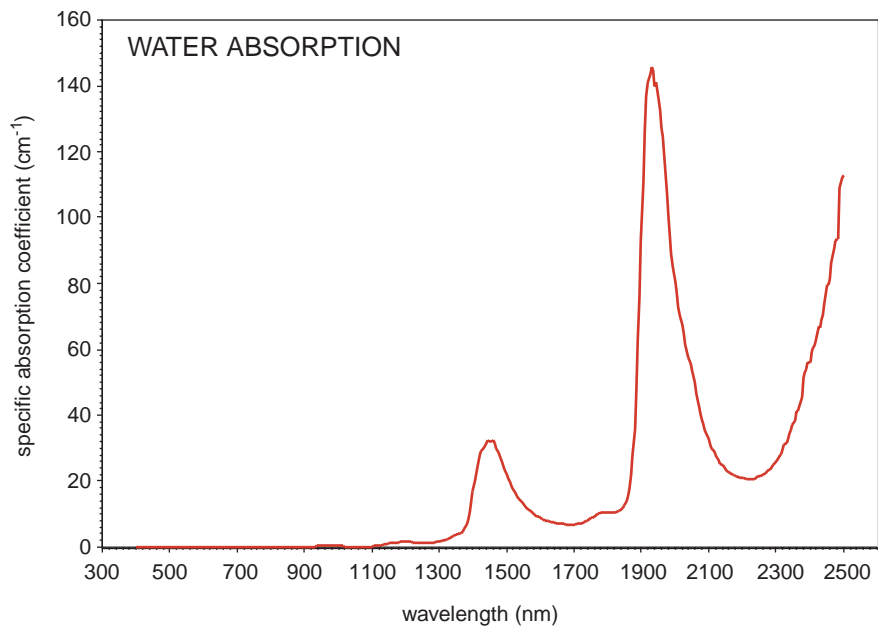


Figure 3.14: Green vegetation absorption spectrum: effect of water.

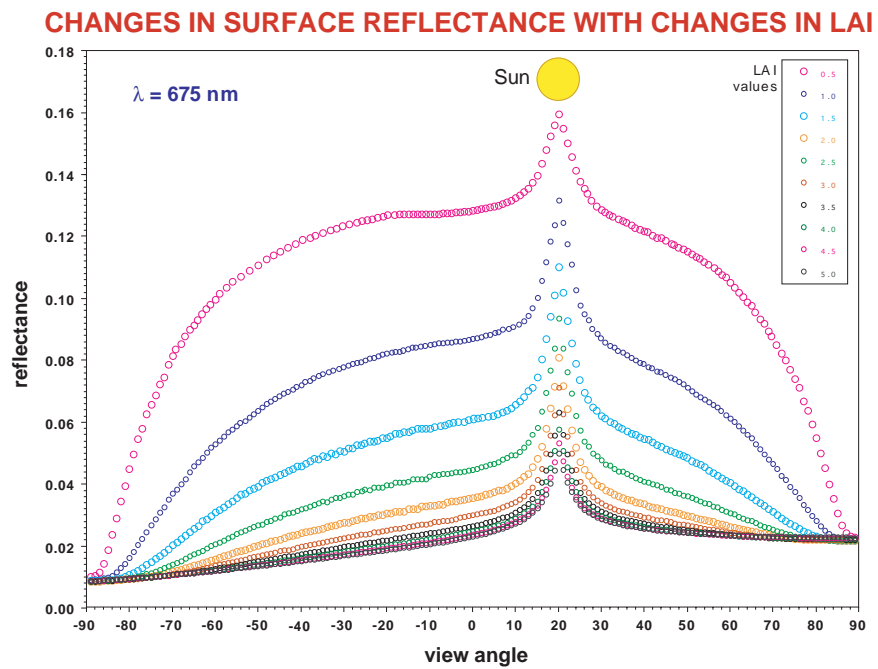


Figure 3.15: Angular variations of surface reflectance for 10 values of vegetation LAI.

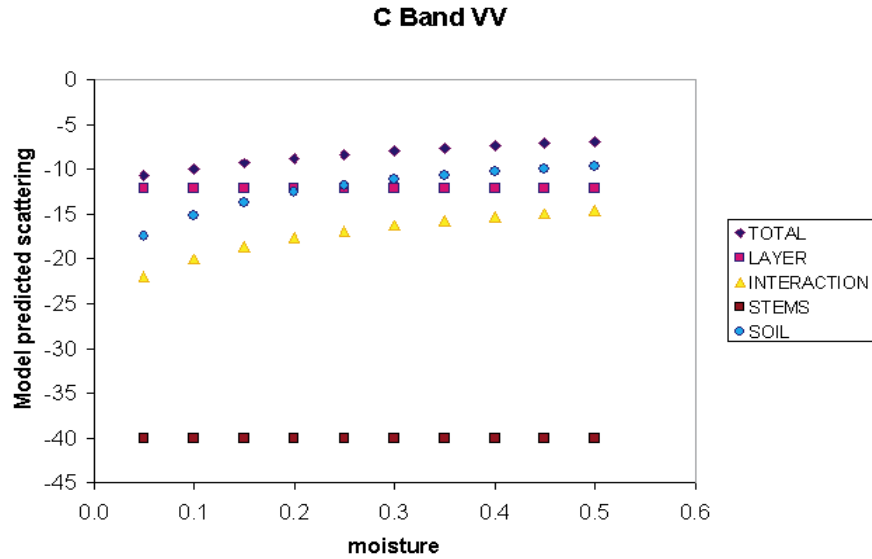


Figure 3.16: Example of crop C-band  $\sigma_{vv}^0$  vs. SMC simulated by the Tor Vergata model. Contributions from the soil and the various canopy elements are singled out.

Among the effects to be considered in the optical domain, the strong angular changes of surface reflectance when observation and illumination angles are close to a hot-spot configuration are a characteristic feature. The hot spot effect is strongly related to the canopy structural parameters, such as LAI, leaf size and crop height. Fig. 3.15 shows the angular variation of surface reflectance for various LAI values and evidentiates the sharp peak of reflectance about the hot spot configuration.

Microwave backscattering contains information about soil moisture. However, the presence of vegetation attenuates the soil contribution, thus introducing difficulties in soil moisture retrieval. This effect can be appreciated from Fig. 3.16, which shows simulation results obtained by the microwave scattering model made available by Tor Vergata University, for the case of low vegetation. On the other hand, we point out that it is possible to estimate the canopy water content by means of optical data through the absorption band depth. The accuracy of the estimate increases when hyperspectral data are used, as the shape of the absorption band is better reconstructed, than when using multispectral data.

The above considerations indicate that the type of information contained in the optical measurements is different from that in microwave data. As a consequence, synergy between the two kinds of data is expected, with possible benefits from a joint use of both sources of remotely sensed information.

### 3.6 Elements of synergy in snow cover measurements

The multiangle, multipolarization, multifrequency and multitemporal backscattering observations of snowcover, performed by a Network Analyzer-based scatterometer in the Swiss and Austrian Alps [11] can be assembled and compared with those of the ERS SAR to assess their global potential in retrieving snowcover properties.

The capability of mapping wet snowcover by means of SAR is well known. However, the ERS configuration does not provide all needed information. In Fig. 3.17, C-Band  $vv$  backscattering is presented as a function of the incidence angle for different snow situations. The signatures of dry and wet snowcover and of the snow-free test-site are in general different, but at  $20^\circ$  incidence angle, dry snowcover, wet snowcover with a rough surface, and snowcover with a thin wet layer at the surface present close responses. Discrimination of wet snow is therefore critical with the ERS SAR at  $23^\circ$  incidence angle when the wet snow surface is rough or when the integrated column height of liquid water in the snow pack is smaller than 1 mm. At large incidence angles and at cross-polarization (Fig. 3.18), on the other hand, this problem does no longer exist.

At 35 GHz, cross-polarization (Fig. 3.19), there is a very clear signature difference between dry and wet snowcover. The enhanced backscattering from the snow grains allows discrimination of dry snowcover from snow-free terrain and, in some cases, makes backscatter sensitive to snow depth. Refrozen crusts on the snow cover surface can be easily identified at this frequency, so that the complementary use of C- and Ka-band scatterometry does allow discrimination if the refrozen crust is on the surface of a completely dry snowcover (high backscattering at C- and Ka-band) or of a snowcover wet at the bottom (high backscattering at Ka-band and low backscattering at C-band).

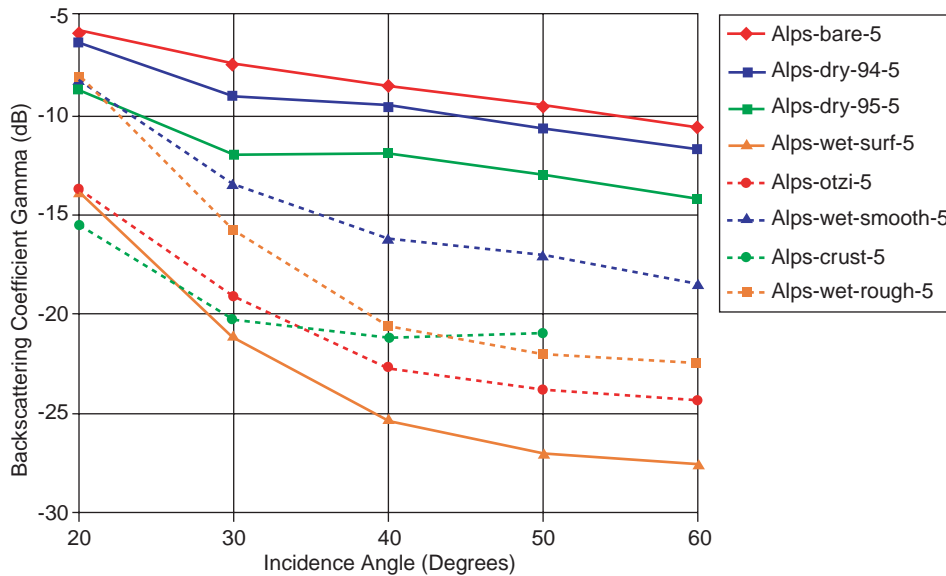


Figure 3.17: C-band  $vv$  backscattering vs. incidence angle for various snow characteristics.

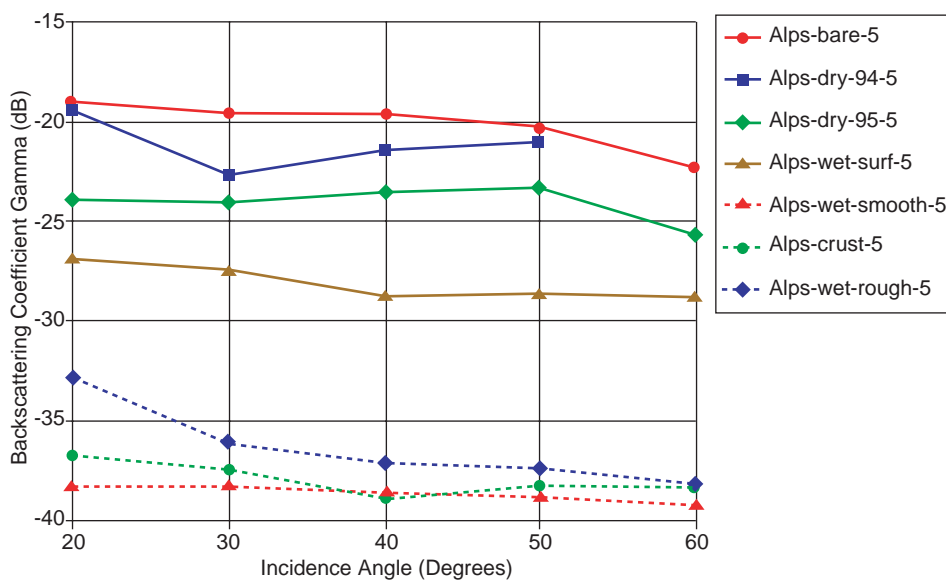


Figure 3.18: C-band hv backscattering vs. incidence angle for various snow characteristics.

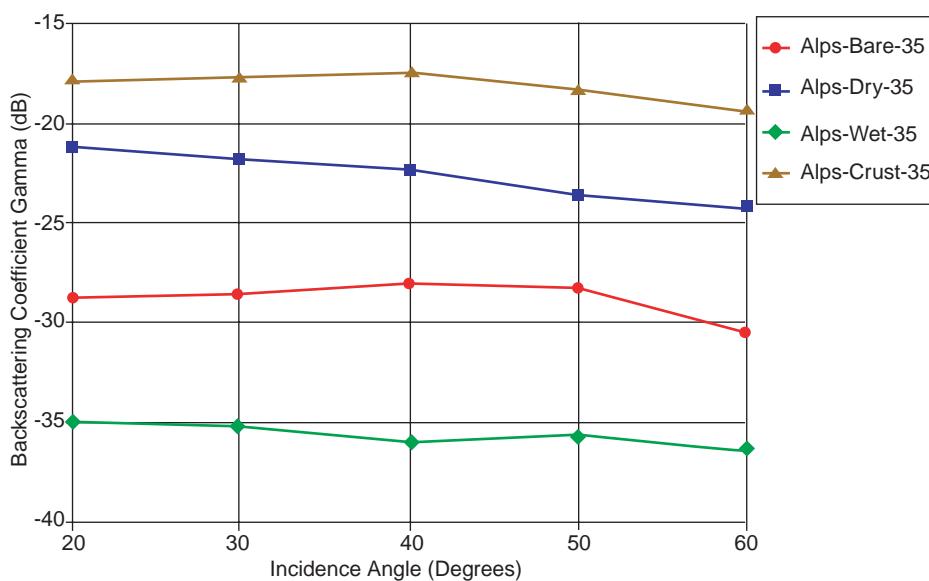


Figure 3.19: Ka-band hv backscattering vs. incidence angle for various snow characteristics.



# Bibliography

- [1] F.T. Ulaby, R.K. Moore, A.K. Fung, “*Microwave Remote Sensing. Active and Passive. Vol. III*”, Artech House, 1986.
- [2] B.A.M. Bouman, D.H. Hoekman, “Multi-temporal multi-frequency radar measurements of agricultural crops during the Agriscatt-88 campaign in The Netherlands”, *Int. J. Remote Sensing*, vol. 14, 1595-1614, 1993.
- [3] U. Wegmüller, “Signature research for crop classification by active and passive microwaves”, *Int. J. Remote Sensing*, vol. 14, 871-883, 1993.
- [4] P. Ferrazzoli, S. Paloscia, P. Pampaloni, G. Schiavon, S. Sigismondi, D. Solimini, “The potential of multifrequency polarimetric SAR in assessing agricultural and arboreous biomass”, *IEEE Trans. Geosci. Remote Sensing*, vol. 35, pp. 5-17, 1997.
- [5] T. Le Toan, F. Ribbes, L.-F. Wang, N. Floury, K.-H. Ding, J. Kong, M. Fujita, T. Kurosu, “Rice crop mapping and monitoring using ERS-1 data based on experiment and modeling results” *IEEE Trans. Geosci. Remote Sensing*, vol. 35, pp. 41-56, 1997.
- [6] H. Skriver, M.T. Svendsen, A.G. Thomsen, “Multitemporal C- and L-band polarimetric signatures of crops”, *IEEE Trans. Geosci. Remote Sensing*, vol. 37, pp. 2413-2429, 1999.
- [7] P. Saich, M. Borgeaud, “Interpreting ERS SAR signatures of agricultural crops in Flevoland, 1993-1996”, *IEEE Trans. Geosci. Remote Sensing*, vol. 38, pp. 651-657, 2000.
- [8] G. Cookmartin, P. Saich, S. Quegan, R. Cordey, P. Burgess-Allen, A. Sowter, “Modeling microwave interactions with crops and comparison with ERS-2 SAR observations”, *IEEE Trans. Geosci. Remote Sensing*, vol. 38, pp. 658-670, 2000.
- [9] P. Ferrazzoli, L. Guerriero, G. Schiavon, “Experimental and model investigation on radar classification capability”, *IEEE Trans. Geosci. Remote Sensing*, vol. 37, pp. 960-968, 1999.
- [10] A. Zell, et al., *SNNS Stuttgart Neural Network Simulator User Manual*, Report N° 6/95, University of Stuttgart, Institute for Parallel and Distributed High Performance Systems, Stuttgart, Germany, 1995.
- [11] T. Strozzi, A. Wiesmann, and C. Mätzler, “Active Microwave Signatures of Snowcovers at 5.3 and 35 GHz”, *Radio Science*, vol. 32, 479-495, 1997.



## Chapter 4

# The Model Library (WP 102, WP 202)

### 4.1 Introduction

This chapter introduces the models which are available to the ERA-ORA library and reports selected results of the analysis carried out by the Working Party on Models (WP 202),

The Model Distributed Library (M.D.L.) includes three computer codes, based on the Radiative Transfer Theory, which simulate the microwave backscattering coefficients of soil and vegetation.

*POLSCAT* is a radiative transfer model contributed by Université Catholique de Louvain, which computes the polarimetric radar response from vegetation using leaf, branch, trunk, and soil parameters as input. A four-layer vector radiative transfer model contributed by Université Paul Sabatier computes the backscattering coefficients and the Müller matrix for arboreous vegetation. Finally, a multiple-scattering model has been contributed by Università Tor Vergata for computing co- and cross-polar backscattering from crops. Besides the description of the main features of the models, a discussion of some examples of results is given.

It is extensively recognized that, when interactions between electromagnetic waves and the earth surface are investigated, experimental studies must be combined with electromagnetic modeling. Indeed, models give a physical basis to observed correlations with ground data, and allow parametric investigation. This can be quite useful especially when, as is often the case, the analysis of the effect of a single bio-geo-physical parameter on the sensor response is difficult to carry out from experimental data, since the whole set of parameters characterizing the earth surface undergo simultaneous variations.

The three theoretical models present in the ERA-ORA M.D.L. are able to simulate microwave backscattering measurements; they can provide an insight into the physical interpretation of experimental results, and can drive the development of retrieval algorithms. The ground truth data present in the D.D.L. can be used as inputs to the available theoretical models. In this way, their validation can be performed and the modeling accuracy may be improved.

## 4.2 Overview of the models

### 4.2.1 UTOV model features

The model developed at Tor Vergata, is based on the Radiative Transfer Theory, and can simulate the radar response of terrain covered with vegetation as a function of the sensor parameters (frequency, polarization and observation angle) and of the relevant bio- geo-physical parameters characterizing the observed surface (that is vegetation components and underlying soil). In the source code, which is available to the ERA-ORA Library, several comments have been provided in order to lead the user through the various steps of the simulation procedure.

It is worth mentioning that, although the ERA-ORA model version yields only the backscattering coefficient, other models under development and test at Tor Vergata can compute in a unified approach also the emissivity of a vegetated terrain. Passive and active simulations have been described in a number of papers [1]–[8]

### 4.2.2 POLSCAT model features

The Polarimetric Radiative Transfer Model (UCLRMTM), developed at UCL, allows the simulation of polarimetric radar (and SAR) observations of bare soils, vegetated areas and forested areas. The motivation for this work has not been to duplicate existing software, but to develop a tool

- that would include a number of important features, not all present in the available codes, and
- for which the user would have a precise knowledge of all the components of the scattering models and of their limits of validity.

Such a tool is important for the simulation of backscattering and polarimetric signatures, for sensitivity analysis, for the interpretation of (polarimetric) radar (SAR) measurements, and ultimately for the development of retrieval algorithms.

Testing of the upgraded version of the code on some data sets is still underway, at UCL, at Universitat de Valencia, and at VITO (Vlaams Instelling voor Technische Onderzoek) in Mol (Belgium), with which UCL has a common project sponsored by the Belgian Federal Funding OSTC.

A User Manual [9] has been prepared that provides a summary of the main characteristics of the model, recalls some required basic relationships for radar polarimetry, and gives detailed explanations with examples on the input file content and specifies the output data. The manual, an example of input data file and two versions of the code executable (low and high precision) are available on the WEB site of the Laboratory.

As is generally the case for models, refinements and additions are almost permanent. In its present form the UCL code is still not completely finalized. Indeed further improvements could be included, in order to describe for instance forests with gaps, anisotropic targets such as corn fields, to include a higher number of layers to better match more complicated situations, to develop a better scattering model for curved leaves, etc.. Also recent tests have shown that a few specific features are still giving some problems and need to be checked and corrected.

### 4.2.3 UPS model features

The model developed at the UPS is based on the vector radiative transfer theory applied to a multilayered discrete random medium. The expression of the first-order solution of the radiative transfer equation for the upward-going Stokes vector is given as the sum of volume scattering and surface-volume scattering, taking place in layer  $n$ . The attenuation due to the presence of layers other than  $n$  are taken into account. Then the total backscattering coefficient is given as a sum over the contributions from different scattering mechanisms taking place in each layer. The contribution of the direct rough surface scattering is also evaluated. The model accounts for different classes of scatterers, allowed to have different size, shape and permittivity. Details about the model description and validation can be found in [10].

## 4.3 The models

This section discusses in some detail the models made available to the ERA-ORA Model Library.

### 4.3.1 UTOV model description

The model developed at Tor Vergata describes the crop medium as sketched in Fig. 4.1. The medium is subdivided into three main regions:

- the top layer, which can be filled by twigs, leaves and/or ears;
- an intermediate layer containing near vertical cylinders representing stems;
- the bottom layer, representing soil.

The canopy components are modeled by lossy scatterers of simple geometrical shape, such as discs to represent leaves, and cylinders to represent ears, twigs and stems.

The Rayleigh-Gans approximation [11] is used up to 5 GHz to model the electromagnetic properties of thin cylinders (twigs) and of discs (leaves). According to this theory, the inner field of an object with at least one dimension small with respect to the wavelength can be approximated by a homogeneous field along this dimension, while, in the other two dimensions, phase differences must be taken into account. At high frequencies, the Physical Optics approximation [12], which replaces the field inside a thin disc with that of a slab with the same thickness, has been implemented to compute the disc electromagnetic properties. The Infinite Length approximation [13], which approximates the field inside a finite cylinder with that of an infinite one, is used for cylindrical objects, like stalks. This approximation is valid when the half-length is much higher than the radius, a condition satisfied also in ears and twigs at high frequencies.

The dielectric constant of vegetation elements has been computed through the semi-empirical formula, given in [14], which needs the moisture content and the wet to dry density ratio as inputs.

It must be pointed out that the top layer and the stem layer can be inhomogeneous, since scatterers may follow any probability distribution of dimensions, orientation and moisture content. Furthermore the top layer can be subdivided into sublayers, in order to represent canopy components with a preferentially vertical distribution. This model flexibility can be fully exploited only if a detailed knowledge of the geometrical and dielectric properties of the canopy is available. Since in most practical cases this is not the case, a single homogeneous layer has been chosen for the crop canopy represented in the code made available to the ERA-ORA project.

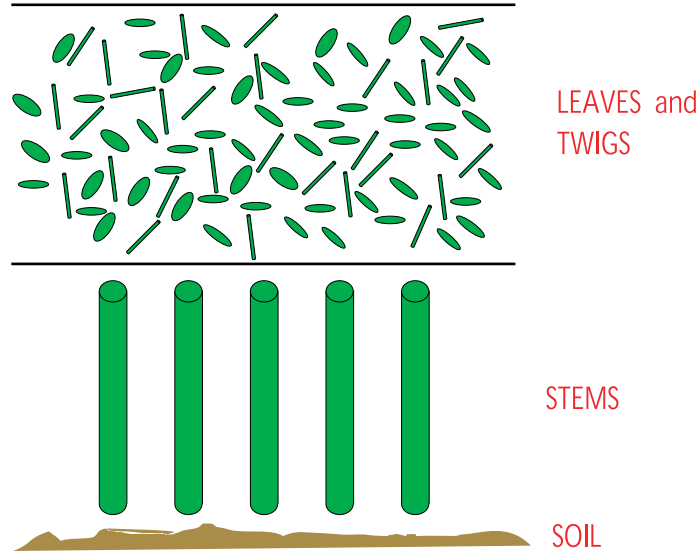


Figure 4.1: Sketch used to model vegetation canopies.

The electromagnetic properties of the soil are described by its bistatic scattering coefficient. According to the analysis developed in [15] and [16], the latter is given by the superposition of a specular coherent contribution and a diffuse incoherent contribution. The coherent contribution, which is proportional to the specular reflectivity given in [15] and [16], is important at L-band, while it is relatively low at C-band and usually negligible at the higher frequencies. To compute the diffuse incoherent contribution, the bistatic version of the Integral Equation Method, given in [5], is used at L- and C-bands. The Geometrical Optics model, with the shadowing function proposed by Smith, is used at higher frequencies [21]. These choices are based on the results of recent studies about validity ranges of surface models summarized in [5].

By using the above mentioned approximations, the amplitude scattering functions  $f_{pq}(\theta, \phi; \theta_s, \phi_s)$  of individual canopy scatterers are computed for the assumed Eulerian angles  $\alpha, \beta, \gamma$  (see pp. 452-454 of [5]).  $\theta$  and  $\theta_s$  denote incidence and scattering off-normal angles, respectively, while  $\phi$  and  $\phi_s$  indicate incidence and scattering azimuth angles;  $p$  and  $q$  denote polarizations of scattered and incident fields, respectively. The bistatic scattering cross-sections  $\sigma_{pq}(\theta, \phi; \theta_s, \phi_s) = 4\pi \langle f_{pq}^2(\theta, \phi; \theta_s, \phi_s) \rangle$  are then obtained, averaging over the assumed range of Eulerian angles. The extinction cross-sections  $\sigma_{eq}(\theta, \phi)$  of individual canopy scatterers are also computed; to this aim, the forward scattering theorem is generally used, while the sum of absorption and scattering cross-sections is taken when the Rayleigh-Gans approximation is applied, since, in that case, the forward scattering theorem does not properly compute the contribution of scattering to extinction. The stem absorption cross-section and the soil bistatic scattering coefficient are also computed.

All scattering cross sections are computed under far-field approximations. Once the above indicated quantities are known, the different contributions are combined by means of the Matrix Doubling algorithm and the overall bistatic scattering coefficient is obtained. Finally, the backscattering coefficient of the whole medium is computed. From this result contributions coming from different canopy layers can be

singled out: the backscattering coefficient of the top layer, of the stems, of the soil, and that arising from multiple interactions between them.

To simulate the emissivity, the energy conservation law is applied. Details about the Matrix Doubling and the mathematical procedures are given in the appendices of [4] and [6].

The Tor Vergata model is able to include multiple scattering effects and shows the advantage of flexibility, since the dimensions, the orientation and the position of the scatterers may be properly selected in order to represent realistically a given crop geometry. The simplification of assuming azimuthal symmetry is required: this is reasonable for dense canopies such as those of wheat ( $\sim 600 \text{ stems}\cdot\text{m}^{-2}$ ).

In principle, the model is valid in the whole microwave spectral range, provided the suitable approximations are adopted to compute the cross-sections of the single elements. However, the use of simple geometrical shapes, such as discs and cylinders, is acceptable at low frequencies but gradually loses validity when the frequency increases, since the microstructure of the elements becomes more and more important. Nevertheless, the frequency range between 1.4 GHz and 21 GHz, which is significant for both theoretical studies and applications in radar remote sensing of the earth surface, is covered.

### 4.3.2 The POLSCAT model

In the following we provide a basic summary of radar polarimetry and a short description of the model.

#### Definitions in radar polarimetry

We recall briefly in this section the basic relationships of radar polarimetry. A short description is given in [19], while more details can be found for instance in [20, 18]. To the random plane wave  $\mathbf{E} = (E_1 \ E_2)^T$ , with components  $E_1, E_2$  in an orthonormal basis in a plane perpendicular to the propagation direction, are associated Stokes parameters that contain information on the power density and polarisation of the wave. The superscript  $T$  stands for the transposed vector or matrix. The Stokes parameters are arranged in a Stokes vector, whose modified form is

$$\mathbf{J}_m = \begin{pmatrix} I_1 \\ I_2 \\ U \\ V \end{pmatrix} = \begin{pmatrix} \langle E_1 E_1^* \rangle \\ \langle E_2 E_2^* \rangle \\ 2 \Re \langle E_1 E_2^* \rangle \\ -2 \Im \langle E_1 E_2^* \rangle \end{pmatrix} \quad (4.1)$$

where the symbol  $\langle \rangle$  denotes ensemble averages.

As the wave is scattered by a target, the scattered wave  $\mathbf{E}^s$  at distance  $r$  from the target is related to the incident wave  $\mathbf{E}^i$  by the scattering matrix

$$\mathbf{E}^s = G(r) \mathbf{S} \mathbf{E}^i \quad \text{with} \quad \mathbf{S} = \begin{pmatrix} S_{11} & S_{12} \\ S_{21} & S_{22} \end{pmatrix} \quad \text{and} \quad G(r) = \exp(-jkr) / kr \quad (4.2)$$

where  $\mathbf{S}$  is the scattering matrix,  $G(r)$  is the Green's function for a spherical wave and  $k$  is the wave number. As defined, the Green's function is dimensionless, as is the case of the scattering matrix. Note that we are using the radioelectrician convention for the propagating wave, i.e. a  $\exp(+j\omega t)$  factor is assumed. With this convention the complex permittivity has a *negative* imaginary part. Here we shall use only the *forward scattering alignment*, or FSA, convention [18], in which a right-handed basis with respect to the propagation direction is used for both the incident and the scattered field.

Scattering by random targets, such as volume distribution of leaves and branches, or rough surfaces, must be described by statistical quantities. The scattered Stokes vector is related to the incident Stokes vector by the Mueller matrix  $\mathbf{M}$ , or the modified Müller matrix  $\mathbf{M}_m$  if the modified Stokes vector is used,

$$\mathbf{J}_m^s = \mathbf{M}_m \mathbf{J}_m^i \quad (4.3)$$

The modified Müller matrix has a simpler expression than the Müller matrix. It is easily obtained by a simple matrix transformation of the direct product

$$\mathbf{W} = \langle \mathbf{S} \otimes \mathbf{S}^* \rangle = \left\langle \begin{pmatrix} S_{11}S_{11}^* & S_{11}S_{12}^* & S_{12}S_{11}^* & S_{12}S_{12}^* \\ S_{11}S_{21}^* & S_{11}S_{22}^* & S_{12}S_{21}^* & S_{12}S_{22}^* \\ S_{21}S_{11}^* & S_{21}S_{12}^* & S_{22}S_{11}^* & S_{22}S_{12}^* \\ S_{21}S_{21}^* & S_{21}S_{22}^* & S_{22}S_{21}^* & S_{22}S_{22}^* \end{pmatrix} \right\rangle \quad (4.4)$$

The modified Müller matrix  $\mathbf{M}_m$  is given by

$$\mathbf{M}_m = \mathbf{R}_m \mathbf{W} \mathbf{R}_m^{-1} \quad \text{with} \quad \mathbf{R}_m = \begin{pmatrix} 1 & 0 & 0 & 0 \\ 0 & 0 & 0 & 1 \\ 0 & 1 & 1 & 0 \\ 0 & j & -j & 1 \end{pmatrix} \quad (4.5)$$

The four elements in the upper right corner of  $\mathbf{M}_m$  are the average norm squared of the  $S_{ij}$  ( $i, j = 1, 2$ ) and are directly proportional to the radar cross sections for the corresponding polarisations. The power received by the radar for arbitrary polarisations is obtained from

$$P_r = \frac{1}{2} (kr)^{-2} F (\mathbf{J}_m^r)^T \mathbf{K}_m \mathbf{J}_m^t \quad (4.6)$$

The factor  $F$  is proportional to the antenna gain  $G(\theta, \phi)$  in the observation direction  $(\theta, \phi)$

$$F(\lambda, \theta, \phi) = \frac{\lambda^2}{8\pi\eta} \frac{G(\theta, \phi)}{|\vec{E}^r|^2} \quad (4.7)$$

The quantities  $\mathbf{J}_m^t$  and  $\mathbf{J}_m^r$  are the modified Stokes vectors associated with the transmitted field and to the field that would be transmitted if the antenna were emitting with the receiving polarisations. These Stokes vectors are defined with respect to the antenna reference frame in the emitting mode. Other quantities are : the free space impedance  $\eta$ , and the electric field  $\vec{E}^r$ , or  $\mathbf{E}^r$  in matrix notations. The matrix  $\mathbf{K}_m$  is the modified Kennaugh matrix [19, 20], related to the modified Müller matrix by

$$\mathbf{K}_m = \mathbf{V} \mathbf{M}_m \quad (4.8)$$

with the following definition of the matrix  $\mathbf{V}$

$$\mathbf{V} = \text{diag} \{2, 2, -1, 1\} \quad (4.9)$$

### Model description

The UCL model includes size distributions of trunks, branches and leaves, it allows vertical distributions within the canopy, it provides a precise description of the vegetation and trees, and it takes account

of the main vegetation characteristics. It is a fully polarimetric radiative transfer model, based on the fundamental assumption that the scattering processes from the various constituents are incoherent, and that consequently powers (and more generally Stokes parameters) add together. However caution has been taken to handle properly particular situations of backscattering enhancement, related to double bounce cases, and reciprocity is forced for those component scattering models that do not satisfy that property. The model provides as main output the complete Müller (or Kennaugh) matrix, and therefore the complete polarimetric response of a distributed target.

The canopy is represented by a distribution of leaves and three classes of branches (one of which can be used for pine needles), with random dimensions and orientations. The branches are modelled by circular cylinders, the leaves by circular, rectangular or elliptic flat dielectric disks and the needles by thin circular cylinders. The trunks are modelled either by dielectric circular cylinders or by dielectric circular cones, with a distribution of inclination angles with respect to the vertical. For all dimensions and orientation distributions, as well as for the vertical distribution, a choice is given between several probability distribution functions. For each individual component, a manual or automatic choice is also possible between several scattering models, depending on the electrical dimensions and properties of the component.

For random rough surfaces, we have developed a two-scale surface scattering model, based on a boundary perturbation approach. This was primarily devised for the ocean surface, but can be transposed to soil surfaces. We have also implemented the Integral Equation Method (IEM) [5]. However this approach raises some open questions regarding the domain of validity and divergence problems in the calculation of the surface field.

The following first order contributions to backscattering are evaluated:

- the direct canopy contribution **DC**,
- the canopy ground contribution **CG**,
- the ground canopy ground contribution **GCG**,
- the trunk ground contribution **TG**,
- the direct ground contribution **DG**.

Since the double bounce canopy contribution **DC2** requires a very long computation time and provides in most cases a rather low contribution, it has not yet been included.

The polarimetric radiative transfer model has been implemented in a computer code in FORTRAN. A detailed input file allows the user to introduce all the data required by the code. A practical problem is probably that many agronomic data are very difficult to measure on the terrain and need to be estimated. The computing time is mostly related to the orientation integration of components with dimensions large compared with the wavelength. The standard output file provides for each mechanism, as well as for the total, the complete modified Müller matrix, the scattering coefficients in the four polarisations  $hh$ ,  $vv$ ,  $hv$ , and  $vh$ , the co-polar correlation in amplitude and phase, the amplitude of the cross correlations, and the four attenuations (diagonal elements of the  $4 \times 4$  extinction matrix).

### 4.3.3 UPS model

This program calculates the backscattering coefficients and the Müller matrix. The bistatic scattering coefficients can be obtained by some minor modification of the program. The model considers the vegetated surface composed of several layers, i.e.,

1. Air
2. Crown Layer
3. Trunk Layer
4. Understory Layer
5. Homogeneous Grass Layer
6. Homogeneous medium (ground)

All the boundaries between different layers are diffuse boundaries except between region 3 and region 4 and between region 4 and region 5 where the reflection from the interface is taken into account. The first-order iterative solution of the radiative transfer equation with the flat or rough surface boundary condition between Region 3 and Region 4 is used.

The medium is characterized by discrete scatterers, such as circular cylinders with radius  $a$  and length  $d$  to represent trunks, branches, and coniferous leaves or circular disks with radius  $R$  and thickness  $d$  to represent deciduous leaves. Other parameters such as branch distribution and the relative permittivity of scatterers have to be supplied by the user.

To take into account ground slope, the model keeps trees vertical and tilts the ground. The program uses coordinate transformation to solve for the case where the ground is horizontal but trees are tilted, then transforms the results back to the original setup.

The outputs of the model consist of:

- backscattering coefficients and one-way attenuation;
- Müller matrix, with identification of contributions from different scattering mechanisms.

## 4.4 Model tests and validation

### 4.4.1 UTOV model validation

The validation of the UTOV theoretical model has been carried out independently by the University of Valencia and by the Tor Vergata University itself. Their activities are separately summarized in the following sections.

#### Validation at UVAL

With reference to two of the three scattering models available, POLSCAT is totally polarimetric and is based on a very detailed description of the canopy architecture, while the canopy description in the UTOV model is simpler, which has some advantages for the required inputs. The performances of POLSCAT have some disadvantages due to the increase in the computational costs. Hence, the work at UVAL has focused mostly on the validation of the UTOV model.

Originally, the UTOV model had two inputs related to the vegetation: crop height and crop type (for corn or sun-flower). By means of fits to some empirical data it computed several parameters (LAI, leaf size,...) that account for a more detailed description of the canopy architecture. UVAL has slightly modified the code, so that all those parameters are initial inputs, instead of being computed by the subroutine. This is convenient when studying the variation of the predicted scattering with those variables for a wide variety of crops. The model provides five quantities as outputs: total power, and four contributions due to the stems, layer, soil and soil-vegetation interaction. In Fig. 4.2 to 4.10 those five quantities as functions of the Leaf Area Index (LAI) are shown as examples at three wavelengths and for  $vv$ ,  $hh$ , and  $hv$  polarizations. At C-band,  $\sigma_{vv}^0$  is sensitive to the canopy layer properties, as occurs in the optical domain, due to the relatively small penetration depth at that frequency, while the soil contribution is very small. In this particular case,  $vv$  and  $hh$  polarizations have very similar responses, which can be explained because the models assume a uniform distribution of the leaves. At L-band, there are two main contributions to the total  $\sigma_{vv}^0$ , i.e., from soil and from stems, as the penetration depth is larger. In this case  $\sigma_{vv}^0$  and  $\sigma_{hh}^0$  are not as similar as at C-band. For L-band  $\sigma_{hv}^0$ , the model predicts a negligible scattering for soil and stems, as is expected because there is no diffuse scattering.

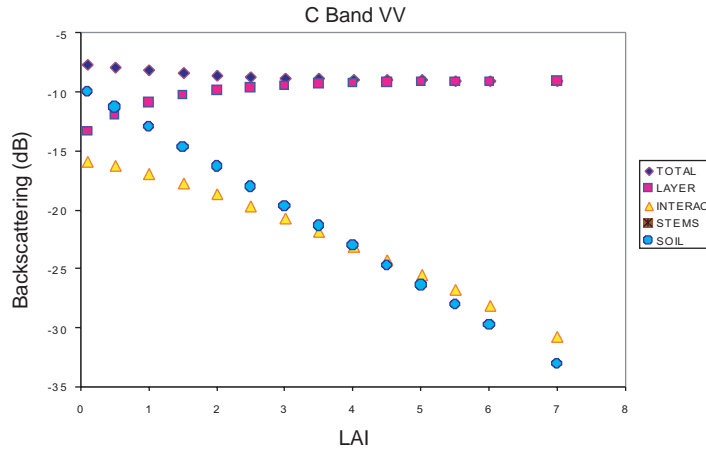


Figure 4.2: C-band  $\sigma_{vv}^0$  vs. LAI simulated by the Tor Vergata scattering model.

It can be concluded that the model reproduces qualitatively the expected results. However, as is for all theoretical models, it involves several simplifications that introduce some limitations in its applicability. The ERA-ORA UTOV model describes vegetation using two layers as shown in Fig. 4.1, and it uses a uniform distribution of the leaves. This description is suitable for plants like alfalfa or dense forest but may be less useful for plants such as corn.

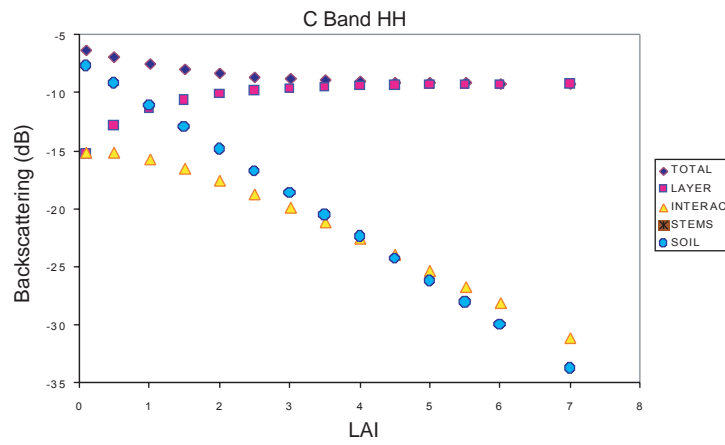


Figure 4.3: C-band  $\sigma_{hh}^0$  vs. LAI simulated by the Tor Vergata scattering model.

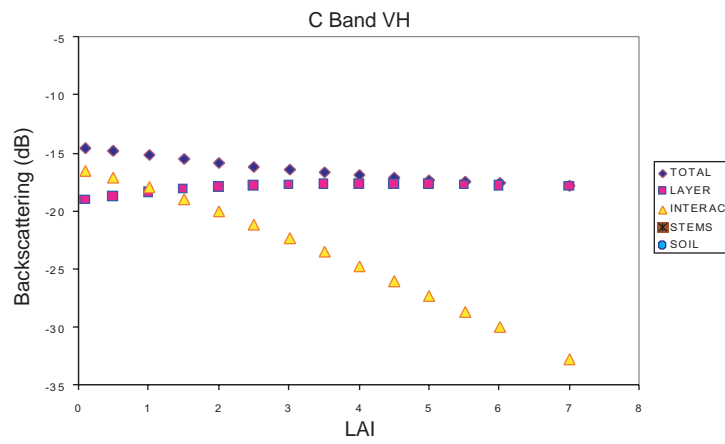


Figure 4.4: C-band  $\sigma_{hv}^0$  vs. LAI simulated by the Tor Vergata scattering model.

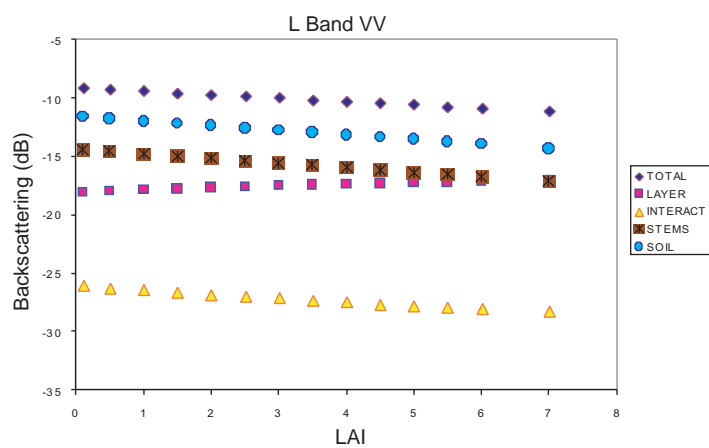


Figure 4.5: L-band  $\sigma_{vv}^0$  vs. LAI simulated by the Tor Vergata scattering model.

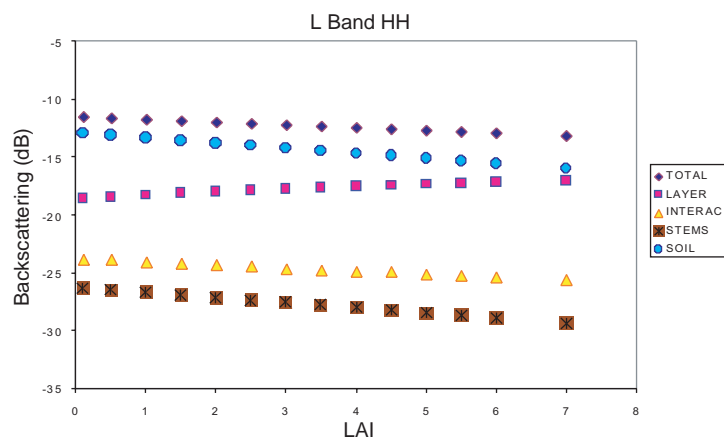


Figure 4.6: L-band  $\sigma_{hh}^0$  vs. LAI simulated by the Tor Vergata scattering model.

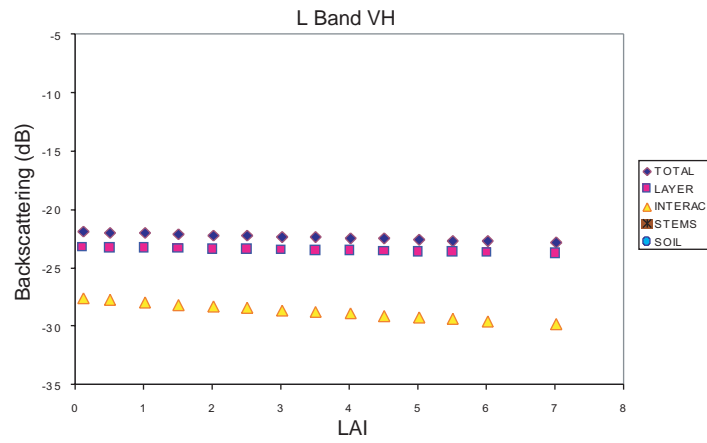


Figure 4.7: L-band  $\sigma_{hv}^0$  vs. LAI simulated by the Tor Vergata scattering model.

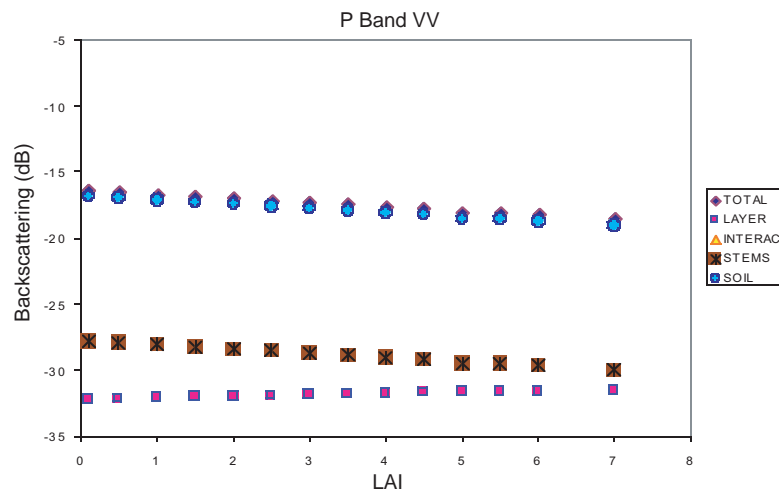


Figure 4.8: P-band  $\sigma_{vv}^0$  vs. LAI simulated by the Tor Vergata scattering model.

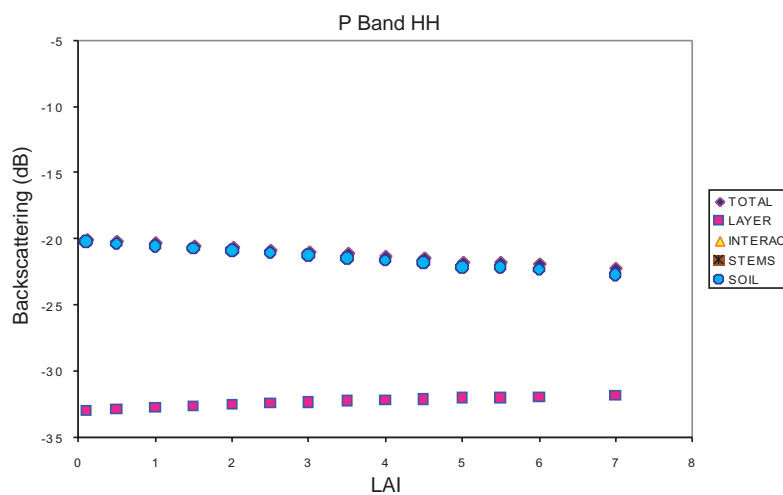


Figure 4.9: P-band  $\sigma_{hh}^0$  vs. LAI simulated by the Tor Vergata scattering model.

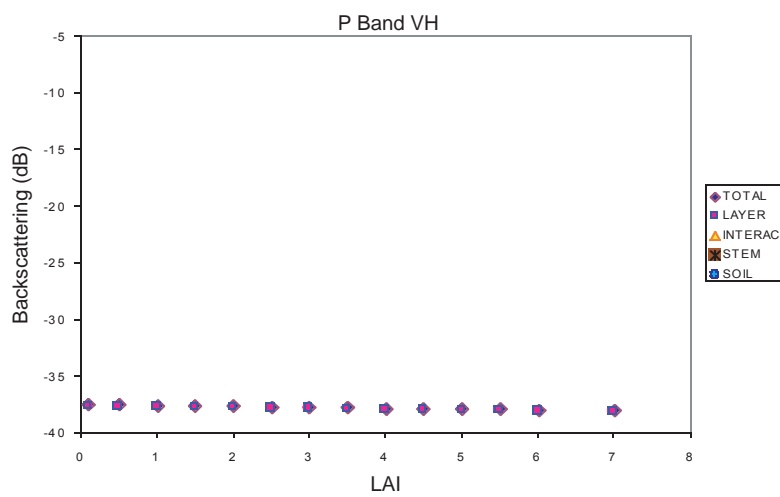


Figure 4.10: P-band  $\sigma_{hv}^0$  vs. LAI simulated by the Tor Vergata scattering model.

### Validation at UTOV

A first validation of the Tor Vergata model has been performed using the model in its passive version. The emissivity simulations were compared with passive measurements carried out with the PORTOS radiometer in 1993 on a wheat field at Avignon (F), provided by INRA, Avignon. This situation was chosen since, during that experiment, an extensive ground truth campaign was carried out ensuring the completeness and reliability of the parameters to be input to the model. In particular, the following vegetation and soil parameters were measured:

- Fresh and dry biomass of leaf, stem, ears and total
- Volume fraction of leaf, stem, ears and total
- Stem density
- Leaf Area Index
- Dimensions of stems, ears and leaves
- Gravimetric and volumetric soil moisture content at 8 depths between 0 and 10 cm
- Roughness standard deviation and correlation length of soil

The measurements (both radiometric and botanical) took place from day of year n.108 to day of year n.180, that is following the whole development cycle of wheat. The revisit time was 3 days. Two of the most significant ground data (soil moisture content and total biomass) are reported in Fig. 4.11.

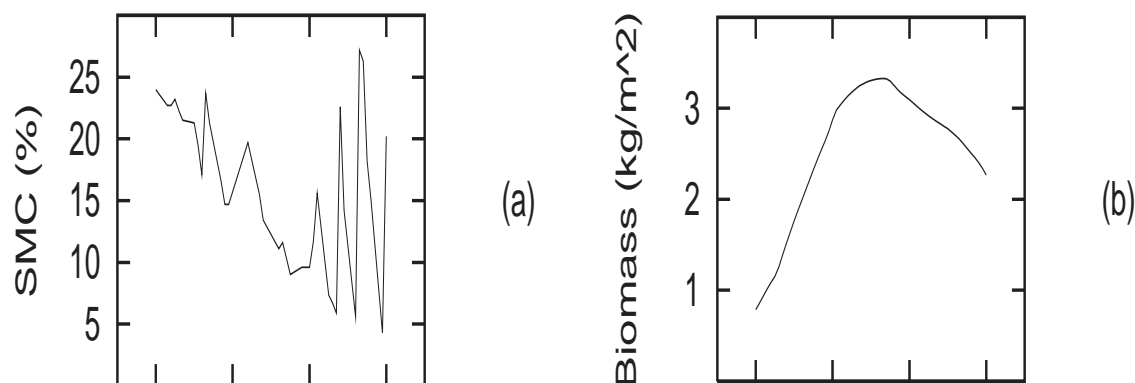


Figure 4.11: Soil moisture content (a) and biomass (b) measured at Avignon on a wheat field during the Portos experiment in 1993.

This extensive set of ground truth data was used as input to the Tor Vergata model that simulated the temporal emissivity trend of wheat at L-, C- and X-band.

The particular geometry of a wheat crop has been introduced, taking benefit from the above mentioned model flexibility. We have considered a lower layer filled with thin vertical cylinders, representing stems, and an upper layer filled with elliptical discs and vertical cylinders, representing leaves and ears, respectively. As far as leaf orientation is concerned, the data available in the literature are sparse and

spread, varying from the almost uniform distributions given in [22] to those of [23], where an erectophile behaviour is indicated for particular wheat species, like Arcane. In the absence of more detailed information, we have kept the basic assumption of a uniform distribution.

The number of stems per  $\text{m}^2$  has been derived from ground data. Also the dimensions of ears and stems have been taken by ground measurements; since stems are partially hollow cylinders, the diameter of a solid cylinder with the same volume has been considered. The leaf (disc) thickness was directly measured, while the number of discs per unit surface has been derived from the measured total leaf volume per unit area. The gravimetric moisture  $m_v$  was measured for all vegetation constituents, i.e. stems, leaves and ears; we have derived the permittivity from  $m_v$  by fitting the low-moisture data of [24] for  $m_v \leq 0.5$ , while we have used the high-moisture formula of [25] for  $m_v > 0.5$ .

At L-band we have taken the average gravimetric SMC in the 0-3 cm range; average values in the 0-1 cm and the 0-0.5 cm ranges have been taken at C-band and at the higher frequencies, respectively. The soil permittivity has been derived by computing the volumetric SMC and using the semiempirical formula of [26]. A bulk density of  $1.43 \text{ g}\cdot\text{cm}^{-3}$  was measured.

Soil roughness was measured at the end of crop development; the surface height standard deviation  $\sigma_z$  was in the range 0.4-0.9 cm, while the correlation length  $l_c$  was in the range 5-11 cm.

Details about ground measurements collected at Avignon and related model simulations can be found in [8].

The model results at an observation angle of 30 degrees, with superimposed experimental data, are reported in Figs. 4.12. Good agreement is shown at the three reported frequencies, and the temporal trend is also well reproduced by the model.

The SAR data available in the ERA-ORA D.D.L. were also used to directly validate the Tor Vergata model, in particular, the data collected by ERS over the Driffield site (UK) in 1997 (13 overpasses over 3 fields) and the Orgeval site (F) in 1996 (10 overpasses over 1 field) and in 1997 (9 overpasses over 1 field). In the period of the ERS data takes, the following vegetation and soil parameters were also measured:

At Driffield:

- Soil moisture
- Roughness standard deviation and correlation length of soil
- Total dry biomass
- Total Volume fraction
- Stem density
- Leaf Area Index
- Moisture content of crop components

At Orgeval:

- Soil moisture
- Roughness standard deviation and correlation length of soil
- Crop height

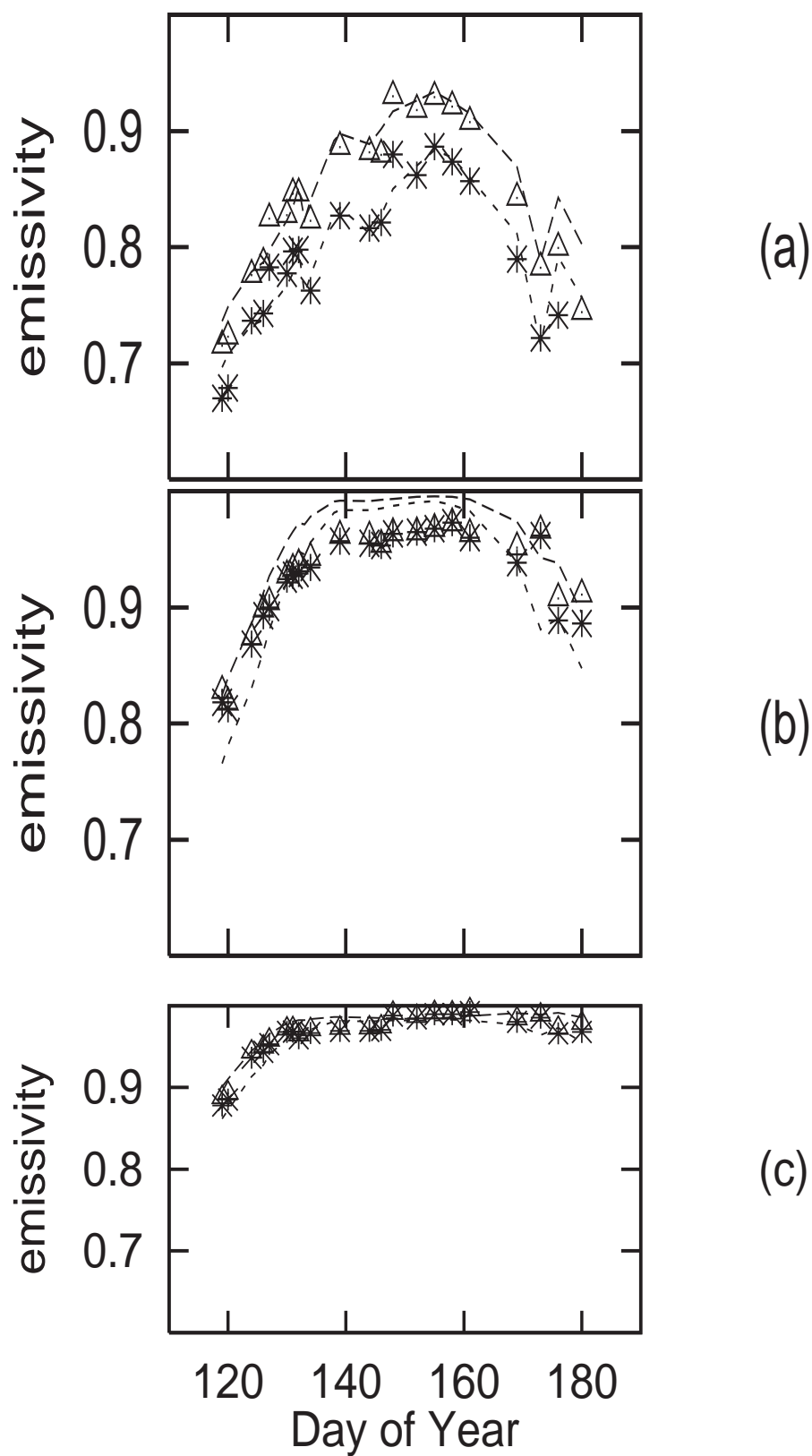


Figure 4.12: Tor vergata model validation with passive data measured at Avignon on a wheat field during the Portos experiment in 1993. Model results are reported by lines; experimental data are reported by stars (horizontal polarization) and triangles (vertical polarization). a) L-band. b) C-band. c) X-band.

The lack of a complete set of vegetation measurements did not allow a direct simulation of radar measurements. To this end, the Driffield and Orgeval ground data had to be integrated with the ones derived from the Avignon campaign. The possibility that the crop cycle were shifted in time, and that it had a different duration was taken into account. Also the possibility that the crop were more or less developed was considered. Summarizing, the geometrical data not available for the Driffield and Orgeval sites (that is stem, ear and leaf dimensions) were calculated with the aid of Avignon data through the following relationship:

$$V_i(DoY) = K \cdot V_{iA}(a \cdot DoY + b)$$

where  $V_i$  are the Driffield and Orgeval parameters,  
 $V_{iA}$  are the Avignon ground data,  
 $K$  is the development factor (0.5, 1, 1.5),  
 $a$  and  $b$  are factors which modify the temporal cycle.

First of all,  $a$ ,  $b$  and  $K$  were selected in order to match multitemporal patterns of data available at Driffield and Orgeval. Examples of this “assimilation” procedure are reported in Figs. 4.13. In these plots the LAI and Biomass, measured over one field of the Driffield site, indicate that the wheat growth cycle is longer and earlier with respect to that measured in Avignon, and also that the English crop is denser than the French one.

Secondly, the  $a$  and  $b$  parameters obtained by fitting the experimental data with the curve reported in Figs. 4.13 were used to calculate the missing geometrical parameters. Stem height obtained in this way is shown in Fig. 4.13 (c) as an example. Note that no development factor  $K$  was applied to obtain the plant geometrical variables, that is stem, ear and leaf dimensions, since it was supposed that fully grown plants cannot be bigger than a certain amount.

Following this procedure, all input parameters necessary to the model were calculated, and the backscattering coefficient as a function of DoY was simulated. The results are reported in Figs. 4.14, where also the ERS backscattering coefficients are reproduced as a function of time.

In Figs. 4.15 the simulations and the SAR measurements related to the site at Orgeval are reported. Beside each plot, the crop height obtained with the same assimilation procedure applied on the Driffield data, is also shown.

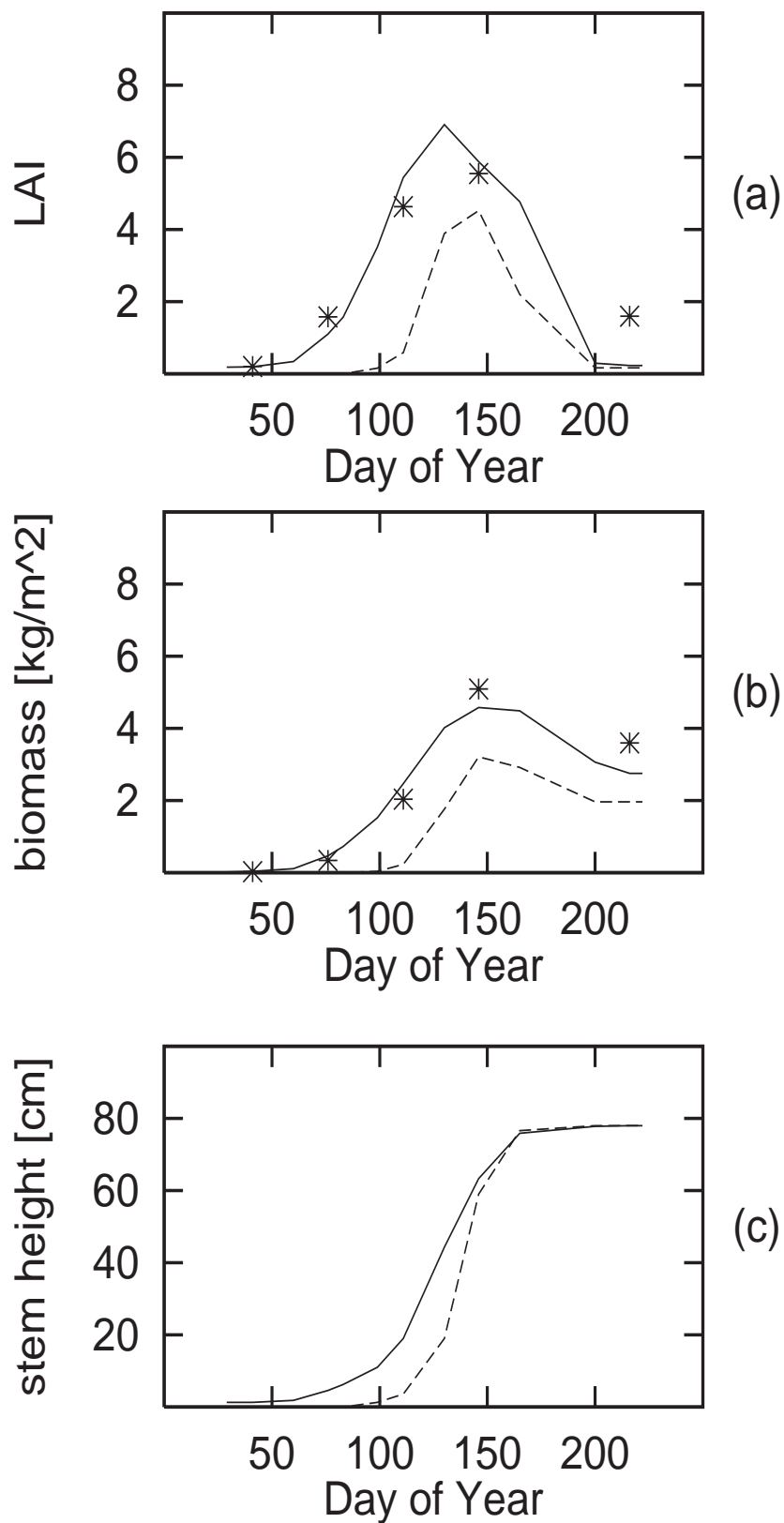


Figure 4.13: LAI (a) and biomass (b) measured on a wheat field at Driffield in 1997 (stars) and at Avignon in 1993 (dashed lines). The continuous lines represent the results of the “assimilation” procedure described in the text. (c) Stem height, same legenda as in (a) and (b). No ground data were measured at Driffield for this parameter.

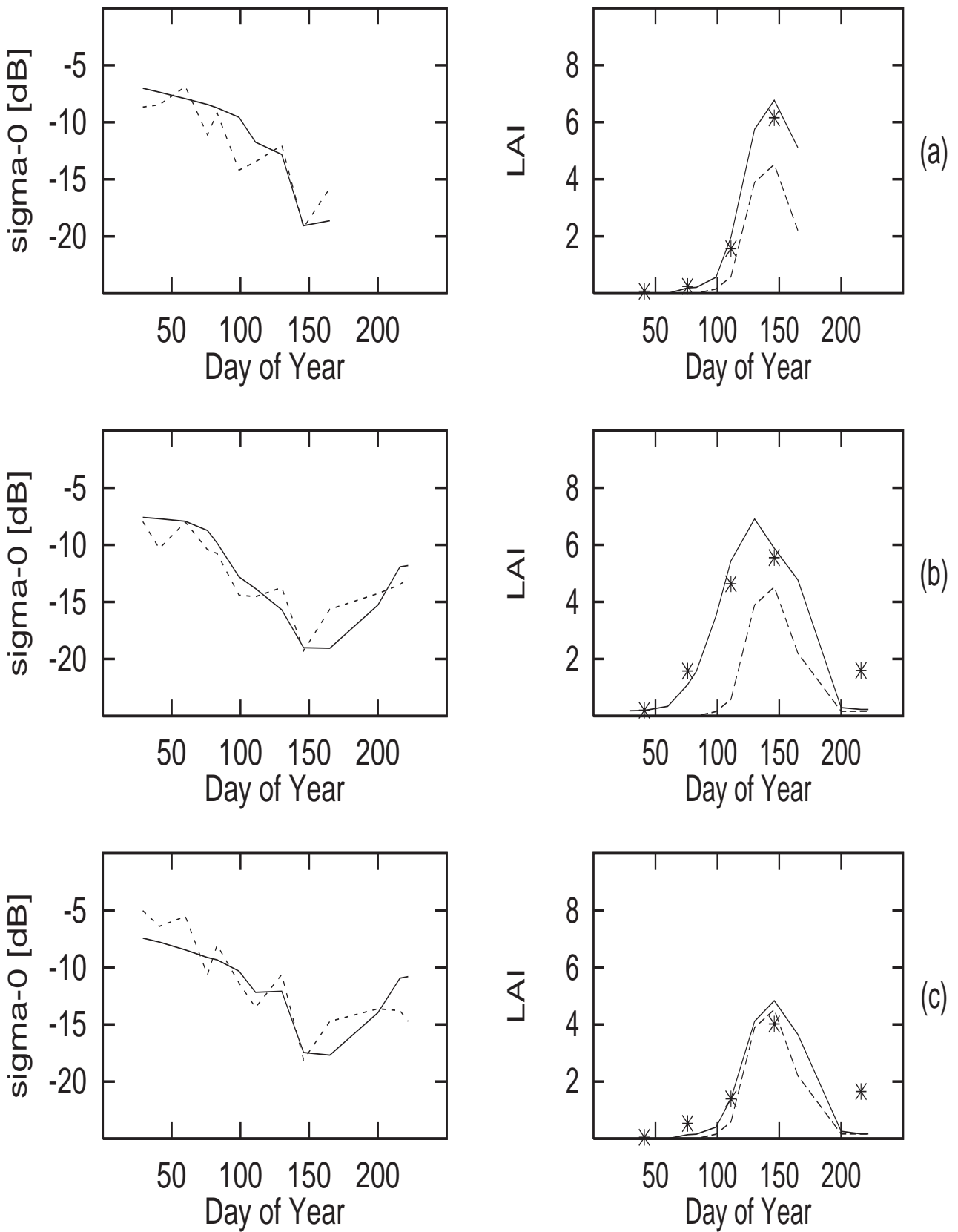


Figure 4.14: Left column: Comparison between data measured by ERS (dashed lines) at the Driffield site and Tor Vergata model results (continuous lines). Right column: LAI measured at Avignon (dashed line), measured at Driffield (stars), input to the model (continuous line). Three studies are presented: field 2 (row a), field 3 (row b), field 5 (row c).

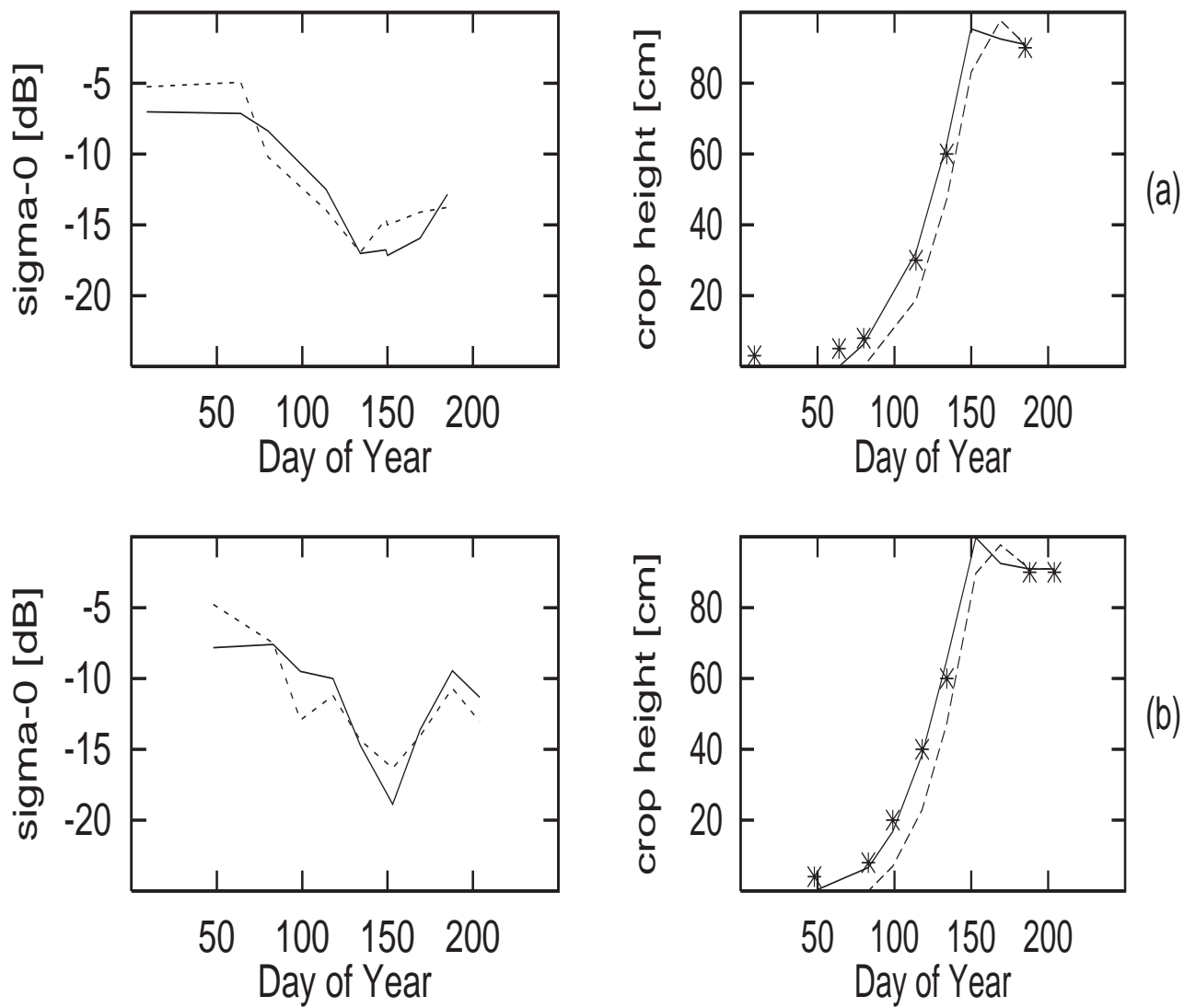


Figure 4.15: Left column: Comparison between data measured by ERS (dashed lines) at the Orgeval site and Tor Vergata model results (continuous lines). Right column: Crop height measured at Avignon (dashed line), measured at Orgeval (stars), input to the model (continuous line). Two studies are presented: 1996 data (row a), 1997 data (row b)

### 4.4.2 POLSCAT model test and validation

#### Examples of results

Some examples of the results that can be obtained by the *POLSCAT* model and computer code are presented in the following.

**Forest** Detailed results are presented for a typical secondary forest in Ivory Coast, using ground data provided by the VITO Institution (Belgium). Figs. 4.16, 4.17 and 4.18 show the contributions of the various scattering mechanisms for 3 frequencies and 3 polarisations as functions of the incidence angle. Fig. 4.19 is a comparison of the total backscattering coefficients for the three frequencies. Figs. 4.20 and 4.21 show the co-polar and cross-polar signatures for the secondary forest, while Figs. 4.22 and 4.23 give detailed co-polar and cross-polar signatures respectively of the four main scattering mechanisms. Finally, Fig. 4.24 compares the signatures of the trunk-ground mechanism with that of a dielectric dihedral reflector, with vertical and horizontal planes permittivities equal to the trunk and ground permittivities respectively.

**Low vegetation** Results for low vegetation cases, described by one layer of mixed leaves and stalks above ground are shown in Fig. 4.25, which displays the backscattering coefficients from mature maize at the three polarisations and for the same frequency bands as previously. Fig. 4.26 shows the same information for natural savanna in Ivory Coast, with input data also provided by the VITO Institute.

**Sensitivity analysis** The last examples are concerned with sensitivity analysis. Fig. 4.27 shows the comparison between the relative contributions from leaves and branches in a teak plantation in Ivory Coast (ground data from VITO) at  $20^\circ$  incidence angle, 3 frequency bands and 3 polarisations. The four cases displayed are:

1. normal situation, leaves of 17 cm average radius,
2. smaller leaves of 10 cm average radius, with leaf density adjusted in such a way that the leaf biomass is unchanged,
3. branches suppressed
4. leaves suppressed.

From Fig. 4.28, the effect of vegetation variability for natural savanna can be appreciated. The variability is introduced in the input file by the element size, orientation and vertical distribution pdf's. The backscattering coefficients with the variability included (continuous lines) are compared with those obtained by reducing the geometric dimensions and orientations distributions to a minimum (only symbols). Some influence of the variability on the response, principally at C-band can be observed.

It should be pointed out that the results shown in this report are only preliminary results from the updated version of the code. They need to be carefully analysed and compared with experimental data and with the outputs from other models. As an example, a comparison of Fig. 4.28 with similar results presented previously [27, figure 4] would seem to indicate some discrepancies for the same situation.

However, the differences are related to the improvements introduced into the computer code. The results in [27, figure 4] were based on the old version of the code, where the leaves and stalks were placed in separate layers; also the stalks were assumed to be oriented exactly along the vertical. In the new version, the leaves and stalks are mixed in the same layer, which corresponds to the real situation, and the stalk orientation is not strictly vertical. This example indicates how important it is to have a model as close as possible to the physics of the scene.

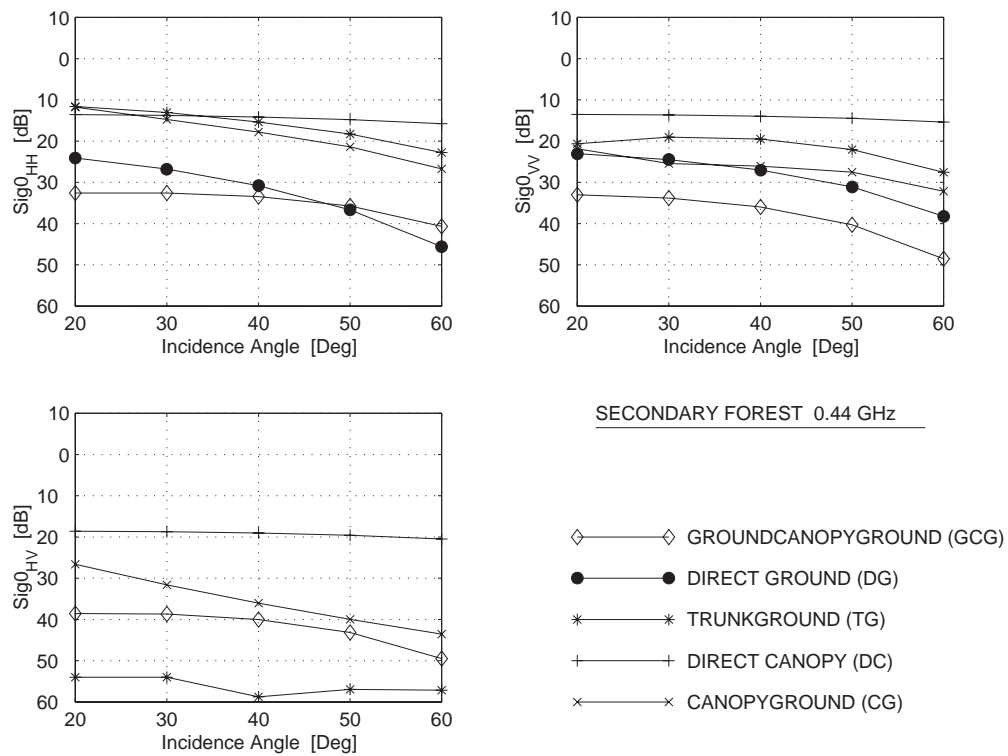


Figure 4.16: Secondary forest: backscattering contributions from various mechanisms at 0.44 GHz, for  $hh$ ,  $vv$  and  $hv$  polarisations.

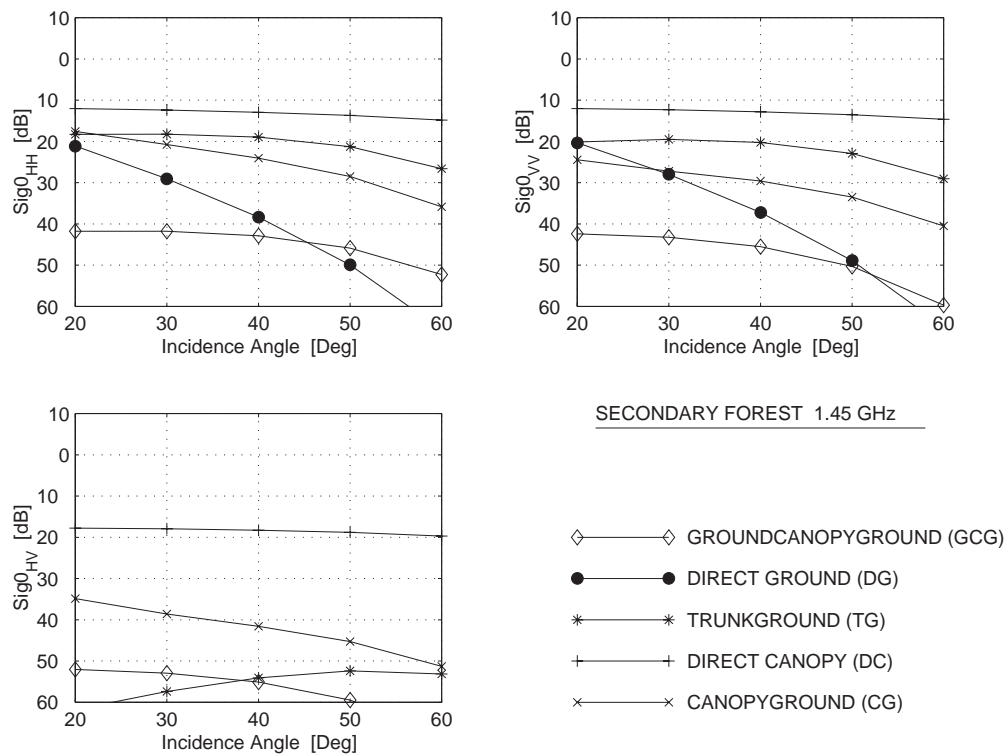


Figure 4.17: Secondary forest: backscattering contributions from various mechanisms at 1.45 GHz, for  $hh$ ,  $vv$  and  $hv$  polarisations.

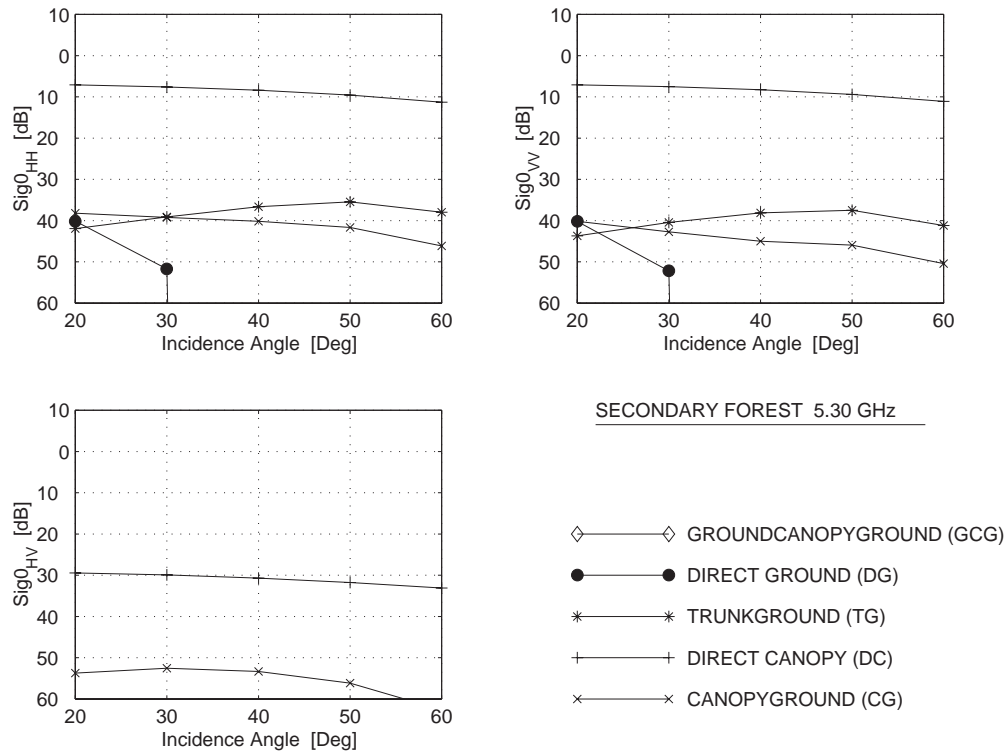


Figure 4.18: Secondary forest: backscattering contributions from various mechanisms at 5.30 GHz, for  $hh$ ,  $vv$  and  $hv$  polarisations.

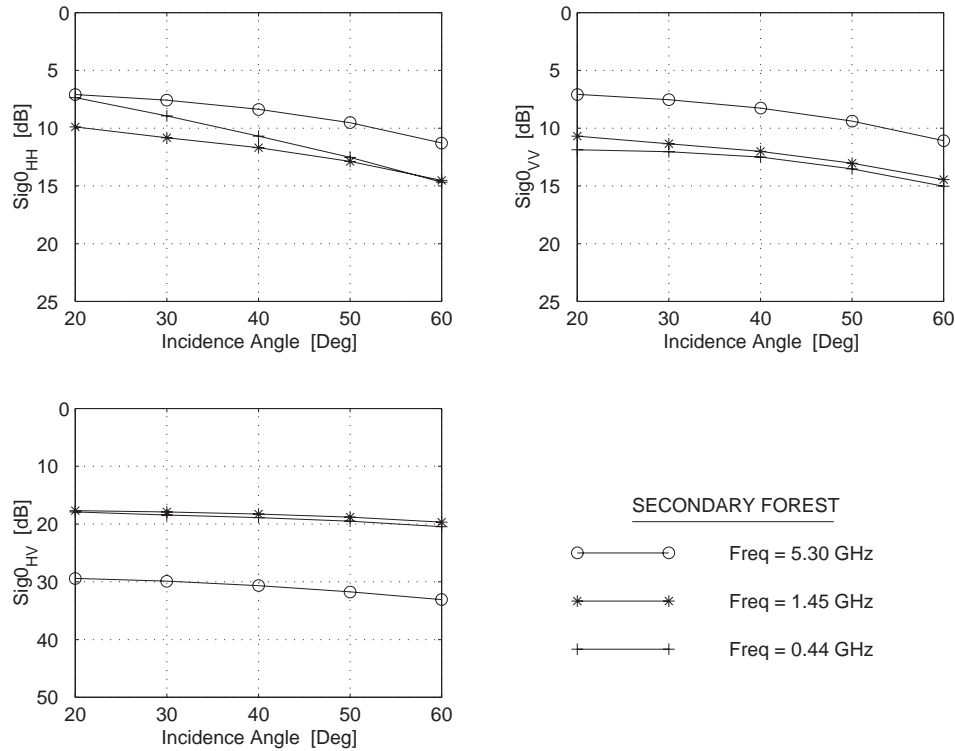


Figure 4.19: Secondary forest: total contributions at 0.44, 1.45 and 5.30 GHz, for  $hh$ ,  $vv$  and  $hv$  polarisations.

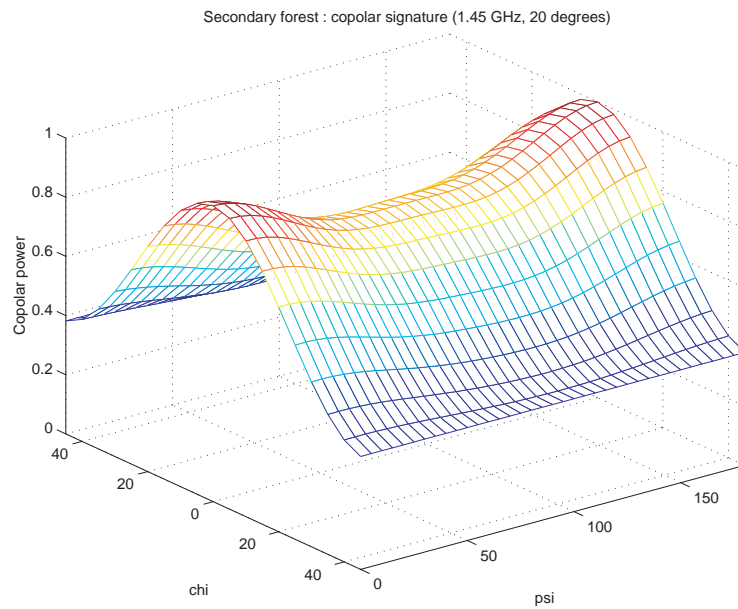


Figure 4.20: Secondary forest: copolar signature (1.45 GHz, 20°).

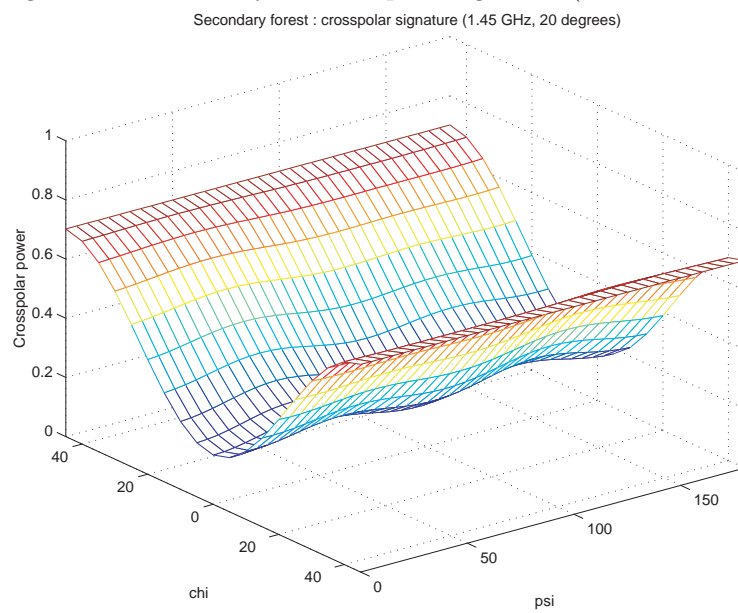


Figure 4.21: Secondary forest: crosspolar signature (1.45 GHz, 20°).

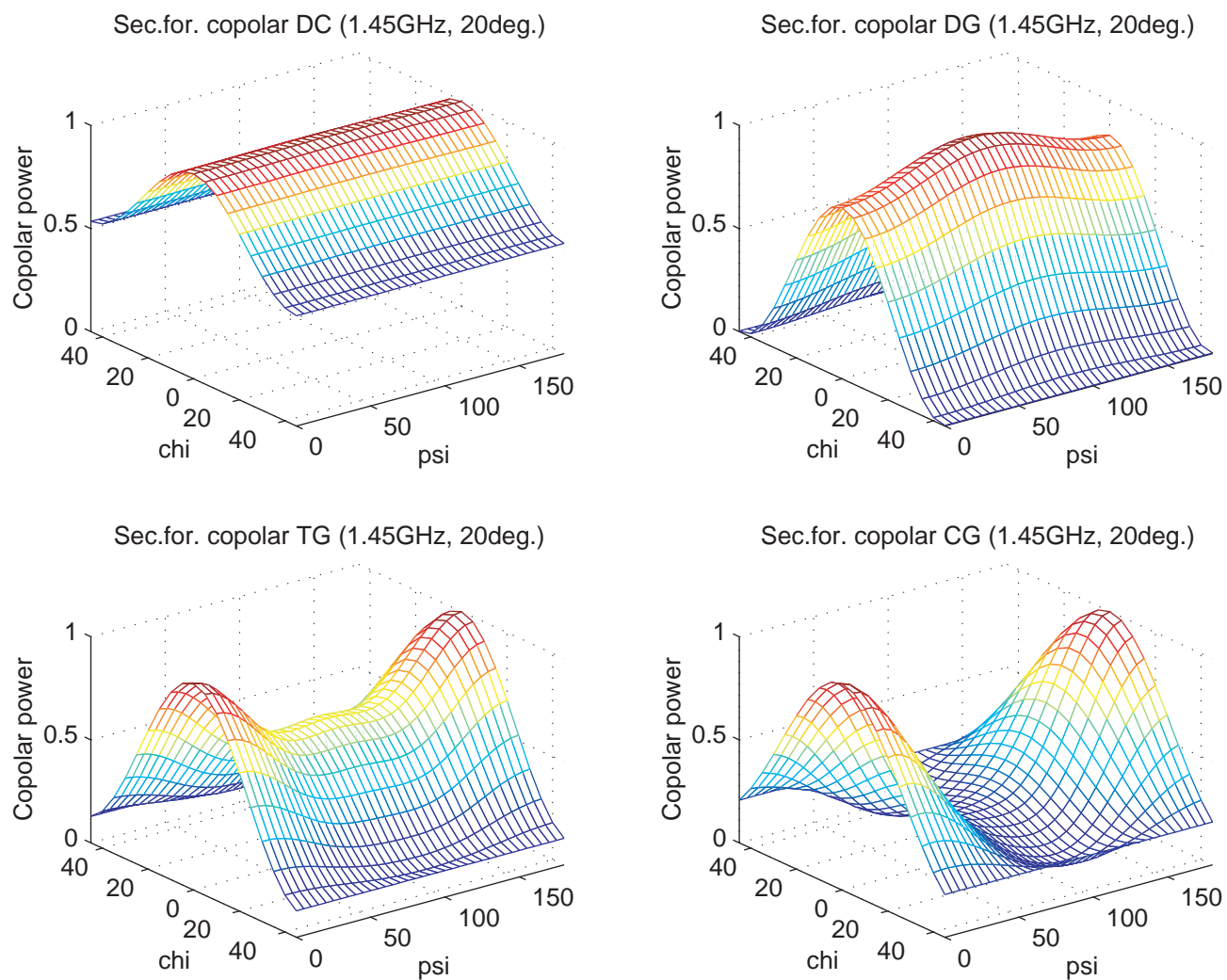


Figure 4.22: Secondary forest: copolar signatures of four separate mechanisms (1.45 GHz, 20°).

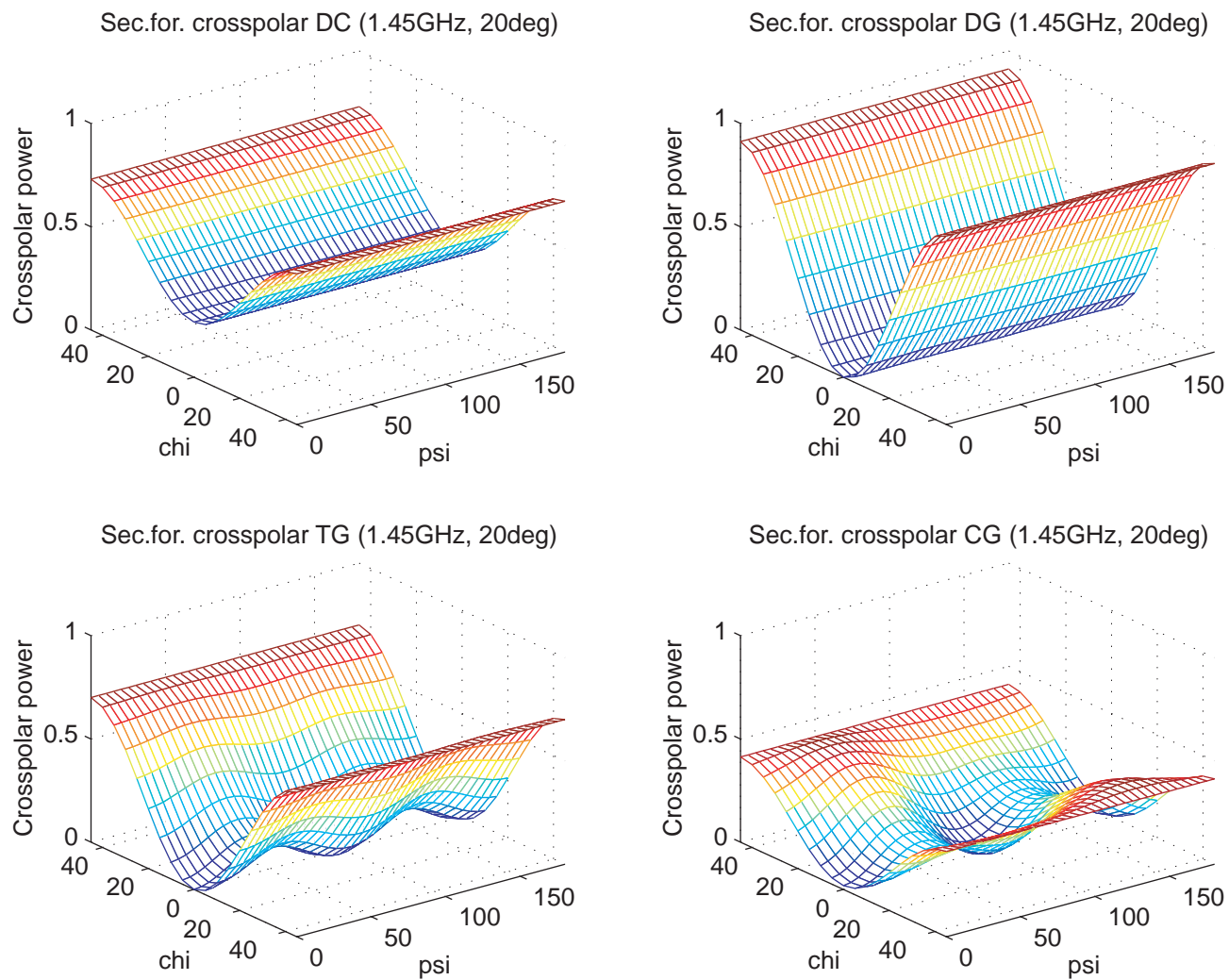


Figure 4.23: Secondary forest : crosspolar signatures of four separate mechanisms (1.45 GHz, 20°).

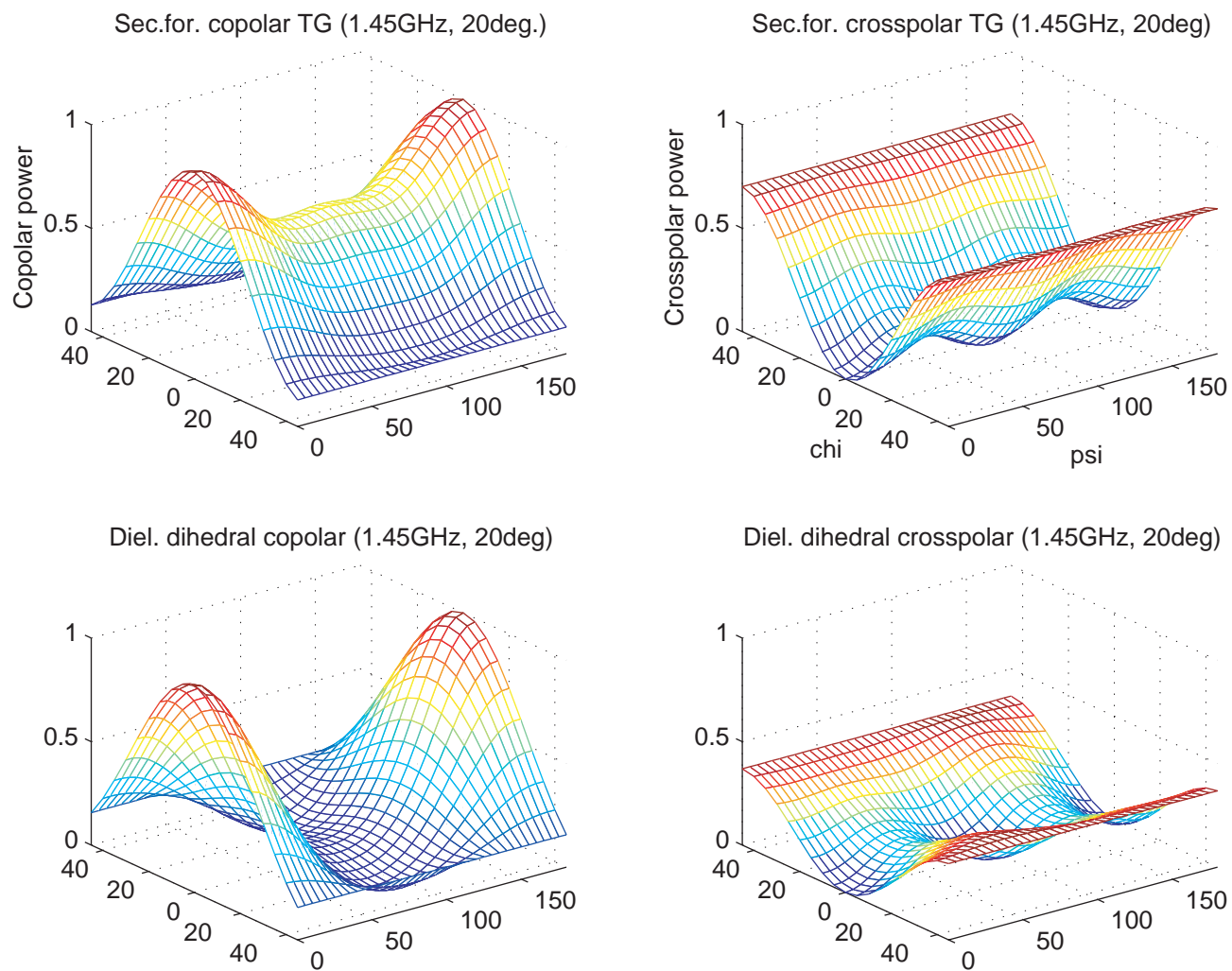


Figure 4.24: Comparison of signatures for TG mechanism and for dielectric dihedral (1.45 GHz, 20°,  $\epsilon_{-tr} = 16.4-j5.3$ ,  $\epsilon_{-soil} = 26.4-j7.3$ ).

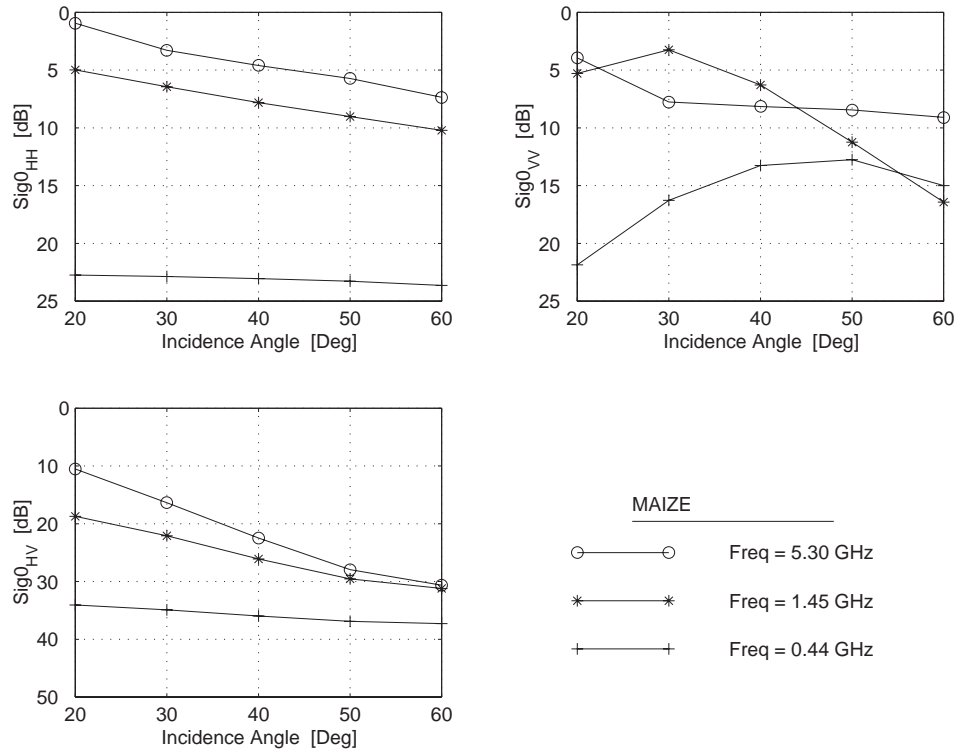


Figure 4.25: Backscattering from mature maize for three frequency bands (P, L and C) and three polarisation combinations.

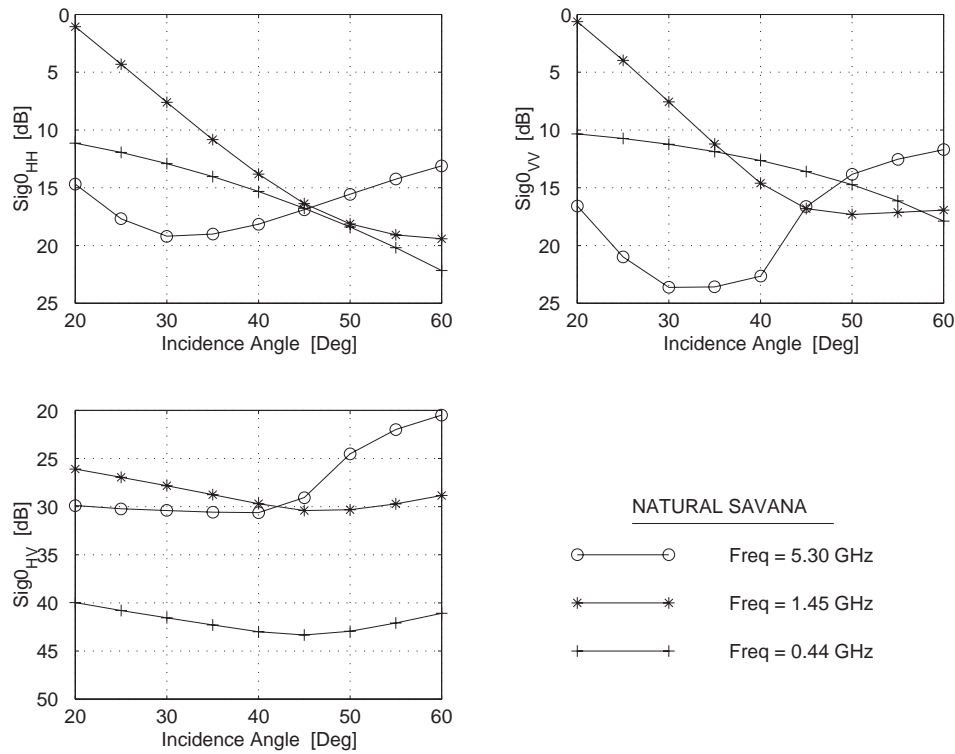


Figure 4.26: Backscattering from natural savanna for three frequency bands (P, L and C) and three polarisation combinations.

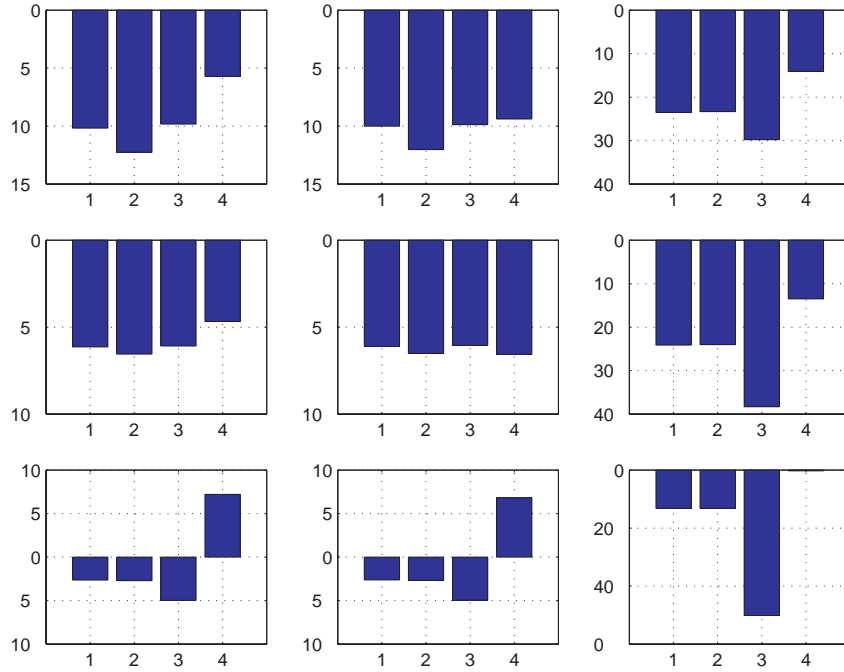


Figure 4.27: Backscattering by a teak plantation for three frequency bands and three polarisation combinations for the four cases detailed in the text.

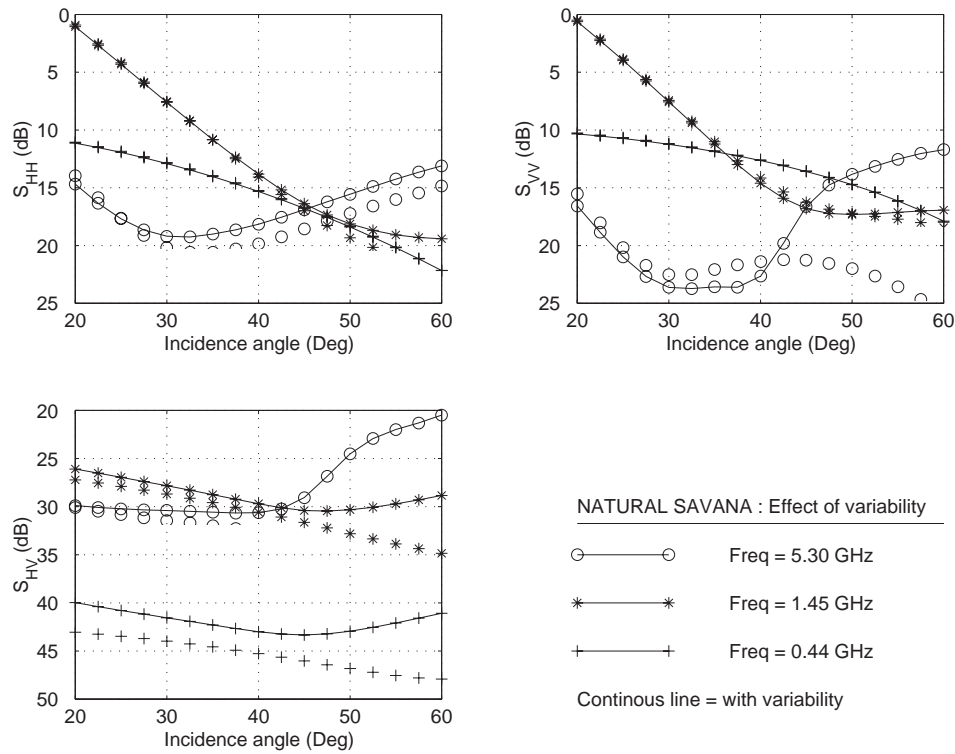


Figure 4.28: Backscattering by a natural savanna for three frequency bands (P, L and C) and three polarisations combinations: effect of natural variability.

# Bibliography

- [1] P. Ferrazzoli, L. Guerriero, and D. Solimini, "Numerical model of microwave backscattering and emission from terrain covered with vegetation," *Applied Computational Electromagnetic Society Journal*, vol. 6, pp. 175-191, 1991.
- [2] P. Ferrazzoli and L. Guerriero, "Interpretation and model analysis of MAESTRO-1 Flevoland data," *International Journal of Remote Sensing*, vol. 15, pp. 2901-2915, 1994.
- [3] P. Ferrazzoli, L. Guerriero, S. Paloscia, and P. Pampaloni, "Modeling X and K<sub>a</sub> band emission from leafy vegetation", *Journal of electromagnetic Waves and Applications*, vol. 9, pp. 393-406, 1995.
- [4] P. Ferrazzoli and L. Guerriero, "Radar sensitivity to tree geometry and woody volume: a model analysis," *IEEE Trans. Geosci. Remote Sensing*, vol. 34, pp. 433-443, 1995.
- [5] P. Ferrazzoli and L. Guerriero, "A fully polarimetric multiple scattering model for crops," *IEEE Trans. Geosci. Remote Sensing of the Environment*, vol. 54, pp. 170-179, 1995.
- [6] P. Ferrazzoli and L. Guerriero, "Passive microwave remote sensing of forests: a model investigation," *IEEE Trans. Geosci. Rem. Sens.*, vol. GE-33, pp. 360-371, 1996.
- [7] P. Ferrazzoli, L. Guerriero, and G. Schiavon, "Experimental and model investigation on radar classification capabilities," *IEEE Trans. Geosci. Rem. Sens.*, vol. GE-37, pp. 960-968, 1999.
- [8] P. Ferrazzoli, J.-P. Wigneron, L. Guerriero, and A. Chanzy, "Multifrequency emission of wheat: modeling and applications," *IEEE Trans. Geosci. Rem. Sens.*, vol. GE-38, pp. 2598-2607, 2000.
- [9] A. Guissard, and S. Matusiak, POLSCAT - UCL *polarimetric radiative transfer model - user manual*, Internal reports, Université Catholique de Louvain, Laboratoire de Télécommunication et Télédétection, Place du Levant, 2, B1348 Louvain-la-Neuve, Belgique, pp. 45, September 2000.
- [10] C.C. Hsu, H. Han, R.T. Shin, J.A. Kong, A. Beaudoin, T. LeToan, "Radiative transfer theory for polarimetric remote sensing of pine forest", *Int. J. of Rem. Sens.*, 15, pp. 2943-2954.
- [11] R. Schiffer, and K.O. Thielheim, "Light scattering by dielectric needles and disks," *J. Appl. Phys.*, vol. 50, pp. 2476-2483, 1979.
- [12] D. M. Le Vine, R. Meneghini, R. H. Lang, and S. S. Seker "Scattering from arbitrarily oriented dielectric disks in the physical optics regime," *Journal of the Optical Society of America*, vol. 73, pp. 1255-1262, 1983.

- [13] M. A. Karam and A. K. Fung, "Electromagnetic scattering from a layer of finite length, randomly oriented, dielectric, circular cylinders over a rough interface with application to vegetation," *Int. J. Remote Sensing*, vol. 9, pp. 1109-1134, 1988. ‘
- [14] M. A. El-Rayes and F. T. Ulaby, "Microwave dielectric spectrum of vegetation - Part I: Experimental observations," *IEEE Trans. Geosci. Rem. Sens.*, vol. GE-25, pp. 541-549, 1987.
- [15] P. Beckmann and A. Spizzichino, *The scattering of electromagnetic waves from rough surfaces*, Pergamon Press, 1963.
- [16] R. Schiffer, "Reflectivity of a slightly rough surface," *Applied Optics*, vol. 26, pp. 704-712, 1987.
- [17] A. K. Fung, *Microwave scattering and emission models and their applications*, Norwood: Artech House, 1994.
- [18] F.T. Ulaby, and C. Elachi, *Radar polarimetry for geoscience applications*, Artech House, Norwood, MA, USA, 1990.
- [19] A. Guissard, "Mueller and Kennaugh matrices in radar polarimetry", *IEEE Trans. Geosc. Remote Sensing*, 32, pp. 590-597, 1994.
- [20] A. Guissard, *Introduction to radar polarimetry*, Internal report, Université Catholique de Louvain, Laboratoire de Télécommunication et Télédétection, Place du Levant, 2, B1348 Louvain-la-Neuve, Belgique, pp. 89, November 2000.
- [21] F. T. Ulaby, R. K. Moore, and A. K. Fung, *Microwave Remote Sensing: Active and Passive*, vol.II-*Surface Scattering and Emission Theory*, Reading, MA: Addison-Wesley, 1982.
- [22] N. S. Goel and D. E. Strebel, "Simple Beta distribution representation of leaf orientation in vegetation canopies," *Agronomy Journal*, vol. 76, pp. 800-802, 1984.
- [23] F. Baret, "Contribution au suivi radiometrique de cultures de cereales", Thesis, University of Paris Sud, Orsay, 1986.
- [24] M. A. El-Rayes and F. T. Ulaby, "Microwave dielectric spectrum of vegetation - Part I: Experimental observations," *IEEE Trans. Geosci. Remote Sensing*, vol. 25, pp. 541-549, 1987.
- [25] C. Mätzler "Microwave (1-100 GHz) dielectric model of leaves," *IEEE Trans. Geosci. Remote Sensing*, vol. 32, pp. 947-949, 1994.
- [26] F. T. Ulaby, R. K. Moore, and A. K. Fung, *Microwave Remote Sensing: Active and Passive*, vol.III-*From Theory to Applications*, Dedham, MA: Artech House, 1986.
- [27] A. Guissard, S. Matusiak, and E. Robin, "Polarimetric radiative transfer model applied to radar remote sensing of vegetation and forest cover", *Proceedings 8th International Symposium : Physical Measurements and Signatures in Remote Sensing*, Aussois, France, January 8-12, 2001, pp. 621-626, 2001.

# Chapter 5

## Towards Retrieval (WP 203)

### 5.1 Objectives

This chapter aims at showing how the modelling activities described in the previous chapter can be exploited to develop retrieval procedures. To this end, selected results of the analysis carried out by the Working Party on Retrieval (WP 203) are reported.

Results of the retrieval of vegetation parameters of wheat fields by means of ERS measurements, carried out at Tor Vergata University, are described in section 5.2, while in section 5.3 the description of a procedure for the retrieval of the soil moisture from ERS SAR data, developed at Université Paul Sabatier, is reported.

### 5.2 Retrieval of crop parameters

#### 5.2.1 General aspects

Two main variables are required in monitoring agricultural crops: soil moisture and an indicator of plant growth, such as Plant Water Content ( $\text{kg}\cdot\text{m}^{-2}$ ) or Leaf Area Index ( $\text{m}^2\cdot\text{m}^{-2}$ ). However, it is now generally agreed that backscattering coefficients are influenced by several additional soil and canopy variables. As an example, let's consider a simple canopy made by stems and leaves only, described by an incoherent model with single-scale representation of surface roughness. Even in this rather simple case,  $\sigma^\circ$  is at least dependent on eleven variables, as indicated below:

- soil moisture,
- soil height standard deviation and correlation length,
- stem height, diameter and permittivity,
- leaf length, width and permittivity,
- number of stems per unit area,

- number of leaves per unit area.

Considering all variables of a canopy as independent and retrieving all of them at every overpass would be not only difficult, but also scarcely effective. Rather, efforts towards exploiting a-priori information would be beneficial. For instance, in a given environment and a given season, reasonable links among some of the variables and with the sought canopy indicator (PWC or LAI) could be established and used in retrieval.

As already stressed, the data stored in the ERA-ORA D.D.L. are of the utmost importance for developing retrieval procedures, since they provide statistically significant and unbiased training and evaluation sets. The availability of models is also quite important for retrieval. Indeed, in Chapter 4, the model developed at Tor Vergata [1] has been employed in a direct approach: that is, given a certain multitemporal ground data set, the backscattering coefficient of vegetated surface was simulated. However, as was mentioned, ground truth data are not always available or, more often, they do not cover the whole set required as input by the theoretical model. For this reason, an “assimilation” procedure has been applied, and it has been shown that the model yields estimated  $\sigma^0$ 's vs. time which closely resemble the experimental ones. Used from another point of view, the model can become a tool of retrieval itself, since it can also be used for an inverse approach, in which available *a-priori* information on and among the canopy parameters is exploited.

### 5.2.2 Data assimilation and use of the UTOV model

In the following, an assimilation/retrieval method using a model will be suggested, which is based on the knowledge of a reference temporal trend of the parameters of a crop. That is, given a certain crop, the various geometrical and dielectric variables ( $V_{iR}$ ) have been measured in a controlled field of reference for the whole growth cycle:

$$V_{iR} = V_{iR}(DoY)_R$$

where subscript  $R$  stands for reference, and  $(DoY)_R$  is the day of year of the crop cycle of reference. Then, the assumption is made that other crops of the same type will have similar growth cycle, but shifted in time and/or with different duration. That is, the vegetation parameters  $V_i$  of a generic crop of a given type may be connected to the same parameter of the crop of reference through the following relationship:

$$V_i(DoY) = K \cdot V_{iR}(a \cdot (DoY)_R + b) \quad (5.1)$$

$a$  and  $b$  are factors which modify the temporal cycle, and  $K$  is a development factor. This corresponds to assuming that, although the crop type is the same, possible differences in measured backscattering coefficients are due to differences in the crop development cycle.

The method we proposed and tested consists of the retrieval of the  $a$  and  $b$  factors in (5.1) running an electromagnetic model in its direct mode: the a-priori known  $V_{iR}$  reference variables are input to the model, and  $a$  and  $b$  which minimize the sum of the square differences between simulated and remote sensed  $\sigma^0$  are then selected.

The method presented above has been implemented to extract vegetation parameters using the Tor Vergata model. As an example, the three wheat fields observed by ERS SAR at the Driffield site have been considered.

First, a configuration has been selected according to the radar parameters: in this case, frequency, observation angle and polarization of ERS SAR (5.3 GHz,  $23^\circ$ ,  $vv$ ). Then, for each day of observation, the following inputs have been given to the model:

- soil parameters, derived from known ground truth (height standard deviation, correlation length, soil moisture content);
- multitemporal vegetation parameters, taken from an a-priori known reference crop cycle. In our case, ground data of the Avignon wheat field mentioned in Chapter 4 [2] have been assumed.

In this way, a temporal set of simulated backscattering coefficients is produced, which are compared with the measured  $\sigma^0$ 's. The temporal trend of the model results is then modified by introducing the following variation on the temporal variable  $DoY$  (Day of Year):

$$DoY = a \cdot (DoY)_A + b$$

where  $(DoY)_A$  is the date of observation of the site of Avignon, while  $a$  and  $b$  are the factors which modify the temporal cycle, as in (5.1). In the above formula, it is assumed that a shift in development time, and a different duration of the crop cycle exists between the Avignon wheat field and the observed one.

Finally, the pair of  $a$  and  $b$  which gives the minimum rms difference between the simulated  $\sigma_0$ 's and the measured backscattering coefficients is chosen. These values are then used to retrieve the desired vegetation parameter according to the following relationship:

$$V_i(DoY) = K \cdot V_{iA}(a \cdot (DoY)_A + b)$$

where  $V_i$  is the retrieved vegetation parameter,  $V_{iA}$  are the ground data measured at Avignon, and  $K$  is a development factor.

A complete retrieval of all soil and vegetation parameters cannot be accomplished by a single-frequency, single-polarization, single-angle SAR, such that of ERS. Therefore, in our exercise, we assumed soil parameters and the  $K$  development factor to be *a priori* known.

The results are shown in Fig. 5.1. In the left column, the ERS experimental data are shown, as well as multitemporal  $\sigma^0$ 's obtained by model outputs and application of  $a$  and  $b$  selected in order to minimize rms differences. The right column compares the measured LAI's with the retrieved ones, obtained by applying the  $a$ ,  $b$  and  $K$  coefficients to data of the Avignon cycle (also shown as a reference).

The correspondence between experimental and retrieved ground data is good for fields 3 and 5, while some discrepancies are observed in field 2. However, it must be considered that the multitemporal data set was not complete in field 2. It is expected that better results could be achieved using multifrequency and/or multipolarization SAR systems.

A new inversion procedure, based on neural networks, which already proved their usefulness in a rather similar approach [3], is under development. In this case a technique similar to that previously described is implemented, where the estimation of parameters  $a$  and  $b$  is performed by means of a neural network instead of a minimization of rms differences. This kind of implementation has already been tested for the retrieval of the wheat crop cycle using radiometric data, yielding promising results [4].

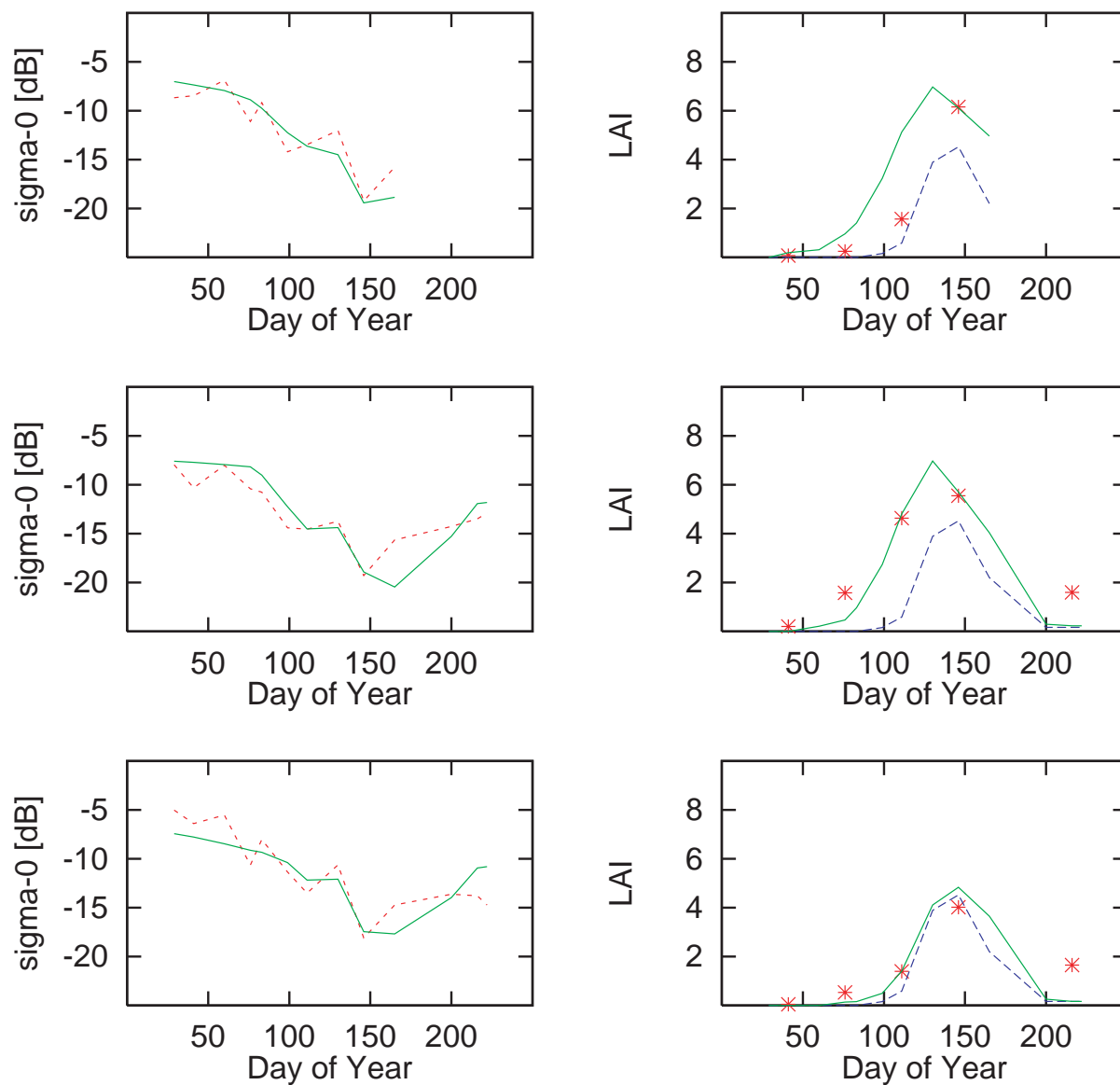


Figure 5.1: Left column: Comparison between data measured by ERS (dashed lines) at the Driffield site and the model results with minimum rms difference (continuous lines). Right column: LAI measured at Avignon (dashed line), measured at Driffield (stars), retrieved by the model (continuous line). Three cases are presented: field 2 (top), field 3 (middle), field 5 (bottom).

### 5.3 Retrieval of soil moisture

In general, the problem of retrieving soil moisture from single specification SAR data (i.e. ERS SAR data) is an ill posed problem. This happens because several surface parameters concur to determine the surface backscattering whereas only single frequency, single incidence angle and single polarisation data are available. Consequently, the same backscattering coefficient may be associated with different combinations of surface parameters and the obtained soil moisture estimate (i.e. the average between all possible solutions) is intrinsically *inaccurate*.

This ambiguity (i.e. inversion error) may be reduced either by introducing *a-priori* information about the surface status or by using multi-specification SAR data, i.e. multi-frequency, multi-incidence information.

A second aspect to be evaluated in a soil moisture retrieval algorithm is its robustness with respect to corruption of input data (i.e. calibration or model errors). More precisely, the algorithm is robust if a slight perturbation of the input SAR data will produce only a slight change in the correct soil moisture value. Such a property is ensured when an appropriate regularisation technique is exploited in the retrieval algorithm.

As a general result, the more accurate the algorithm, the less robust it is. In this respect, a trade off must be achieved.

In a recent study [7], the feasibility of retrieving soil moisture from ERS SAR data and future multi-parameter SAR systems such as ENVISAT ASAR has been investigated. The derived soil moisture retrieval algorithm is based on inverting the IEM model [5]. The inversion technique consists of a Neural Network (NN) which is trained with simulated data obtained by exploiting the IEM model (both in its single and multi-scale version [6]). Different C-band multi-specification SAR configurations are simulated. For each configuration, the impact of inversion, model and calibration errors is assessed. The main results are summarised in the following.

- For the ERS-1/2 configuration the attainable accuracy, quantified by the overall rms in the retrieved volumetric soil moisture content, is of the order  $\Delta Mv = \pm 6\%$ . The uncertainties in  $Mv$  are due almost exclusively to variations in roughness conditions which influence the relationship between soil moisture-radar backscattering coefficient.
- For a sensor configuration using two co-polarisations at the same time, the overall error (assuming a calibration error of  $\pm 0.5$  dB and an accurate direct model) in the retrieved soil moisture is reduced to  $\Delta Mv = \pm 5.2\%$  at  $23^\circ$  incidence angle.
- For a sensor imaging simultaneously at two polarisations and two incidence angles (e.g.  $23^\circ$  and  $45^\circ$ ) the best accuracy is attained. In this case, still under the hypothesis of  $\pm 0.5$  dB of calibration error and an accurate direct model, results show that soil moisture can be retrieved with an accuracy of  $\Delta Mv = \pm 3.3\%$ .

An important result of the study shows that modelling errors influence to a great extent the accuracy of soil moisture retrieval using multi-parameter SAR. This was seen in the results obtained when inverting MLS-IEM data using a NN trained with IEM data. As a consequence it would appear that forward models better adapted to the modelling of backscatter from natural surfaces such as MLS-IEM could play a crucial role in the development of retrieval algorithms for future multi-parameter systems. If the model errors can be reduced then the results show that three moisture classes may be realistically separated using multi-specification C-band SAR data provided that a reliable direct forward model is available and the calibration errors are within 0.5 dB.



# Bibliography

- [1] M. Bracaglia, P. Ferrazzoli, L. Guerriero, “A fully polarimetric multiple scattering model for crops,” *Remote Sensing of Environment*, vol. 54, pp. 170–179, 1995.
- [2] P. Ferrazzoli, J. P. Wigneron, L. Guerriero, A. Chanzy, “Multifrequency emission of wheat: modeling and applications,” *IEEE Trans. Geoscience and Remote Sensing*, vol. 38, pp. 2598–2607, 2000.
- [3] F. Del Frate, L.F. Wang, ” Sunflower biomass estimation using a scattering model and a neural network algorithm ”, *International Journal of Remote Sensing*, vol. 22, pp. 1235–1244, 2001.
- [4] F. Del Frate, P. Ferrazzoli, G. Schiavon, J-P. Wigneron, A. Chanzy, “Retrieving agricultural variables by microwave radiometry using a neural network algorithm trained by a physical model,” *Proc. IGARSS '99*, Hamburg, Germany, pp. 2134–2136, 1999.
- [5] Fung, A.K., *Microwave scattering and emission models and their applications*, Artech House, 1994.
- [6] F. Mattia, T. Le Toan, “Backscattering Properties of Multi Scale Rough Surfaces,” *J. of Electromagnetic Waves and Applications*, Vol. 13, No. 4, 1999.
- [7] Satalino, F. Mattia, M. Davidson, T. Le Toan, G. Pasquariello, M. Borgeaud, “Current limits and future perspectives of soil moisture retrieval using C-band SAR data,” submitted to *IEEE TGARS*.



## Chapter 6

# Conclusions and Recommendations

### 6.1 The Data Library (WP101)

The activity promoted by the ERA-ORA project has been successful in collecting a large amount (more than 1,500,000 measurements) and a wide assortment of radar data individually acquired by the pool of participating European experimenters in the course of various campaigns on different test sites. The variety of sensors, types of surface, climatic conditions, and dates of acquisition makes the content of the Data Distributed Library a definitely value added set. Its completeness is likely to improve the understanding of the information content of remote sensing measurements and their employment in applications such as classification of the earth surface and retrieval of necessary bio- geo-physical parameters.

The additional availability of optical/IR data allows further progress in comprehending the wave-surface interaction mechanisms over large portions of the whole electromagnetic spectrum available for remote sensing.

The present ERA-ORA data set, which is potentially useful in pushing forward the exploitation of remote sensing data by users in different fields, looks particularly appropriate to applications in agriculture.

#### 6.1.1 Data calibration

##### Remote sensing data

It is well known to many experimenters how crucial is the calibration of data in remote sensing. In particular, imaging synthetic aperture radars are complex systems whose outputs are not easily controllable. Analogous difficulties are encountered in the optical/IR domain, where atmospheric conditions and observation geometry can introduce artifacts into the measurements. As a consequence, the calibration of remote sensing data cannot be taken for granted, nor is it a trivial issue. The institutions participating in ERA-ORA in many cases rechecked the quality of their data and eventually proceeded to re-calibration, as detailed in Sect. 2.2.

Due to the obvious cost of remote sensing campaigns and processing, the final quantity of data in the D.D.L. has been kept as large as possible. On the other hand, the ERA-ORA team is aware of the fact that corrupted data can be harmful to the advancement of applications. Hence, in addition to the individual calibration efforts, a careful analysis of data has been undertaken, taking advantage of the cross-checks

allowed by the high number of measurements altogether available (Sect.2.3.3). This enhanced capability of assessing the quality of data is a further outcome of the ERA-ORA project and another *value added* by the project.

As a general consideration, the **benefits from cross-calibrating the remote sensing data stored by single institutions is stressed and possible coordination and support to this kind of activity from international institutions is recommended.**

### Ground truth data

With reference to studies and applications in agriculture, the crop ground truth present in the ERA-ORA library allows several investigations to be carried out, since in most cases available ground data provide the necessary information on important general variables like biomass, leaf area index, moisture, etc., or are at least sufficient to identify the crop status. Again, the availability of values of surface parameters measured in a variety of conditions allows intercomparisons and checks, to the benefit of accuracy, which, globally, seems adequate for the applications considered.

The situation is a little different when the use of scattering models is considered, since all inputs needed by the computer codes are not generally available to researchers. In particular, geometric data, such as dimensions and orientations of stems and leaves, or individual snow grain sizes are rarely measured. A basic consideration is that nature is complex and it is probably impossible to measure through a fairly limited set of numbers the particular features of the surface one could want as model input. Even if the approximation is pushed further, at the expense of time and cost, the numbers are probably never exactly what is found in nature. Rather, a compromise must be reached between the accuracy of a model in reproducing the signature of a single portion of a particular surface and the applicability of the model to a sufficiently wide class of surfaces.

A similar crucial issue is the characterization of the roughness of the soil surface through its r.m.s. height and correlation length, since especially the latter is difficult to measure and, moreover, may not be adequate to represent the features of the surface relevant to the wave scattering simulation by theoretical models. However, if the studies are based on a classical approach, the data present in the ERA-ORA D.D.L. are adequate in most cases.

## 6.2 Remote sensing data in agriculture (WP 201)

The library contains data taken on agricultural areas, forests, bare soil, and snow. Data relevant to the first type of surface are definitely more abundant and most of the important European crop species are represented, so that, although hydrology and, to a more limited extent, forestry, can profit from the ERA-ORA library, agriculture is expected to gain substantial benefit from it.

Within the frame of potential applications of the data and model libraries created by the project, three main topics have been considered: data synergy, model validation and retrieval algorithms. Although the considerable extent of the data base and the complexity of the modeling approaches require that studies be continued and extended, some conclusions may be presently drawn.

### 6.2.1 Classifying and monitoring crops

It is believed that the ERA-ORA data base has the potential of fostering a number of applications of remote sensing in agriculture, some of which have already been tackled within the frame of the project.

A particularly suggestive example regards the enhancement of the knowledge about radar potential in classification. In this field substantial improvements are expected from the availability of the D.D.L.

Several classification algorithms have been proposed, but in most cases they have been based on data from single sites and single years. Hence, the results could have been influenced by the peculiar environmental characteristics of one area or of one year. Analyzing the wide set of data deposited in the ERA-ORA D.L., which spans different sites and different years, allows more reliable conclusions to be drawn about the radar classification potential. Careful interpretation of data based on the available ground truth makes the process sounder. Algorithms developed and tested on the basis of polygon data, i.e., on average values, could be extended to the pixel level by exchanging full SAR images among experimenters.

A better insight into the classification potential of radar multitemporal, multi-frequency, multi-polarization patterns is attainable, because of the variety of multitemporal data, which stretch over the multi-frequency, polarimetric measurements spanning a time interval of the order of a month and the multi-year observations by the ERS SAR or by multi-frequency multi-polarization scatterometers. The improvement brought by the interferometric coherence can also be assessed.

Finally, results obtained from the variety of the ERA-ORA C-band data can be useful in predicting the expected performance of schemes exploiting the forthcoming ENVISAT signatures.

In a more general perspective, our studies confirm that radar is a valid instrument for classification among different land covers. Good classification results may be achieved both by using multitemporal data collected by satellite SAR's and by using multifrequency polarimetric data collected by single flights.

### 6.2.2 Monitoring bare soil and plant moisture

ERA-ORA has assembled data for several bare fields observed by different radars (ERS, AIRSAR, RASAM) and optical instruments (AVIRIS, TMS). Fairly conclusive studies are feasible on sensitivity to soil moisture content of both multitemporal radar observations over single fields and observations over different fields.

In addition to conventional measurements, full roughness profiles are available over the Swiss Central Plain fields, simultaneously with RASAM measurements. This means that tests and possible use of more advanced surface scattering models, requiring the full profile as input, can also be suggested.

The availability of the TerraDew radar measurements, specifically intended for plant moisture observation, provides additional value to the ERA-ORA data base and new opportunities in this field.

We observe that, in general, radar/optical synergy may be a way to improve the exploitation of SAR images and, conversely, the limited capabilities of optical data can be extended by the greater canopy penetration capabilities of radar waves. Moreover, due to the diverse interaction mechanisms, optical and radar data contain different pieces of information, so that their combination may provide more information than just adding the information coming from each source independently.

## 6.3 The Model Library (WP 102, WP 202)

The need for reliable physical models is widely recognized, not only for scientific understanding, but also for applications like retrieval, where the complexity of the interactions between electromagnetic waves and natural surfaces prevents estimating the needed parameters by simple empirical methods.

The model section of the library is unique in containing three microwave models, all based on the Radiative Transfer Theory, which are able to simulate the microwave backscattering coefficients of soil, crops and arboreous vegetation.

Tremendous efforts have been done in recent years to improve the accuracy of electromagnetic models. For surface scattering, the advanced Integral Equation Method is presently available and several advances towards a multi-scale representation of surface roughness are in progress. For vegetation scattering, the approach based on the Radiative Transfer Theory with discrete elements is widely used and, indeed, the three models available in the ERA-ORA M.D.L. are based on such a theory. Also coherent models, considering the location of scattering phase centers, have been developed by the scientific community. Presently, the correspondence between simulated and experimental data is generally good, but further refinements are needed in order to make a full and reliable use of physical models in applications, like training retrieval algorithms.

Due to the complexity of the problem, involving both a difficult electromagnetic approach and the representation of very complicated structures, the theoretical scattering models developed by the scientific community have not yet reached their complete maturity, but they are undergoing continuous evolution. The three computer codes present in the M.D.L. are intended as *frozen* versions, which, nevertheless, are very useful for a variety of applications.

It should be noted that, with some exceptions, the use of a model is generally restricted to a single research group and is validated by the limited set of data available to that group. The availability of a collection of models like that assembled by ERA-ORA, has considerable potential in advancing modelling capabilities. First of all, comparison among the output of the different codes gives indications on the features of the models in the various ranges of the input parameters, and possibly suggests modifications and improvements. Second, comparison between the theoretical estimates and the ERA-ORA ample set of measurements yields a validation procedure which is not biased by the restricted individual data sets.

As a general recommendation, **it is suggested that an extended activity of test and validation of models developed and used by different European groups be fostered and supported by the relevant international institutions.**

### 6.3.1 The problem of the model inputs

The meaningful use of a modelling computer code is quite demanding, especially in terms of understanding its features and selecting the appropriate inputs. In the approach followed in developing the three models, soil features, plant geometry, shape, dimensions and permittivity of different vegetation elements such as stem, leaf, ear, etc., are taken into account. This implies that the modelling computer codes be fed on sets of input data sufficient to characterize the relevant features of the surface whose scattering is being simulated. Although the collection of ground data stored in the ERA-ORA library is unusually complete, a major problem experienced when trying to validate a model with the available ground data is the difference between the *many* input required by the model and the *few* ground measurements. Fig. 6.1 summarizes required vs. available data. The difficulties increase with increasing bio-geo-physical detail needed by the model. Highly detailed models probably yield accurate simulation results, but require expensive ground measurements and the significance of their output might be limited to one particular realization of the ensemble of surfaces.

In principle, one means of reducing these difficulties is the use of plant growth models and/or other agricultural information. The available ground truth data, if not sufficient, can be supplemented by data provided by an architectural vegetation model, so that the canopy geometrical variables, whose values are often lacking, are derived from the more commonly measured global variables (such as plant water content, LAI, crop height, day after sowing, etc.).

A drawback of this method is the present general lack of usable growth models for many crops, and a number of issues, such as the invariance of a growth model with respect to climatic areas and conditions,

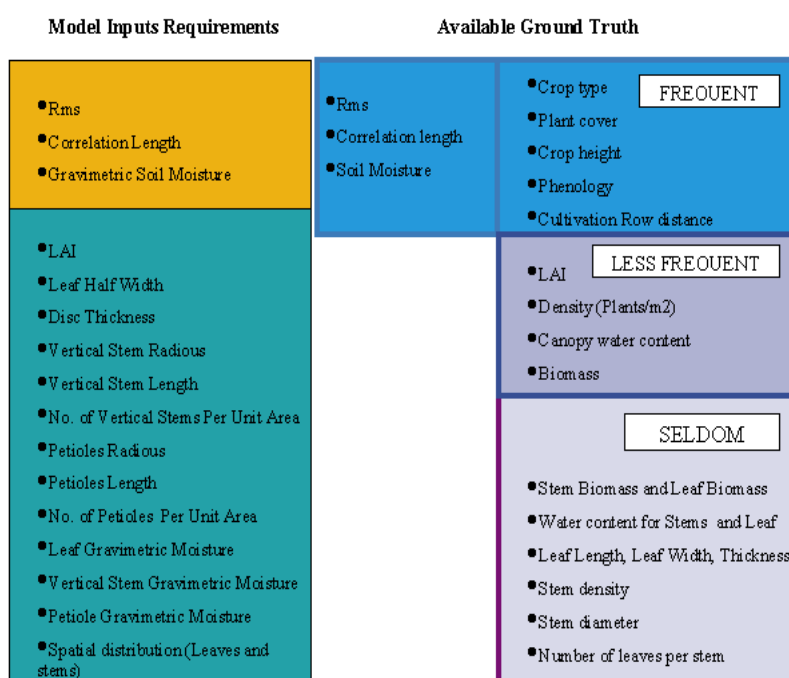


Figure 6.1:

remain open. It can be pointed out that **sponsoring and supporting an activity of development of crop growth models, involving both botanists and remote sensing specialists would be beneficial.**

As a further general consideration, in addition to continuing efforts aimed at improving the electromagnetic accuracy, the procedures to establish a correspondence between the properties of the model structure (based on simple geometries such as discs and cylinders) and the ground measured variables must be established with care and agreed among the experimenters. **New studies aimed at refining the permittivity models of leaf, stem and ear are recommended too.**

## 6.4 Towards data assimilation and retrieval (WP 203)

Retrieving the bio-geo-physical parameters of interest to applications is a primary objective of remote sensing technology. Many research groups are active in devising and developing schemes and algorithms for retrieving surface parameters from radar and optical/IR measurements. Sometimes, the retrieval procedures take advantage of theoretical scattering models. As noted before, the usually limited extent of models, remote sensing and ground data available to single groups somewhat hampers this activity and may introduce biases into the algorithms produced. The complexity of the retrieval problem, which requires calibrated data, validated models and retrieval schemes, has allowed partial progress to the scientific community.

The unusual composition and extent of the ERA-ORA library, including both many data and several models, offers new opportunities in this field. **Further extensive use of the library can be anticipated to aid progress towards retrieval of bio- geo-physical parameters and, again, promotion and support from international institutions is recommended.**

Moreover, we observe that considering many plant parameters as independent and retrieving all of them at every overpass would be difficult and scarcely useful. Efforts aimed at including a-priori information on the links among canopy (and soil, eventually) parameters into the retrieval algorithms are required. Within the ERA-ORA project, a suggestive exercise has been carried out in the case of wheat, for which detailed ground truth, measured on a French site during the whole cycle, was available. As detailed in Sect. 5.2, the retrieval method makes use of an electromagnetic scattering model, a plant growth model and a neural network algorithm. By this combination, SAR data and climatology enter a *surface processes* model approach, where radar measurements are assimilated into the information rather than being used simply to retrieve an isolated parameter.

As a general comment, for a given environment and a given season when observations are done, reasonable links among relevant bio- geo-physical variables should be established and used. Cooperation between electromagnetic and agricultural expertise is essential to this aim.

## 6.5 Suggesting future satellite radar features

On the basis of our studies, some suggestions about configurations of future radar systems for monitoring vegetation may be given. For forest applications, it is widely recognized that low frequencies ( i.e. P-band or, even, VHF band) are possibly needed, and cross-polarized data are very important. These statements are confirmed by us. For agricultural applications, some conclusions may be drawn on the basis of this study, as indicated below.

- Radar signatures are influenced by crop geometry, hence, there is not a unique sensor optimization strategy valid for all crops.
- For some crops with predominant thin stems, such as wheat and barley, interesting results have already been achieved by C-band single-polarization ERS and RadarSat. On the basis of previous studies, a similar statement is valid also for rice.
- The launch of Envisat ASAR will represent an important step, in that the availability of cross-polarization and relatively high acquisition angle will improve both the monitoring and the classification capability.
- C-band signatures suffer some limits of dynamic range, especially for wide leaf crops such as corn, potato, sugarbeet and sunflower. At least for these crops, lower frequencies (i.e. L-band) would expand the dynamic range.

In conclusion, a future satellite network including both L-band and C-band SAR's, operating at  $hh$ ,  $vv$  and  $hv$  polarization, would be optimal for agricultural applications. In a more remote future, further advantages could be achieved by polarimetry, especially for classification.

## 6.6 General conclusions and recommendations

ERA-ORA has succeeded in assembling a library of measurements and simulation software which has considerable potentiality on promoting use of remote sensing in environmental monitoring. Classification of crop types and retrieval of agricultural vegetation biomass have been specifically investigated; monitoring snow covers and soil moisture has also been considered.

The critical analysis of data and scattering modelling software has led to identifying issues which require further research and development efforts. The status of the procedures for retrieving crop biomass and soil moisture has been assessed and suggestions have been provided on possible future radar configurations intended for soil and vegetation remote sensing.

Finally, recommendations for coordination and support of the following main activities have been originated in the project:

- cross-calibrating remote sensing data stored by single institutions;
- test and validation of models developed and used by different European groups;
- development of crop growth models, involving both botanists and remote sensing specialists;
- refining the permittivity models of vegetation elements (leaf, stem, etc.);
- extensive use of the ERA-ORA library.



## Appendix A

# The Wageningen Agricultural University Data Set

### A.1 The Flevoland agricultural test site

The test site is located in Southern Flevoland, a polder reclaimed from Lake IJssel in 1966. Flevoland is an agricultural area eminently suitable for remote sensing experiments. Here, since the mid-seventies, microwave experiments have been performed on a regular basis by Dutch experimenters (the ROVE team). The land surface is flat and the soils are very homogeneous over vast areas. The agricultural parcels are large and rectangular. According to the World Soil Map (FAO) the soil can be classified as a fine textured Calcaric Fluvisol.

In the Flevoland area large parcels of about 80 ha in extent are cultivated by the development authority for the polders; the "Directie Flevoland" (DF). Usually one crop is grown per parcel. The average dimensions of these parcels are 1600 x 500 m. The cultivation by the DF is temporary and the large parcels are eventually leased to individual farmers. All farmers grow several crops within one parcel. This results in the parcels being subdivided into fields characterized by a single crop type. Typical crops for this area are potatoes, sugar beet, barley, wheat and maize. A sketch of the area is shown in Fig.A.1

### A.2 The MAESTRO-I campaign in The Netherlands.

The MAESTRO-I airborne radar campaign was carried out under the auspices of the European Space Agency (ESA) and the Joint Research Centre (JRC). It focused on the deployment of the AIRSAR, a modern polarimetric imaging radar system developed by the Jet Propulsion Laboratory (JPL) of the National Aeronautics and Space Administration (NASA). It offered the European research community the prospect of studying the capabilities of multi-band polarimetric radar data. Moreover, the introduction of P-band data, acquired simultaneous with the C- and L-band data, was recognized as being very interesting for development of certain applications, notably in forestry and soil studies. The campaign was also considered to be a good preparation for the SIR-C/X-SAR space shuttle experiment to be carried out starting in 1993. The AIRSAR as well as the SIR-C space shuttle radar systems are prototypes of the multiband polarimetric spaceborne radar systems proposed for the future Earth observing system

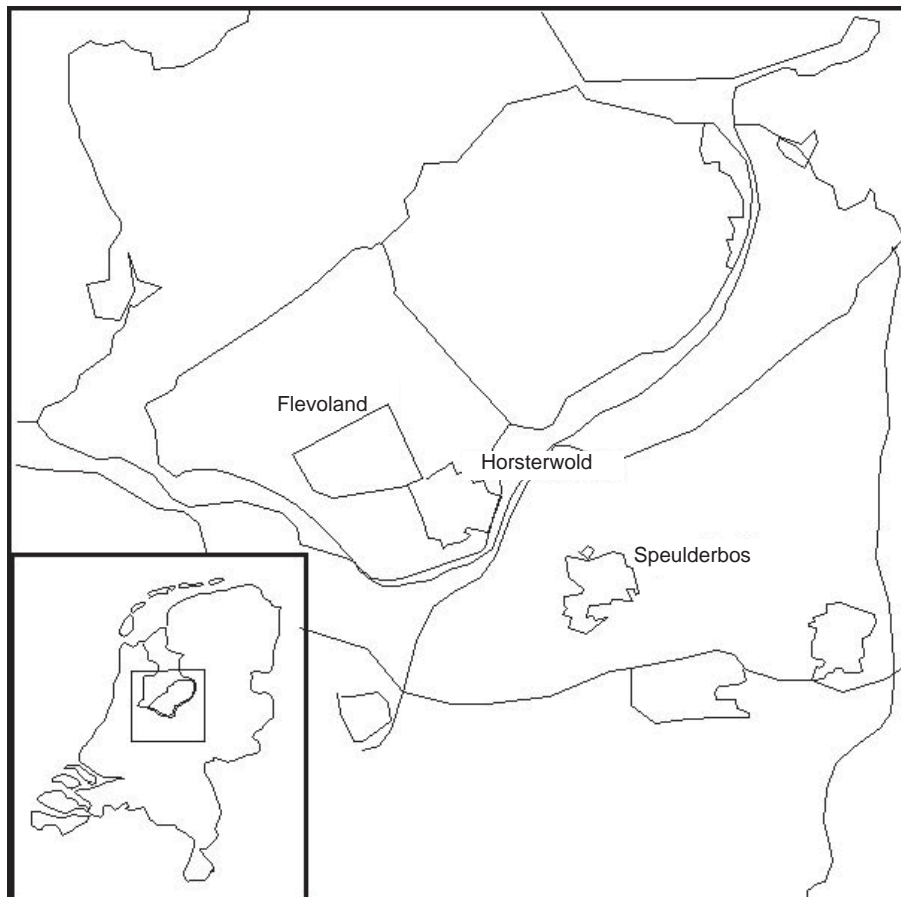


Figure A.1: Location of Flevoland in The Netherlands.

Crop type	Field number
Wheat	101, 102, 103, 104
Sugar beet	105, 106, 107
Potato	108, 109
Maize	111, 112
Bare soil	113, 114, 115, 116, 117, 118

Table A.1: Agricultural fields selected for extensive ground data collection (derived from Droesen et al., 1989).

(Eos). The current studies, therefore, focus on development of applications for the Eos radar which may be operational from 1999 onwards (Way and Smith, 1991).

On the 16th and 18th of August 1989 test sites in four countries were covered: the Feltwell site in the U.K., the Freiburg site in Germany, Les Landes in France and the Flevoland/Speulderbos site in The Netherlands. The sites in France and Germany comprise forests, the sites in the U.K. and The Netherlands comprise forests as well as agricultural areas.

The Flevoland/Speulderbos test site consists of three adjacent study areas: an agricultural area, a young forest plantation in Flevoland and an old forest at The Veluwe. A description of these areas is given below. All three areas could be partly covered in one 30 km track and in such a way that a significant part of each area was contained in a single AIRSAR scene with dimensions of approximately 10 km in azimuth and 7 km in range. For calibration four trihedral corner reflectors were deployed in the agricultural area, the northern part of the track.

### A.3 Ground data collection.

On August 16, the day of flight in The Netherlands, an extensive set of ground data was collected according to specifications standardized for European radar campaigns for agricultural areas (Churchill and Sieber, 1988). The collection of forest data was carried out conform the guidelines drafted by Churchill (1989). In order to elaborate a sampling concept for leaf/branch moisture and forest soils several preliminary field experiments were performed (Droesen et. al., 1989).

For agricultural areas the ground truth comprised, amongst other quantities: top soil volumetric moisture content for layers at 0-5 cm, 10-15 cm and 20-25 cm depth, surface roughness spectra, soil cover of the crop, crop height, fresh and dry biomass, leaf area index (LAI), leaf and stalk dimensions and spatial orientation distributions. The soil moisture was measured at 9 locations per field. Per location three sample rings of 100 cm<sup>3</sup> were used. The biomass was measured from five samples of 1 m<sup>2</sup> per field, and the LAI was determined from a subsample of these five square meter samples. This extensive sampling was performed for 18 fields (Fig. A.2 and Table A.1). In addition a crop type map of the area, including over two hundred fields, was prepared. Visual observations were made of phenological development stage and of anomalies like disease or weed infection, layering and hail damage. For bare soils and stubble fields observations of roughness conditions resulting from harvesting, ploughing or harrowing were made. All data were compiled into a ground data report (Droesen et.al., 1989).

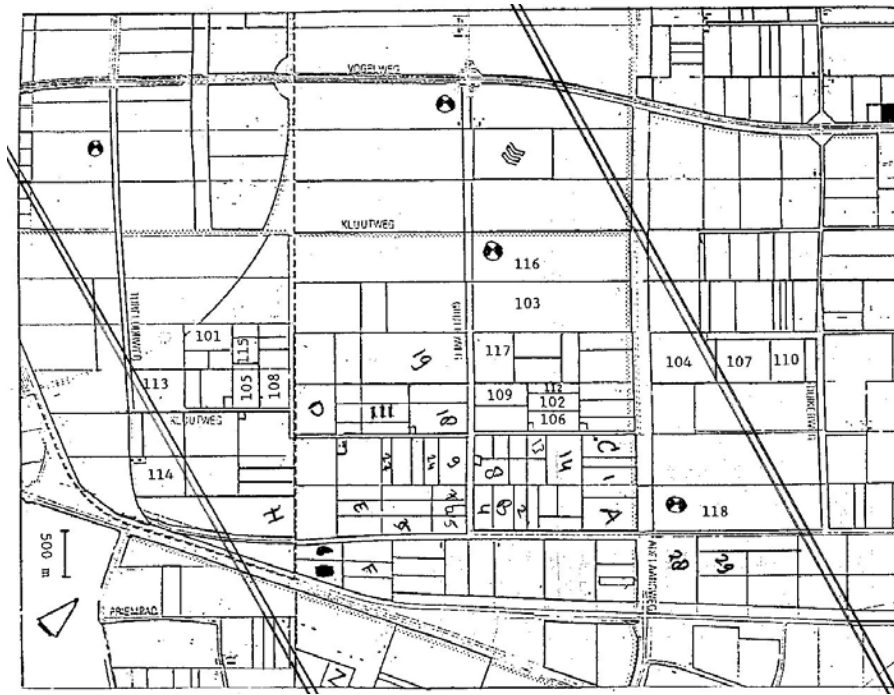


Figure A.2: The Flevoland site showing test fields. See Table A.1 for descriptions.

## A.4 The JPL AirSAR-91 campaign in The Netherlands.

In the framework of the SIR-C/X-SAR (space shuttle) project an airborne campaign with the NASA/JPL multiband polarimetric SAR (a prototype of the space shuttle SAR) is carried out over a number of the selected European sites. The campaign (JPL-SAR experiment 1991) was planned for a six-weeks period on a multi-temporal basis starting the last week of June until the first week of August. Thus it coincided with a substantial part of the agricultural growing season. The Flevoland site has obtained the status of international 'supersite' for the SIR-C/X-SAR project and was visited four times during the campaign (June 15th, July 3rd, July 12th and July 28th 1991). The data acquired will strongly support the development of the application of polarimetric radar data.

Aircraft imaging radar such as SLAR and SAR indicated their use for crop identification. The data also provide information about the physical properties of the surface of the vegetation and the soil. As with radar satellite systems images are obtained on a regular base, they are promising for monitoring purposes. The aim of the project, land use monitoring with ERS-1, is the development of a monitoring system applying ERS-1 SAR imagery in combination with SPOT and TM, dealing with agricultural crop growth, the occurrence of diseases in forestry and the monitoring of vegetation for nature areas.

Within both projects ground data was collected for soil and vegetation in agricultural areas comprising crops (Flevoland) and grasslands (Veluwe). Forest data was collected in selected study stands in the Horsterwold and Speulderbos. A data base has been established suitable for the study of land use and soil moisture mapping. In particular:

- Soil moisture was measured by the Heidemij and the Wageningen Agricultural University department of Water Resources (WAU-WR).
- Soil surface roughness was measured by WAU-WR.
- Field reflectance measurements were taken by the Centre for Agrobiological Research (CABO) and Wageningen Agricultural University department of Landsurveying and Remote Sensing (WAU-LRS).
- Crop observations were made by CABO, WAU-WR, and WAU-LRS.
- Field inventory was done by CABO WAU-WR and Directorate Flevoland (DF).
- The vegetation map was processed by the Winand Staring Centre (WSC), WAU-WR, CABO, Heidemij and DF.
- The Forest stands parameters were collected by WAU-WR.

## A.5 Vegetation map.

A vegetation map was constructed by the Winand Staring Centre (WSC) and the Wageningen Agricultural University department of Water Resources (WAU-WR) based on observations and inventory done by Heidemij, Directorate Flevoland (DF), Centre for Agrobiological Research (CABO) and WAU-WR. This inventory reflects only a situation in July, therefore fields at a later stage can differ in size. Figs. A.3 and A.4, show a crop color-coded map, and a field number coded map, respectively.

The crop labels in the database are reported in Table A.2:

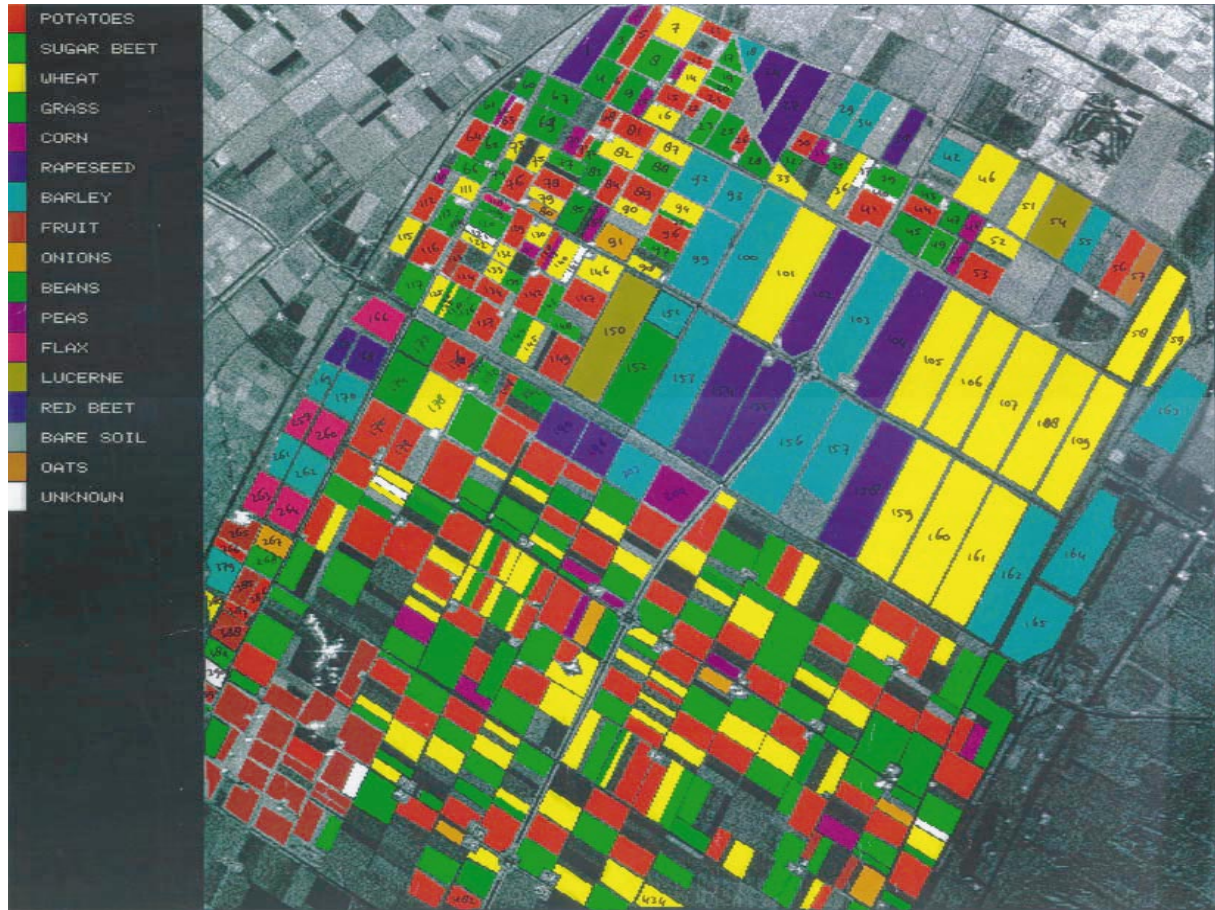


Figure A.3: Vegetation map with legend.

SBT: beet	POT: potato	WHE: wheat
BAR: barley	MAI: maize	GRA: grass
LUZ: lucerne	FAL: flax	OAT: oats
ONI: onions	RAP: rapeseed	BEA: beans
PEA: peas	FRU: fruit trees	?: unknown

Table A.2: The crop labels in the database.

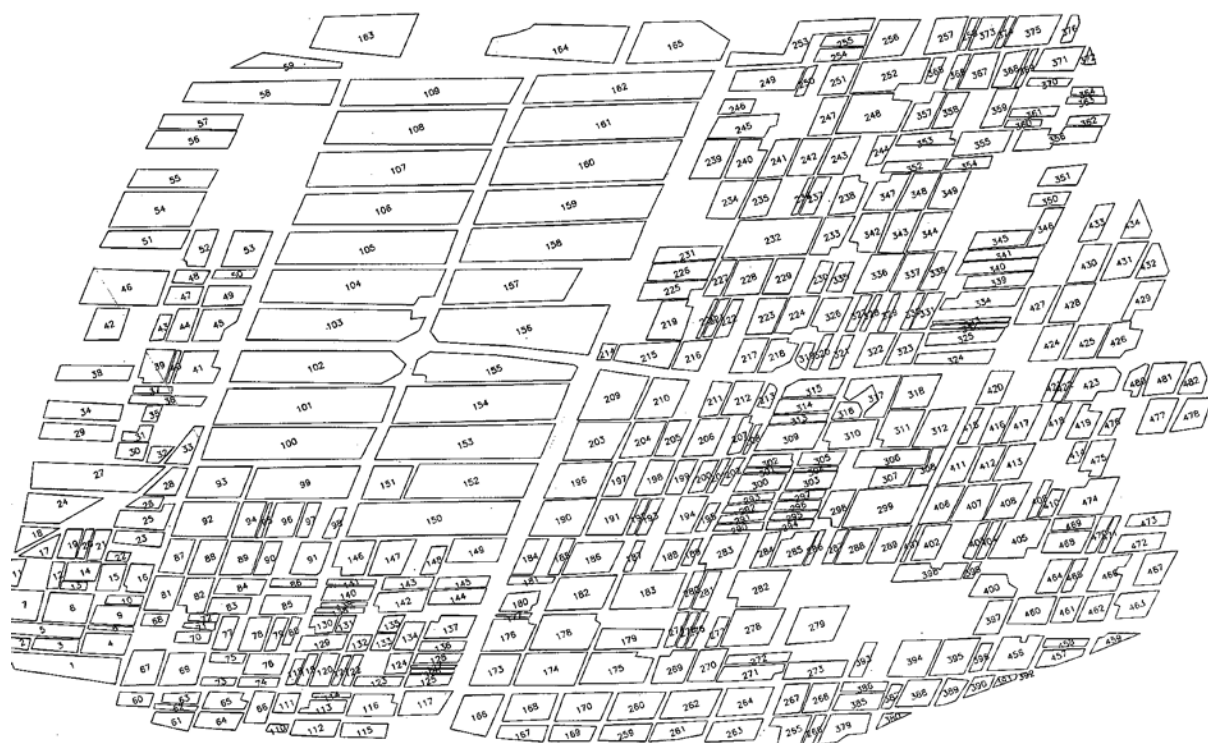


Figure A.4: Test field numbering during JPL-AirSAR 91 campaign.



# Bibliography

- [1] Büker, C., J.G.P.W. Clevers, H.J.C. van Leeuwen, B.A.M. Bouman and D. Uenk, 1992. Optical component MAC Europe ground truth report Flevoland 1991. Department of Landsurveying and Remote Sensing (LUW-LMK), Centre for Agrobiological Research (CABO), report no 199204, 55p.
- [2] Churchill, P.N. and A.J. Sieber, 1988, EURACS: A European radar cross-section database, Proc. IGARSS'88, Edinburgh, 12-16 September, pp.29-32.
- [3] Churchill, P.N., 1989, Procedures for the collection and compilation of forest ground data in microwave experiments, MAESTRO-I Campaign 1989 Experiment plan, Annex 2, JRC, Ispra.
- [4] Churchill P.N. 1990. MAESTRO-1 Airborne SAR Campaign - Proceedings of the Data Workshop. JRC/ESA, report IRSA/MWT/4.90, Ispra, Italy
- [5] Drogen W.J., D.H. Hoekman, H.J.C. van Leeuwen, J.J. van der Sanden, B.A.M. Bouman, D. Uenk, M.A.M. Vissers and G.G. Lemoine, 1990, MAESTRO 89 Ground Data Collection Horsterwold/Speulderbos/Flevoland (NL). Final Report. Agric. Univ. Wageningen, the Netherlands.
- [6] Faber, P.J., 1990. Handleiding en toelichting bij de empirische groeimodellen OPTAB - PEPPEL en RUIM - SIMU. Wageningen, Dorschkamp mededelingen band 23, no.1, 80 p.
- [7] Grandi G.F. de, G.G. Lemoine and A.J. Sieber, 1992, Supervised Fully Polarimetric Classification, An Experimental Study on the MAESTRO1 Freiburg Data Set, submitted to: Int. Geosci. Remote Sensing Symp. (IGARSS 1992), May 26-29th, Houston.
- [8] Groot J. and A. Freeman, 1990, Calibration Equipment Deployed on the Flevoland Test Site During the 1989 NASA/JPL DC-8 SAR Experiment, Proc. MAESTRO-1 Data Workshop, JRC Ispra, Italy 5-6 July, 1990.
- [9] Heidemij, 1991. Ground Data Collection 1991 JPL-SAR CAMPAIGN. Heidemij adviesbureau, no 635/21044, 80 p.
- [10] Lemoine G.G., D.H. Hoekman and H.J.C. van Leeuwen, 1991, Separability of Agricultural Fields and Forest Stands Using Multi-Frequency Polarimetric SAR Data of the Flevoland Site. Int. Geosci. Remote Sensing Symp. (IGARSS 1991) Digest, 681-684, Helsinki, Finland, June 3-6, 1991.
- [11] Roth, K., R. Schulin, H. Fluhler and W. Attinger, 1990. 'Calibration of Time Domain Reflectometry for Water Content Measurement Using a Composite Dielectric Approach'. Water Resources Research, Vol.26, no.10, pp.2267-2273.

- [12] Uenk, D., B.A.M. Bouman and H.W.J. van Kasteren, 1992. Reflectiemetingen aan landbouwgewassen. Handleiding voor het meten van gewasreflectie. Standaardlijnen voor de bepaling van bodembedekking en LAI. CABO-DLO verslag 156. 56 p.
- [13] Uenk, D., B.A.M. Bouman and M.A.M. Vissers, 1992. Veldbeschrijvingen in Z. Flevoland t.b.v. ERS-1 campagne in Nederland 1991. CABO.
- [14] Vries, P.G. de, 1986. Sampling Theory for Forest Inventory. A Teach-Yourself Course. Berlin (Springer-Verlag), 399 p.
- [15] Vissers, M.A.M. and J.J. van der Sanden, 1993. Groundtruth collection for the JPL-SAR and ERS-1 campaign in Flevoland and the Veluwe (NL) 1991. BCRS report no. NRSP-2 92-26.

## Appendix B

# Data Structure and Format

The database has been filled following the guidelines listed below. These have to be considered as indications: in some cases slight modifications have been applied. In any case, the data formats have been reported in "description" files included where needed.

Sections:

1. Ground data for bare soil;
2. Ground data for crops;
3. Ground data for forests;
4. Ground data for snow-covered terrains;
5. Scatterometer data;
6. Non-polarimetric SAR data;
7. Polarimetric SAR data;
8. Interferometric SAR data;
9. Optical data
10. Directory structure.

Notes:

- Each data set is associated to a "homogeneous polygon";
- Radar data must be provided if concurrent with a ground data set;
- Optical data must be provided if concurrent with a radar data set;
- Two data sets may be considered "concurrent" if the time difference between the two acquisitions is sufficiently small to make the comparison significant;
- SAR data have to be considered polarimetric if *hh-vv* phase information is available;

- Corrections for eventual slope effects must be carried out before storing the radar data;
- 8 polygon types are defined:
  - bsa: bare soil with detailed ground data;
  - bsb: bare soil with coarse ground data;
  - cra: crop with detailed ground data;
  - crb: crop with coarse ground data;
  - foa: forest with detailed ground data;
  - fob: forest with coarse ground data;
  - sna: snow with detailed ground data;
  - snb: snow with coarse ground data.

A ground data format must be defined for each available polygon type. The definition must be given in a file, in the same directory in which ground data are stored. The file must also indicate the number of samples per field and the number of measurements per sample. Sections 1-4 contain lists typical of detailed ground data. The experimenter may decide to store also coarse ground data, if supposed to be useful for some applications.

#### 1. GROUND DATA FOR BARE SOIL

- Date and time of measurements;
- Soil type;
- Tillage technique;
- Direction of eventual periodic structures or soil tracks (degrees vs. NS);
- Bulk density ( $\text{kg}/\text{m}^3$ );
- For the available layers:
  - Depth of upper layer limit (m);
  - Depth of lower layer limit (m);
  - Gravimetric moisture (% , average);
  - Gravimetric moisture (% , st.deviation. or range);
- Profilometer type;
- Profilometer length;
- Profilometer direction (degrees vs. NS);
- Surface height st. deviation. (m, average);
- Surface height st. deviation. (m, st. deviation. or range);
- Correlation length (m, average);
- Correlation length (m, st. deviation. or range);
- Profiles data:
  - distance between samples,

- number of samples,
- a list containing heights for each sample;
- Available information about stones;
- Available weather information.

## 2. GROUND DATA FOR CROPS

- Date and time of measurements;
- Crop type and variety;
- Sowing date;
- Phenological state;
- Cover fraction;
- Row direction angle (degrees vs. NS);
- Row separation distance (m);
- Plant separation distance (m);
- Average and st.deviation (or range) for the following variables:
  - Total height (m);
  - Fresh and dry biomass, possibly subdivided among components (kg/m<sup>2</sup>);
  - Gravimetric moisture (%);
  - Stem density (m<sup>2</sup>);
  - main stem diameter (m);
  - main stem height (m);
  - LAI;
  - n. of leaves per stem;
  - leaf width, length and thickness (m);
- All available data (even if qualitative) on secondary stems, petioles and (in case of wheat or barley) ears, including orientation and non-regularity;
- Available data on canopy stratification;
- The same soil data provided for bare soils, excluding the list of profile data;
- Available weather information.

## 3. GROUND DATA FOR FORESTS

- Date and time of measurements;
- Forest type; species, percentage of species if mixed;
- Age (years);
- Average values and st.deviation. (or ranges) for the following variables:
  - Row direction vs. NS (degrees);
  - Row separation distance (m);

- Tree separation (within row) distance (m);
- Total height (m);
- Dominant tree height (m);
- Canopy height (m);
- Fresh and dry total biomass ( $\text{kg}/\text{m}^2$ );
- Fresh and dry stem biomass ( $\text{kg}/\text{m}^2$ );
- Wood density ( $\text{kg}/\text{m}^3$ ) (if available);
- Stem density ( $\text{m}^{-2}$ );
- Stem dbh (m);
- Stem height (m);
- LAI;
- Leaf width, length and thickness (m);
- Leaf density ( $\text{m}^{-1}$ );
- Leaf orientation distribution;
- Gravimetric moisture content and/or dielectric constant of stem, branches and leaves
- All available branch data (in particular density, branch/stem volume ratio, orientation distribution, dimensions distribution, length/diameter ratio);
- All available understory data (e.g. biomass, typical stem dimensions);
- The same soil data provided for bare soils, excluding the list of profile data;
- Available weather information.

#### 4. GROUND DATA FOR SNOW-COVERED TERRAINS

- Date and time of measurements;
- Average and st.deviation. (or ranges) for:
  - Snow thickness (m);
  - Snow density ( $\text{kg}/\text{m}^3$ );
  - Volumetric liquid content;
  - Temperature;
  - Permittivity;
  - Information on layers;
  - Information on grain types;
  - % of liquid water;
- The same soil data provided for bare soils, excluding the list of profile data;
- Eventual information on crop type;
- Available information on snow-free terrain.
- Available weather information.

#### 5. SCATTEROMETER DATA

- Polygon (field) identification;

- Date and time of acquisition;
- Radar name;
- Frequency (GHz);
- Polarization;
- Off-nadir angle (degrees);
- Azimuth angle (degrees vs. NS);
- Average backscatter coefficient (dB);
- Information to ensure calibration quality.

#### 6. NON-POLARIMETRIC SAR DATA

- Polygon identification;
- Date and time of acquisition;
- Radar name;
- Frequency (GHz);
- Polarization;
- Off-nadir angle (degrees);
- Azimuth angle (degrees vs. NS);
- N. of pixels;
- N. of looks;
- Average backscatter coefficient (dB);
- Intensity standard deviation;
- Intensity histogram (n. of samples to be selected by the experimenter);
- Autocorrelation function (optional);
- Information to ensure calibration quality.

#### 7. POLARIMETRIC SAR DATA

- Polygon identification;
- Date and time of acquisition;
- Radar name;
- Frequency (GHz);
- Off-nadir angle (degrees);
- Azimuth angle (degrees vs. NS);
- N. of pixels;
- N. of looks;
- For the backscatter coefficients in  $hh$ ,  $hv$ ,  $vv$ :
  - Average value (dB);

- Intensity standard deviation
- For elements 13,12,32 (i.e.  $hh\ vv^*$ ,  $hh\ hv^*$  and  $vv\ hv^*$ ) of covariance matrix:
  - Average value of module (dB) and phase (degrees);
  - Intensity and phase standard deviations;
- For the polarizations  $hh$ ,  $hv$  and  $vv$ :
  - Intensity histogram (n. of samples to be selected by the experimenter);
  - Autocorrelation function (optional);
- Histograms of  $hh$ - $vv$  phase (n. of samples to be selected by the experimenter);
- Information on calibration (adopted techniques, eventual problems, etc.).

#### 8. INTERFEROMETRIC SAR DATA

- Polygon identification;
- First date and time of acquisition;
- Second date and time of acquisition;
- Radar name;
- Frequency (GHz);
- Polarization;
- Off-nadir angle (degrees);
- Azimuth angle (degrees vs. NS);
- Angle (degrees);
- N. of pixels;
- N. of looks;
- Average backscatter coefficient 1 (dB);
- Intensity standard deviation 1;
- Average backscatter coefficient 2 (dB);
- Intensity standard deviation 2;
- Window size;
- Average degree of coherence;
- Standard deviation of degree of coherence;
- Interferometric baseline (m);
- Information to ensure calibration quality and eventual problems related to the use of two overpasses.

#### 9. OPTICAL DATA

- Polygon identification;
- Date and time of acquisition;

- Instrument name;
- N. of pixels;
- For each band:
  - Lower and upper wavelengths ( $\mu\text{m}$ );
  - Average reflectance;
  - Reflectance standard deviation;
  - Reflectance histogram (n. of samples to be selected by the experimenter);
  - Reflectance autocorrelation function (optional);
  - Techniques used to consider sun irradiation and correct atmospheric effects.
- DIRECTORY STRUCTURE
  - /eraora/yourname/data/site/sensor/date (radar/optical data)
  - /eraora/yourname/data/site/g-data/date (ground data)
  - where
  - yourname: partner code
  - sensor: ers1, ers2, airsar, ...
  - site: choose a 4 characters abbreviation
  - date: in the format YYMMDD (YYMMDD\_YYMMDD for interferometric data)
  - file names should be of the type:
  - sensor data: yourname\_sensor\_site\_date\_nnn\_typ
  - ground data: yourname\_site\_date\_nnn\_typ
  - where
  - nnn is a progressive file number
  - (nnn for sensor data file is the same as the corresponding ground data file); typ is the polygon type (bsa, bsb, cra, crb, foa, fob, sna, snb).
  - Other naming conventions are acceptable if your system does not support long filenames, provided that no files with the same name exist.
  - Each file contains ground data or sensor data for a polygon and a date (2 dates for interferometric data). When multifrequency and/or multipolarization and/or multiangle data are available, the same polygon file contains data for all the frequencies and/or polarizations and/or angles, in sequence.
  - Files should be ASCII with one datum per line
  - each directory with files must contain:
    - 1 file with the list of files in the directory
    - files describing formats for those available among the 8 types of data.
  - 1 README file in top directory describing directory structure and directory index, and giving references for more detailed information.



## Appendix C

# Papers on pilot applications of the ERA-ORA Library

Presented at the 3<sup>rd</sup> International Symposium  
*Retrieval of Bio- and Geophysical Parameters from SAR Data  
for Land Applications*  
Sheffield, U.K., 11-14 September 2001.

- P. Ferrazzoli, “SAR for agriculture: Advances, problems and prospects”  
(Keynote address), ..... pp. 47–56
- M.C. Gonzales-Sampedro, T. Le Toan, M.W.J. Davidson, and J. Moreno, “Assessment of crop  
discrimination using multi-site databases”, ..... pp. 63–68
- F. Del Frate, G. Schiavon, D. Solimini, M. Borgeaud, D. Hoekman, and M. Vissers, “The potential  
of SAR in crop classification using multi-configuration data”, ..... pp. 93–98
- F. Del Frate, P. Ferrazzoli, L. Guerriero, T. Strozzi, U. Wegmüller, G. Cookmartin, and S. Quegan,  
“Monitoring crop cycles by SAR using a neural network trained by a model”, ..... pp. 239–244

**ESA SP-475, January 2002**



# SAR FOR AGRICULTURE: ADVANCES, PROBLEMS AND PROSPECTS

P. Ferrazzoli

Università Tor Vergata, Ingegneria, DISP, Via di Tor Vergata 110, I-00133 Rome, Italy  
Tel. +39 06 72597420, Fax +39 06 72597460, E-mail ferrazzoli@disp.uniroma2.it

## ABSTRACT

The aim of this paper is to illustrate the state of the art in SAR data use for agricultural applications, discuss the main problems and give suggestions for future work.

The paper is introduced with some short historical notes about the evolution of ground based, airborne and spaceborne radar observations, as well as about the advances in scattering modeling.

Then, the paper considers three aspects of the retrieval problem, corresponding to three fundamental steps: i) identification of a convenient radar configuration; ii) development of reliable relationships between backscatter coefficient and agricultural variables (direct problem); iii) retrieval in the strict sense (inverse problem). For each of the three topics, the important recent advances are summarized and the author's point of view about the state of the art is given.

## 1. INTRODUCTION

The objective of this paper is to illustrate and discuss the state of the art in SAR data use for agricultural applications. This topic has been the object of many investigations, in the last decades.

A first extensive experimental data base was provided by several ground-based measurements carried out in the 70's and early 80's, mainly in the US, using calibrated scatterometers. Single fields of various crop types, e.g. corn, soybeans, alfalfa, wheat, grass, etc., were monitored during their growth cycle. Observations over vegetated fields were mainly carried out in a frequency range between 4 and 18 GHz and in a linear copolar configuration (i.e. at VV and HH polarizations). Extensive results were published in several papers, e.g. Ulaby (1980), and summarized in important books (Ulaby et al., 1986; Ulaby & Dobson, 1989). In general, experimental results indicated that the radar backscatter coefficient  $\sigma^\circ$  is sensitive to vegetation parameters. Over some specific fields, a very nice correlation versus important vegetation variables was observed, e.g. in Figure 21.53 of Ulaby et al. (1986) This first activity gave a fundamental stimulus to microwave remote sensing for agricultural applications.

In the late 80's, some airborne campaigns made radar signatures available to a wide community of users (Hoekman, 1992; Churchill & Attema, 1992). The instruments, in this case, observed large agricultural areas including several fields. In order to monitor fields developments, the areas were observed 3-4 times during the Summer season. However, the temporal extension of the observations was more limited than in the case of ground based observations. The correlation between  $\sigma^\circ$  and ground parameters was investigated considering several fields observed simultaneously during limited time intervals. In general, correlations versus vegetation variables were not as good as with multitemporal single-field ground based observations. Soil properties and plant structure were different among the various fields. Therefore,  $\sigma^\circ$  was not simply correlated to a single variable, but was influenced by complex interactions among soil scattering, vegetation attenuation and vegetation scattering, as well as differences in geometry and permittivity of vegetation components (stem, leaf, petiole, ear, etc.). Moreover, the calibration problems were not yet completely solved, especially for airborne observations.

In the late 80's and in the 90's important advances were achieved, opening prospects of a full future utilization of SAR data for agricultural applications. First of all, significant improvements in calibration techniques were obtained using corner reflectors, extended targets and active calibrators (Van Zyl, 1990; Zebker & Lou, 1990; Freeman et al., 1990). Moreover, fully polarimetric instruments were realized. A lot of sites worldwide were overflown by AIRSAR (Held et al., 1988) and SIR-C (Stofan et al., 1995), thus allowing several scientists to get an insight into the problem of interaction between waves and natural media. Important activities were also carried out by means of EMISAR (Christensen et al., 1998). The launches of ERS-1, ERS-2, JERS-1 and RADARSAT made spaceborne multitemporal signatures available to many users for the first time. Finally, in parallel with the quantitative and qualitative improvements of experimental data bases, very important progresses were achieved in modeling, leading to a significant expansion of our capabilities in interpreting radar signatures. A simple "cloud" model gave a first key to understand  $\sigma^\circ$  dependence on main soil and vegetation variables (Ulaby & Attema, 1978). Important studies led to simulate  $\sigma^\circ$  using a discrete Radiative Transfer (RT) model, with vegetation elements represented as discs and cylinders (Eom &

Fung, 1984), (Karam & Fung, 1988). Further studies, aimed at refining the models in order to include leaf curvature and/or coherent effects, are in progress.

To summarize, tremendous efforts have been carried out, leading both to a significant expansion of experimental data bases available to us and to an important improvement of our capability to interpret the data. From the application point of view, the main objective is the retrieval of important agricultural variables such as Water Content (WC, kg/m<sup>2</sup>) and Leaf Area Index (LAI, m<sup>2</sup>/m<sup>2</sup>). The work aimed at solving this problem may be subdivided into three main steps. The first step consists in identifying a convenient radar configuration, i.e. one or more combinations of frequency, incidence angle and polarization for which  $\sigma^\circ$  is sensitive to the variable to be retrieved. As a second step, a relationship between  $\sigma^\circ$  and all soil and vegetation variables by which it is influenced has to be established. The relationship must be reliable, in the sense that must be valid in different sites and under different operational conditions. Finding this relationship, which is constituted by a model, solves the direct problem. Finally, the inverse problem has to be solved, i.e. retrieving the variables of interest using data collected in a convenient radar configuration and with the aid of a reliable direct model.

The three steps will be the objects of Sections 2, 3 and 4, respectively. For each of them, some important recent advances will be summarized and the author's point of view about the state of the art and the main present problems will be illustrated. Suggestions about future research directions will be given.

## 2. STUDIES ON RADAR SENSITIVITY

In order to retrieve a variable, the remote sensing system must be sensitive to the variable itself. In case of agricultural crops, since we are generally interested on variables associated to crop growing and crop senescence (i.e. WC and LAI), we need to identify combinations of frequency, incidence angle and polarization for which the  $\sigma^\circ$  value is significantly influenced by the crop cycle. This is ensured by a high  $\sigma^\circ$  dynamic range between full growth and early stage and a gradual transition between the extreme values. Since the various crop types show different geometries, the convenient radar configuration is not the same for all crops, but must be considered for any specific type, as it will be evident in Section 2.2.

### 2.1. Recent advances

As stated in the Introduction, the problem of radar sensitivity to vegetation variables has been investigated since the 70's using experimental data and models of various complexity. Some important pa-

pers, published during the last three years, are shortly summarized below.

Skriver et al. (1999) have illustrated polarimetric multitemporal signatures collected by EMISAR at L and C band over several crop types in Denmark. Main features have been discussed in comparison with previous works.

Saich & Borgeaud (2000) have analyzed ERS SAR signatures collected at Flevoiland (NL) site in 93, 94, 95 and 96 over potato, sugarbeet, wheat, barley and grass fields. Crop typical temporal patterns and year-to-year variabilities have been analyzed, also using a second order RT model.

Macelloni et al. (2001) have investigated the different relationships between  $\sigma^\circ$  and biomass of narrow and broad leaf crops. Critical comparisons with previous works have been shown. Radar signatures collected by various airborne and spaceborne instruments, as well as a first order RT model, have been used.

De Roo et al. (2001) have investigated the radar sensitivity to soil moisture and vegetation water content of soybeans fields. L and C band signatures and a semiempirical model have been used.

Important advances have been achieved in studies on rice cycle monitoring. Ribbes & Le Toan (1999) have investigated the performance of RADARSAT SAR, also in comparison with ERS SAR. Rosenquist (1999) has studied the temporal and spatial characteristics of JERS-1 SAR signatures.

### 2.2. Survey

Considerations about convenient radar configurations, based on studies carried out till now, are shown in this Section. For sake of concreteness, a set of 7 crop types, i.e. potato, corn, sugarbeet, rape, wheat, barley and rice, has been selected. This set is limited, but statistically significant, in that covers a high fraction of world crop area. For each of the seven crop types, diagrams or references to the literature are used to identify convenient radar configurations, on the basis of multitemporal trends or comparisons vs.  $\sigma^\circ$ 's of bare soils and other crops. Most of the diagrams are plotted using  $\sigma^\circ$  data made available in the framework of the ERA-ORA Project, founded by ECC. Results are interpreted by means of electromagnetic considerations.

#### 2.2.1. Potato crop

At L band, HV polarization, higher angles,  $\sigma^\circ$ 's of developed potato fields are clearly higher than  $\sigma^\circ$ 's of other crops and bare soils. This configuration appears to be convenient since produces a high dynamic range. Figure 1 shows results, obtained by AIRSAR over Flevoiland site in 1991, made available by University of Wageningen. Signatures collected in other

experiments, shown by Ferrazzoli et al. (1998) and by Skriver et al. (1999), are in agreement with data of Figure 1. Stem density of potato is low ( $10\text{-}15\text{ m}^{-2}$ ). Crop structure is ramified with large twigs (diameter  $> 4\text{ mm}$ ). The feature of Fig. 1 may be explained by the crosspolar scattering of twigs.

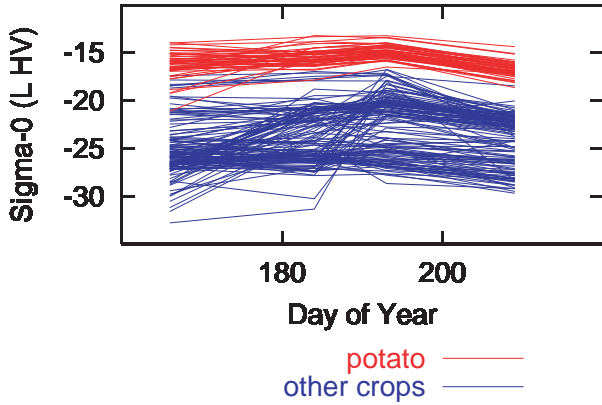


Figure 1. Multitemporal signatures collected at Flevoland in 1991. L band, HV polarization. Comparison between potato and other crops

#### 2.2.2. Corn crop

At L (S) band, HV polarization, high angles, an appreciable  $\sigma^\circ$  increase is observed in corn fields during the time interval of plant growth. This property is observed in Figure 2, showing again L band AIRSAR data collected at Flevoland in 1991. Results shown by Ferrazzoli et al. (1997) and Macelloni et al. (2001) confirm this increasing trend. Experimental data collected by the RASAM multifrequency scatterometer at the Central Plain site in Switzerland (Wegmüller, 1993) show a similar trend also at S band. Stem density of corn is low ( $7\text{-}10\text{ m}^{-2}$ ). The crop shows broad leaves with large ribs and petioles. The feature of Fig. 2 may be explained by the crosspolar scattering of ribs and petioles.

#### 2.2.3. Sugarbeet crop

For sugarbeet, a clearly convenient configuration is not easy to be identified. A good contrast with respect to bare soil is generally achieved at HV polarization, high angles. Moreover,  $\sigma^\circ$  increase vs. frequency is more evident than in other crops or in bare soils. These properties may be observed in Figure 3, showing crop averaged  $\sigma^\circ$ 's measured by RASAM and made available by GAMMA. Stems are sparse ( $7\text{-}10\text{ m}^{-2}$ ) and low. Scattering is dominated by the wide and thick leaves, particularly at the higher frequencies.

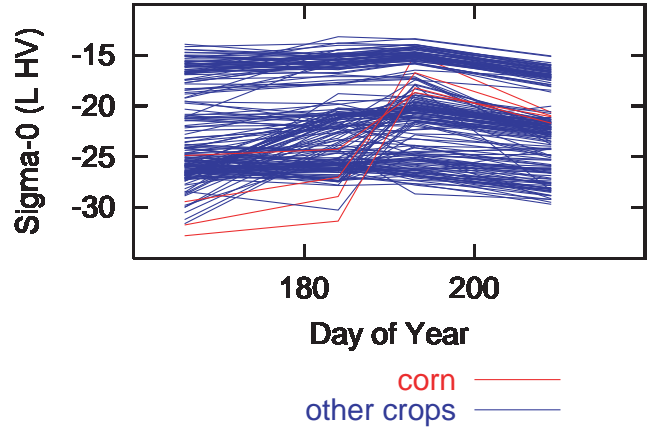


Figure 2. Multitemporal signatures collected at Flevoland in 1991. L band, HV polarization. Comparison between corn and other crops

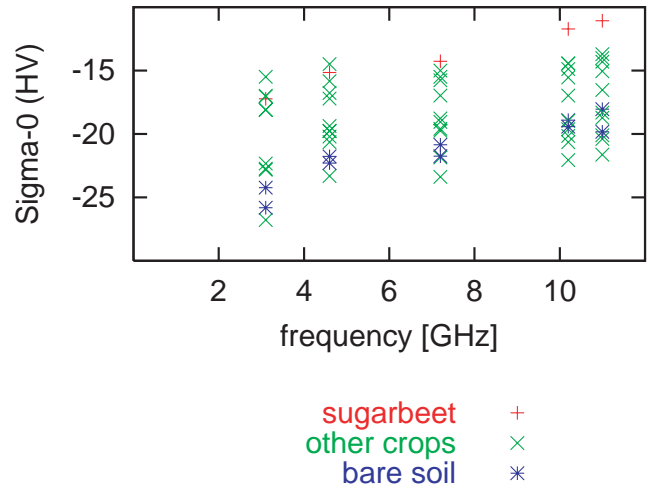


Figure 3. Multifrequency signatures collected by RASAM at Central Plain. HV polarization. Comparison between sugarbeet, bare soil and other crops

#### 2.2.4. Rape crop

At C band, HV polarization, high angles,  $\sigma^\circ$ 's of developed rape crops are clearly higher than  $\sigma^\circ$ 's of other crops and bare soils. Therefore, this radar configuration is convenient for rape. Figure 4 compares C band HV signatures collected by AIRSAR at Flevoland. The high rape backscatter before harvest is evident. Signatures collected in Italy (Ferrazzoli et al., 1997) and in Denmark (Skriver et al., 1999) agree with these statements. Stem density of rape is typically  $70\text{-}80\text{ m}^{-2}$ . Plants are ramified, with several small twigs ( $< 2\text{ mm}$  diameter) and pods. The feature of Fig. 4 finds explanation in the crosspolar scattering of twigs and pods.

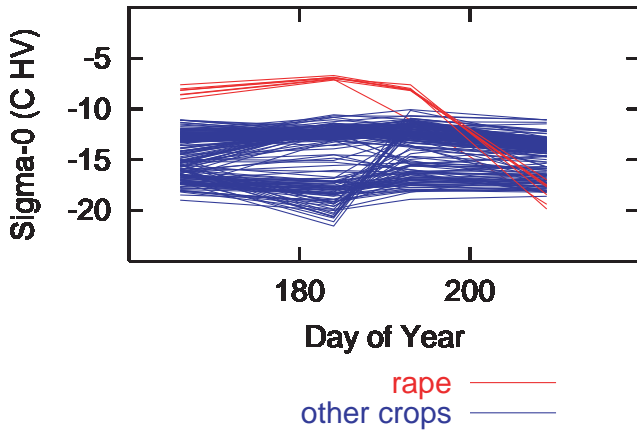


Figure 4. Multitemporal signatures collected at Flevoland in 1991. C band, HV polarization. Comparison between rape and other crops

#### 2.2.5. Wheat crop

At C, VV polarization, low angles ( $20^{\circ}$ - $30^{\circ}$ ) wheat  $\sigma^{\circ}$ 's show an evident lowering during crop growth. This is clearly observed in Figure 5, where multitemporal ERS SAR  $\sigma^{\circ}$ 's of wheat fields are compared against the ones of potato, corn and sugarbeet fields. Data were collected at the Flevoland site in a 4-years period, from 93 to 96, and have been made available by ESA/ESTEC. This wheat behavior is observed and discussed also by Saich & Borgeaud (2000), Cookmartin et al. (2000) and Macelloni et al. (2001). The ERS SAR configuration appears to be convenient for cycle monitoring. According with the results published by Del Frate et al. (2001), VV polarization contains useful information also at S and X band. Wheat stems are thin and dense ( $500$ - $1000$   $m^{-2}$ ) with narrow leaves. Ears are present on top in the mature stage. The feature of Fig. 5 finds explanation in the increasing attenuation suffered by VV soil backscattering due to growth of vertical stems and ears.

At HV polarization, wheat  $\sigma^{\circ}$  is mostly related to ear bending; therefore, this polarization does not appear to be reliable for crop monitoring. As far as L band is concerned, useful information could be added by its availability, in that the sensitivity to crop density is improved. However, L band signatures are heavily influenced by azimuth orientation, as demonstrated by Stiles et al. (2000).

#### 2.2.6. Barley crop

The general behavior of barley signatures is similar to the one observed for wheat. This may be explained by the general similarity between the two crop structures. Figure 6 compares multitemporal ERS signatures of barley with the ones measured

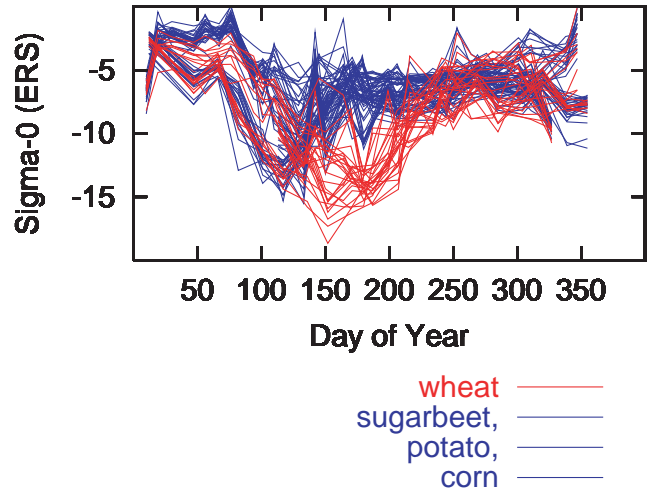


Figure 5. Multitemporal ERS signatures collected at Flevoland. Comparison between wheat and other crops

over potato and sugarbeet. Considerations similar to the ones of Fig. 5 may be applied. In the mature stage, barley ear bending is more enhanced than wheat ear bending. Therefore, the use of HV polarization for growth monitoring is not appropriate, and may be even misleading.

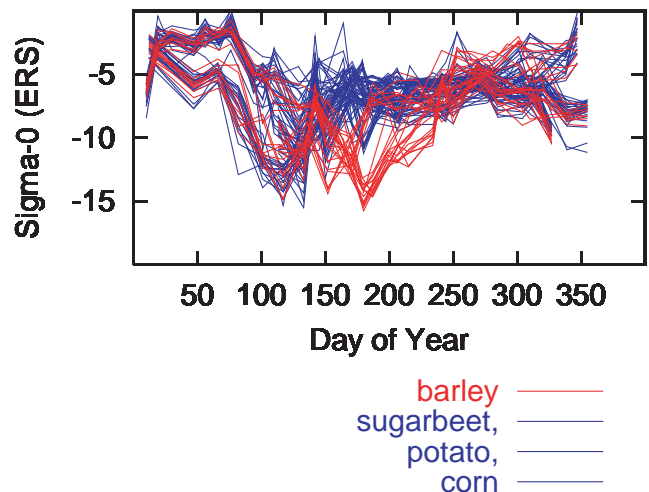


Figure 6. Multitemporal ERS signatures collected at Flevoland. Comparison between barley and other crops

#### 2.2.7. Rice crop

Rice crop backscatter has been the object of several experimental and modeling studies, in the recent years. Measurements carried out over various

sites indicate ERS SAR configuration to be convenient. An evident  $\sigma^\circ$  increase is observed during crop growth, with limited variability. Model simulations give a theoretical basis to this result (Le Toan et al., 1997). Rice stem density is relatively high ( $\sim 200 \text{ m}^{-2}$ ). Stems are grouped in bounces. The soil is flooded during the growing phase. At early stage  $\sigma^\circ$  is low, since the flooded soil is smooth. Crop growth is associated with a soil/stem double bounce effect, producing a gradual  $\sigma^\circ$  increase. The direct vegetation backscatter dominates in full growth.

Also RADARSAT and JERS-1 rice signatures have been analyzed. The  $\sigma^\circ$  contrast between full growth and early stage is lower in RADARSAT than in ERS signatures. This is explained by the lower interaction of stem with HH polarization, with respect to VV polarization (Ribbes & Le Toan, 1999). Investigations carried out by Rosenquist (1999) indicate that, for manual planting, also L band signatures (JERS-1 configuration) are well correlated with crop growth. The situation is more complex in case of mechanical planting, since a significant dependence on azimuth angle is observed, due to coherent interactions.

Studies about rice are at an advanced stage. Some applications, such as classification and crop monitoring, are preoperational (Ribbes & Le Toan, 1999). Unfortunately, few data in HV polarization are available.

### 2.3. Considerations about coherence

The considerations of Section 2.2 are relevant to  $\sigma^\circ$  amplitude. In the recent years, the application potential of interferometric coherence data collected by using SAR tandem overpasses has been investigated. This research has been stimulated by the availability of tandem images obtained by ERS-1 and ERS-2 with 1 day time delay. Some works indicate that the coherence contains useful information about vegetation type and vegetation status (Wegmüller & Werber, 1997). In order to get an insight into this problem, some coherence data made available by GAMMA have been analyzed. Figure 7 shows some multitemporal trends, obtained over the Flevoland site in 1995, relevant to wheat, potato and sugarbeet fields. For most of potato and sugarbeet fields, coherence is low in full growth and increases during drying. However, there are some anomalous samples of difficult interpretation. Coherence of wheat fields is high: this property could be due to a more advanced drying, with respect to other crops, or to the differences in geometrical characteristics. According to the data of Fig. 7, coherence confirms to have a good potential for agricultural applications, but its dependence on canopy and soil properties needs further investigations.

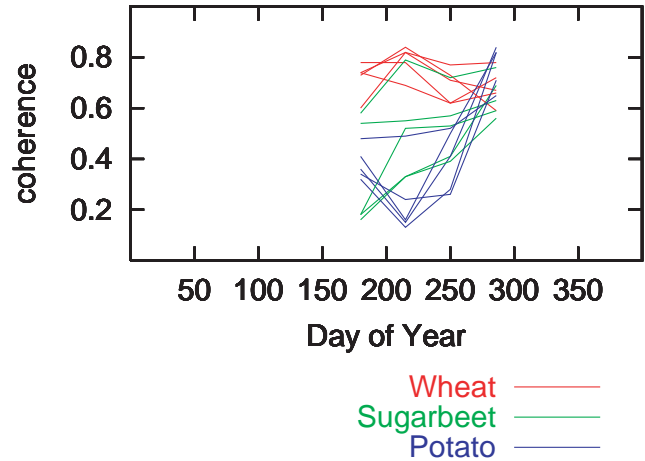


Figure 7. Multitemporal coherence data collected at Flevoland by ERS tandem overpasses. Comparison between potato, sugarbeet and wheat

### 2.4. Summarizing considerations

The analysis of section 2.2 indicates that general conclusions, valid for all crop types, cannot be drawn, since the radar sensitivity is affected by single crop properties. However, two observations of general validity may be done.

- An increase in stem density, generally associated to a decrease in stem diameter, leads to an increase of the convenient frequency. For wheat, barley, rice, rape (higher stem density, lower stem diameter) a high interaction with C (X) band waves is observed, making high frequencies interesting for monitoring. For corn and potato (higher stem diameter, lower stem density) lower frequencies (L and S band) appear to be more convenient.
- HV polarization is particularly useful when crops are well ramified, i.e. the relative weight of twigs, pods, petioles and leaf ribs becomes important. It is the case of potato, corn and rape. For crops dominated by vertical structures, such as wheat and barley, the most significant information is contained in the attenuation and/or double bounce effects produced at VV polarization.

It must be remembered that L band, HV polarization, has proved to be a convenient configuration also for sunflower (Ferrazzoli et al., 1997) and soybeans (De Roo et al., 2001).

The above considerations are valid when scattering is dominated by cylindrical elements. Their applicability to sugarbeet, characterized by large leaves and very low stems, is not straightforward.

From a system point of view, the forthcoming considerations apply.

- The configurations of present spaceborne SAR's, particularly ERS SAR, are interesting for some crops, such as rice, wheat and barley.
- ENVISAT ASAR signatures, provided ground resolution will be sufficient, will produce a significant improvement in monitoring, in that may contain HV polarization.
- A general good potential in monitoring of the main crops could be achieved in the future by simultaneous availability of L and C band observations.

The analysis has been limited to linear polarizations. However, previous studies indicate that the availability of fully polarimetric data is very useful for classification (Ferrazzoli et al., 1998; Skriver et al., 1999) and, to a lesser extent, for crop monitoring (Ferrazzoli et al., 1997; Skriver et al., 1999).

### 3. MODELING

It is well recognized that  $\sigma^\circ$  of crops depends on several soil and vegetation variables. The latter may show simultaneous variations. As an example, crop growth and soil drying processes, both influencing  $\sigma^\circ$ , generally occur simultaneously in springtime and early summertime. In order to correctly describe the scattering process, it is necessary to single out vegetation effects from soil effects and to distinguish among the influences of the various vegetation variables. To this aim, a model is required. A model is a relationship linking  $\sigma^\circ$  to the observation parameters (i.e. frequency, incidence angle, polarization) and to  $N$  surface variables:

$$\sigma^\circ = F(f, \theta, \psi_r, \chi_r, \psi_t, \chi_t; a_1, a_2, \dots, a_N)$$

where  $f$  is the frequency,  $\theta$  is the incidence angle  $\psi_r$  and  $\chi_r$  are the rotation and ellipticity angles in reception,  $\psi_t$  and  $\chi_t$  are the rotation and ellipticity angles in transmission (Ulaby & Elachi, 1990). The  $N$  variables ( $a_1, a_2, \dots, a_N$ ) include the objectives of the observation, useful for applications, as well as other variables less useful for applications but influencing  $\sigma^\circ$  anyhow. The complexity of the model ranges from a simple empirical relationship, linking  $\sigma^\circ$  with few general vegetation and soil variables, to complex physical models taking the canopy geometry and the complex interactions among scatterers into account.

#### 3.1. Recent advances

A fully phase-coherent model has been proposed, including coherent interactions among single plant el-

ements and among different plants (Stiles & Sarabandi, 2000; Stiles et al., 2000). Leaf and stem curvature effects have been also considered. The model has been tested over scatterometer data collected over a wheat canopy. It has been found that L band signatures are severely affected by coherent effects, depending on azimuth direction and radar resolution. At C band, single scatterer geometry is important. Soil direct backscatter is low.

Chauhan & Lang (1999) have modeled alfalfa canopies as conical clumps of stems that are clustered with leaflets. Coherent effects are considered within each clump. The model is able to explain some high  $\sigma^\circ$  values measured over alfalfa canopies at L band.

Chiu & Sarabandi (2000) have developed a coherent model and tested it against experimental soybeans signatures, collected at L and C band. Coherent effects result to be appreciable at L band.

Cookmartin et al. (2000) have tested a second order RT model against multitemporal ERS signatures collected over wheat fields. The agreement is good in the growing season, but crop attenuation is overestimated in the drying season. Laboratory studies are in progress to investigate the problem (Brown et al., 2001)

#### 3.2. The state of the art

A lot of models have been proposed till now to represent  $\sigma^\circ$ 's of agricultural fields. Models may be classified in increasing order of complexity, as indicated below.

- The simplest approach may consist in an empirical formula relating  $\sigma^\circ$  to soil moisture and crop WC (or LAI) with 2 regression coefficients. The latter may be computed by fitting over a statistically significant amount of experimental data at a given frequency, angle and polarization.
- The "Water Cloud" approach (Ulaby & Attema, 1978) is physically based, in that considers soil scattering, vegetation attenuation and vegetation scattering. For each frequency, angle and polarization  $\sigma^\circ$  is related to WC (or LAI) and soil moisture by 4 coefficients to be computed by statistical fitting over experimental data.
- A significant progress in physical representation is achieved using discrete RT models, representing soil as a homogeneous half-space with rough interfaces, and vegetation elements, i.e. stem, leaf, twig, ear, etc. as lossy dielectric scatterers. In general, stems, twigs, ears, etc. are represented as cylinders, while leaves are represented as circular or elliptic discs (Eom & Fung, 1984; Karam & Fung, 1988). The various scattering contributions may be combined by a simple single scattering model or by a more complex

multiple scattering model. The number of variables is higher than in the case of empirical and semiempirical models. As a minimum, the following inputs are requested: soil permittivity; soil hstd. and correlation length; permittivity of stem, ear and leaf; height and diameter of stem and ear; length, width and thickness of leaf; distribution of Eulerian angles describing leaf orientation.

- Refinements of RT models include near field interactions among scatterers (Fung et al., 1987) and/or leaf curvature (Stiles & Sarabandi, 2000). New input variables are required: the average distance among scatterers in the first case, curvature parameters (typically 3) in the second case.
- The models indicated above are based on an incoherent approach, i.e. the contributions of the different scattering sources are summed incoherently within each pixel. Of course, this is an approximation. As pointed out in Section 3.1, several works are in progress, aimed at considering coherent interactions. In coherent models the number of variables is even larger, since geometrical locations of several kinds of scatterers must be correctly characterized.

In order to be useful for remote sensing applications, models must be reliable, i.e. must save their validity under different operational and environmental contexts. From this point of view, empirical models suffer the disadvantage of depending on coefficients fitted over limited data sets. Physical models have an intrinsic more general validity. Moreover, they allow us to understand scattering processes more deeply and compute scattering effects more accurately. However, while increasing model complexity, the input variables characterization becomes more and more critical. In fact, the influence on  $\sigma^\circ$  played by some variables (e.g. scatterer orientation and/or location) is smoothed by something like an averaging process in simple models, while is explicitly considered in physical models. Therefore, the latter lead to a real accuracy improvement only if the input variables characterization is accurate as well.

Model reliability is ensured by comparisons with calibrated experimental data. This leads to: “fitting” for (semi)empirical models, “validation” for physical models. In the reality, some parameters are sometimes defined as “equivalent” and “fitted” also in physical models.

In spite of the important progresses recently achieved, some discrepancies with experimental data are observed and recognized in some papers, see e.g. (Cookmartin et al., 2000; Del Frate et al., 2001). Discrepancies may be due to various reasons, as indicated below.

- Interactions among scatterers are not correctly considered by incoherent models. Coherent

models may be more accurate with this respect, provided vegetation elements locations are described with high precision.

- The vegetation canopy is often subdivided into various layers. Some unavoidable arbitrary decisions are taken in this process.
- The single scatterer characterization is not yet a solved problem. Leaves are neither plane nor regularly bent. Stems are hollow cylinders. Ears are not homogeneous cylinders, but have a complex internal geometry and are partially empty. Moreover, presently used permittivity models have not received so many new validations, in the recent years.

Studies aimed at solving the above mentioned problems are recommended. Moreover, if the physical model has to be used to train a retrieval algorithm (see next Section) it could be appropriate to define some variables as equivalent and fit their values over experimental data, provided the model represents well the basic physics of the scattering process and fitting is carried out over multifrequency and multitemporal data sets, and over various fields of the same crop type.

## 4. RETRIEVAL

As observed in Section 3, modeling studies are still in progress and refinements are under way. Nevertheless, what has been learned till now by experimental and modeling investigations may be used to develop preliminary retrieval algorithms. Future refinements in the direct problem will produce parallel refinements in the retrieval techniques as well.

### 4.1. Recent advances

Wigneron et al. (1999) have retrieved crop biomass of a soybeans field using a multitemporal set of  $\sigma^\circ$  data, collected by a C band scatterometer, using a simple “cloud” model calibrated by a discrete RT model.

Prévoit et al. (2001) have retrieved the temporal evolution of wheat variables using the STICS crop model in addition to RT models. An assimilation technique has been adopted. Results obtained using only optical data have been compared with the ones obtained by using both optical and SAR data.

Bouman et al. (1999) have tested a composite model including crop growth (SUCROS), water balance (SAHEL) and radar backscatter (CLOUD). ERS signatures collected at Flevoland site over potato, sugarbeet and wheat fields have been used. The paper contains information useful to develop retrieval algorithms.

#### 4.2. State of the art

Among the several variables influencing  $\sigma^\circ$ , WC and LAI are considered particularly important for applications, and studies are mainly aimed at retrieving them. A list of possible approaches to the problem is given below.

- Direct inversion of simple empirical models. This is a straightforward method. However, empirical relationships are validated over restricted data sets and do not prove to be accurate when used in different operational or environmental contexts.
- Inverting simple models after calibration by physical models. This approach shows a more general validity with respect to the previous one. However, also this procedure has been tested over limited data sets, till now. Therefore, further checks are required.
- Multi-variable inversion of physical models. As stated in Section 3, physical models represent a scattering process in which  $\sigma^\circ$  is dependent on several soil and vegetation variables. From a purely mathematical point of view, the inverse problem may be solved, provided the site is observed in several radar configurations, in such a way as to achieve a number of  $\sigma^\circ$  data at least equal to the number of unknowns. The mathematical complexity of the problem could be overcome, due to the tremendous advances recently achieved in computational systems and in retrieval techniques (e. g. neural networks). However, even limited inaccuracies of the direct model may produce severe effects.
- Using multitemporal radar data, eventually associated with optical data, and assimilation of a-priori information provided by crop models. This technique appears to be promising, although requires further work.

In the author's opinion, due to the high number of variables influencing  $\sigma^\circ$ , a feasible and reliable algorithm should take the maximum benefit from: i) multitemporal observations, ii) available a-priori information. The vegetation variables are not independent from each other, but evolve following some rules, for a given crop type and crop variety. Moreover, the temporal evolution is different from field to field, but shows some common aspects which may be assumed as a-priori known.

In order to clarify these concepts, the temporal evolutions of WC measured at different sites have been compared. Ground measurements were carried out over wheat fields at Avignon (F) in 93 and 96 and at Central Plain (CH) in 88 and 89. Central Plain data have been provided by GAMMA in the framework of ERA-ORA Project, while Avignon data have been made available by INRA. The various trends are shown in Figure 8.

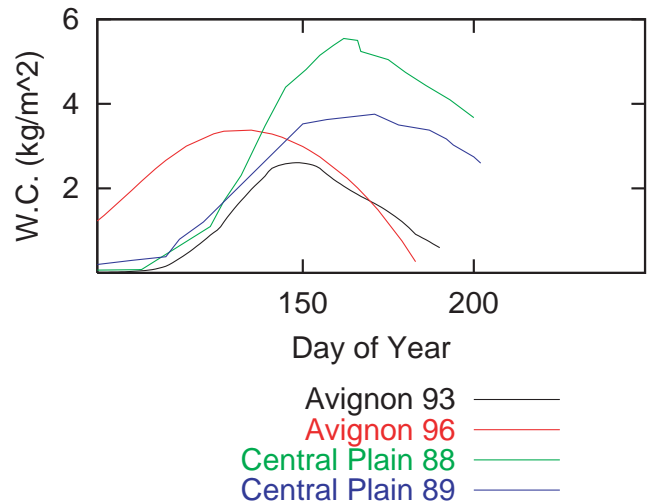


Figure 8. Examples of multitemporal WC trends of wheat fields

All trends show a typical “bell” shape, but there are large differences in maximum WC value (full growth value) as well as in temporal location and temporal duration of the cycles. By applying a simple normalization as:

$$WC_n(t) = K \cdot WC(at + b)$$

(where  $t$  is the time) and optimizing the  $a$ ,  $b$  and  $K$  parameters for each cycle, the trends of Figure 9 are obtained. The latter appear to be well close to each other.

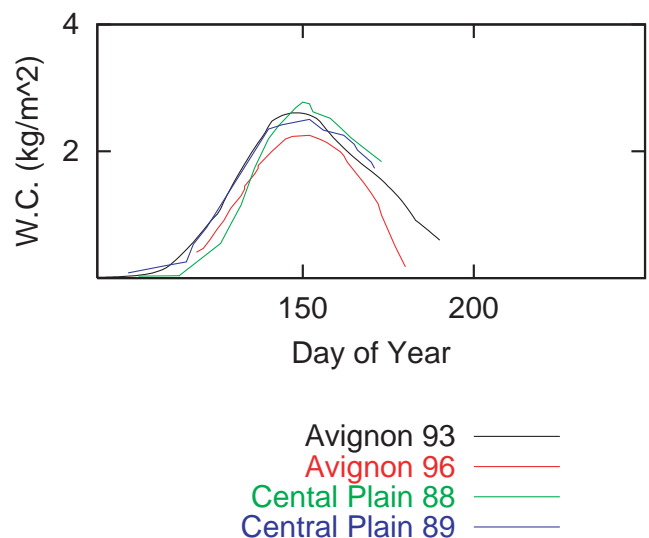


Figure 9. Multitemporal WC trends of wheat fields after normalization

Therefore, a possible retrieval technique could assume a reference “bell” function as a priori known and use remote sensing data to find the  $a$ ,  $b$  and  $K$  parameters, which are specific of the observed field. This could be done using: i) a crop model and a simple model relating  $\sigma^\circ$  to WC with coefficients fitted over data collected in previous experiments, possibly over fields of the same variety and in the same environment; ii) multitemporal ground truth previously collected over fields of the same crop type and a physical model. An attempt to retrieve the cycle of a wheat field using the second approach is shown by Del Frate et al. (2001). The inaccuracy of the results is mainly due to the direct model, while the algorithm works well. Figure 2 of the same paper indicates that, for 3 fields of the same site, geometrical variables are different from field to field, but evolve following similar trends.

## 5. CONCLUSIONS

In the work aimed at retrieving crop variables, three main phases have been considered: i) identification of a convenient radar configuration, ii) modeling and iii) solution of the inverse problem. According with the results obtained till now, a future satellite radar system, operating at L and C band, at linear co- and cross-polarization and at an intermediate  $\theta$  range ( $30^\circ - 40^\circ$ ), should acquire most of the potential information for crop monitoring. Advances in modeling have been important, but further refinements are needed to correctly describe single scatterers and understand the importance of coherent interactions. Retrieval techniques based on multitemporal data and assimilation of crop models appear to be promising.

## ACKNOWLEDGMENTS

The data collected at Flevoland and Central Plain sites have been made available in the framework of the ERA-ORA Concerted Action, founded by ECC (Contract No. ENV4-CT97-0465).

The author wishes to thank all the colleagues who gave a tremendous help in several ways: direct cooperation, data exchange, suggestions, severe criticism. In particular: D. Solimini, G. Schiavon, L. Guerriero, F. Del Frate, P. Pampaloni, S. Paloscia, J.-P. Wigneron, A. Chanzy, T. Strozzi, U. Wegmüller, D. Hoekman, M. Vissers, M. Borgeaud, S. Quegan.

## REFERENCES

Bouman B.A.M., van Kraalingen D.W.G., Stol W., van Leeuwen H.J.C., 1999, “An agroecological modeling approach to explain ERS SAR radar backscatter of agricultural crops”, *Remote Sens. Environ.*, vol. 67, 137-146

Brown S.C.M., Quegan S., Bennett J.C., 2001, “High resolution measurements of scattering in wheat canopies - Implications for crop canopy retrieval”, *This issue*

Chauhan N.S., Lang R.H., 1999, “Radar backscattering from alfalfa canopy: a clump modelling approach”, *Int. J. Remote Sensing*, vol. 20, 2203-2220

Chiu T., Sarabandi K., 2000, “Electromagnetic scattering from short branching vegetation”, *IEEE Trans. Geosci. Remote Sensing*, vol. 38, 911-925

Christensen E.L., Skou N., Dall J., et al., 1998, “EMISAR: an absolutely calibrated polarimetric L- and C-band SAR”, *IEEE Trans. Geosci. Remote Sensing*, vol. 36, 1852-1865

Churchill P.N., Attema E.P.W., 1992, “The MAESTRO-1 European airborne polarimetric Synthetic Aperture Radar campaign”, MAESTRO-1/AGRISCATT Final Workshop Proceedings, ESA wpp-31, 1-11

Cookmartin G., Saich P., Quegan S., et al., 2000, “Modeling microwave interactions with crops and comparison with ERS-2 SAR observations”, *IEEE Trans. Geosci. Remote Sensing*, 658-670.

Del Frate F., Ferrazzoli F., Guerriero L., et al., 2001, “Monitoring crop cycles by SAR using a neural network trained by a model”, *This issue*

De Roo R.D., Du Y., Ulaby F.T., et al., 2001, “A semiempirical backscattering model at L-band and C-band for a soybean canopy with soil moisture inversion”, *IEEE Trans. Geosci. Remote Sensing*, vol. 39, 864-872

Eom H.J., Fung A.K., 1984, “A scatter model for vegetation up to Ku-band”, *Remote Sens. Environ.*, vol. 19, 139-149

Ferrazzoli P., Schiavon G., Solimini D., et al., 1997, “The potential of multifrequency polarimetric SAR in assessing agricultural and arboreous biomass”, *IEEE Trans. Geosci. Remote Sensing*, vol. 35, pp. 5-17

Ferrazzoli P., Guerriero L., Schiavon G., 1998, “Experimental and model investigation on RADAR classification capability”, *IEEE Trans. Geosci. Remote Sensing*, vol. 37, pp. 960-968

Freeman A., Shen Y., Werner C.L., 1990, “Polarimetric SAR calibration experiment using active radar calibrators”, *IEEE Trans. Geosci. Remote Sensing*, vol. 28, 224-240

Fung A.K., Chen M.F., Lee K.K., 1984, “Fresnel field interaction applied to scattering from a vegetation layer”, *Remote Sens. Environ.*, vol. 23, 35-50

Held D.H., Brown W.E., Freeman A., et al., 1988, “The NASA/JPL multifrequency multipolarization airborne SAR system”, *IGARSS'88 Proceedings*, 345-349

Hoekman D. H., 1992, “Introduction to the Agriscatt'87 and '88 campaigns”, MAESTRO-1/AGRISCATT Final Workshop Proceedings, ESA wpp-31, 13-21

- Karam M.A., Fung A.K., 1988, "Electromagnetic scattering from a layer of finite length, randomly oriented, dielectric, circular cylinders over a rough interface with application to vegetation", *Int. J. Remote Sens.*, vol. 9, 1109-1134
- Le Toan T., Ribbes F., Wang L.-F., et al, 1997, "Rice crop mapping and monitoring using ERS-1 data based on experiment and modeling results", *IEEE Trans. Geosci. Remote Sensing*, vol. 35, 41-56.
- Macelloni G., Paloscia S., Pampaloni P., et al., 2001, "The relationship between the backscattering coefficient and the biomass of narrow and broad leaf crops", *IEEE Trans. Geosci. Remote Sensing*, vol. 39, 873-884
- Prévoit L., Chauki H., Troufleau D., et al, 2001, "Assimilating optical and radar data into the STICS crop model for wheat", 8th ISPRS Proceedings, 753-758.
- Ribbes F., Le Toan T., 1999, "Rice field mapping and monitoring with RADARSAT data", *Int. J. Remote Sensing*, vol. 20, 745-765
- Rosenquist A., 1999, "Temporal and spatial characteristics of irrigated rice in JERS-1 L-band SAR data", *Int. J. Remote sensing*, vol. 20, 1567-1587
- Saich P., Borgeaud M., 2000, "Interpreting ERS SAR signatures of agricultural crops in Flevoland, 1993-1996", *IEEE Trans. Geosci. Remote Sensing*, vol. 38, 651-657
- Skriver H., Svendsen M.T., Thomsen A.G., 1999, "Multitemporal C- and L-band polarimetric signatures of crops", *IEEE Trans. Geosci. Remote Sensing*, vol. 37, 2413-2429
- Stiles J.M., Sarabandi K., 2000, "Electromagnetic scattering from grassland - part I: a fully phase-coherent scattering model", *IEEE Trans. Geosci. Remote Sensing*, vol. 38, 339-348
- Stiles J.M., Sarabandi K., Ulaby F.T., 2000, "Electromagnetic scattering from grassland - part II: measurement and modeling results", *IEEE Trans. Geosci. Remote Sensing*, vol. 38, 349-356
- Stofan E.R., Evans D.L., Schmullius C., et al., 1995, "Overview of results of spaceborne imaging radar-C, X-band Synthetic Aperture Radar (SIR-c/X-SAR)", *IEEE Trans. Geosci. Remote Sensing*, vol. 33, 817-828
- Ulaby F.T., Attema E.P.W., 1978, "Vegetation modeled as a water cloud", *Radio Science*, vol. 13, 357-364
- Ulaby F.T., 1980, "Vegetation clutter model", *IEEE Trans. Antennas Propagat.*, vol. 28, 538-545
- Ulaby F.T., Moore R.K., Fung A.K., 1986, *Microwave Remote Sensing. Active and Passive. Vol III*, Artech House
- Ulaby F.T., Dobson M.C., 1989, *Handbook of Radar Scattering Statistics from Terrain*, Artech House
- Ulaby F.T., Elachi C., eds., 1990, *Radar Polarimetry for Geoscience Applications*, Artech House
- van Zyl J.J., 1990, "Calibration of polarimetric radar images using only image parameters and trihedral corner reflectors responses", *IEEE Trans. Geosci. Remote Sensing*, vol. 28, 337-347
- Wegmüller U., 1993, "Signature research for crop classification by active and passive microwaves", *Int. J. Remote Sensing*, vol. 14, 871-883.
- Wegmüller U., Werner C., 1997, "Retrieval of vegetation parameters with SAR interferometry", *IEEE Trans. Geosci. Remote Sensing*, vol. 35, 18-24
- Wigneron J.-P., Ferrazzoli P., Oliosio A., et al., 1999, "A simple approach to monitor crop biomass from C-band radar data", *Remote Sensing Environ.*, vol. 69, 179-188.
- Zebker H., Lou Y., 1990, "Phase calibration of imaging radar polarimeter Stokes matrices", *IEEE Trans. Geosci. Remote Sensing*, vol. 28, 246-252

# ASSESSMENT OF CROP DISCRIMINATION USING MULTI-SITE DATABASES

M.C. Gonzalez-Sampedro (1), T. Le Toan (2), M.W.J. Davidson (2) and J. Moreno (1)

(1) Universitat de València  
Facultad de Física, Departamento de Termodinámica  
Dr. Moliner 50, Burjassot (Valencia), 46100, Spain  
tel: + 34963983112 / fax: + 34963983385  
e-mail: [mcgonzal@uv.es](mailto:mcgonzal@uv.es) / [moreno@uv.es](mailto:moreno@uv.es)

(2) CESBIO (Centre d'Etudes Spatiales de la Biosphère)  
18 Avenue Edouard. Belin  
31401 Toulouse Cedex 4, France  
Tel: + 33561556671/ Fax: + 33561558500  
e-mail: [Thuy.Letoan@cesbio.cnes.fr](mailto:Thuy.Letoan@cesbio.cnes.fr) / [Malcolm.Davidson@esa.int](mailto:Malcolm.Davidson@esa.int)

## ABSTRACT

Within the framework of the ERA-ORA (European Radar-Optical Research Assemblage) project funded by the EC, an extensive database including both remote sensing data and coincident ground data, collected by several institutes in Europe, has been assembled and organized. The remote sensing data consists of radar data acquired mainly by ERS and airborne SARs at different sites across Europe.

Overall, this compilation of data from different sites represents an opportunity to examine the generality and robustness of remote sensing methods and algorithms. In the past much of the literature published on retrieval algorithms has been based on observations over a single site. The extension of these results to larger areas and different sites thus represents an important step in the development and validation of generalized retrieval algorithms applicable to a variety of situations.

## INTRODUCTION

In this paper, we will analyze and interpret part of the database collected at different European agricultural sites to address several questions related to crop classification, keeping in mind that the launch of ENVISAT in the next few months will open new perspectives for radar satellite applications. In particular, this work addresses the following questions related to the classification of crops:

- a) Can multitemporal ERS data be used to discriminate crop types based on their temporal backscatter signal?
- b) With the known limitations of current systems, can ENVISAT/ASAR with its different polarisations and incidence angles be used to

discriminate crop types at a given time with fewer temporal acquisitions.

- c) What are the relative contributions of polarimetry at C, L and P bands to the overall crop classification results?
- d) What is the role of synergy between optical and radar sensors (e.g. ASAR and MERIS) for large agriculture fields?

## MULTI-SITE DATABASE

### Study Areas

This work has been focused on the following study areas (Fig. 1):

Flevoland (The Netherlands):

This area is located in Zuid Flevoland (centered at 52.4° North and 5.4° East) in the Netherlands, approximately 30 Kilometers east of Amsterdam. The Zuid Flevoland polder was reclaimed from lake IJsselmeer in 1966 and its topography is almost perfectly flat, the general altitude of the area being three meters below the mean sea level. The reclaimed polder is used mainly for agriculture and forestry, the main cultivated crops are sugar beet, potato and winter wheat [1].

Barrax (Spain):

This area is located in Castilla-La Mancha, Spain (with coordinates 39° 3' North and 2° 6' West) and it has been used for several previous experiments: EFEDA (Field Experiment in Desertification-threatened Areas), STAAARTE (Scientific Training and Access to Aircraft for Atmospheric Research Throughout Europe), MAC (Multisensor Aircraft Campaign), DAISEX (Digital Airborne Imaging Experiment) among others. Its flat topography is of great advantage for remotely sensed data corrections and its interpretation. In Barrax, there are large uniform crop fields both irrigated and non

irrigated mostly consisting of barley, corn, sugar beet, wheat, as well as bare soils areas.



Figure 1.- Location of the study areas

ERS-SAR time series

ERS-SAR temporal series from Flevoland over the period 1993 to 1996 have been used to assess crop separability and annual variations in crop radar signatures.

Polarimetric data

We have used JPL-AIRSAR data (C, L and P band) from the Flevoland site that were acquired in two different experiments, MAESTRO-89 and MAC-Europe 1991. The data collection was conducted from August 16, 1989 to July 28, 1991 (there are a total of five acquisition dates: 89-08-16, 91-06-15, 91-07-03, 91-07-12, 91-07-28). The crop signatures were averaged in every field. The incidence angle for both years falls in the 26 to 65 degrees range.

Optical-radar synergy

In addition, we have used hyperspectral optical data to investigate the radar-optical synergy from the ESA/DAISEX-1999 and EFEDA campaigns that took place at Barrax. The airborne hyperspectral scanner HyMap [2] has 128 channels covering the 0.4-2.5 μm spectral range. HyMap images from the DAISEX-1999 campaign were compared with the ERS-SAR images. The JPL-AVIRIS [3] airborne sensor images (224 bands along the 0.4-2.5 μm range) acquired during the EFEDA campaign were used in combination with AIRSAR data.

Ground measurements:

Detailed crop maps for each year were available for the Flevoland and for the Barrax area as well. For some of

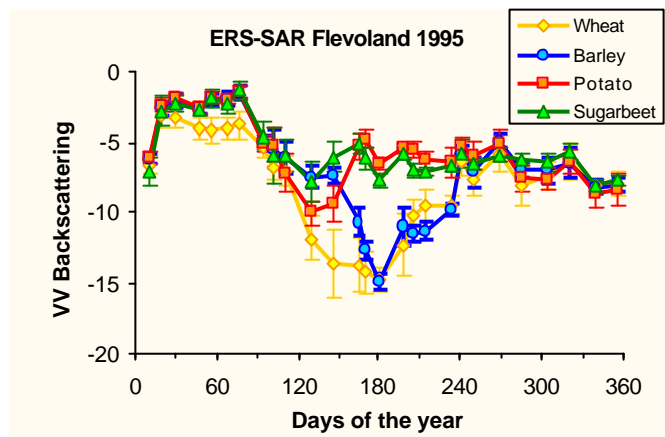
the fields, several agronomic parameters such as biomass, crop height, canopy water content and soil moisture status were measured.

RESULTS

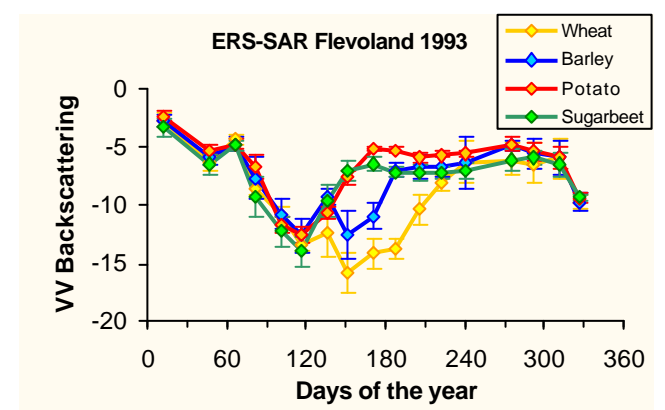
Temporal series:

We have selected two complete ERS-SAR annual series data from the Flevoland area, corresponding to the years 1993 and 1995. Figure 2 shows those temporal series for four crops (barley, wheat, sugarbeet and potato). The curves were obtained by averaging all the crops of the same kind. Standard deviation is shown as error bars.

For one particular year it is possible to distinguish between two main groups (cereals and broad leaves crops) in the period that follows the maximum cereals development: for 1995 near day 180 (beginning of July) and for 1993 near day 150 (end of May). It is important to notice that even for the same site there are shifts of one month in crops phenology. Bigger shifts are expected when comparing temporal curves from different sites.



a)



b)

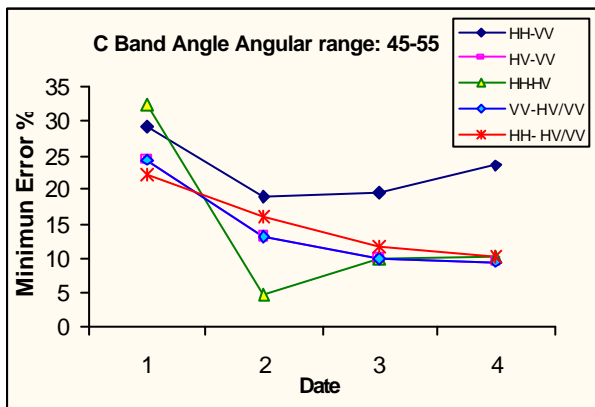
Figure 2.- Radar signatures of the dominant crops in the region of Flevoland a) Year 1995, b) Year 1993.

AIRSAR data:

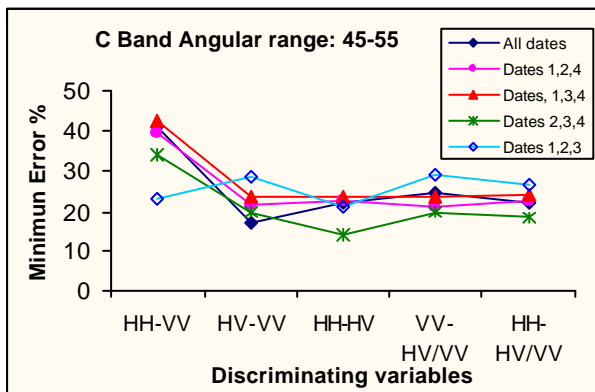
Using more than one polarisation channel, higher levels of separation between crops can be achieved, even if the information comes from only one frequency. Among the available Flevoland AIRSAR data we have selected field averaged C band signatures with incident angle between 45 and 55 degrees. The reason to choose this angular interval was that it included the biggest amount of fields. A total number of 450 signatures were available (88 of sugarbeet, 134 of wheat, 129 of potato, 51 of barley and 48 of grass) corresponding to 4 dates from the same year. Table 1 contains these details.

Date	Sugar-beet	Wheat	Potato	Barley	Grass
91/06/15	15	30	28	16	10
91/07/03	19	32	26	12	17
91/07/12	25	35	34	13	11
91/07/28	29	37	41	10	10

Table 1.- Number of crops per date used for the analysis



a)



b)

Figure 3.- Minimum error achieved in the classification of 5 crop types using the maximum likelihood algorithm.

Figure 3 shows the minimum error in the classification of five types of crops (sugar beet, potato, barley, wheat

and grass) using the algorithm of maximum likelihood [4]. A case has been considered in which only one day and two discriminating variables were utilized (Figure 3.a) as well as the case in which all the dates or combinations of the three dates are utilized (Figure 3.b). For all the combinations of different polarisations (HH-VV, HV-VV, HH-HV, VV-HV/VV, HH-HV/VV) we have found that date 1, which corresponds to June 15 has the largest errors. Date 2, corresponding to July 3, is the optimum date due to the separation between crops which is maximum utilising HH and HV polarisations. We have seen that including more than one date in the analysis does not improve the error of the classification but worsens it as it is seen in Figure 3.

Optical-radar synergy:

The error of the separability among the 5 classes in our dataset was never lower than 10% even when using polarisation information. For some combinations of dates, errors were higher than 40%. In these cases, other sources of information, such as optical data, may help to overcome the limitations of radar data.

For exploring the optical-radar synergy we have done a pixel by pixel comparison of two pairs of images from the Barrax site:

- a) ERS-SAR (2<sup>nd</sup> of June, 1999) / HyMap (3<sup>rd</sup> of June, 1999)
- b) AIRSAR (19<sup>th</sup> of June, 1991)/ AVIRIS (29<sup>th</sup> of June, 1991)

In order to make possible a pixel by pixel comparison of the images we need first to superpose them. After georectification of the optical images and slant-to-ground range correction of the radar images, these have been registered over optical images by means of ground control points. The final resolution is that of the optical images (5 meters for HyMap and 20 meters for AVIRIS). HyMap image was geometrically and atmospherically corrected at DLR [5]. Due to the flat topography of the Barrax site the topographic effects are not critical.

In Figure 4, we have compared a near infrared band, where the vegetation response is very high, with radar backscattering. The grey scale represents the density of points. If the same information were contained in both optical and radar data, a high correlation between the two quantities would be found. However, Figure 4 shows a very low correlation. Points are grouped into two clouds, corresponding to the optical signal of soils (low reflectance) and to green vegetation (high reflectance). Radar signal was not able to distinguish these two classes. For each surface type, the variability in radar images was due to roughness and moisture changes. Higher levels of noise were present in the ERS-SAR image as opposed to the HyMap image.

Figure 6 shows very clearly the complementarity of optical and radar data. The CHV/LHV ratio obtained from the AIRSAR (radar) image has been represented against two indexes derived from the AVIRIS (optical) image. These two indexes are: a chlorophyll index (Fig 6a) and a plant water index (Fig 6b). In Fig 6a there is an imaginary line parallel to the x-axis illustrating how bare soils (very low index) and vegetation (higher index) have the same radar backscatter value. However, in the region of bare soils all the sensitivity comes from the radar signal. Although a low level of correlation between both kinds of data is justified by the fact that radar signal is insensitive to chlorophyll, the comparison between the water in the plant (Fig 6b) shows how information coming from the two different sources (optical and radar) is not redundant.

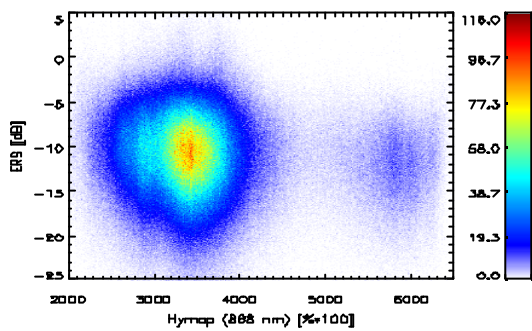


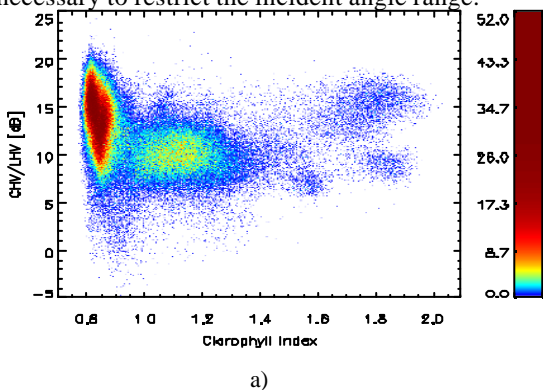
Figure 4.- ERS (radar) CVV backscattering versus HyMap (optical) 868 nm band reflectance in %\*100

#### DRAWBACKS

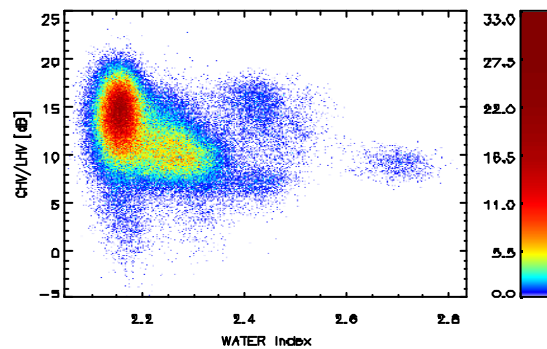
In the classification of crops with radar data two main drawbacks are present:

- a) Angular Variability
- b) Temporal Variability

Airborne radar systems have a wide range of incident angles. In Figure 5, the angular variability (in some cases it can be of more than 6 dB for the same crop type) is higher than the variation from one crop to another, thus there is confusion among classes. To obtain better results in the classification it is necessary to restrict the incident angle range.



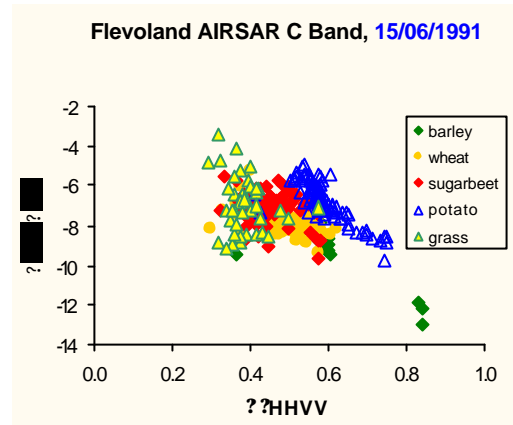
a)



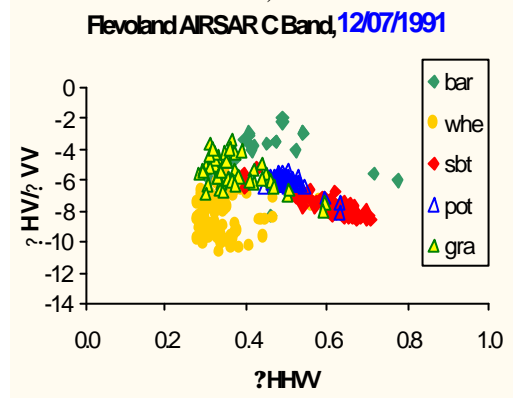
b)

Figure 6.- CHV/LHV ratio from the AIRSAR (radar) image versus to two indexes from AVIRIS (optical) image. a) chlorophyll index and b) plant water index.

Classification results are strongly dependent on the time sequence because of the differences in the phenological state of the crops. Development of crops occurs very quickly in a short period of time, which is different for every crop and changes from one site to another. So depending on the overlapping of the phenological cycles of every kind of crop, there will be an optimal date or an optimal combination of dates that ensure the highest crop separability. With the current satellite systems with time resolutions of 35 days (ERS case) it is not possible to guarantee an image acquisition in those optimal dates for an particular area.

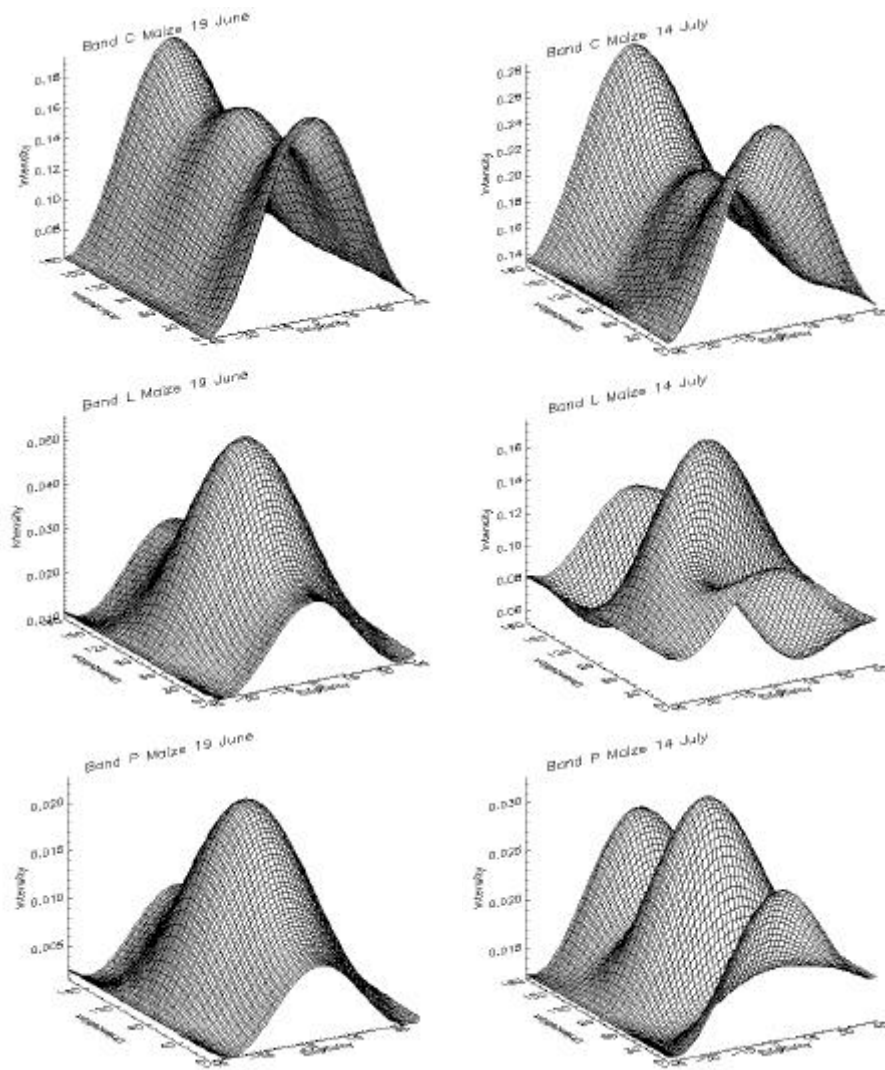


a)

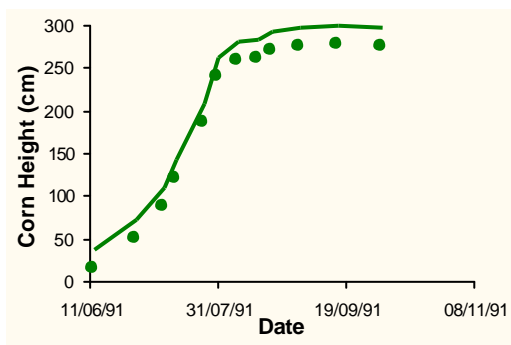


b)

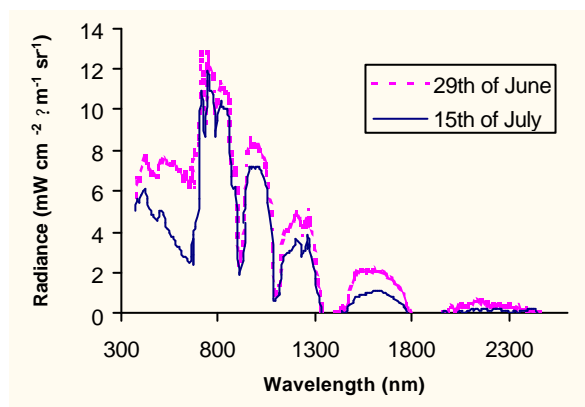
Figure 5.- C band HV/VV ratio versus HH-VV correlation for two different dates at Flevoland



a)



b)



c)

Figure 7.- Ideal case for the optical-microwave synergistic study.

a) In these figures the averaged radar backscattering intensity for a corn pivot in the area of Barrax has been plotted for all the possible polarisation states of the transmission and received co-polarised waves. We can observe that for longer wavelengths the response is more sensitive to the surface structure. b) This figure shows a considerable increase in the height and biomass of corn from June 19<sup>th</sup> through July 14<sup>th</sup>. c) AVIRIS hyperspectral signatures of the same corn pivot.

## FUTURE PERSPECTIVES

In the frame of the points we deal with in this paper ENVISAT satellite opens two new perspectives:

### a) Use of polarimetric information

ASAR sensor on board ENVISAT operating in C band, is technologically more advanced than ERS and will acquire images in VV (as ERS), HH and cross polarisations allowing for the first time the use of polarimetric information from satellite.

Although homogeneous surface have a characteristic polarisation signatures (see Fig. 7), at satellite resolutions polarimetric information may be difficult to interpret for non homogeneous surfaces.

### b) Radar/optical synergy

Radar/optical synergy is not a well explored field of study, partly due to the sparse availability of radar/optical data for the same study area. This lack of data comes from two different causes: 1) For the time being, there are no satellites equipped with both kinds of sensors. Referring to airborne remote sensing, there have been few campaigns in which radar data together with optical data were acquired. 2) In regions where the probability of having clouds is high, available optical data are not always useful.

The launch of ENVISAT will allow for the first time to have radar and optical images systematically acquired for the same study area by means of the ASAR and MERIS sensors. The MERIS optical sensor will provide high spectral resolution images (bandwidth in nm) that will allow new applications, not possible with broad band sensors (LANDSAT, SPOT). Although its spatial resolution (300x300 m) is much coarser than the spatial resolution of SPOT (20x20 m), radar/optical synergy for areas with extensive crops, such as Barrax, would still be possible (see Figure 8).

## CONCLUSIONS

- Temporal evolution is confirmed as the dominant effect in crop discrimination for single band (CVV) imagery.
- The potential of polarimetric information in crop discrimination cannot be demonstrated by means of airborne polarimetric systems with a wide range of incidence angles. Spaceborne polarimetric systems can be more effective with a limited range of incidence angles for the same area coverage.
- ENVISAT/ASAR opens new perspectives, but radar-optical synergy is still necessary to discriminate between soil and vegetation scattering with C band.



Figure 8.- RGB composition in a Barrax HyMap image showing MERIS pixel size. One of the channels has been degraded to 300x300m resolution.

## ACKNOWLEDGEMENT

This work has been supported by the European Union under contract ENV4-CT95-0465 for the ERA-ORA project (European Radar-Optical Research Assemblage) and by ESA under the contract no. 13390/98/NL/GD for the ESA/DAISEX-1999 campaign.

## REFERENCES

- [1] M. Engdahl and M. Bourgeaud, "ERS-1/2 Tandem Interferometric Coherence and Agricultural Crop Height", Proc. 2<sup>nd</sup> International Workshop on Retrieval of Bio-&Geo-physical Parameters from SAR Data for Land Applications, ESA SP-441, December 1998, ISBN 92-9092-764-X.
- [2] T. Cocks, R. Janssen, A. Stewart, I. Wilson, and T. Shields, 1998, "The HyMap Airborne Hyperspectral Sensor: The System, Calibration and Performance", Proc. 1st EARSeL Workshop on Imaging Spectroscopy, October 1998, Zurich, EARSeL, Paris, p. 37-42.
- [3] G. Vane, R. O. Green, T. G. Chrien, H. T. Enmark, E. G. Hansen and W. M. Porter, 1993, "The Airborne Visible/Infrared Imaging Spectrometer (AVIRIS)", Remote Sensing of Environment, 44:127-143.
- [4] J. A. Richards, "Remote Sensing Digital Image Analysis" An Introduction. Springer-Verlag, ISBN 3 540-58219-3
- [5] R. Richter, "Atmospheric correction methodology for imaging spectrometer data", Proc. of the Final Results Workshop on DAISEX (Digital Airborne Imaging Spectrometer Experiment), ESA SP-499, July 2001, ISBN 92-9092-809-3.

# THE POTENTIAL OF SAR IN CROP CLASSIFICATION USING MULTI-CONFIGURATION DATA

F. DelFrate<sup>1</sup>, G. Schiavon<sup>1</sup>, D. Solimini<sup>1</sup>

M. Borgeaud<sup>2</sup>, D. Hoekman<sup>3</sup>, M. Vissers<sup>3</sup>

<sup>1</sup>Università Tor Vergata, Ingegneria, DISP, Viale Politecnico 1, I-00133 Roma, Italy  
tel: +39 06 72597422, fax +39 06 72597460, e-mail: schiavon@disp.uniroma2.it

<sup>2</sup>European Space Agency, Electromagnetics Division TOS-EEP  
Postbus 299, 2200 AG Noordwijk, The Netherlands  
tel: +31 71 565 4830, fax: +31 71 565 4999, e-mail: maurice@xe.estec.esa.nl

<sup>3</sup>Department of Water Resources, Wageningen Agricultural University  
Bode 82, Postbus 9101, 6700 HB Wageningen, The Netherlands  
tel: +31 317 4 82894, fax: +31 317 4 84885, e-mail: dirk.hoekman@users.whh.wau.nl

## ABSTRACT

This paper reports on a quantitative investigation which has been carried out, aimed at evaluating the performances of a neural network based crop classification technique. Backscattering coefficients measured in different SAR configurations (multipolarization/multitemporal) have been used as inputs of the algorithm. For this purpose, AirSAR and ERS data collected at the Flevoland site have been extracted from the ERA-ORA distributed library.

## 1. INTRODUCTION

The potential of SAR in classifying among different agricultural crop species has been demonstrated in several studies (Ulaby et al., 1986; Bouman and Hoekman, 1993; Ferrazzoli et al., 1999; Saich and Borgeaud, 2000). The performance of a classification exercise depends on the sensitivity of the measured backscattering coefficient to the differences in the bio-morphological structures of different species, which cause different interaction behaviour between the incident electromagnetic waves and the vegetation structures. It has been experienced that observations by SAR systems in a single configuration, which means one image taken at a certain time at one fixed frequency, polarization and incidence angle, are often inadequate to classify with the required accuracy, mainly when similar crops have to be separated. In those cases, the potential of a classification algorithm may be improved by operating in multifrequency and/or multipolarization and/or multiangle configuration. Additional benefits may be achieved by repeated overpasses (multitemporal techniques).

This paper reports on a quantitative investigation which has been carried out, aimed at evaluating the

performances of a neural network based crop classification technique for different SAR configurations. A wide data set, consisting of AirSAR signatures collected at the Flevoland site in 1991 and of ERS backscattering coefficients collected at the same site through years 1993–95, has been used. The considered data set has been assembled within the ERA-ORA (European RADar-Optical Research Assemblage) project, a concerted action supported by the European Commission within the RTD Programme on Environment and Climate (Fourth Framework Programme) in the field of space techniques applied to environmental monitoring and research. The essential objective of the Concerted Action is to improve the radar data analysis and utilization tools developed by European researchers for Earth observation from space.

AirSAR signatures span 3 frequencies, are fully polarimetric and partially multitemporal, since the site was overflown 4 times in summertime. Several combinations of SAR parameters have been considered, starting from a simple single configuration system, at C band, vv polarization, one date, through gradually increasing complexities, adding polarizations and number of overpasses, up to a C band system with hh, vv, hv polarizations, and multitemporal data. The percentage of misclassified fields, which in the first case is more than 40%, drops to very low values in the last cases (less than 4%), although only C band and linear polarizations (without phase information) have been considered. This is indeed a promising result in view of future exploitation of Envisat ASAR.

ERS data are single frequency and single polarization but are collected during the whole year. In this case the multitemporal character of the data has been fully exploited in the algorithm.

Table 1. Data set characteristics.

type	AirSAR		ERS (95 vs. 95)		ERS (93, 94 vs. 95)	
	training	test	training	test	training	test
barley	10	4	5	3	18	8
corn	2	2	8	4	0	0
grass	11	8	21	9	68	30
potato	28	25	15	15	109	30
rape	4	3	1	1	0	0
s.beet	23	19	18	12	95	30
wheat	33	18	19	11	123	30
total	111	79	87	55	413	128

## 2. NEURAL NETWORK CLASSIFICATION ALGORITHM

The classification algorithm consists in a neural network with feedforward configuration. The neural network simulator (SNNS) developed at the University of Stuttgart (Germany) (Zell et al., 1995) has provided the basic software for the algorithm implementation. The net consists of a multilayer perceptron with two hidden layers. A typical architecture of the used nets is reported in Fig. 1. Training has been pursued by a scaled conjugate gradient (SCG) algorithm. This is a member of the class of conjugate gradient methods, general purpose second order techniques that help to minimize goal functions of several variables. Second order indicates that such methods use the second derivatives of the error function, while a first-order technique, like standard backpropagation, only uses the first derivatives. By using the SCG method the nets have generally been trained after a few hundreds of epochs, that is, the training phase was very short time consuming. For the purpose of classification, in the training phase the component of the output vector corresponding to the true class has been set to 1 while the others to 0. In the test phase a winner-and-take approach has been considered.

## 3. RESULTS

### 3.1. AirSAR data

The Flevoland '91 AirSAR signatures have been used to carry out a classification exercise intended to assess the improvement of accuracy brought in by progressively richer (in terms of polarizations and measurement dates) sets of data.

A training set of backscattering coefficients has been generated, by selecting the C-band 50° data relative to a number of fields, listed in column 2 of Table 1, of the crops listed in column 1, within the total number of fields imaged on the Flevoland '91 site. Multipolarization and/or multitemporal C-band  $\sigma^0$ 's of the fields have trained the NN algorithm.

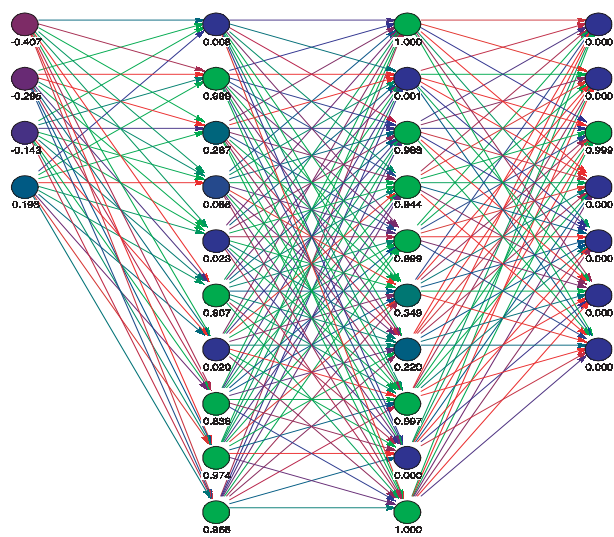


Figure 1. Neural network feedforward topology.

Then, the trained network has been used to classify the fields of the test set, which included the remaining Flevoland '91 fields (column 3 of Table 1). The work has been repeated several times using different subsets of the available data. First of all, a very simple data set has been taken, i.e.,  $\sigma^0$  for C-band, vv polarization, one single flight. The data set complexity has gradually been increased, up to the most complete case, relative to C-band, hh, vv and hv polarizations, 4 flights (15 June, 3, 12, 28 July 1991). Poor classification performance has been obtained for the single polarization single flight case (overall accuracy (OA) = 55.7 %), while it improves when data acquired during all the four available flights in the same vv polarization are used (OA = 83.5 %). Still better performance is obtained when exploiting the other mentioned polarizations, achieving OA = 96.2 % in the most complete case. Table 2 reports the complete confusion matrix for the hh-vv-hv combination, one flight, while in Table 3 the same polarization combination, but for all the four dates, is considered. It is noticeable to observe that a quite high OA have been achieved in the last case, although only C-band and linear polarizations (without phase information) have been considered.

Tables 4 to 6 report the resulting confusion matrices for the hh-hv combination for increasing number of acquisition dates (1 to 3). Comparable results have been obtained for the vv-hv configuration. It can be observed that the addition of the crosspolar polarization produces an improvement of the OA even in the case of data acquired during one single flight (from 55.7 % to 88.6 %), but particularly when multitemporal data are used. This is a promising result in view of the future exploitation of the Envisat ASAR data, although before generalizing the results obtained in this exercise, the effects of the different incidence angles should be assessed. Note, however, that 50° is close to the maximum ASAR incidence angle.

### 3.2. ERS data

Fig. 2 compares multitemporal ERS trends collected over many different fields and in different sites and years. Three different codes are associated with different crop types. During vegetation development, i.e. from Day of Year ~150 to Day of Year ~200,  $\sigma^0$ 's of wheat fields are clearly lower than  $\sigma^0$ 's of potato and sugarbeet fields. In the other periods of the year, when soil scattering dominates,  $\sigma^0$  variations are mainly due to soil conditions (moisture effects, essentially). As a consequence of this, small differences are observed among samples belonging to the same site and year, while site-to-site or year-to-year variations may be large. Fig. 2 indicates that a single-frequency, single-polarization radar, such as ERS SAR, may be useful for classification, provided multitemporal data are used, and that the most suitable data for this task are those acquired during the vegetation development period.

Therefore, a classification exercise has been performed, using ERS data collected over the Flevoland test site. At first all the available data collected during year 1995, which include acquisitions in 27 days from Day of Year 10 to 355, have been used. A training set of backscattering coefficients has been generated, with data relative to a number of fields of the same crops of the AirSAR case. Then, the trained network has been used to classify the remaining fields, which formed the test set (columns 4 and 5 of Table 1). The resulting confusion matrix is reported in Table 7, which shows a very good classification performance with only one field misclassified. Based on the considerations made commenting Fig. 2, the classification exercise has then been repeated selecting data acquired only on seven days during the vegetation development period. Results are reported in Table 8, not showing a substantial difference with the previous case, and therefore confirming what previously stated.

An inter-year classification exercise has then been performed, training a neural network algorithm using data acquired in years 1993 and 1994, and testing it on 1995 data. Data of the first two years didn't include all the crop types present in 1995, therefore

results obtained in this case, and reported in Table 9, are not directly comparable with the others. Nevertheless, they can give some useful information. Dates of acquisition were not the same from year to year, therefore the dates of one year included in the datasets have been selected to be no more than one week apart from those of the other two years. The 1995 overpasse dates were the same seven days of the previous case. Despite, as expected, the OA is lower, the obtained results are encouraging, and substantial improvements might be envisaged when using the future Envisat ASAR data, with the addition of the crosspolar channel.

### ACKNOWLEDGMENTS

This work has been partially supported by Agenzia Spaziale Italiana (ASI).

### REFERENCES

- Bouman B.A.M., D.H. Hoekman, 1993, "Multitemporal multi-frequency radar measurements of agricultural crops during the Agriscatt-88 campaign in The Netherlands", *Int. J. Remote Sensing*, vol. 14, 1595-1614.
- Ferrazzoli P., L. Guerriero, G. Schiavon, 1999, "Experimental and model investigation on radar classification capability", *IEEE Trans. Geosci. Remote Sensing*, vol. 37, pp. 960-968.
- Saich P., M. Borgeaud, 2000, "Interpreting ERS SAR signatures of agricultural crops in Flevoland, 1993-1996", *IEEE Trans. Geosci. Remote Sensing*, vol. 38, pp. 651-657.
- Ulaby F. T., Moore R. K, Fung A. K, 1986, *Microwave Remote Sensing: Active and Passive - vol.III*, Artech House, Dedham (MA, USA).
- Zell A., G. Mamier, M. Vogt, et al., 1995, *SNNS Stuttgart Neural Network Simulator User Manual*, Report n. 6/95, University of Stuttgart, Institute for Parallel and Distributed High Performance Systems, Stuttgart, Germany.

Table 2. Confusion matrix describing the neural algorithm crop classification performance. Algorithm input characteristics: 3 polarizations (hh-vv-hv), 1 date, AirSAR measurements (Flevoland 1991).

classified as	true class						
	barley	corn	grass	potato	rape	s.beet	wheat
barley	3	0	3	0	0	0	0
corn	0	2	0	0	1	0	0
grass	1	0	5	0	0	0	0
potato	0	0	0	25	0	0	2
rape	0	0	0	0	2	0	0
s.beet	0	0	0	0	0	19	0
wheat	0	0	0	0	0	0	16
total number of samples					=	79	
correctly classified					=	72	
overall accuracy					=	91.1 %	

Table 3. Confusion matrix describing the neural algorithm crop classification performance. Algorithm input characteristics: 3 polarizations (hh-vv-hv), 4 dates, AirSAR measurements (Flevoland 1991).

classified as	true class						
	barley	corn	grass	potato	rape	s.beet	wheat
barley	4	0	0	0	0	0	0
corn	0	2	0	0	0	0	0
grass	0	0	7	0	0	0	0
potato	0	0	1	25	0	0	1
rape	0	0	0	0	3	0	0
s.beet	0	0	0	0	0	19	1
wheat	0	0	0	0	0	0	16
total number of samples					=	79	
correctly classified					=	76	
overall accuracy					=	96.2 %	

Table 4. Confusion matrix describing the neural algorithm crop classification performance. Algorithm input characteristics: 2 polarizations (hh-hv), 1 date, AirSAR measurements (Flevoland 1991).

classified as	true class						
	barley	corn	grass	potato	rape	s.beet	wheat
barley	3	0	2	0	0	0	0
corn	0	1	0	0	0	2	0
grass	0	0	6	0	0	0	3
potato	1	0	0	25	0	0	0
rape	0	0	0	0	3	0	0
s.beet	0	1	0	0	0	17	0
wheat	0	0	0	0	0	0	15
total number of samples					=	79	
correctly classified					=	70	
overall accuracy					=	88.6 %	

Table 5. Confusion matrix describing the neural algorithm crop classification performance. Algorithm input characteristics: 2 polarizations (hh-hv), 2 dates, AirSAR measurements (Flevoland 1991).

classified as	true class						
	barley	corn	grass	potato	rape	s.beet	wheat
barley	3	0	1	0	0	0	1
corn	0	1	0	0	0	0	0
grass	0	0	6	0	0	0	1
potato	0	0	1	25	0	0	0
rape	0	0	0	0	3	0	0
s.beet	0	0	0	0	0	18	0
wheat	1	1	0	0	0	1	16

total number of samples = 79  
 correctly classified = 72  
 overall accuracy = 91.1 %

Table 6. Confusion matrix describing the neural algorithm crop classification performance. Algorithm input characteristics: 3 polarizations (hh-hv), 3 dates, AirSAR measurements (Flevoland 1991).

classified as	true class						
	barley	corn	grass	potato	rape	s.beet	wheat
barley	3	0	1	0	0	0	0
corn	0	2	0	0	0	0	0
grass	0	0	7	0	0	1	0
potato	1	0	0	25	0	0	2
rape	0	0	0	0	3	0	0
s.beet	0	0	0	0	0	18	0
wheat	0	0	0	0	0	0	16

total number of samples = 79  
 correctly classified = 74  
 overall accuracy = 93.7 %

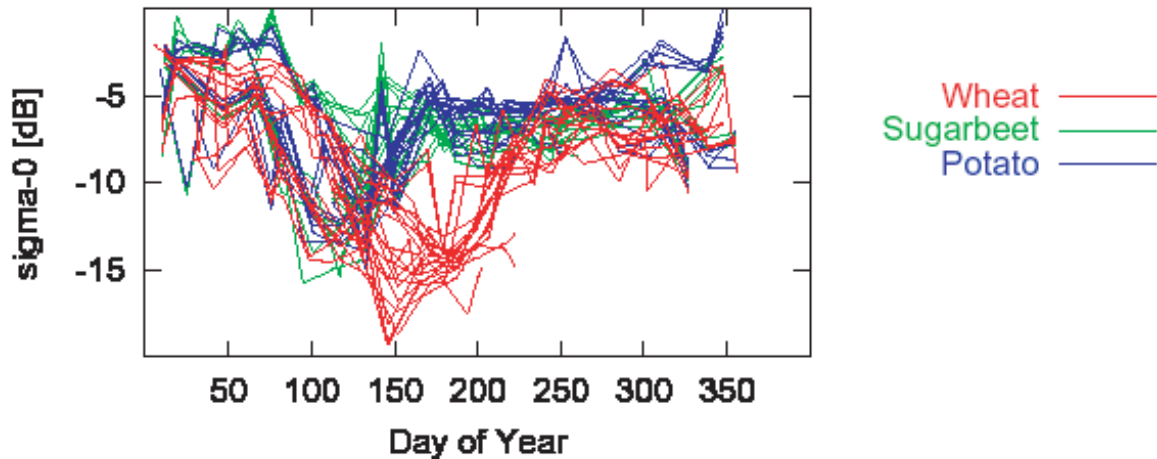


Figure 2. Different behaviours of  $\sigma^0$ 's of different crops as resulting from ERS measurements taken over different sites and years.

Table 7. Confusion matrix describing the neural algorithm crop classification performance. Algorithm input characteristics: 1 polarization (vv), 27 dates, ERS measurements (Flevoland 1995).

classified as	true class						
	barley	corn	grass	potato	rape	s.beet	wheat
barley	3	0	0	0	0	0	0
corn	0	3	0	0	0	0	0
grass	0	0	9	0	0	0	0
potato	0	0	0	15	0	0	0
rape	0	0	0	0	1	0	0
s.beet	0	1	0	0	0	12	0
wheat	0	0	0	0	0	0	11

total number of samples = 55  
correctly classified = 54  
overall accuracy = 98.2 %

Table 8. Confusion matrix describing the neural algorithm crop classification performance. Algorithm input characteristics: 1 polarization (vv), 7 dates, ERS measurements (Flevoland 1995).

classified as	true class						
	barley	corn	grass	potato	rape	s.beet	wheat
barley	3	0	0	0	0	0	1
corn	0	4	0	0	0	0	0
grass	0	0	9	0	0	0	0
potato	0	0	0	15	0	1	0
rape	0	0	0	0	1	0	0
s.beet	0	0	0	0	0	11	0
wheat	0	0	0	0	0	0	10

total number of samples = 55  
correctly classified = 53  
overall accuracy = 96.4 %

Table 9. Confusion matrix describing the neural algorithm crop classification performance. Algorithm input characteristics: 1 polarization (vv), 7 dates, ERS measurements. Training set: Flevoland 1993/94, test set: Flevoland 1995.

classified as	true class				
	barley	grass	potato	s.beet	wheat
barley	8	0	0	0	5
grass	0	30	0	0	1
potato	0	0	30	2	0
s.beet	0	0	0	28	0
wheat	0	0	0	0	24

total number of samples = 128  
correctly classified = 120  
overall accuracy = 93.8 %

# MONITORING CROP CYCLES BY SAR USING A NEURAL NETWORK TRAINED BY A MODEL

F. Del Frate<sup>1</sup>, P. Ferrazzoli<sup>1</sup>, L. Guerriero<sup>1</sup>  
T. Strozzi<sup>2</sup>, U. Wegmüller<sup>2</sup>, G. Cookmartin<sup>3</sup>, S. Quegan<sup>3</sup>

<sup>1</sup>Università Tor Vergata, Ingegneria, DISP, Via di Tor Vergata 110, I-00133 Rome, Italy  
Tel. +39 06 72597420, Fax +39 06 72597460, E-mail ferrazzoli@disp.uniroma2.it

<sup>2</sup>Gamma Remote Sensing, Thunstrasse 130, CH-3074 Muri BE, Switzerland  
Tel. +41 31 951 70 05, Fax +41 31 951 7008, E-mail strozzi@gamma-rs.ch

<sup>3</sup>Sheffield Centre for Earth Observation Science, Hicks Building  
University of Sheffield, Sheffield S3 7RH, UK  
Tel. +44 114 22 3803, Fax +44 114 222 3809, E-mail s.quegan@sheffield.ac.uk

## ABSTRACT

An algorithm, based on an electromagnetic model and a neural network, aimed at monitoring the multitemporal evolution of wheat fields, is described. Three different sites are used to validate the model, provide reference ground data, and test the algorithm.

## 1. INTRODUCTION

In the last decades, important advances have been achieved in the agricultural applications of SAR. Since the 70's, several ground based experiments proved a significant radar sensitivity to crop parameters, and results were summarized in important books (?). Further experimental studies were carried out by means of airborne SAR campaigns. Finally, the launches of ERS, RADARSAT and JERS made it possible to monitor crop cycles continuously by means of spaceborne SAR's.

In parallel, crop scattering models are being refined. Vegetation elements such as leaf, stem and ear have been represented as discrete elements and their scattering and absorption cross-sections computed by theories developed for canonical shapes, that is discs and cylinders. Further developments are in progress, leading to include multiple scattering, leaf curvature and coherent interactions.

From the application point of view, the objective is the solution of the retrieval problem. It means that the evolution of important vegetation variables such as Leaf Area Index (LAI,  $m^2/m^2$ ) and Biomass ( $kg/m^2$ ) has to be estimated by means of SAR acquisitions. This problem is considered in the present paper, with specific reference to wheat fields. Three main steps may be identified: i) to adopt a convenient radar configuration, ii) to establish a reliable

relationship between the backscatter coefficient  $\sigma^\circ$  and the vegetation variables, and iii) to solve the inverse problem. As far as the first step is concerned, several studies indicate that the ERS configuration (i.e. C band, VV polarization,  $23^\circ$ ), in spite of its limitations, may lead to interesting results for some crops, such as wheat and rice (??). The second step is still in progress. Important advances have been achieved, but some studies indicate that present models are not yet sufficiently accurate (?). Finally, the third problem is very complex, since  $\sigma^\circ$  depends on several soil and vegetation variables. Therefore, inversion based on a single radar observation is not feasible. Multiple observations are needed, and the problem shows difficult aspects in any case.

The idea suggested in this work is to use an electromagnetic model and a known multitemporal set of detailed ground data, collected in a reference site, to generate a multitemporal set of simulated  $\sigma^\circ$ 's which, on its turn, is used to train a neural network. Then, a test site is considered. The network, using as input a multitemporal set of experimental  $\sigma^\circ$ 's collected over the test site, estimates the differences between the crop cycle of the reference site and the crop cycle of the test site and, hence, the time evolution of its vegetation variables. Of course, the so obtained algorithm is based on some approximations, which will be critically discussed in the paper. However, it shows the advantage of fully exploiting the potential of multitemporal data and training the network with model outputs which consider the evolution of all vegetation variables.

Section 2 describes the experimental data, collected by the ERS-2 SAR over wheat fields of the Driffield (UK) site and by the RASAM scatterometer over wheat fields of the Central Plain (CH) site. The experimental data have been made available in the framework of an EEC Concerted Action, named ERA-ORA. Also some information about the reference site is given. Section 3 describes the electro-

magnetic model used to train the retrieval algorithm. The latter is described in Section 4. Section 5 shows and discusses the obtained results. Finally, indications about further studies, required to improve the accuracy of the algorithm, are given.

## 2. THE EXPERIMENTS

Three data sets are considered in this work. ERS-2 signatures collected at the Driffield site in 1997, as well as detailed ground truth, are used to critically estimate the accuracy of the electromagnetic model. RASAM signatures collected at the Central Plain site in 1988, with some fundamental ground data, are used to test the retrieval procedure. Finally, in order to train the neural network, the model is run using as input a detailed ground data set, collected at the French Avignon site with a sampling time of 3 days.

### 2.1. Model validation site (Driffield)

In 1997, several fields were monitored at the Driffield site by ERS-2 SAR. During the campaign, the important soil and vegetation variables were measured. In particular, multitemporal signatures of 3 wheat fields (numbered by 2, 3 and 5) are available. Radar data are accompanied by detailed information about soil moisture and soil roughness, as well as dimensions and moisture of leaf, stem and ear. The experiment is described and discussed by ?, where details are available. Some aspects, which are important to our objective, are summarized below.

Figure 1 shows the temporal evolution of volumetric Soil Moisture Content (SMC), crop biomass and backscatter coefficient measured by ERS-2. It is evident that simultaneous effects of soil drying and crop growing occur in springtime. Both effects contribute to lower the backscatter coefficient. Therefore, inversion of a single parameter by means of empirical methods is not reliable, but physical models are required to single out the different effects. For all the three fields a clear  $\sigma^\circ$  minimum is observed at Day of Year (DoY)  $\sim 150$ , followed by a slight  $\sigma^\circ$  increase. The biomass, on its turn, shows the highest values in a subsequent time interval, i.e. between DoY 150 and DoY 200.

Figure 2 compares, in the three fields, the trends of geometrical variables, such as leaf width, stem diameter and ear diameter. Although with some differences, the time evolutions follow similar rules among the three fields. Therefore, developing retrieval algorithms based on a reference field, as it is done in this paper, appears to be reasonable. Of course, the accuracy of the algorithm will be improved if the reference field is taken in the same climatic zone and is of the same species and variety.

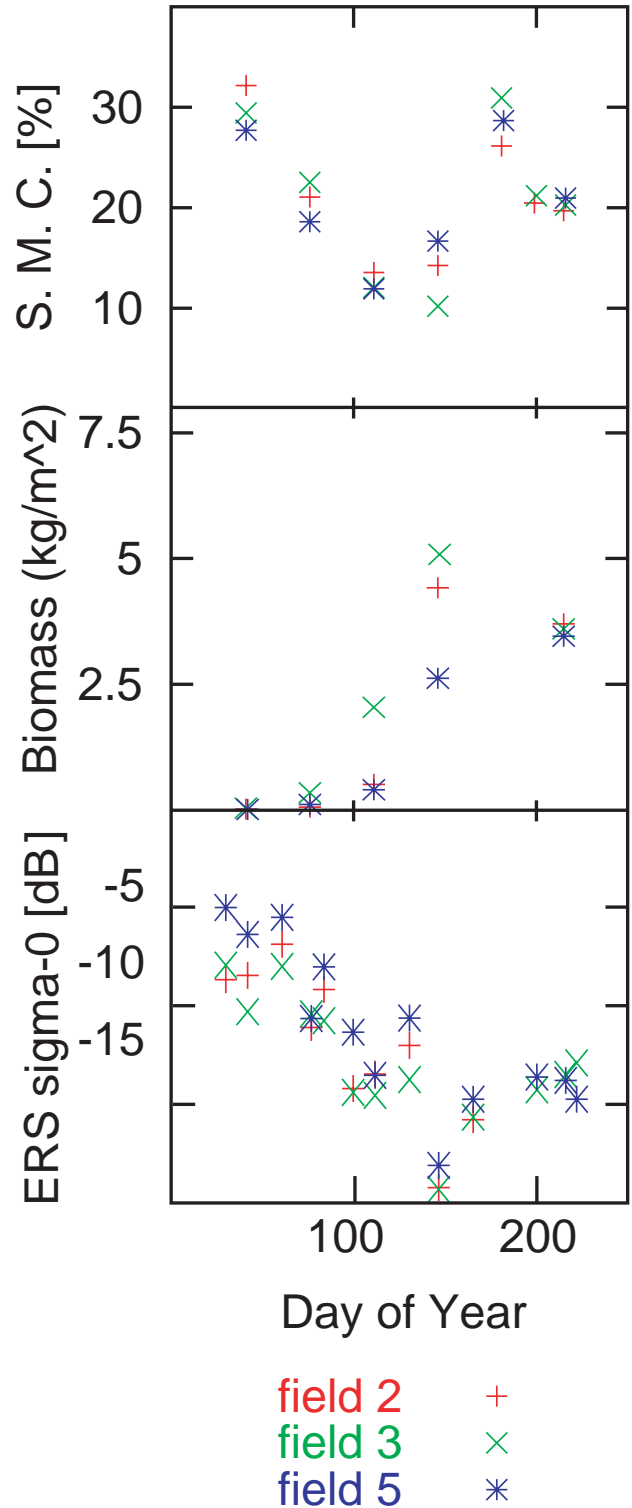


Figure 1. Temporal evolution of Soil Moisture Content, biomass, and  $\sigma^\circ$  (measured by ERS) in the 3 fields of Driffield-site (Central Plain)

RASAM is a microwave radiometer/scatterometer system. It operated over several fields in Switzerland between 1984 and 1991. Signatures were collected at the frequencies of 2.5, 3.1, 4.6, 7.2, 10.2 and 11.0 GHz, at several angles between  $10^\circ$  and  $70^\circ$ , and at VV, HH, HV and VH polarizations (?).

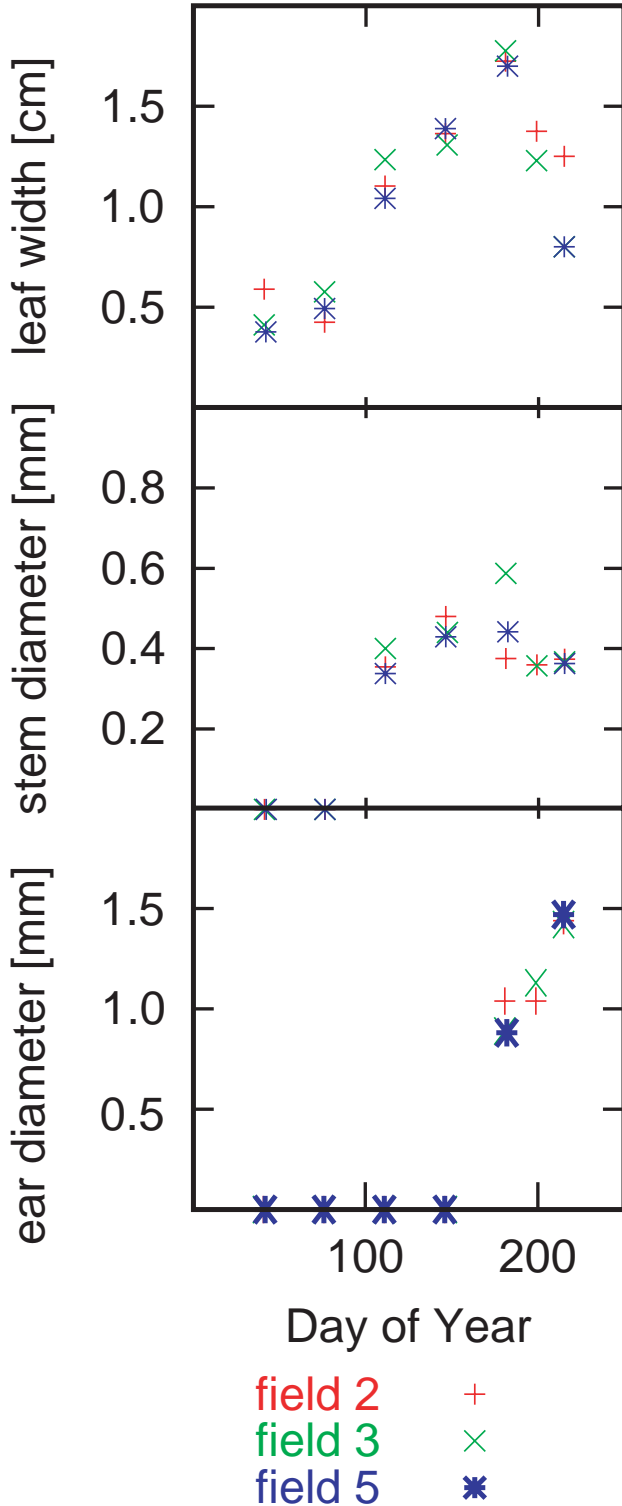


Figure 2. Temporal evolution of leaf width, stem diameter and ear diameter in the 3 fields of Driffield site

Ground data covered some significant parameters such as soil moisture, soil roughness, crop height, crop biomass, etc. In this paper, the retrieval procedure is tested using multitemporal signatures collected over a wheat field in 1988 at the Central Plain site.

Figure 3 shows the time evolution of Soil Moisture Content, biomass and  $\sigma^\circ$ . Two frequency bands, i.e. 3.1 GHz (S) and 10.2 GHz (X), two polarizations, i.e. VV and HH, and an angle of  $30^\circ$  are taken. The SMC remains relatively high (i.e.  $> 25\%$ ) during the whole cycle, with some limited and rapid variations. SMC effects on  $\sigma^\circ$  are appreciable at S band, HH polarization, while are not evident at X band and/or at VV polarization. As far as general  $\sigma^\circ$  trends are considered, a minimum similar to the one observed in Fig. 1 for ERS is noted at S band (particularly at VV polarization), while at X band the trend is monotonic decreasing.

### 2.3. Reference site (Avignon)

As it will be shown in the next Section, the neural network has been trained using a multitemporal set of simulated signatures with short sampling time. Of course, the same short sampling time was required for the ground data used as model inputs. Measurements carried out over a wheat field in 1993 at the French Avignon site have been used. Data covered all the important biophysical and geometrical vegetation variables, with a sampling time of 3 days. Details about the site and the measurements are given by ?.

## 3. THE MODEL

The model assumes the vegetation medium to be a homogeneous half-space with rough interface, representing the soil, overlaid by an ensemble of discrete lossy scatterers, representing the plant constituents.

The electromagnetic properties of the soil are described by its bistatic scattering coefficient. The latter is computed by the Integral Equation method with an exponential correlation function. The electromagnetic properties of the scatterers, which represent the plant constituents, are described by their bistatic scattering cross sections. Dielectric elements of simple shape, such as discs and cylinders, are used. For discs, representing leaves, the Physical Optics approximation is adopted. Cylinders represent stems and ears. For these kinds of scatterers computations are carried out assuming the internal field to be the same as that of an infinite length cylinder.

Once the bistatic scattering cross sections of the scatterers have been computed for a discrete set of incidence and scattering directions, the electromagnetic

behaviour of the ensemble of scatterers is obtained. To this end, the matrix doubling algorithm is used, under the assumption of azimuthal symmetry. The same algorithm is used to combine the vegetation layer scattering contribution with that due to the soil. The backscatter coefficient of the whole medium is finally computed.

Details about the model are given in ?. In order to simulate the particular geometry of a wheat crop, we consider a lower layer filled with thin vertical cylinders, representing stems, and an upper layer filled with vertical cylinders, representing ears, respectively (?). Discs, representing leaves, are distributed along the vertical direction. A uniform lower half-space with rough interface represents the soil.

The model is tested against Driffield data, since ground truth in this site are sufficiently detailed to be used as inputs. Figure 4 shows the results for the three wheat fields. A general agreement is observed during the growing phase, up to  $\sim$  DoY 150. Both the model and the experimental data show a decreasing  $\sigma^\circ$  trend, which is due to both the soil drying and the vegetation attenuation increase. After this decreasing period, both simulated and experimental data sets show a minimum, followed by a slight increase in the late part of the cycle. A disagreement is observed in the location of the minimum. In the experimental data, it occurs at  $\sim$  DoY 150, i.e in the early earing, while in the simulations is located in the mature phase. Apparently, the model overestimates ear attenuation. This problem, which has been observed in other works and leads to an inaccuracy in the retrieval, needs further investigations.

#### 4. THE RETRIEVAL ALGORITHM

A retrieval algorithm has been developed and tested over the Central Plain site. Neural simulations are based on the Stuttgart University neural network simulator (SNNS). The topology is formed by a multi-layer perceptron with two hidden layers, while a sigmoid function is applied as activation function of the network units. The retrieval process is subdivided into two phases: training and test.

##### 4.1. Training

A reference site, for which a multitemporal set of detailed ground truth is available, is selected. For each Day of Year of the reference site  $[DoY]_{REF}$  the model is run to simulate  $\sigma^\circ$ 's at the required frequencies, polarization and angles. Vegetation inputs are given by the ground data measured at the reference site. As far as soil variables are concerned (i.e. soil moisture, height std. and correlation length), a parametric approach is adopted: computations are carried out for several values of soil variables. It is

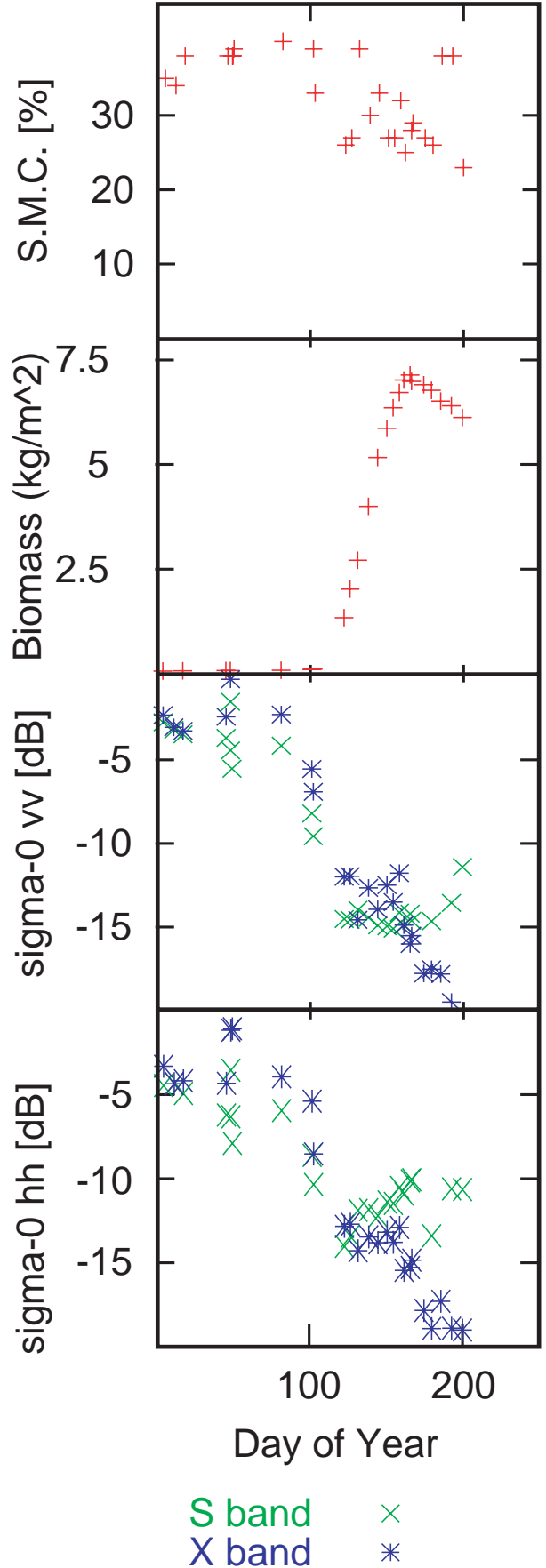


Figure 3. Temporal evolution of Soil Moisture Content, biomass, and  $\sigma^\circ$  in the field of Central Plain site.

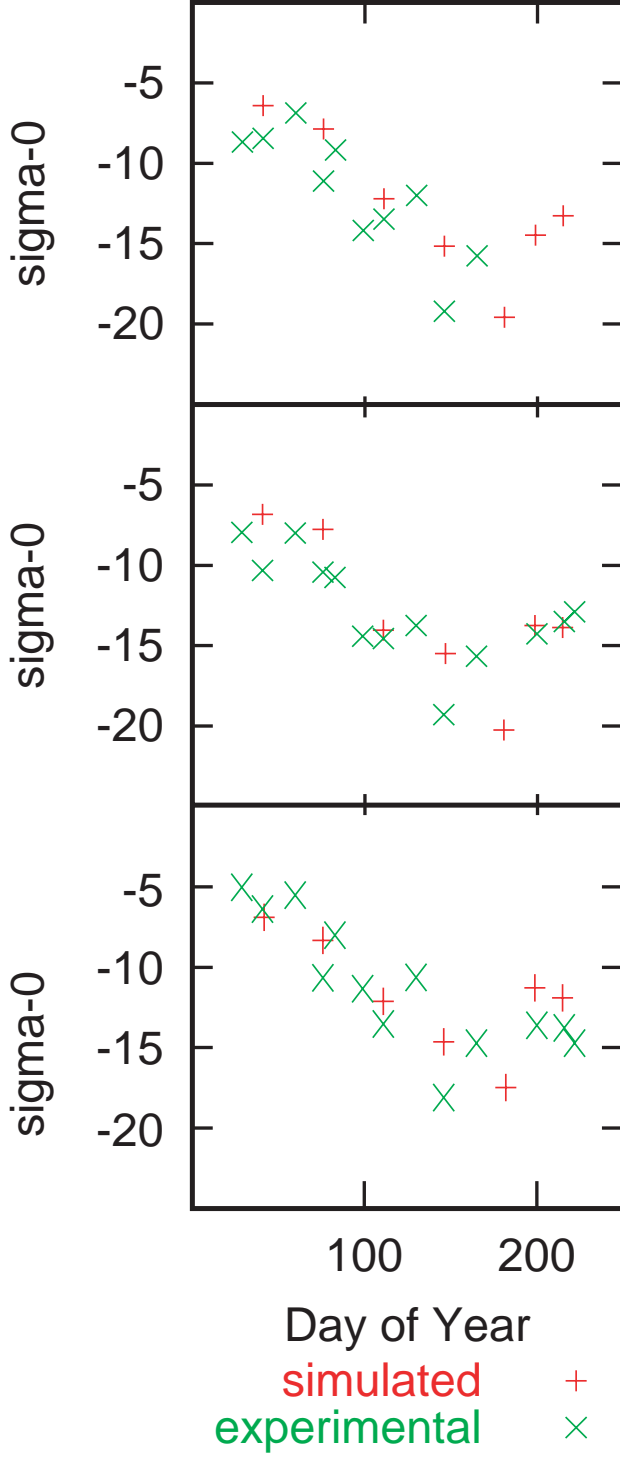


Figure 4. Comparison between experimental (ERS) and simulated  $\sigma^{\circ}$ 's in the 3 fields of Driffield site.

also introduced a “density factor”  $F_d$  in the computations. This means that  $\sigma^{\circ}$ 's are simulated for a field with a number of plants per  $m^2$  ( $N$ ) which may be different from the value measured at the reference site ( $N_{REF}$ ). The  $F_d = N/N_{REF}$  ratio is varied up to a maximum value of 2. In this way a set of simulated  $\sigma^{\circ}$ 's is generated, covering several  $[DoY]_{REF}$ 's, several situations of soil variables and  $F_d$ 's, and the selected frequencies, polarizations and angles. Model outputs are used to train the neural network. As a

result of the training phase, multitemporal sets of backscatter coefficients are associated to crop cycles which may differ from the reference cycle in crop density, and also in temporal location and temporal duration, as it will be better clarified in the next Section.

#### 4.2. Test

A test site is considered. A multitemporal set of  $\sigma^{\circ}$ 's measured at the same frequencies, polarizations and angles as those of the training phase, is taken. Soil parameters are assumed to be known, and taken from ground data of the test site. As far as vegetation parameters are considered the network, using experimental  $\sigma^{\circ}$ 's as input, estimates the differences between the multitemporal ground data of test field and the ones of reference field. These differences may concern the density factor, the temporal location and the temporal duration. The outputs provided by the network are the  $F_d$  factor and a couple of parameters, named  $a$  and  $b$ , containing information about the temporal evolution of the cycle, as indicated below.

Let  $Y_R$  be the retrieved value of a vegetation variable for a given Day of Year in the test site,  $[DoY]_{TEST}$ , and  $Y_M$  be the measured value of the same variable for a given Day of Year in the reference site  $[DoY]_{REF}$ . Some variables, such as biomass and LAI, are dependent on density. In this case we have:

$$Y_R([DoY]_{TEST}) = F_d \cdot Y_M([DoY]_{REF}) \quad (1)$$

with:

$$[DoY]_{REF} = [DoY]_{REF0} + a \cdot ([DoY]_{TEST} - [DoY]_{REF0} + b) \quad (2)$$

where  $[DoY]_{REF0}$  is the starting day of the reference cycle.

Other variables, such as dimensions and moistures of leaf, stem and ear are not dependent on the density. For these variables, formula (1) is modified into:

$$Y_R([DoY]_{TEST}) = Y_M([DoY]_{REF}) \quad (3)$$

while formula (2) is unmodified. In this way all vegetation variables may be estimated for the whole test cycle.

The proposed method adopts some simplifying assumptions which could be restrictive. In the reality, the test field may differ from the reference field in other properties besides density, temporal location and temporal duration. However, this restriction could be overcome in the future by some refinements such as: i) introduction of other parameters, besides  $a$ ,  $b$  and  $F_d$ , ensuring a higher degree of flexibility to the algorithm; ii) availability of reference ground data taken in the same environment as that of the test field.

In spite of its limits, the proposed algorithm may be a step towards the solution of the retrieval problem. It must be considered that, in the model adopted by us, the backscatter coefficient is influenced by: soil moisture, surface height std. and correlation length, number of plants per  $m^2$ , dimensions and moistures of leaf, stem and ear, leaf orientation distribution, for a total of 14 variables. The number is even higher in models adopting multi-scale surface representations and/or coherent approaches. Therefore, a direct mathematical inversion of such a large system of relationships is extremely difficult. On the other hand, methods based on simple relationships between  $\sigma^\circ$  and a single variable are much less general, in that are heavily influenced by the specific properties of the adopted data sets.

## 5. RESULTS

The procedure described in Section 4 has been applied using a wheat field of Avignon site as reference and another wheat field of Central Plain site as test. Among the several frequencies, polarizations and angles of RASAM, the following ones have been selected: 3.1 GHz, 4.6 GHz, 10.2 GHz frequencies; HH and VV polarizations,  $30^\circ$  angle.

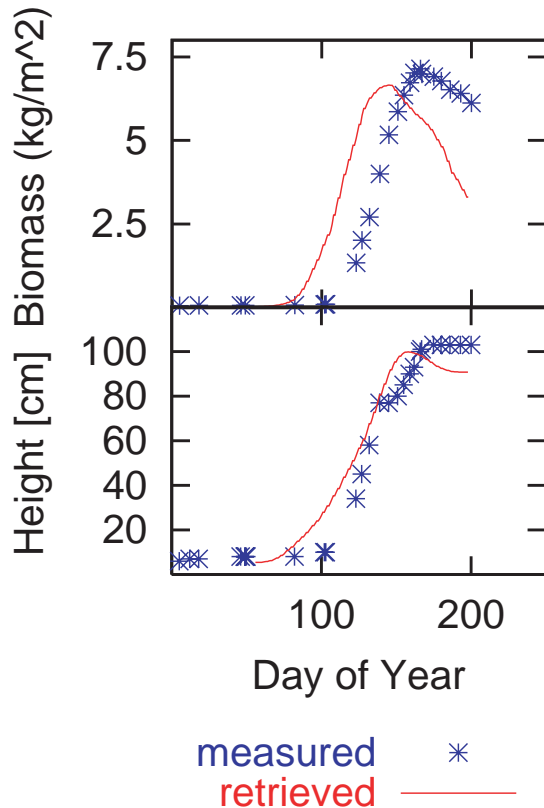


Figure 5. Comparison between experimental and retrieved vegetation parameters at Central Plain site

This selection ensures the use of diversified information sources, but it avoids to introduce too many

nodes in the network. On the basis of available ground data of Avignon site,  $[DoY]_{REF0}$  has been set equal to 110.

The procedure leads to the following results:

$$a = 0.71, b = 26, F_d = 2$$

By using formulas (1) and (3), respectively, the multitemporal trends of crop biomass and crop height may be retrieved. Figure 5 compares the retrieved data sets with the directly measured ones. As far as biomass is concerned, the algorithm correctly predicts the Central Plain field to be denser than the Avignon field, with  $F_d = 2$ . On the contrary, there is an evident error in the time evolution, since the cycle predicted by the algorithm is earlier than the measured one. This inaccuracy, which is less evident in crop height trends, is related to the modeling problems already identified in Figure 4 for the Driffield site. The algorithm tends to predict an earlier cycle to compensate for the delay in  $\sigma^\circ$  introduced by the model. The latter, on its turn, is due to an overestimation of ear attenuation in the late part of the cycle. Therefore, refinements in the electromagnetic model are required. In particular, geometric and dielectric properties of stem and ear need to be better represented.

A good fitting of biomass trend at test site would have been obtained with:

$$a = 0.6, b = 10, F_d = 2$$

The height trend is better reproduced than the biomass trend. This result could be due to some agronomic differences between the Avignon field and the Central plain field, not sufficiently considered by three simple parameters such as  $a$ ,  $b$  and  $F_d$ . Algorithms with a higher degree of flexibility could lead to better results, in the future.

## 6. CONCLUSIONS

An algorithm has been proposed to retrieve the multitemporal evolution of wheat fields using a reference site, a model and a neural network. The accuracy of the results needs to be improved. Further studies, aimed at refining the electromagnetic model and introducing a higher degree of flexibility in the algorithm, are required.

## ACKNOWLEDGMENTS

The data of Avignon test site have been kindly made available by J.-P. Wigneron, from INRA. The data of Driffield and Central Plain sites have been made available in the framework of the ERA-ORA Project, funded by ECC.

## REFERENCES

- Bracaglia M., Ferrazzoli P., Guerriero L., 1995, "A fully polarimetric multiple scattering model for crops", *Remote Sensing of Environment*, vol. 54, 170-179.
- Cookmartin G., Saich P., Quegan S., et al., 2000, "Modeling microwave interactions with crops and comparison with ERS-2 SAR observations", *IEEE Trans. Geosci. Remote Sensing*, vol. 38, 658-670.
- Ferrazzoli P., Wigneron J.-P., Guerriero L., Chanzy A., 2000, "Multifrequency emission of wheat: modeling and applications", *IEEE Trans. Geoscience and Remote Sensing*, vol. 38, 2598-2607.
- Le Toan T., Ribbes F., Li-Fang W., et al., 1997, "Rice crop mapping and monitoring using ERS-1 data based on experiment and modeling results", *IEEE Trans. Geosci. Remote Sensing*, vol. 35, 41-56.
- Stiles J. M., Sarabandi K., Ulaby F. T., 2000, "Electromagnetic scattering from grassland - part II: measurement and modeling results", *IEEE Trans. Geosci. Remote Sensing*, vol. 38, 349-356.
- Ulaby F. T., Moore R. K, Fung A. K, 1986, *Microwave Remote Sensing: Active and Passive - vol.III*, Artech House, Dedham (MA, USA).
- Wegmüller U., 1993, "Signature research for crop classification by active and passive microwaves", *Int. J. Remote Sensing*, vol. 14, 871-883.